PARAMETRIC FINITE ELEMENT MODELING AND FULL-SCALE TESTING OF TRUNNION-HUB-GIRDER ASSEMBLIES FOR BASCULE BRIDGES

Glen Besterfield, Autar Kaw & Roger Crane
Department of Mechanical Engineering
University of South Florida

November 2001

A Report on a Research Project Sponsored by the Florida Department of Transportation[1]

[1] Contract Number B-C008

DISCLAIMER

The opinions, findings and conclusions expressed in this publication are those of the authors who are responsible for the facts and accuracy of the data presented herein. The contents do not necessarily reflect the views or the policies of the Florida Department of Transportation or the Federal Highway Administration.

The report is prepared in cooperation with the Florida Department of Transportation.

UNIT CONVERSION TABLE

To convert from	To	Multiply by
inch	centimeter	2.54
square inch	square centimeter	6.4516
kip	kiloNewton (kN)	4.44747
kip/sq.in. (ksi)	kN/sq.m (kPa)	6,894.28
kip-foot	kN-meter	1.3556
btu	joule	1,055
btu	kilowatt-hrs.	0.0002928
btu/hr.	watt	0.2931
degrees fahrenheit – 32	degrees celsius	0.5555
lb/cu.in.	kgs./cu.m	27,680
btu/sq.ft./min.	watts/sq.in.	0.122

PREFACE

The investigation reported in this document was funded by a contract awarded to the University of South Florida, Tampa by the Florida Department of Transportation (FDOT). Mr. Thomas A. Cherukara was the Project Manager. It has been a pleasure to work with "Tom" and we would like to acknowledge his numerous contributions to this study.

This project could not have been successfully completed without enormous support and help from other members of the FDOT. We would like to especially acknowledge Mr. Jack Evans and Mr. Angel Rodriguez.

We wish to thank Mr. James Allison, PE of Steward Machine Co. in Birmingham, AL for machining trunnion, hub and girder test specimens. We are also very grateful to Mr. Paul Hillis of PGH Engineering in Tampa, FL for giving tremendous insight into the assembly of a trunnion-hub-girder and to Mr. George Patton of EC Driver in Tampa, FL for his assistance.

This project could not have been completed without the support and invaluable assistance of the College of Engineering's Machine Shop staff. The contribution of graduate students Mr. Michael Denninger, Mr. Niranjan Pai, Mr. Badri Ratnam, and Mr. Sanjeev Nichani is gratefully acknowledged and we are deeply indebted to them for their excellent work ethic and insight into the project. We also acknowledge the assistance of numerous undergraduate students who helped with the experimental testing. Some of them (not in any order) were Ms. Erika Rosand, Mr. Kevin Edwards, Mr. Raoul Rodriguez, Mr. Thomas Wasik, Mr. Chris Hampton, and Mr. Saul Sanchez, to name a few.

EXECUTIVE SUMMARY

Failures during fabrication of trunnion-hub-girder (THG) assemblies of bascule bridges can result in losses of hundreds of thousands of dollars. Crack formation in the hub of the Miami Avenue Bridge, Christa McAuliffe Bridge and Brickell Avenue Bridge during assembly led the Florida Department of Transportation (FDOT) to commission a project to perform a complete numerical and experimental study to investigate why the assemblies failed.

Two different procedures are currently utilized for the assembly of the trunnion-hub-girder. Assembly procedure 1 (AP1) involves cooling the trunnion and shrink fitting it into the hub, and subsequently cooling the trunnion-hub assembly to shrink fit it into the girder. In assembly procedure 2 (AP2), the hub is shrink fitted into the girder first, followed by cooling the trunnion and shrink fitting it into the hub-girder assembly. Several problems can occur during the assembly, including development of cracks on the hub as well as improper assembly due to insufficient cooling of the parts.

A preliminary study of the steady state stresses using the Bascule Bridge Design Tools revealed that the stresses are well below the yield strength of the material and could not have caused failure. This called for a further investigation of the transient thermal and structural stresses developed during the assembly process.

In the second study, a numerical modeling of the different assembly procedures of the THG assembly is developed. A parametric finite element model is designed in ANSYS called the Trunnion-Hub-Girder Testing Model (THGTM) to analyze the stresses, temperatures and critical crack lengths in the THG assembly during the two assembly procedures. The THGTM is used to compare the hoop stress and critical crack lengths during the two assembly procedures for different bridges. The critical points in the assembly and the critical stages during the two assembly processes are identified based on the critical crack length.

A third study presents results from experiments used to determine the thermal and structural response of the trunnion-hub-girder assembly during the two assembly procedures. Quarter-scale and full-scale trunnion-hub-girders were instrumented with cryogenic strain gages and thermocouples to determine stresses and temperatures at critical points.

It was found that large tensile hoop stresses develop in the hub at the trunnion-hub interface in AP1 when the trunnion-hub assembly is cooled for insertion into the girder. These stresses occur at low temperatures, and result in low values of critical crack length. Peak stresses during AP2 occur when the hub is cooled for insertion into the girder. Note that the critical crack length allowed under AP1 is less than half that could be allowed under AP2. In other words, the critical crack length for AP2 could be more than double that could be allowed under AP1.

The conclusions of this report are that for the given full-scale geometry and interference values, AP2 is safer than AP1 in terms of lower hoop stresses, lower Von-Mises stresses and larger critical crack lengths.

TABLE OF CONTENTS

LIST OF TABLES

LIST OF FIGURES

LIST OF SYMBOLS

a	crack length	in
a_c	critical crack length	in
A	hoop stress with infinite meshing	psi
B	constant in convergence equation	psi
C_p	specific heat at constant pressure	BTU/(lb-ºF)
cdiv	number of divisions in the circumferential direction for every 60º (between a pair of gussets)	nondimensional
coolt1	hub cooling time/trunnion cooling time	min
coolt2	trunnion cooling time/trunnion-hub cooling time	min
cptemp	cool temperature factor	nondimensional
D	hydraulic diameter	in
E_0	Young's modulus at absolute zero	psi
$E_i(T)$	temperature dependent Young's modulus where i=1, 2, 3 represents the trunnion, the hub, and the girder, respectively	psi
E_T	Young's modulus at a temperature T	psi
ex	distance from the end of the backing ring to the end of the hub	in
exdiv	number of divisions along the ex	nondimensional
f_e	edge effect factor for stress intensity factor	nondimensional
fdiv	number of divisions along the length to the hub on the gusset side	nondimensional
g	acceleration due to gravity	in/sec^2
$G_i(T)$	temperature dependent shear modulus, where i=1, 2, 3 represents the trunnion, the hub and the girder, respectively	psi
gfdiv	number of divisions along the girder flange width	nondimensional
Gr	Grashof number	nondimensional
h	convective heat transfer coefficient	BTU/(hr-ºF-in^2)
$h_c(T)$	temperature dependent convective heat transfer coefficient for cooling medium	BTU/(hr-ºF-in^2)
h_m	heat transfer coefficient	BTU/(hr-ºF-in^2)
$h_w(T)$	temperature dependent convective heat transfer coefficient for air	BTU/(hr-ºF-in^2)
*hcoot*1	time at which user defined exit criteria are met in the hub during the cooling process	min
*hcoot*2	time at which the hub meets the user defined exit criteria	min
*hgct*1	time at which the interference between the hub and the girder is breached	min
*hgct*2	time at which the interference between the hub and the girder is breached	min
hgf	height of the girder flange	in
hgfdiv	number of divisions along the girder flange height	nondimensional

hgw	height of the girder	in
*hptemp*1	warm temperature factor	nondimensional
*hptemp*2	warm temperature factor	nondimensional
*hwarm*2	time at which the hub meets the user defined exit criteria	min
k	thermal conductivity	BTU/(hr-in-ºF)
$K_i(T)$	temperature dependent thermal conductivity, where i=1, 2, 3 represents the trunnion, the hub and the girder, respectively	BTU/(hr-in-ºF)
$K_{Ia}(T)$	temperature-dependent critical crack arrest factor	ksi-in$^{1/2}$
$K_{Ic}(T)$	temperature-dependent critical stress intensity factor	ksi-in$^{1/2}$
L	length of sleeve	in
l	extension of the trunnion on the gusset side (length to hub on the gusset side of the trunnion)	in
l_e^1	trunnion end coordinate	in
l_e^2	hub end coordinate	in
l_e^3	girder-hub contact end coordinate	in
l_s^1	trunnion start coordinate	in
l_s^2	hub start coordinate	in
l_s^3	girder-hub contact end coordinate	in
ldiv	number of divisions along the length to the hub on the backing ring side	nondimensional
lf	distance to hub flange	in
lfdiv	number of divisions along lf	nondimensional
lg	width of the girder	in
lh	total length of hub	in
lt	total length of trunnion	in
myref	reference strain temperature	ºF
N_i	number of elements in the THG assembly	nondimensional
Nu	Nusselt number	nondimensional
numdiv	number of divisions in the radial direction in each of the trunnion, the hub and the girder	nondimensional
Pr	Prandtl number	nondimensional
P	load on sleeve-bolt assembly	lb
r	radial coordinate	in
r_i^1	trunnion inner radial coordinate	in
r_i^2	hub inner radial coordinate	in
r_i^3	girder inner radial coordinate	in
r_o^1	trunnion outer radial coordinate	in
r_o^2	hub outer radial coordinate	in
R_{N_i}	hoop stress at a point with N_i elements	psi
rhg	outer radius of the hub(minus flange)	in

rho	outer radius of the hub flange	in
rti	inner radius of the trunnion	in
rto	inner radius of the hub	in
S	constant used in equation for Young's modulus	psi
t_{ac}	time after contact	min
t_{bc}	time before contact	min
t_c	total time (cooling)	min
t_w	total time (warming)	min
T_b	ambient air temperature	ºF
T_c	cooling medium bulk temperature	ºF
T_e	Einstein characteristic temperature	ºF
T_{sat}	saturation temperature	ºF
T_w	wall temperature	ºF
T_s^c	cold temperature criterion	ºF
T_s^w	warm temperature criterion	ºF
T_∞	ambient temperature	ºF
*tcoot*1	time at which the user defined exit criteria are met in the trunnion during the cooling process	min
tg	gusset thickness	in
*thcoot*1	time at which the trunnion-hub assembly meets the user defined exit criteria during the cooling process	min
*thct*1	time at which the conduction between the trunnion and the hub is switched to "on"	min
*thct*2	time at which the interference between the trunnion and the hub is breached	min
*thwarm*1	time at which the trunnion-hub-girder assembly meets user defined exit criteria during the fitting of the trunnion-hub assembly into the girder	min
tinc	time increments (warming) during AP1	min
tincc	time increments (cooling) during AP1	min
tinc2	time increments (warming) during AP2	min
tincc2	time increments (cooling) during AP2	min
*twarm*1	time at which the trunnion-hub assembly meets the user defined exit criteria	min
*twarm*2	time at which the trunnion-hub-girder assembly meets user defined exit criteria during the fitting of the trunnion into the hub-girder assembly	min
TBulk	ambient air bulk temperature	ºF
TCool	cooling medium bulk temperature	ºF
wbr	backing ring width	in
wbrdiv	number of divisions along wbr	nondimensional
wgf	width of the flange of the girder	in
wgw	width of the girder	in

wgwdiv	number of divisions along wgw	nondimensional
whf	width of the hub flange	in
whfdiv	number of divisions along whf	nondimensional
x_l^3	x-coordinate of girder flange on the left side as viewed from the gusset side of the THG assembly	in
x_r^3	x-coordinate of girder flange on the right side as viewed from the gusset side of the THG assembly	in
y_{ib}^3	inner y-coordinate of girder flange (bottom)	in
y_{it}^3	inner y-coordinate of girder flange (top)	in
y_{ob}^3	outer y-coordinate of girder flange (bottom)	in
y_{ot}^3	outer y-coordinate of girder flange (top)	in
z_r^3	z-coordinate of girder flange on backing ring side	in
α	coefficient of thermal expansion	in/in/ºF
$\overline{\alpha}$	constant in convergence equation	nondimensional
β	volume coefficient of thermal expansion	$in^3/in^3/ºF$
δ	change in length	in
ΔT	temperature difference	ºF
γ_e	electronic contribution	$BTU/(lb\text{-}ºF^2)$
μ	absolute viscosity	lb/(in-hr)
ρ	density	lb/in^3
σ_r	radial stress	psi
σ_z	axial stress	psi
σ_θ	hoop stress	psi
ν	kinematic viscosity	in^2-hr
$\nu^i(T)$	Poisson's ratio, where i=1, 2, 3 represents the trunnion, the hub and the girder, respectively	nondimensional

CHAPTER 1

BACKGROUND

1.1 Introduction

A bascule bridge is a type of movable bridge that can be opened or closed to facilitate the movement of water-borne traffic such as ships and yachts. The bascule bridge opens like a lever on a fulcrum (see Figure 1.1). The fulcrum that is fit into the girder of the bridge is made of a trunnion and a hub as shown in Figure 1.2. This trunnion, hub and girder when fitted together are referred to as a trunnion-hub-girder (THG) assembly. To open and close the girder (that is, the leaf) of the bascule bridge, power is supplied to the THG assembly by means of a curved rack and pinion gear at the bottom of the girder.

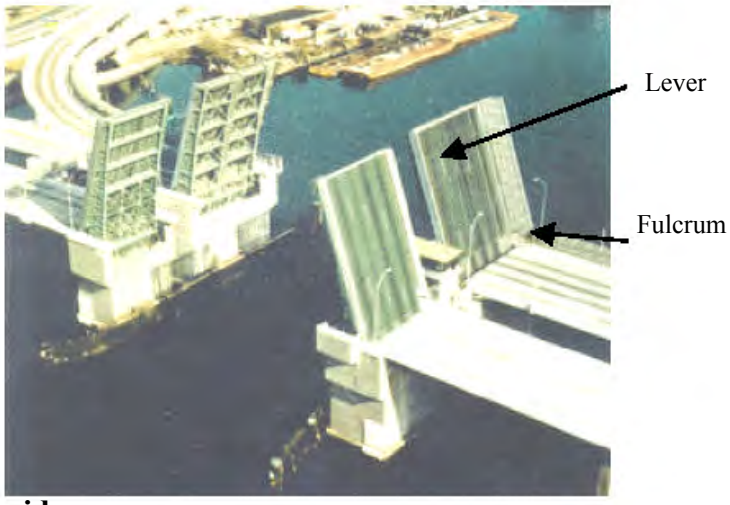

Figure 1.1 Bascule bridge.

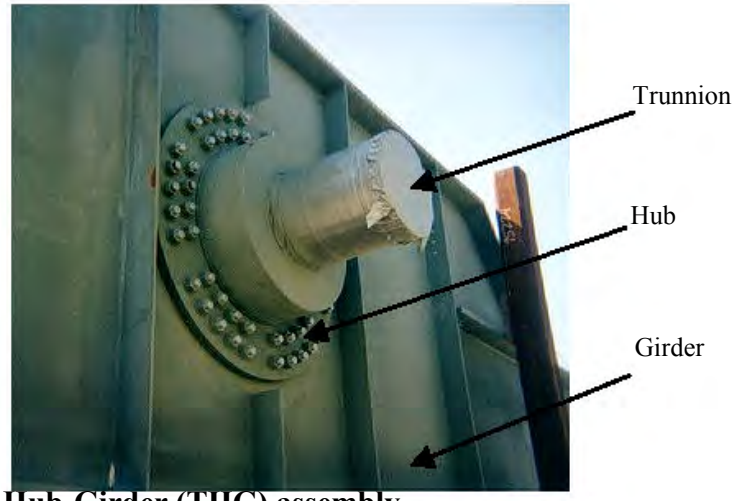

Figure 1.2 Trunnion-Hub-Girder (THG) assembly.

The THG assembly is generally made by interference fits between the trunnion and hub, and the hub and girder. Typical interference fits used in the THG assemblies for Florida bascule bridges are FN2 and FN3 fits (Shigley and Mishke, 1986).

FN2 and FN3 fits are 'US Standard Fits'. FN2 designation is (Shigley and Mishke, 1986) "Medium-drive fits that are suitable for ordinary steel parts or for shrink fits on light sections. They are about the tightest fits that can be used with high-grade cast-iron external members." Furthermore, FN3 designation is (Shigley and Mishke, 1986) "Heavy drive fits that are suitable for heavier steel parts or for shrink fits in medium sections".

The current procedure for assembling THG assemblies (in Florida) involves shrink fitting the trunnion into the hub, then shrink fitting this trunnion-hub into the girder. This assembly can also be done in a manner different from the existing procedure. Some failures associated with the current procedure are described in the next section.

1.2 History

On May 3rd, 1995 during the immersion of the trunnion-hub assembly in liquid nitrogen for the Christa McAuliffe Bridge, a cracking sound was heard. On removing the trunnion-hub assembly out of liquid nitrogen, it was found that the hub had cracked near its inner radius (see Figure 1.3). In a separate instance, during the assembly of the Venetian Causeway Bascule Bridge, while inserting the trunnion into the hub, the trunnion got stuck in the hub before complete insertion took place. A possible reason for this could be insufficient shrinkage of the trunnion in the dry ice-alcohol cooling medium.

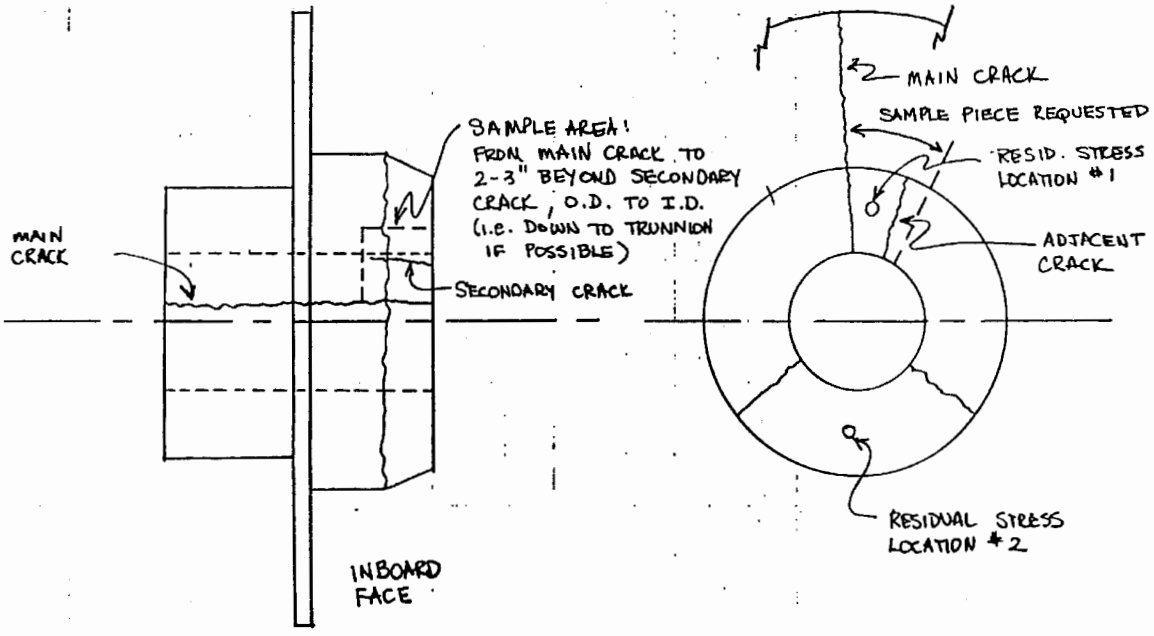

Figure 1.3 Locations of cracks on hub.[2]

[2] Figure 1.3 is reprinted from an independent consultant's report.

Each failure resulted in the loss of hundreds of thousands dollars in material, labor and delay in replacing the cracked assemblies. To prevent their recurrence, the Florida Department of Transportation (FDOT) decided to investigate the cause of failure in the THG assemblies. Preliminary investigations done by independent consulting firms and the assembly manufacturers gave various reasons for the possible failure including high cooling rate, use of liquid nitrogen as a cooling medium, residual stresses in the cast hub, and the assembly procedure itself.

FDOT officials wanted to carry out a complete numerical and experimental study, which would investigate why the assemblies failed and lay down clear specifications for future assemblies to prevent the recurrence of these failures.

So, in 1998, they provided a research grant to the College of Engineering at the University of South Florida to investigate the problem. This final report is the conclusion of this research grant.

1.3 Assembly procedures

The Trunnion-Hub-Girder assembly can be done in two different ways, called "Assembly Procedure 1 (AP1)" and "Assembly Procedure 2 (AP2)" (see Figure 1.4). AP1 involves the following four steps:

Step 1. The trunnion is shrunk by cooling in liquid nitrogen.

Step 2. This shrunk trunnion is then inserted into the hub and allowed to warm up to ambient temperature to develop an interference fit on the trunnion-hub interface.

Step 3. The resulting trunnion-hub assembly is shrunk by cooling in liquid nitrogen.

Step 4. This shrunk trunnion-hub assembly is then inserted into the girder and allowed to warm up to ambient temperature to develop an interference fit on the hub-girder interface.

AP2 consists of the following four steps:

Step 1. The hub is shrunk by cooling in liquid nitrogen.

Step 2. This shrunk hub is then inserted into the girder and allowed to warm up to ambient temperature to develop an interference fit on the hub-girder interface.

Step 3. The trunnion is shrunk by cooling in liquid nitrogen.

Step 4. This shrunk trunnion is then inserted into the hub-girder assembly and allowed to warm up to ambient temperature to develop an interference fit on the trunnion-hub interface.

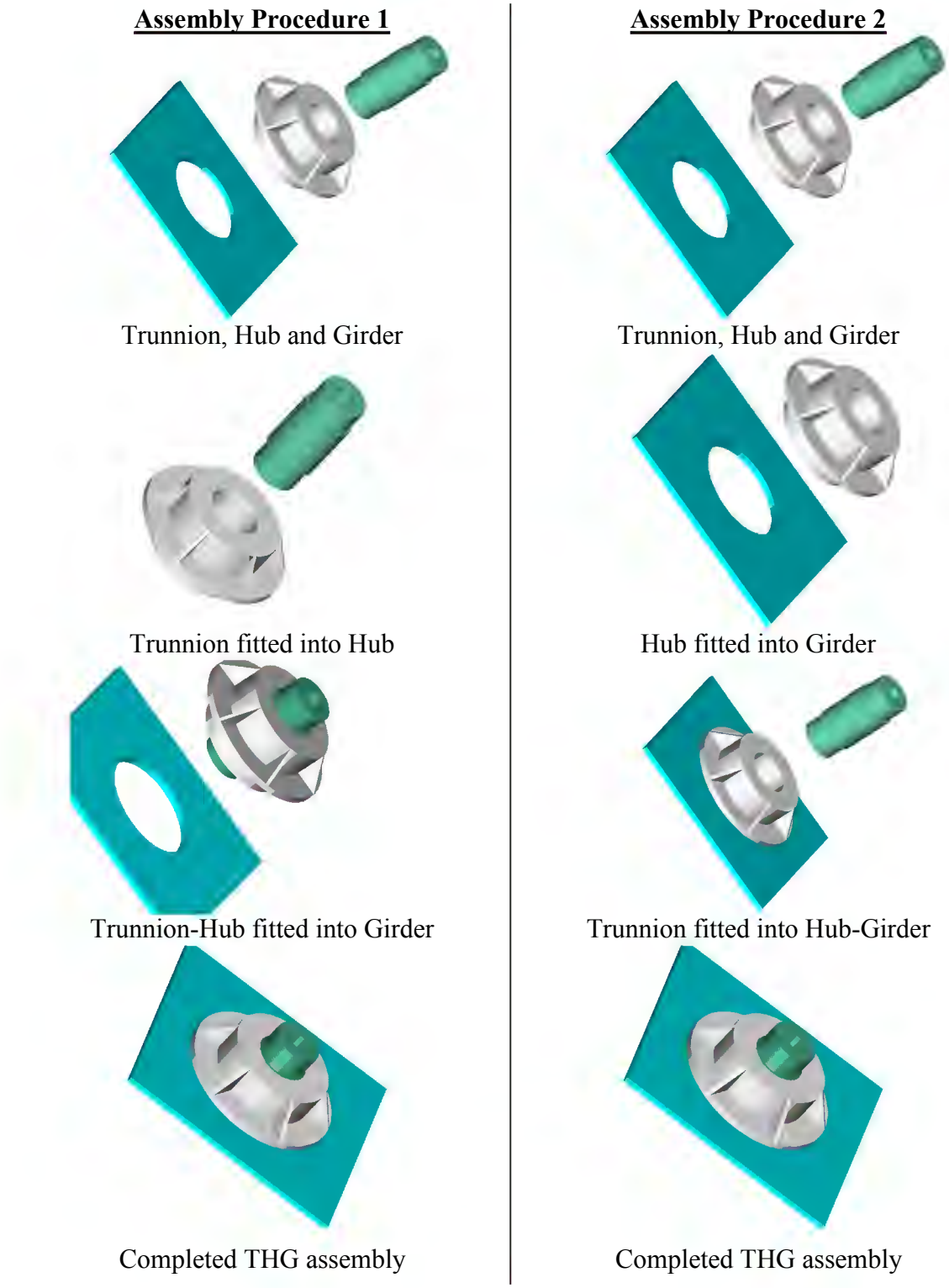

Figure 1.4 Two different assembly procedures.

During either of these assembly procedures, the trunnion, hub and girder develop both structural stresses and thermal stresses. The structural stresses arise due to

interference fits between the trunnion-hub and the hub-girder. The thermal stresses are a result of a temperature gradients within the component. These temperature gradients comes into play when either the trunnion or the hub is immersed in liquid nitrogen or when a cold trunnion is inserted into the hub, which is at room temperature. The term "Transient Stress" will be used in this study to mean stresses during the assembly procedure. The term "Steady State Stress" will be used to mean the stresses in the trunnion, hub and girder at the end of the assembly procedure.

1.4 Objective

Mindful of the losses caused by the failures and eager to prevent their recurrence the Florida Department of Transportation decided to investigate the cause of failure in the THG assemblies. Some questions by the FDOT were as follows. Why were these failures taking place and only on a few of the many THG assemblies carried out in Florida? Why were they not happening on the same THG assemblies again? How can we avoid losses of hundreds of thousands dollars in material, labor and delay in replacing the cracked assemblies? Preliminary investigations done by independent consulting firms and the assembly manufacturers gave various reasons for the possible failure including high cooling rate, use of liquid nitrogen as a cooling medium, residual stresses in the castings and the assembly procedure itself.

FDOT officials wanted to carry out a complete numerical and experimental study to find out why the assemblies failed, how they could be avoided in the future and to develop clear specifications for the assembly procedure. So, in 1998, they provided a two-year $250,000 grant to the College of Engineering at the University of South Florida to investigate the problem.

1.5 Literature review

1.5.1 Transient thermal-structural stresses

This study is primarily focused on analyzing transient stresses and failures caused due to them. This broad scope encompasses topics such as temperature-dependent material properties, thermoelastic contact, thermal shock and fracture toughness. A brief history of previous work done in these areas and the relevance of each to this study is explained. Also, a justification for this study because of the limitations of the previous research efforts and unique requirements of this project is included.

Pourmohamadian and Sabbaghian (1985) modeled the transient stresses in a solid cylinder with temperature dependent material properties under an axisymmetric load. However, their model does not incorporate non-symmetric loading, complex geometries and thermoelastic contact, all of which are present in the THG assembly.

The trunnion-hub interface and the hub-girder interface are in thermoelastic contact. Attempts were made to model thermoelastic contact between two cylinders by Noda (1985). However, the models were only applicable for cylinders and not for non-standard geometries. Also, the issue of temperature-dependent material properties was not addressed in this study.

Takeuti and Noda (1980) studied transient stresses in a cylinder under nonaxisymmetric temperature distribution. This study is relevant to our research efforts due to complex geometry and temperature-dependent material properties of the THG assembly and being under nonaxisymmetric temperature distribution. However, the

issues of thermoelastic contact and complex geometries are not addressed in this study. Noda also modeled a transient thermoelastic contact problem with a position dependent heat transfer coefficient (1987) and transient thermoelastic stresses in a short length cylinder (1985). These efforts, although useful to understanding the thermoelastic modeling, did not address the issues of temperature dependent material properties and complex geometries.

Enumerated below are studies that aided us in the understanding the role of fracture toughness in the study. Thomas, et al. (1985) found the thermal stresses due to the sudden cooling of cylinder after heating due to convection. The results indicated the magnitude of stresses attained during the cooling phase increases with increasing duration of heating. Consequently, the duration of application of the convective load can be a factor influencing the maximum stresses attained in the assembly.

Parts of the THG assembly are subjected to thermal shock when they are cooled down before shrink fitting. Oliveira and Wu (1987) determined the fracture toughness for hollow cylinders subjected to stress gradients arising due to thermal shock. The results covered a wide range of cylinder geometries.

It is clear that the drawback of all previous studies of transient thermal stresses is their inability to deal with non-standard geometries. In addition, previous research efforts address some of the issues (for example, temperature dependent material properties, thermoelastic contact, nonaxisymmetric loading, and thermal shock) but never all of the issues. Our research efforts are concentrated less on isolating the effects of individual factors affecting the stresses in the THG assembly than on observing the interplay of assorted factors acting together. Hence, this study breaks new ground in the study of thermal stresses.

1.5.2 Cryogenic instrumentation

Many researchers have worked on experimental stress analysis under cryogenic temperatures. The principal issues regarding the use of strain gages at such temperatures are:

- Selecting an appropriate bonding agent to bond the gage onto the surface and the curing procedure of this particular bonding agent;
- Compensating for the thermal output of a strain gage due to temperature alone; and
- Moisture proofing the strain gage.

Moore (1997) outlined the application procedures for cryogenic strain gages. Various stages of the application procedure described in Moor (1997) are surface preparation, curing the adhesive M-Bond-610, wiring the gage, conducting initial electrical checks, apparent strain correction and moisture-proofing procedure.

Kowalkowski et al. (1998) discussed the output of a strain gage due to temperature, which is termed ‘Apparent Strain’. Strain gage thermal output (apparent strain) is described as one of the largest sources of error associated with the measurement of strain when temperatures vary. The thermal output of WK-type strain gages is experimentally determined for temperatures ranging from -450^0F to 230^0F.

Hare and Moore (2000) examined the possible service of a RTV (GE-167 Silicone Rubber) as a moisture barrier for cryogenic strain gages. The paper concluded that the RTV is not recommended for temperatures below -150^0 F. This ruled out its use in the

current study. So, a chloroprene rubber coating (N-1) was used for tests conducted in the current study.

Radebaugh and Marquardt (1993) reviewed various types of cryogenic instrumentation. Various sensors for a particular type of measurement were compared to aid in selection of the optimum type of sensor.

1.6 Studies on Trunnion-Hub-Girder Assemblies of Bascule Bridges

At the outset, it became apparent that isolating and pinpointing the causes of failure intuitively is difficult for three reasons. First, it was observed that cracks were formed in some bridge assemblies but not in others. Second, the cracks occurred in different parts of the hub for different bridges and at different loading times. Last, the problem involves an interplay of several issues, that is,

1. Complex geometries, such as, gussets on the hub, make it a 3-D elasticity and heat transfer problem.
2. Thermal-structural interaction, due to the cooling and warming of the THG components and the shrink fitting of these components, results in both thermal and mechanical stresses. In addition, conduction takes place along contact surfaces.
3. Temperature-dependent material properties, such as, coefficient of thermal expansion, specific heat, thermal conductivity, yield strength and fracture toughness, can be highly nonlinear functions of temperature.

Hence, an intuitive analysis is not merely difficult but intractable, so three studies were conducted.

1.6.1 Study 1 – Design tools for trunnion-hub-girder assemblies of bascule bridges

The first study conducted for the grant by Denninger (2000) to find steady state stresses in the THG assembly showed that these stresses are well below the ultimate tensile strength and yield strength of the materials used in the assembly. Hence, these stresses could not have caused the failure. The first study concluded that the transient stresses needed to be investigated since they could be more than the allowable stresses. The stresses during the assembly process come from two sources – thermal stresses due to temperature gradients, and mechanical stresses due to interference at the trunnion-hub and hub-girder interfaces.

Are these transient stresses more than the allowable stresses? Since fracture toughness values decrease with a decrease in temperature, do these transient stresses make the assembly prone to fracture? These are some of the questions to be answered.

1.6.2 Study 2 – Parametric finite element modeling of trunnion-hub-girder assemblies of bascule bridges

The second study for the grant (also called Phase I) was conducted by Ratnam (2000) to find both the transient and steady state stresses developed during the assembly process. This study employed the method of finite element analysis to determine these stresses. ANSYS was used for the finite element analysis. The finite element approach was most suitable because it could handle the interplay of complex geometries, coupled thermal and structural fields, and temperature dependent properties. This study used critical crack length and hoop stress, for comparing the two assembly procedures. Using

a parametric model, transient stresses in the two alternative assembly procedures for different bridges were compared with the aid of time-history plots of temperature and stress.

This study hypothesized that in AP1, a combination of high hoop stress and low temperature result in smaller values of critical crack length, possibly leading to crack development and growth. In AP2, stresses due to interference never occur together with the thermal stresses during the cooling process, resulting in larger values of critical crack length, thereby reducing the probability of crack development and growth. It concluded that the results of the finite element analysis broadly agreed with the hypothesis. It also stated that every bridge was different and needed to be analyzed separately.

1.6.3 Study 3 – Full-scale testing of trunnion-hub-girder assemblies of bascule bridges

The earlier two studies (Denninger (2000) and Ratnam (2000)) had provided theoretical estimates of steady state and transient stresses. Also, the second study had presented a comparison of the stresses in the two assembly procedures. The theoretical values of stresses, from these two studies needed to be validated against experimental values of stresses obtained from full-scale models. This formed the basis of the third study that was to experimentally determine transient and steady state stresses and temperatures during both assembly procedures.

1.7 Overview

Chapter 1 - 'Background' describes the history, objectives and literature review among other topics.

Chapter 2 - 'Technical Details' describes the geometry of the THG assembly and the two different assembly procedures.

Chapter 3 - 'Numerical Modeling and Material Properties' describes the modeling approach and assumptions used. Particular emphasis is given to the interaction between the thermal and structural fields. The nonlinear material properties of the steel used in the THG assembly, and the thermal properties of air and liquid nitrogen are also discussed.

Chapter 4 - 'Summary of Results for Parametric FEA (Phase I)' presents results for THG geometries of three bridges (that is, Christa McAuliffe Bridge, 17th Street Causeway Bridge, and Hillsborough Avenue Bridge) using both assembly procedures, AP1 and AP2. The temperature, critical crack length and hoop stress are used as parameters for comparison between different assembly procedures and different bridges.

Chapter 5 - 'Experimental Set-up' describes the components of the experimental set-up. Details of the data acquisition system and the LabVIEW program are covered in this chapter. This chapter also discusses the selection process of the particular type of thermocouples and strain gages that were used in this study.

Chapter 6 - 'Experimental Quarter-Scale Model' discusses a preliminary THG assembly using a quarter-scale model. Also, a summary of the comparison of the results obtained from the quarter-scale model to those predicted by the finite element analysis is given in this chapter.

Chapter 7 - 'Experimental Full-Scale Models' describes the full-scale testing of the THG assembly. It discusses the two assembly procedures carried out on two nearly identical sets of trunnion, hub and girder. Results of each step of both assembly procedures are discussed.

Chapter 8 - 'Summary of Results for Full-Scale Testing (Phase II)' presents experimental and FEA comparisons of the two assembly procedures, based on criterion of hoop stress, critical crack length and Von-Mises stresses.

Chapter 9 - 'Conclusions and Recommendations' summarizes the conclusions based on the comparisons made in Chapters 4 and 8 and provides recommendations for future work.

Appendix A - 'Trunnion-Hub-Girder Design Tools' presents a program for calculating bridge loading and interference stresses due to a specified interference or a specified fit.

Appendix B - 'User Manual' presents a technical manual to show how a design engineer can use the ANSYS software to find transient stresses for any existing or new THG assembly.

Appendix C - 'Verification Examples' presents numerous experiments conducted to verify the strain and temperature acquisition in a liquid nitrogen environment.

Appendix D - 'X-ray Report' presents the x-ray report of the hub done by an independent consulting company and pictures of the x-rays.

Appendix E - 'Web Site' presents the web site where all of the information pertaining to this research project can be obtained.

CHAPTER 2

TECHNICAL DETAILS

2.1 Introduction

The technical and mathematical aspects of this study are described in this chapter. The objective of this chapter is to define the scope, specifications and details of the phenomena modeled in the parametric finite element model. The subsequent chapter describes how these requirements are met. The existing assembly procedure, AP1 results in crack formation in the hub of some of the bridges. An alternative assembly procedure, AP2 is suggested that can possibly rectify some, if not all the problems associated with the assembly procedure, AP1.

2.2 Geometry of the trunnion-hub-girder assembly

Figures 2.1a and 2.1b, 2.2a and 2.2b, and 2.3a and 2.3b show the geometries of the trunnion, hub and girder, respectively. The interference between the trunnion-hub and the hub-girder is determined by the Bascule Bridge Design Tools (Denninger 2000) for FN2 and FN3 fits.

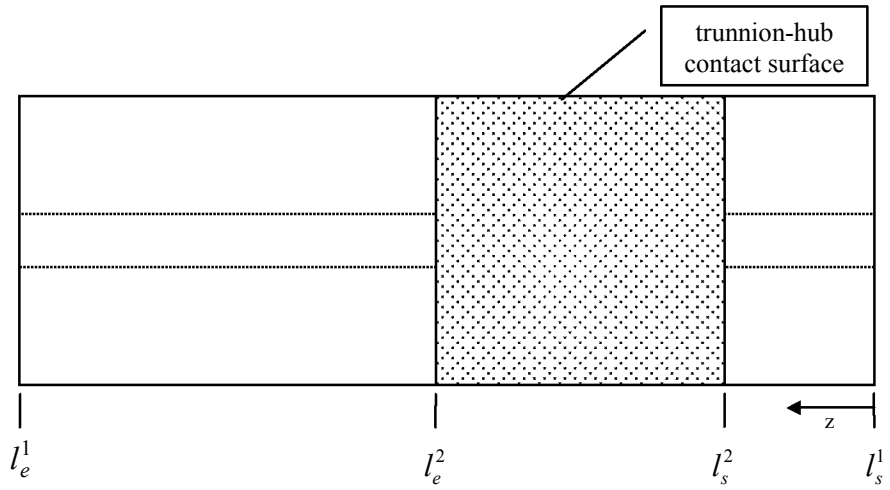

Figure 2.1a Trunnion coordinates (side view).

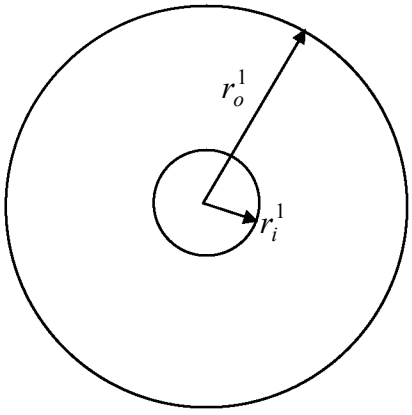

Figure 2.1b Trunnion coordinates (front view).

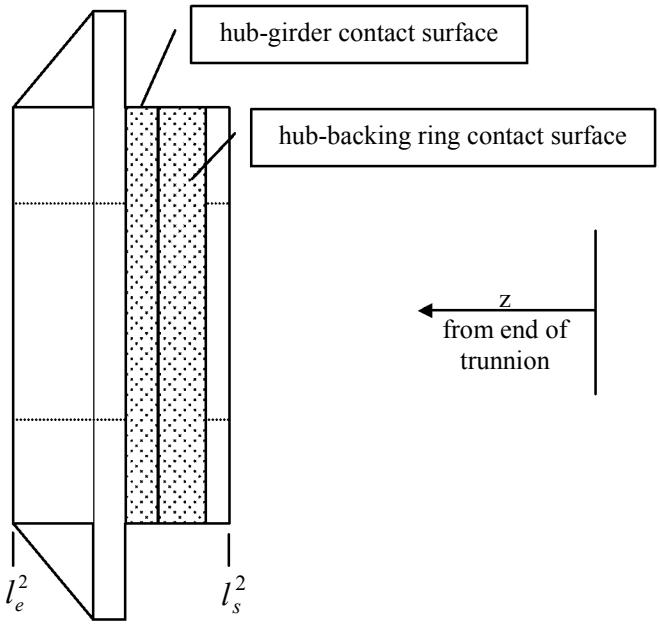

Figure 2.2a Hub coordinates (side view).

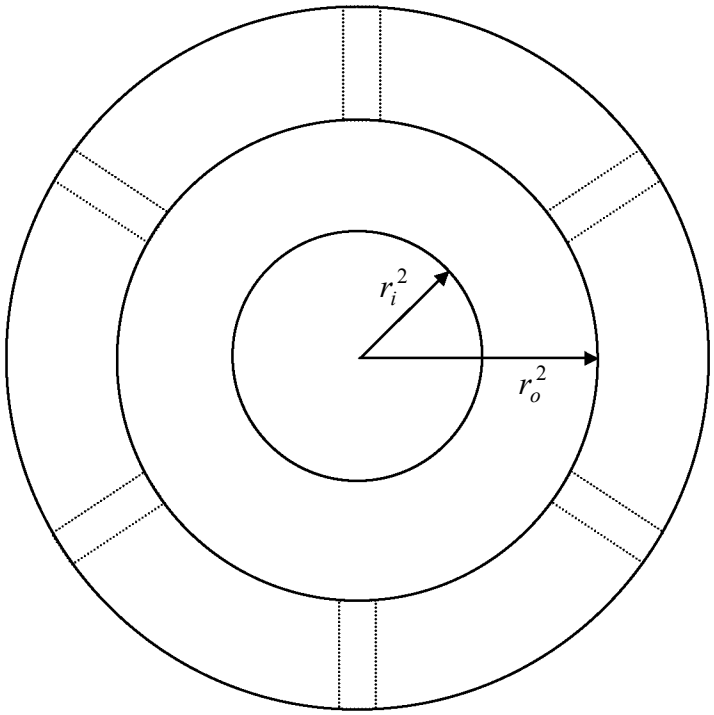

Figure 2.2b Hub coordinates (front view).

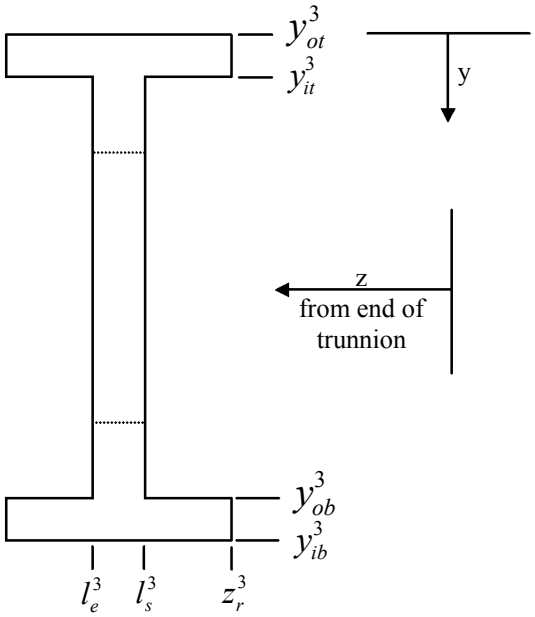

Figure 2.3a Girder coordinates (side view).

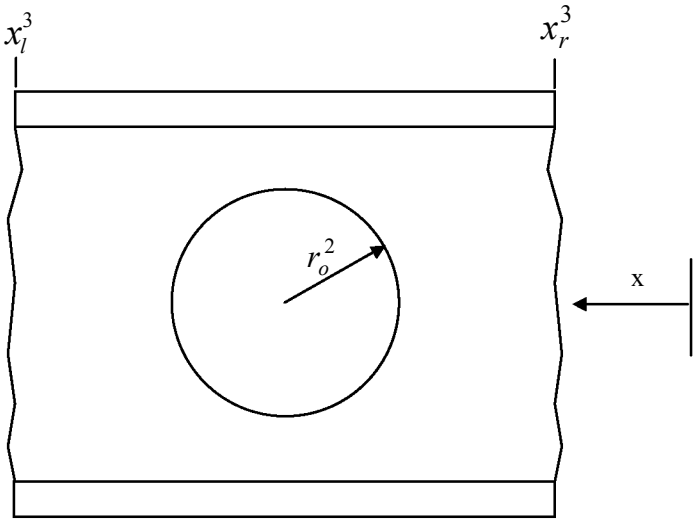

Figure 2.3b Girder coordinates (front view).

2.3 Assembly procedures

Two assembly procedures are studied in this work.

2.3.1 Assembly procedure 1 (AP1)

The present assembly procedure involves the following four steps.

Step 1. The trunnion is shrunk by cooling in liquid nitrogen.

Step 2. This shrunk trunnion is then inserted into the hub and allowed to warm up to ambient temperature to develop an interference fit on the trunnion-hub interface.

Step 3. The resulting trunnion-hub assembly is shrunk by cooling in liquid nitrogen.

Step 4. This shrunk trunnion-hub assembly is then inserted into the girder and allowed to warm up to ambient temperature to develop an interference fit on the hub-girder interface.

2.3.2 Assembly procedure 2 (AP2)

An alternative assembly procedure involves the following four steps.

Step 1. The hub is shrunk by cooling in liquid nitrogen.

Step 2. This shrunk hub is then inserted into the girder and allowed to warm up to ambient temperature to develop an interference fit on the hub-girder interface.

Step 3. The trunnion is shrunk by cooling in liquid nitrogen.

Step 4. This shrunk trunnion is then inserted into the hub-girder assembly and allowed to warm up to ambient temperature to develop an interference fit on the trunnion-hub interface.

CHAPTER 3

NUMERICAL MODELING AND MATERIAL PROPERTIES

3.1 Introduction

An understanding of the modeling approach is necessary to appreciate the validity of the results, inherent assumptions, and consequential limitations of the parametric model. Some problems associated with the Finite Element Modeling (FEM) of thermo-structural analysis and their resolution using some non-conventional approaches are described.

Assumptions made in the model are justified based on the physics of the problem, computational time versus accuracy trade-off, limitations of finite element method, and need for simplicity. Nonlinear material properties for steel, air, and liquid nitrogen are plotted at the end of this chapter.

3.2 Coupled field analysis

Coupled field analysis involves an interaction of two or more types of phenomena. This study involves the coupling of the thermal and structural fields. ANSYS features two types of coupled field analysis: direct and indirect.

3.2.1 Direct coupled field analysis

In direct coupled field analysis, degrees of freedom of multiple fields are calculated simultaneously. This method is used when the responses of the two phenomena are dependent upon each other, and is computationally more intensive.

3.2.2 Indirect coupled field (sequential coupled field analysis)

In this method, the results of one analysis are used as the loads of the following analysis. This method is used where there is one-way interaction between the two fields.

3.3 Design of the model

The sequential coupled field method described above is chosen as the approach best suited to our requirements. The underlying assumption is that the structural results are dependent upon the thermal results, but not vice-versa. This assumption is valid for the requirements of our study. Typically, this involves performing the entire thermal analysis, and subsequently transferring the thermal nodal temperatures to the structural analysis. However, our problem requires some modifications to the pure form of this approach as interaction between the two fields (thermal and structural) is required to determine the time of contact between parts of the assembly during the process of shrink-fitting. This is achieved using a non-conventional approach.

First, the thermal analysis of the cooling down of part(s) to steady state is performed. Subsequently, the structural analysis is performed to determine the time when the interference between the two parts of the assembly is breached. These parameters are used in the complete thermal analysis to switch thermal and structural contact ‘on’ and ‘off’. That is, to determine whether conductance is taking place between the parts of the assembly. The minimum temperature in the assembly during cooling down and the maximum temperature during warming up process are monitored and the

program exits the process in question once it nears steady state. The modeling procedure is described in the Figure 3.1.

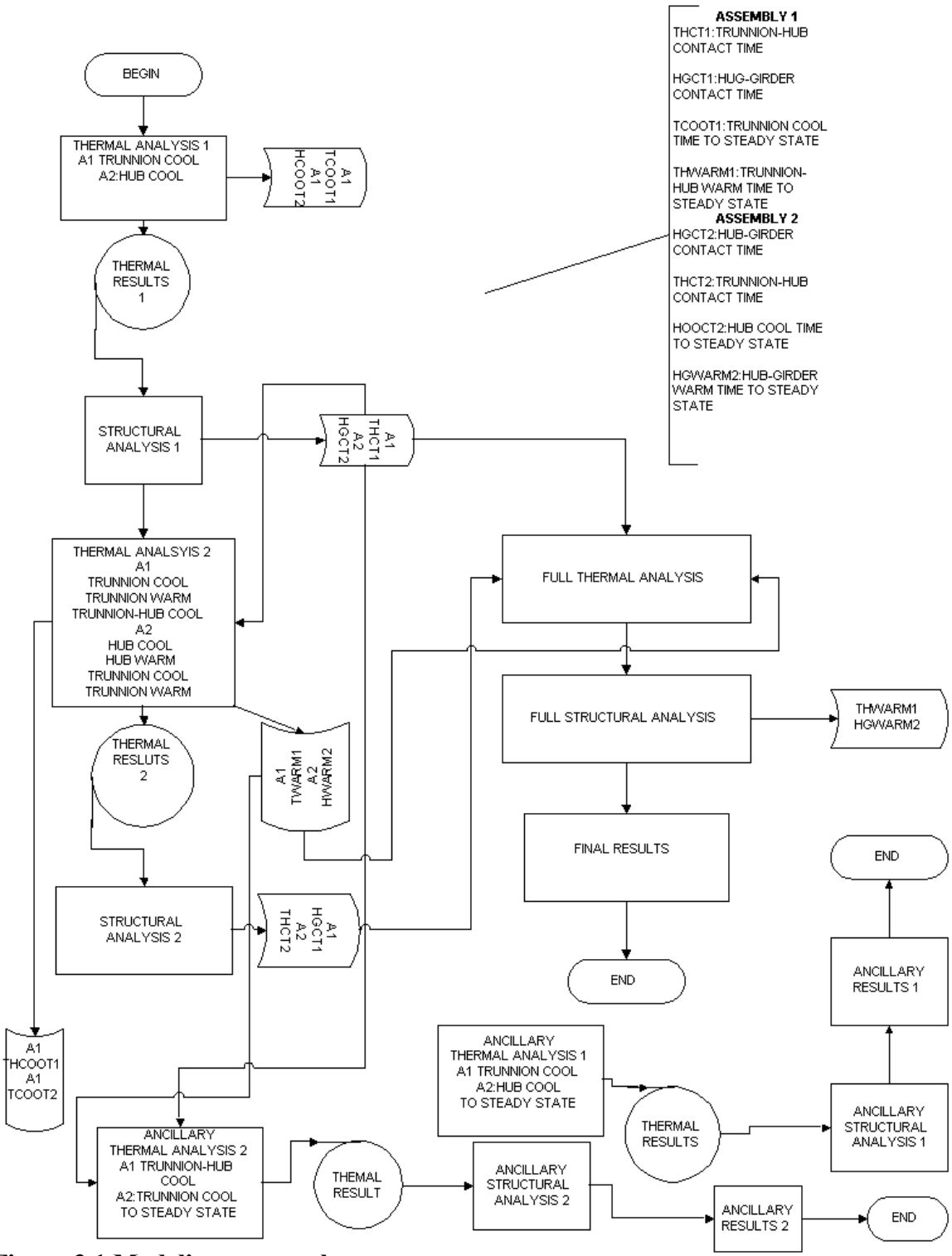

Figure 3.1 Modeling approach.

In this model, we perform multiple thermal and structural analysis to determine time parameters at which certain thermal and structural criteria are met. The thermal results obtained are transferred as nodal temperatures to the structural analysis.

These parameters are used to perform the complete thermal and structural analysis along with the ancillary cooling analyses. Segments of the flowchart shown in Figure 3.1 are explained next. The section headings explain the namesake process boxes in the flowchart.

3.3.1 Cooling process 1

The phenomena modeled are: AP1 - Cooling down of the trunnion and AP2 - Cooling down of the hub

3.3.1.1 Process box-thermal analysis 1

The cooling process is performed till the user defined exit criterion for the cooling process (see Appendix B.3.5.2) is met.

Parameters output for AP1

tcoot1 - time at which the user defined exit criterion (see Appendix B.3.5.2) is met during the cooling down of the trunnion.

Parameters output for AP2

hcoot2 - time at which the user defined exit criterion (see Appendix B.3.5.2) is met during the cooling down of the hub.

3.3.1.2 Process box-structural analysis 1

The nodal temperatures from 'thermal analysis 1' are transferred to this analysis. The structural analysis is performed to determine the time at which the interference between the male and the female parts of the assembly is breached.

Parameters output for AP1

thct1 - time at which the interference between the trunnion and hub is breached during the cooling down of the trunnion.

Parameters output for AP2

hgct2 - time at which the interference between the hub and the girder is breached during the cooling down of the hub.

Note that thct2 and hgct2 determine the time at which the conduction between the two parts (trunnion-hub or hub-girder) of the assembly should be switched 'on' (see element COMBIN37 in Table 3.1).

3.3.2 Cooling process 2

The cooling down of the trunnion-hub in the case of AP1 and the cooling down of the trunnion in the case of AP2 is performed.

3.3.2.1 Process box-thermal analysis 2

The cooling process is performed till the user defined exit criterion is met. (see Appendix B.3.5.2).

Parameters input for AP1

thct1 - time at which the conduction between the trunnion and the hub is to switched 'on'. (see element COMBIN37 in Table 3.1). This parameter is obtained from 'structural analysis 1'.

Parameters input for AP2

hgct2 - determines the time at which the conduction between the hub and the girder is to switched 'on' (see element COMBIN37 in Table 3.1). This parameter is obtained from 'structural analysis 1'.

These parameters are used to perform the thermal analysis of the second cooling process until the user defined exit criterion is met (see Appendix B.3.5.2).

Parameters output for AP1

thcoot1 - time at which the trunnion-hub assembly meets the user defined exit criterion (see Appendix B.3.5.2) during the cooling process.

twarm1 - time at which the trunnion-hub assembly meets the user defined exit criterion (see Appendix B.3.5.2) during the warming up of the trunnion.

Parameters output for AP2

tcoot2 - the time at which the user defined exit criterion (see Appendix B.3.5.2) during the cooling down of the trunnion is met.

hwarm2 - the time at which the user defined exit criterion (see Appendix B.3.5.2) during the warming up of the hub is met.

3.3.2.2 Process box-structural analysis 2

The nodal temperatures from 'thermal analysis 2' are transferred to this analysis. The structural analysis is performed to determine the time at which the interference between the two parts of the assembly is breached.

Parameters output for AP1

hgct1 - time at which the interference between the trunnion-hub and the girder is breached.

Parameters output for AP2

thct2 - time at which the interference between the trunnion and the hub-girder assembly is breached.

3.3.3 Complete analysis

Parameters obtained from previous thermal and structural analysis are used to perform the complete thermal and structural analysis.

3.3.3.1 Process box-full thermal analysis

Parameters input for AP1

thct1 - see previous sections

hgct1 - see previous sections

twarm1 - see previous sections

Parameters input for AP2

hgct2 - see previous sections

thct2 - see previous sections

hwarm2 - see previous sections

Parameters output for AP1

thwarm1 - the time at which the THG assembly meets the user defined exit criterion when the trunnion-hub assembly is fitted into the girder (see Appendix B.3.5.2).

Parameters output for AP2

twarm2 - the time at which the THG assembly meets the user defined exit criterion when the trunnion is fitted into the hub-girder assembly (see Appendix B.3.5.2).

3.3.3.2 Process box-full structural analysis

The nodal temperatures from 'full thermal analysis' are transferred to this analysis. The complete structural analysis is performed for both the assembly procedures.

3.3.4 Ancillary analysis

The stand alone cooling down processes are performed.

3.3.4.1 Ancillary cooling 1

The following cooling process in performed: for AP1 - cooling down of the trunnion, and for AP2 - cooling down of the hub.

3.3.4.2 Ancillary cooling 2

The following cooling process is performed: for AP1 - cooling down of the trunnion-hub, and for AP2 - cooling down of the trunnion

Parameters input for AP1

thct1 - time of contact between the trunnion and the hub (see Appendix B.3.5.2). This parameter is obtained from 'structural analysis 1'.

twarm1 - time at which the trunnion-hub assembly fulfills user defined exit criterion (see Appendix B.3.5.2) during the insertion of the trunnion into the hub.

Parameters input for AP2

hgct2 - time of contact between the hub and the girder. This parameter is obtained from 'structural analysis 1'.

hwarm2 - time at which the hub-girder assembly fulfills user defined exit criterion during the insertion of the hub into the girder.

3.4 The finite element model

Table 3.1 describes the types of element used in the model with a brief description of each. The structural and thermal element meshes for the THG assembly are shown in Figure 3.2a (brick elements) and Figure 3.2b (shell elements). Note that the sequential coupled field analysis requires separate elements to be defined for both the thermal and structural analysis. Hence, Figure3.2a and Figure 3.2b plot both the thermal and the structural elements at the same time. The shell elements used to plot the gussets are shown in Figure 3.2b. Figure 3.2c plots the contact and target elements and Figure 3.2d plots the combination elements.

Table 3.1 Element characteristics.

FIELD	ELEMENT NAME	DESCRIPTION
Thermal	SOLID70	• 3-D 8 node thermal brick element • Option to evaluate the convection coefficient as a function of wall temperature. • Thermal analogue of SOLID45
	SHELL57	• Three dimensional thermal shell element • Used to mesh the gussets
Structural	SOLID45	• 3-D 8 node structural element • Structural analogue of SOLID70
	SHELL63	• Three dimensional structural shell element • Used to mesh the gusset
Contact	CONTACT174	• 3-D surface-to-surface structural contact. • Used to model structural contact between trunnion-hub and hub girder
	TARGET170	• Target element for CONTACT174. • Used to model structural contact between the hub and the girder
Combination	COMBIN37	• Used to create thermal contact between trunnion-hub and hub-girder • Allows thermal contact to be 'switched on' and 'switched off' based on the time parameter

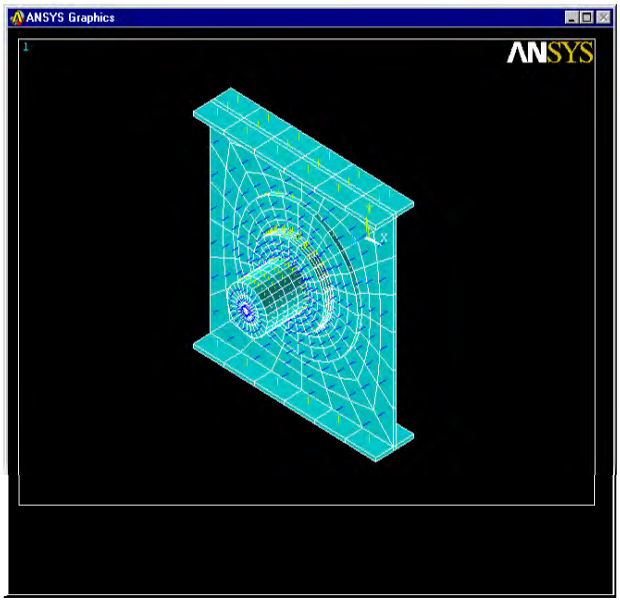

Figure 3.2a Thermal element SOLID70 and structural element SOLID45.

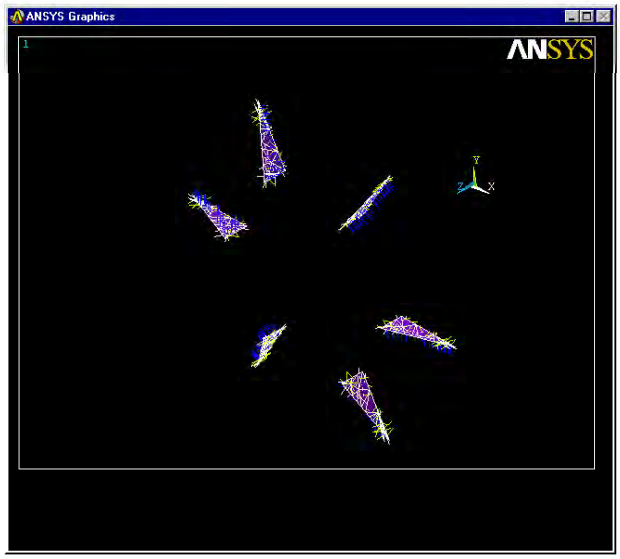

Figure 3.2b Thermal element SHELL57 and structural element SHELL63.

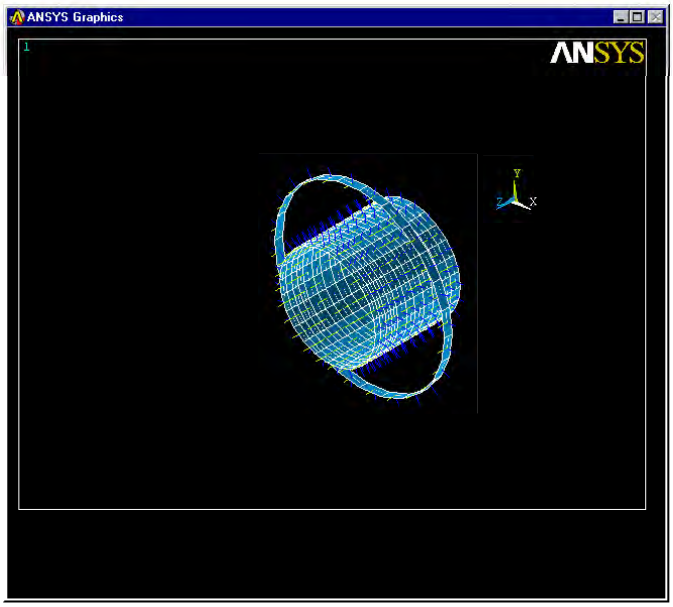

Figure 3.2c Contact elements CONTACT174 and TARGET170.

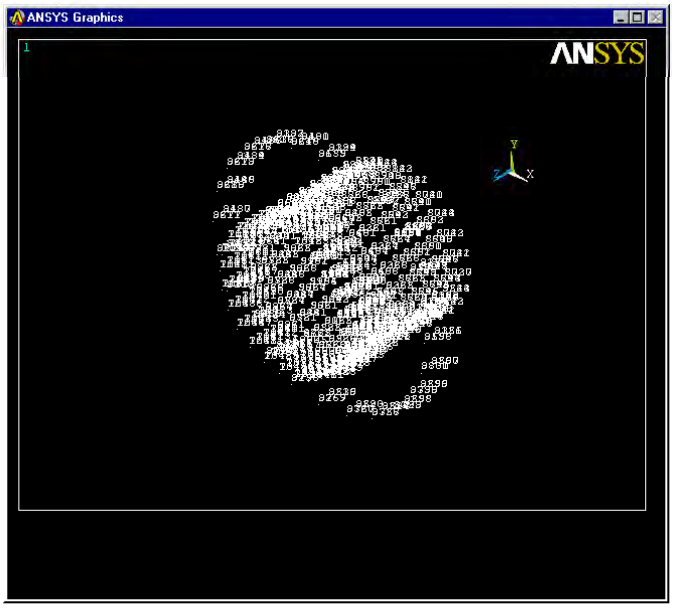

Figure 3.2d COMBIN37 elements.

3.5 Assumptions

3.5.1 Sequential coupled field approach

The assumption in this approach is that the structural results are dependent upon the thermal results but not vice-versa. This is a fair assumption as the effect of strains on the thermal analysis is negligible.

3.5.2 Convection coefficient

The assumptions in the calculation of the convective heat transfer coefficient for air are:

1. The geometry of the assemblies is assumed to cylindrical. To obtain the convective heat transfer coefficient, the Grashoff's number (Gr), Prandtl number (Pr), and the Nusselt number (Nu) are required. The equations to obtain these quantities are discussed next. Grashoff's number is defined by Ozisik (1977) as

$$Gr = \frac{g\beta(T_w - T_\infty)D^3}{\nu^3} \tag{3.1a}$$

where

g = acceleration due to gravity,
β = volume coefficient of thermal expansion,
T_w = wall temperature,
T_∞ = ambient temperature,
D = diameter of cylinder, and
ν = kinematic viscosity.

The Prandtl number, Pr is defined by Ozisik (1977) as

$$\Pr = \frac{c_p \mu}{k} \tag{3.1b}$$

where

c_p = specific heat,
μ = absolute viscosity, and
k = coefficient of thermal conductivity.

The Nusselt's number, Nu is defined by the following equation (Ozisik, 1977).

$$Nu = 0.53(Gr\,\Pr)^{1/3}. \tag{3.1c}$$

The convective heat transfer coefficient, h_m is also obtained from Ozisik (1977) as

$$h_m = \frac{kNu}{D}. \tag{3.1d}$$

2. The value for the hydraulic diameter, D, for the trunnion is the outer diameter of the trunnion; for the hub, it is the hub outer diameter; and for the girder, it is the length of the girder.
3. Turbulent flow is assumed.
4. The convection coefficient is assumed to be dependent on the wall, temperature and the bulk or ambient temperature.

The convection coefficient for air is plotted later in this chapter. Note that the value for the convective heat transfer coefficient is not a function of the hydraulic diameter. Hence, the convective coefficient is independent of the bridge geometry.

3.5.3 Time increments and contact point

The minimum time increment in this model is one minute. Hence, the degree of accuracy of our time of contact between parts of the assembly is less than one minute.

3.5.4 Finite element method assumptions

The standard inaccuracies associated with any finite element model due to mesh density, time increments, number of substeps, etc. are present in this model (Logan, 1996).

3.5.5 Material properties

The material properties of the THG assembly, the air, and the cooling medium are temperature dependent and are evaluated at specified temperature increments. The properties in between or outside the extremes of these values are interpolated and extrapolated, respectively.

3.6 Nonlinear material properties of metal

The nonlinear material properties for a typical steel - Fe - 2.25 Ni (ASTM A203-A) are plotted in the next several pages. Though nonlinear material properties in general are explored, particular emphasis is given to properties at low temperatures.

3.6.1 Young's modulus

The elastic modulus of all metals increases monotonically with increase in temperature. The elastic modulus E_T can be fitted into a semi-empirical relationship:

$$E_T = E_o - \frac{S}{[\exp(T_e / T) - 1]} \tag{3.2}$$

where

E_0 = elastic constant at absolute zero,
S = constant, and
T_e = Einstein characteristic temperature.

The Young's modulus remains stable with change in temperature (see Figure 3.3) and hence is assumed to remain constant throughout this analysis.

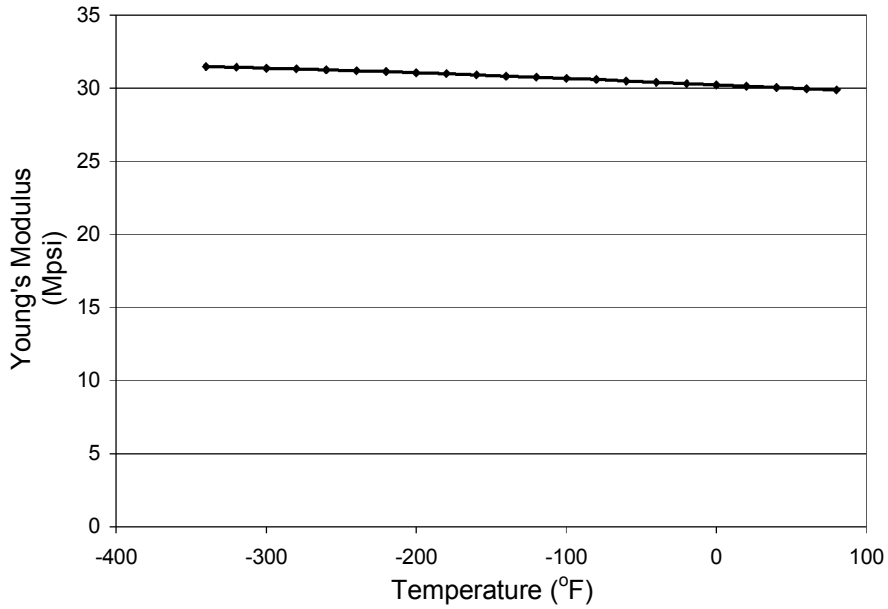

Figure 3.3 Young's modulus of steel as a function of temperature.

3.6.2 Coefficient of thermal expansion

The coefficient of thermal expansion at different temperatures is determined principally by thermodynamic relationships with refinements accounting for lattice vibration and electronic factors. The electronic component of coefficient of thermal expansion becomes significant at low temperatures in cubic transition metals like iron (Reed, 1983). The coefficient of thermal expansion increases with increase in temperature by a factor of three from -321^0F to 80^0F as shown in the Figure 3.4.

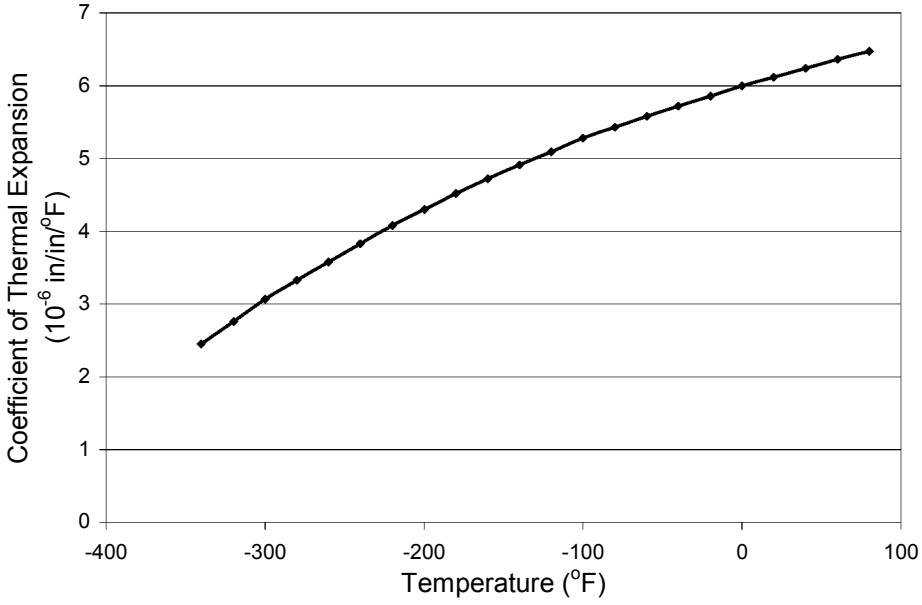

Figure 3.4 Coefficient of thermal expansion of steel as a function of temperature.

3.6.3 Thermal conductivity

The coefficient of thermal conductivity (see Figure 3.5) increases with an increase in temperature by a factor of two from -321^0F to 80^0F. Thermal conduction takes place via electrons, which is limited by lattice imperfections and phonons. In alloys, the defect scattering effect ($\propto T$) is more significant than the phonon scattering effect ($\propto T^{-2}$) (Reed, 1983).

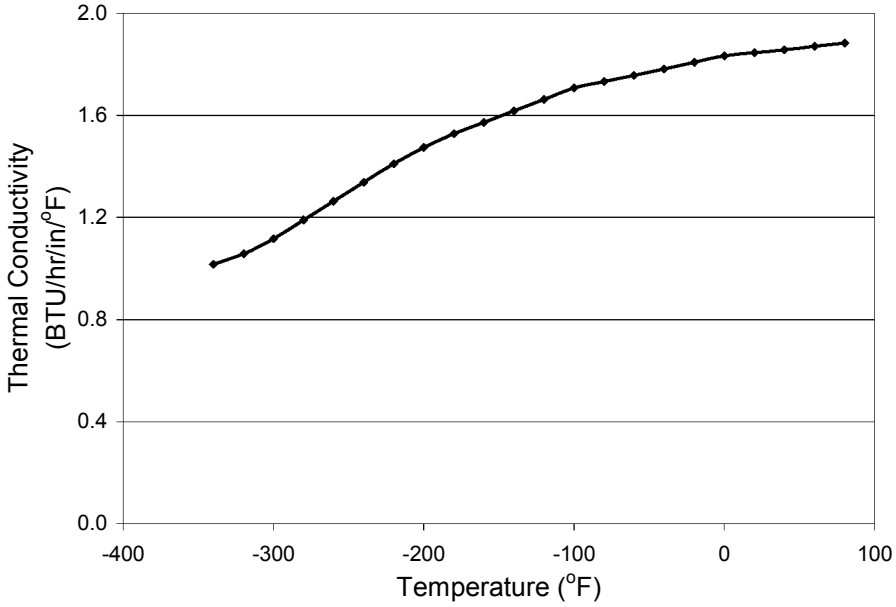

Figure 3.5 Thermal conductivity of steel as a function of temperature.

3.6.4 Density

For the range of temperatures of interest to our study the density remains nearly constant, as shown in Figure 3.6.

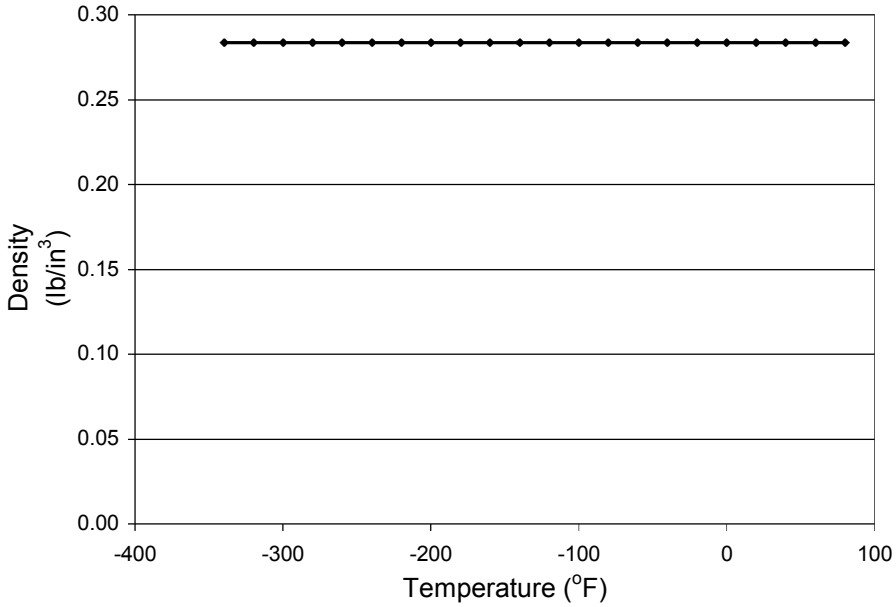

Figure 3.6 Density of steel as a function of temperature.

3.6.5 Specific heat

Lattice vibrations and electronic effects affect the specific heat of a material. The contribution of two effects can be shown by

$$C = \beta T^3 + \gamma T \tag{3.3}$$

where,

βT^3 = lattice contribution,

β = volume coefficient of thermal expansion,

γT = electronic contribution, and

γ = normal electronic specific heat.

Note that specific heat decreases by a factor of five over the temperature range in question, as shown in Figure 3.7.

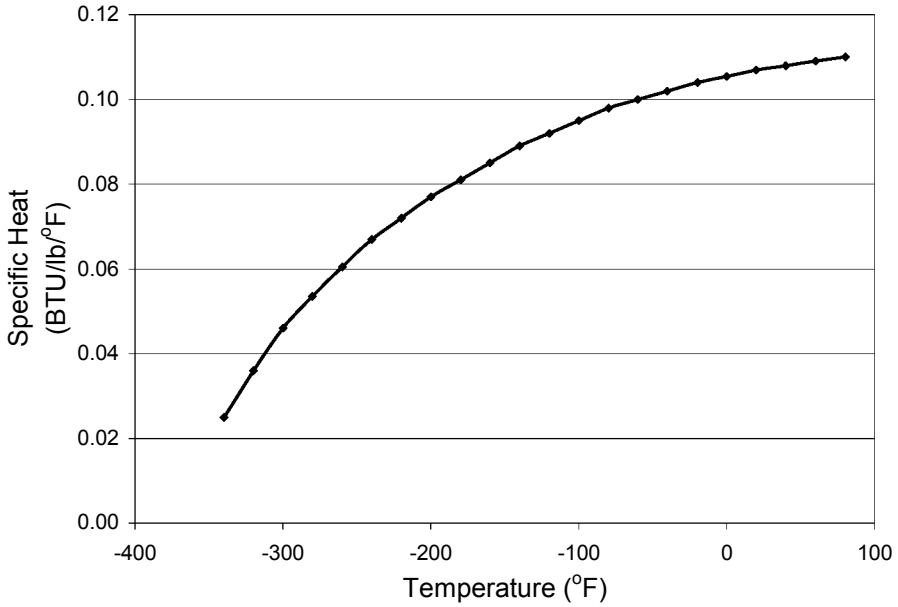

Figure 3.7 Specific heat of steel as a function of temperature.

3.7 Nonlinear material properties of air and liquid nitrogen

The temperature dependent convective heat transfer coefficients for air and liquid nitrogen are plotted next.

3.7.1 Convection to air at 80^0F

The convective heat transfer coefficient is a function of the volume coefficient of thermal expansion (β), the thermal conductivity (k), absolute viscosity (μ), kinematic viscosity (ν), specific heat (c_p) and mass density (ρ) all of which are temperature dependent. The Grashof number, the Nusselt number and the Prandtl number and ultimately the convective heat transfer coefficient can be calculated from these quantities from Equations (3.1a) through (3.1d). The variation of each with temperature is plotted in Figure 3.8a through Figure 3.8f.

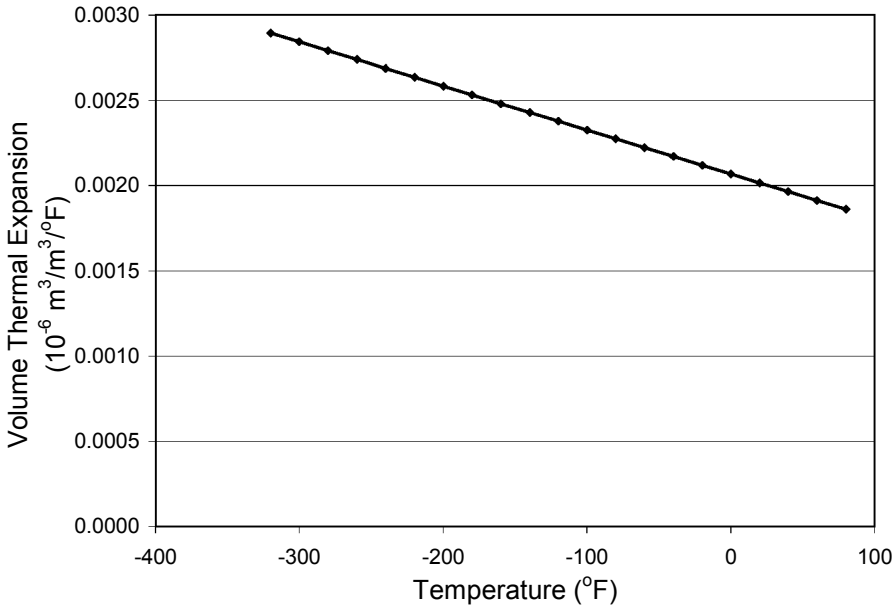

Figure 3.8a Volume coefficient of thermal expansion of air as a function of temperature.

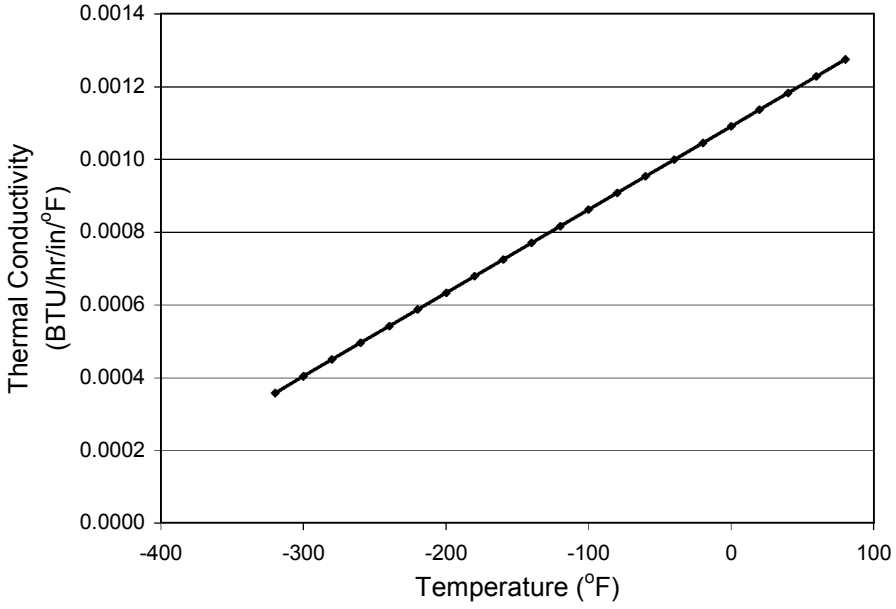

Figure 3.8b Thermal conductivity of air as a function of temperature.

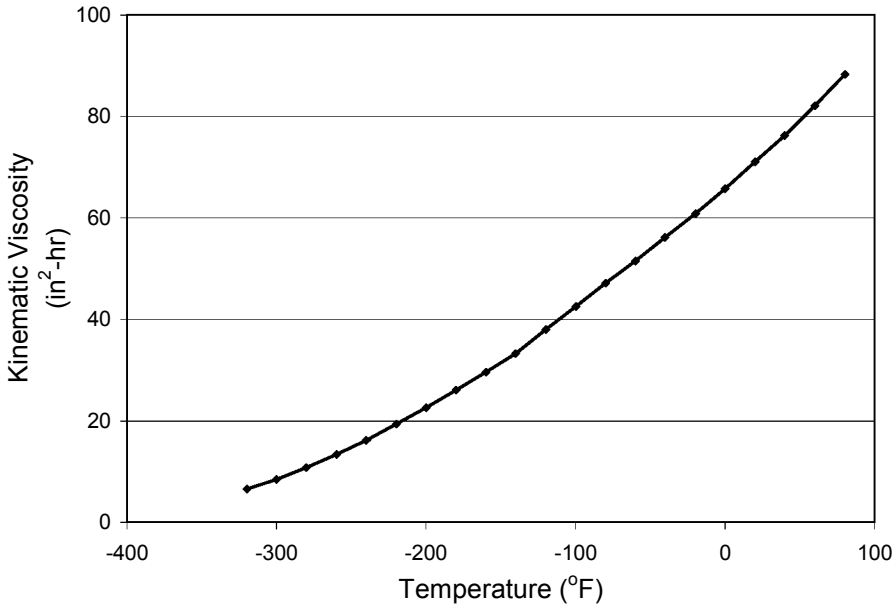

Figure 3.8c Kinematic viscosity of air as a function of temperature.

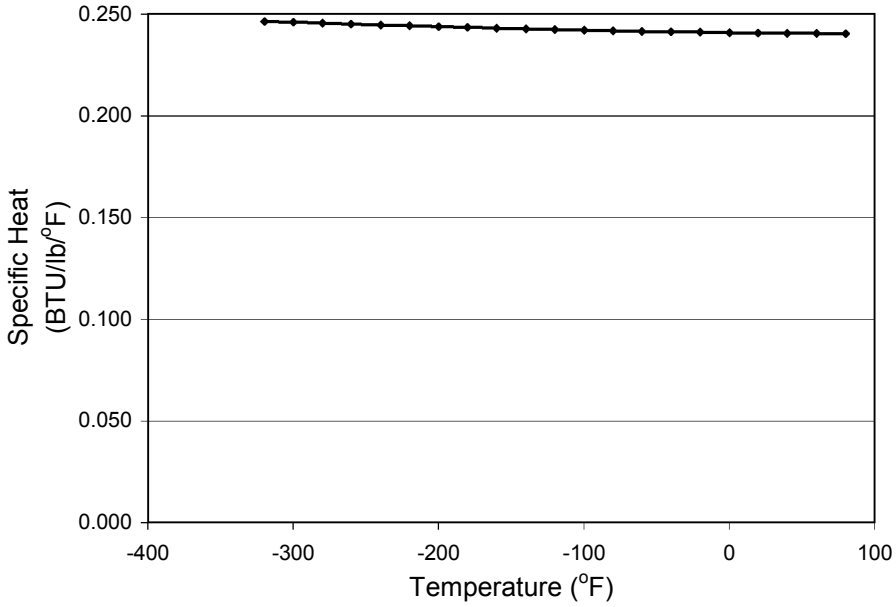

Figure 3.8d Specific heat of air as a function of temperature.

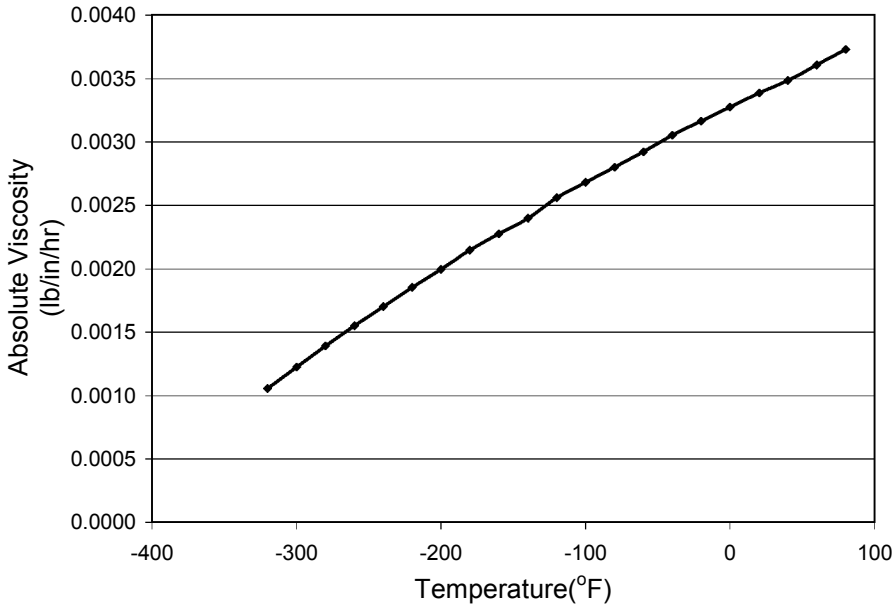

Figure 3.8e Absolute viscosity of air as a function of temperature.

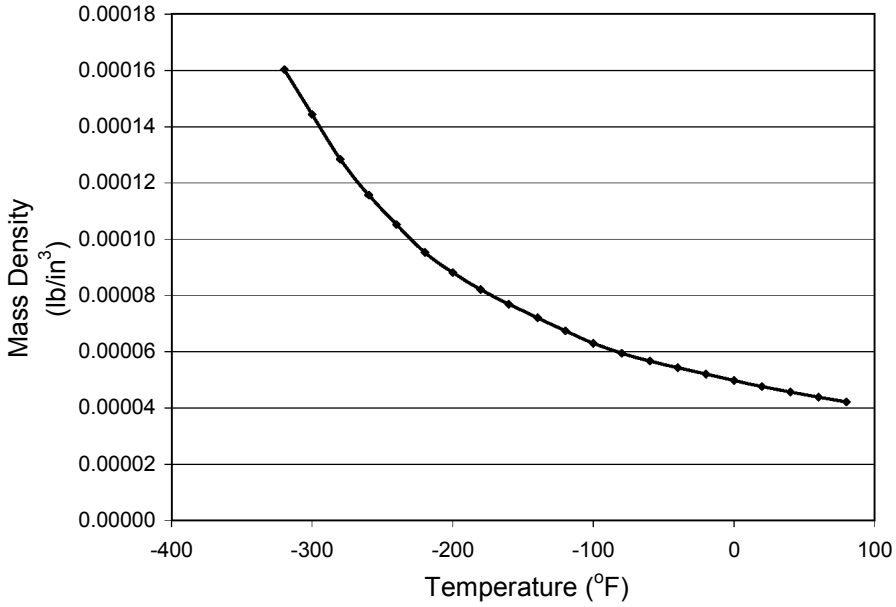

Figure 3.8f Mass density of air as a function of temperature.

The convective heat transfer coefficient for air, based upon the previous five graphs (see Figures 3.8b through 3.8f) and Equations (3.1), is shown in Figure 3.8g. Note that the convective heat transfer coefficient for convection to air is evaluated at the film temperature (that is, the average of the bulk and the wall temperatures).

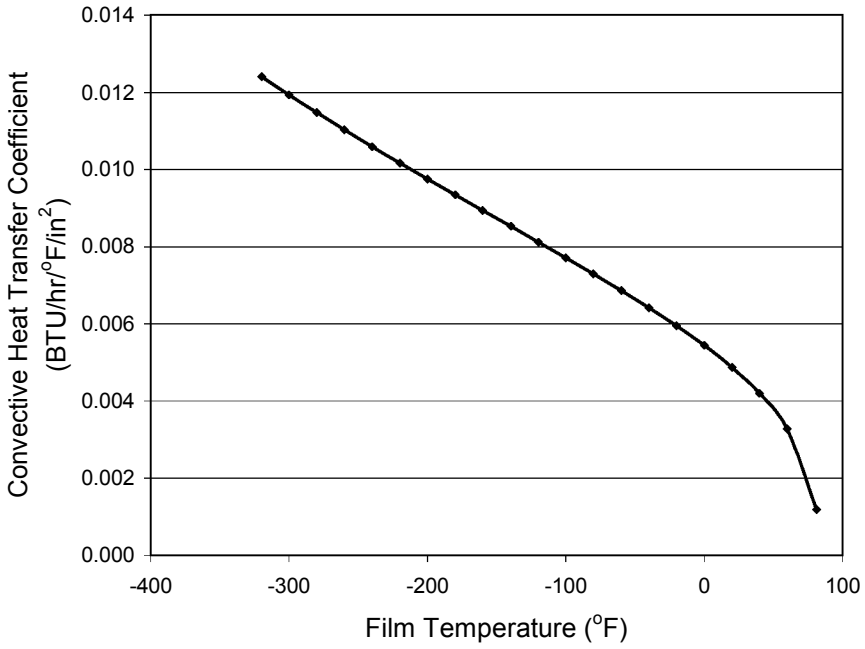

Figure 3.8g Convective heat transfer coefficient of air as a function of temperature.

3.7.2 Convection to liquid nitrogen at -321^0F

The phenomenon of convection to liquid nitrogen is quite complex and involves multi-phase heat transfer. Whenever an object at ambient temperature (that is, 80^0F) comes into contact with liquid nitrogen "film boiling" occurs until the temperature of the object reaches approximately -260^0F. This phenomenon of film boiling occurs when there is a large temperature difference between the cooling surface and the boiling fliud. At the point when film boiling stops, the minimum heat flux occurs and the phenomenon of "transition boiling" occurs until the temperature of the object reaches -290^0F. At the point when transition boiling stops, the maximum heat flux occurs and the phenomenon of "nucleate boiling" occurs until the temperature of the object reaches the temperature of liquid nitrogen. Nucleate boiling occurs when small bubbles are formed at various nucleation sites on the cooling surface. When nucleate boiling starts the object cools very rapidly.

The convective heat transfer coefficient for convection to liquid nitrogen is dependent on many factors, such as, surface finish, size of the object and shape of the object, to name a few. Based on the previous discussion, the convective heat transfer coefficient for convection to liquid nitrogen is shown in Figure 3.9 (Brentari and Smith 1964). This data was chosen because it very closely matches the surface finish, and object sizes and shapes used for trunnions and hubs. Note that the convective heat transfer coefficient for convection to liquid nitrogen is evaluated at the wall temperature.

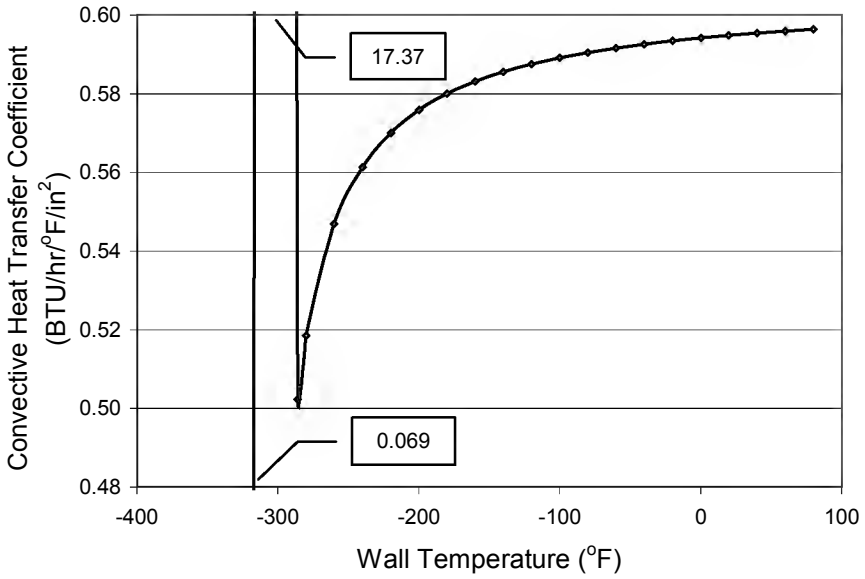

Figure 3.9 Convective heat transfer coefficient of liquid nitrogen as a function of temperature.

CHAPTER 4

SUMMARY OF RESULTS FOR PARAMETRIC FEA (PHASE I)

4.1 Introduction

The results of the study are presented in this chapter. Theories of failure based on fracture mechanics and yield stresses present several alternative causes of failure. The relevant theory for crack formation in the Trunnion-Hub-Girder (THG) was formulated based on several observations. First, the steady state stresses after assembly were well below the yield point and could not have caused failure. Second, experimental observations indicate the presence of small cracks in the assembly. Last, cracks were formed during the immersion of the trunnion-hub assembly in liquid nitrogen. This observation is important as fracture toughness decreases with a decrease in temperature whereas yield strength increases with a decrease in temperature (see Figure 4.1b). Our hypothesis is that the small cracks present in the assembly propagate catastrophically once the size of the crack exceeds the critical crack length. This hypothesis is tested using the THGTM (Trunnion-Hub-Girder Testing Model). A brief explanation of this theory is included.

Time history plots of temperatures, hoop stresses and critical crack lengths at different stages in the assembly process are presented. The plots show the interdependence of the variables and suggest possible avenues of optimizing them by changing the parameters or steps involved in the assembly process. One possible solution, using AP2, is explored and a comparison between the two assembly procedures for different bridges is presented. A phenomenon called crack arrest, that may prevent cracking in some cases despite low critical crack lengths, is described and the possibility of it occurring is explored.

The results are important from two perspectives, one of which is explicitly presented in the results and the other which is implicitly suggested. The explicit result is the comparison between the two assembly procedures. Also, implicitly presented in the results is a comparison of different bridges explaining why some THG assemblies form cracks while others do not.

4.2 Bridge geometric parameters

The geometric parameters for the three bridges, that are, Christa McAuliffe Bridge, Hillsborough Avenue Bridge and 17th Street Causeway Bridge, are presented in Table 4.1a. For a schematic and description of the parameters, refer to Figures B.13a, B.14a, and B.15a of Appendix B.

Interference values for FN2 fits can be obtained from the Bascule Bridge Design Tools (Denninger, 2000). In this study, we analyze the worst case, that is, maximum interference between the trunnion and hub, and minimum interference between the hub and the girder. These values of interference will cause the largest tensile hoop stress in the hub. The interference values, based on FN2 fits, used in this analysis are presented in Table 4.1b.

Table 4.1a Geometric parameters.

Geometric Parameters	Bridge		
	Christa McAuliffe	Hillsborough Avenue	17TH Street Causeway
hgf (in)	1.5	1	0.75
hgw (in)	82	90	60
l (in)	18.5	20	6
lf (in)	4.25	8.5	4.25
lg (in)	82	90	60
lh (in)	16	22	11
lt (in)	53.5	62	23
rhg (in)	16	15.39	8.88
rho (in)	27	24.5	13.1825
rti (in)	1	1.125	1.1875
rto (in)	9	8.39	6.472
tg (in)	1.5	1.5	1.25
wbr (in)	1.75	1.75	0.78125
wgf (in)	17	14	1.25
wgw (in)	1.5	1	0.75
whf (in)	1.75	1.75	1.25

Table 4.1b Interference values.

Diametrical Interference	Bridge		
	Christa McAuliffe	Hillsborough Avenue	17TH Street Causeway
Trunnion-Hub (in)	0.008616	0.008572	0.007720
Hub-Girder (in)	0.005746	0.005672	0.004272

4.3 Bridge loading parameters

The material properties of an equivalent metal, that is, Fe - 2.25 Ni (ASTM A203-A), are presented in Chapter 3. Also presented are the thermal properties of air and liquid nitrogen. Bulk temperatures used for the results presented are given in Table 4.2.

Table 4.2 Bulk temperatures.

Type of bulk temperature	Temperature (^{0}F)
Ambient air bulk temperature	85
Cooling medium bulk temperature	-321

4.4 Convergence test and result verification

A convergence test is performed to verify the suitability of the mesh used in the analysis. The hoop stress is calculated at different levels of meshing, that is, different mesh densities. The hoop stress, R_N, at a point (Logan, 1992) is given by

$$R_N = A + \frac{B}{(N)^{\bar{\alpha}}} \tag{4.1a}$$

where

B and $\bar{\alpha}$ = constants,
A = extrapolated result for infinite mesh density, and
N = number of elements.

Note that as $N \to \infty$, $\frac{B}{N^{\bar{\alpha}}} \to 0$, $R_\infty \to A$ for $\bar{\alpha} > 1$. So, for $\bar{\alpha} > 1$ the results will converge and for $\bar{\alpha} < 1$ the results will diverge. Table 4.3a show the results with different mesh densities (that is, 3096, 4740 and 6336 elements).

Table 4.3a Results with different mesh densities.

NUMBER OF ELEMENTS, N	HOOP STRESS σ_θ (ksi)
3096	27.328
4740	31.158
6336	32.686

Using the information from Table 4.3a and Equation (4.1a) results in the following three simultaneous equations in terms of A, B and $\bar{\alpha}$.

$$R_{3096} = 27.328 = A + \frac{B}{3096^{\bar{\alpha}}} \tag{4.1b}$$

$$R_{4740} = 31.158 = A + \frac{B}{4740^{\bar{\alpha}}} \tag{4.1c}$$

$$R_{6336} = 32.686 = A + \frac{B}{6336^{\bar{\alpha}}} \tag{4.1d}$$

Solving Equations (4.1a) through (4.1c) for A, B and $\bar{\alpha}$ yields A=35.551 ksi, B=1.133 x 10^9, and $\bar{\alpha}$ =1.472208. Since $\bar{\alpha} > 1$, the results will converge.

A comparison of stresses at steady state at the inner radius of the hub with those obtained from the Bascule Bridge Design Tools (BBDT) (Denninger, 2000) is presented in Table 4.3b.

Table 4.3b Comparison between trunnion-hub-girder testing model and bascule bridge design tools results.

BRIDGE	STRESS (ksi)		PERCENT DIFFERENCE
	THGTM	BBDT	
Christa McAuliffe	9.812	9.372	4.59 %
Hillsborough Avenue	10.173	9.813	3.62 %
17th Street Causeway	14.298	13.457	6.06 %

The results are within an allowable difference, especially considering that the geometries of the trunnion, hub and girder in the BBDT are approximated to long annular cylinders.

4.5 Hoop stress, temperature and critical crack length

Our hypothesis is that small cracks present in the assembly propagate catastrophically once they attain a critical crack length, a_c. The critical crack length is calculated as follows. For an edge radial crack in a hollow cylinder that is small in comparison to the radial thickness of the cylinder (see Figure 4.1a), the stress intensity factor at the crack tip is given by

$$K_I = f_e \sigma_\theta \sqrt{\pi a} \tag{4.2a}$$

where

a = crack length,
f_e = edge effect factor[3],
K_I = stress intensity factor, and
σ_θ = hoop stress.

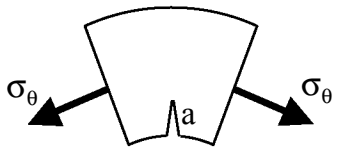

Figure 4.1a Critical crack length.

If $K_I = K_{Ic}(T)$ where $K_{Ic}(T)$ is the temperature dependent critical stress intensity factor or fracture toughness of the material, then the critical crack length (that is, the maximum crack length allowable before a crack propagates catastrophically) is determined by Equation (4.2b) (Kanninen and Popelar, 1985).

$$a_c = \frac{K_{Ic}^2(T)}{f_e^2 \pi \sigma_\theta^2} \tag{4.2b}$$

where

a_c = critical crack length.

The critical crack length is dependent upon the fracture toughness, $K_{Ic}(T)$, and the hoop stress, σ_θ. The critical stress intensity factor, K_{Ic}, in turn is a function of temperature. K_{Ic} decreases with an decrease in temperature as shown in Figure 4.1b

Our hypothesis is that in AP1, a combination of high hoop stress and low temperature results in smaller values of critical crack length, possibly leading to crack formation. In AP2, stresses due to interference never occur together with the thermal stresses during the cooling process, possibly resulting in larger values of critical crack length, thereby reducing the probability of crack formation. *In short, temperature, hoop stress and critical stress intensity factor (fracture toughness) are not optimized in AP1, and AP2 may resolve this problem.* A multiplicity of factors (geometry, temperature dependent material properties, thermal stresses, interference stresses, etc.) affect the stresses in the assembly with some parameters sometimes reinforcing and yet at other

[3] f_e equals 1.125 for an edge crack which would be the worst case scenario.

times negating the effects of each other. Therefore, this intuitive analysis needs to stand the test of a numerical model before gaining engineering acceptability. The THGTM is used for this purpose.

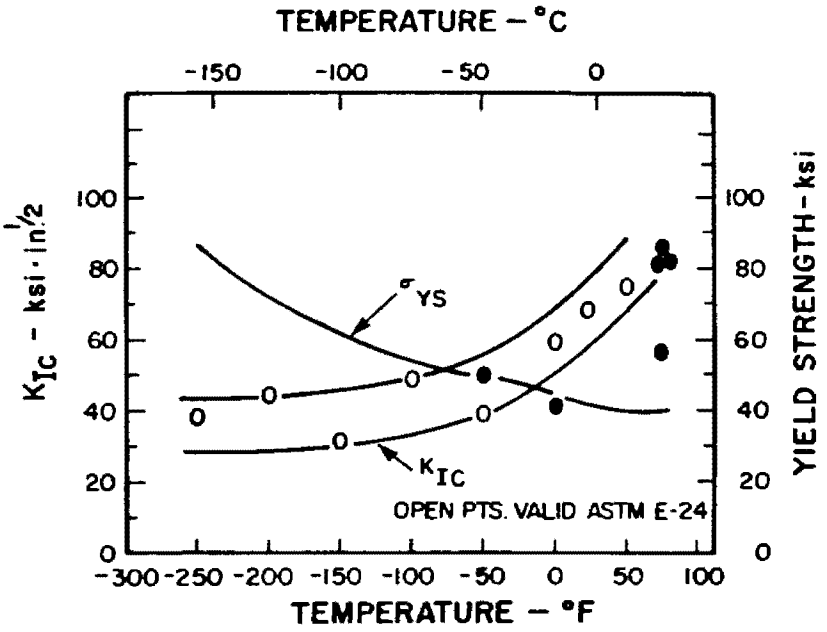

Figure 4.1b Fracture toughness and temperature (Blair et al., 1995).

The THGTM is used to plot the temperature, hoop stress and the critical crack length at possible points of failure in the assembly. The critical crack length is used as the parameter for comparison between different assembly procedures for different bridges. A further study possible with the THGTM (though not included as a part of this study) is analyzing the effect of the different loading parameters on the critical crack length.

4.6 Transient stresses and critical crack length using the trunnion-hub-girder testing model

The THGTM is used to analyze the stresses and critical crack length at possible locations of failure. We choose the point with the greatest probability of failure and plot critical crack lengths, hoop stress and temperature against time for that point.

With the aim of modeling the worst case from the perspective of failure (see Section 4.12) in our model, the male parts of the assembly are inserted into the female parts as soon as the interference between the two is breached. In practice, it is often difficult to shrink-fit an assembly without a clearance, and hence the high stresses after contact may not be observed in practice. It is important to note that in practice it is impossible to perform an insertion without a gap and hence the high stresses noticed immediately after contact may not be observed in practice. Also, the entire assembly process and the ancillary cooling processes are performed separately. Hence, the time periods for which the cooling is performed in the full assembly process (only till interference is breached) will be different from that in the ancillary cooling process (user specified cooling time).

The results are presented with time-history plots for all the bridges. Selected contour plots are presented only for the Christa McAuliffe Bridge.

4.7 Christa McAuliffe Bridge

Possible critical points in the hub are studied using the THGTM. The element at the inner radius of the hub on the gusset side is found to be the most critical element. Figure 4.2 shows the chosen element.

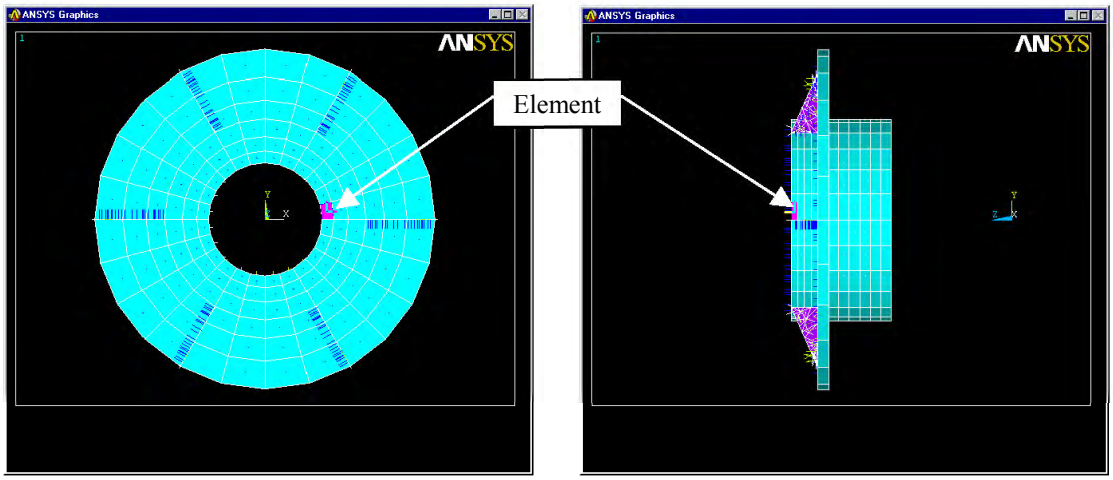

Figure 4.2 Front and side view of the chosen element in the Christa McAuliffe hub.

4.7.1 Assembly procedure 1 (AP1)

4.7.1.1 Full assembly process

The stresses, temperatures and critical crack lengths during AP1 are plotted against time in Figure 4.3. The time period for which each step of the assembly process is performed is given in Table 4.4.

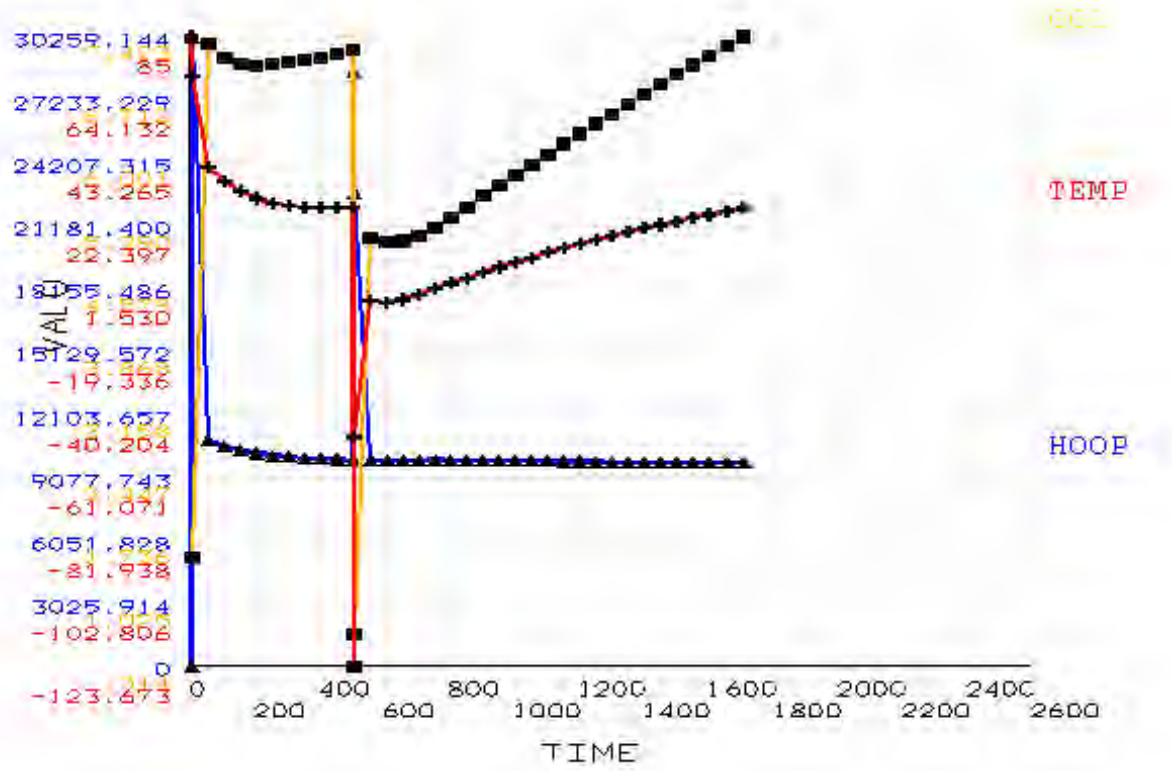

Figure 4.3 Critical parameters (CCL is critical crack length in inches, TEMP is temperature in ^{0}F, and HOOP is hoop stress in psi) plotted against time (full assembly process during AP1 of Christa McAuliffe Bridge).

Table 4.4 Time for each step of AP1 for the Christa McAuliffe Bridge.

STEP	STARTING TIME (min)	ENDING TIME (min)
Cooling down of the trunnion	0	3
Sliding the trunnion into the hub	4	503
Cooling down the trunnion-hub assembly	504	505
Sliding the trunnion-hub assembly into the girder	506	1705

4.7.1.2 Cooling down of the trunnion

The stresses at the hub are not affected during this step.

4.7.1.3 Sliding the trunnion into the hub

The hoop stress, temperature and the critical crack length during this step are plotted against time in Figure 4.4. Almost immediately after contact, a combination of interference and thermal stresses produces high hoop stresses at the inner radius of the hub. Due to the effects of conduction and convection, the temperatures in the trunnion-hub assembly begin to converge to around the same temperature. As a consequence, the thermal stresses play an increasingly marginal role with the passage of time.

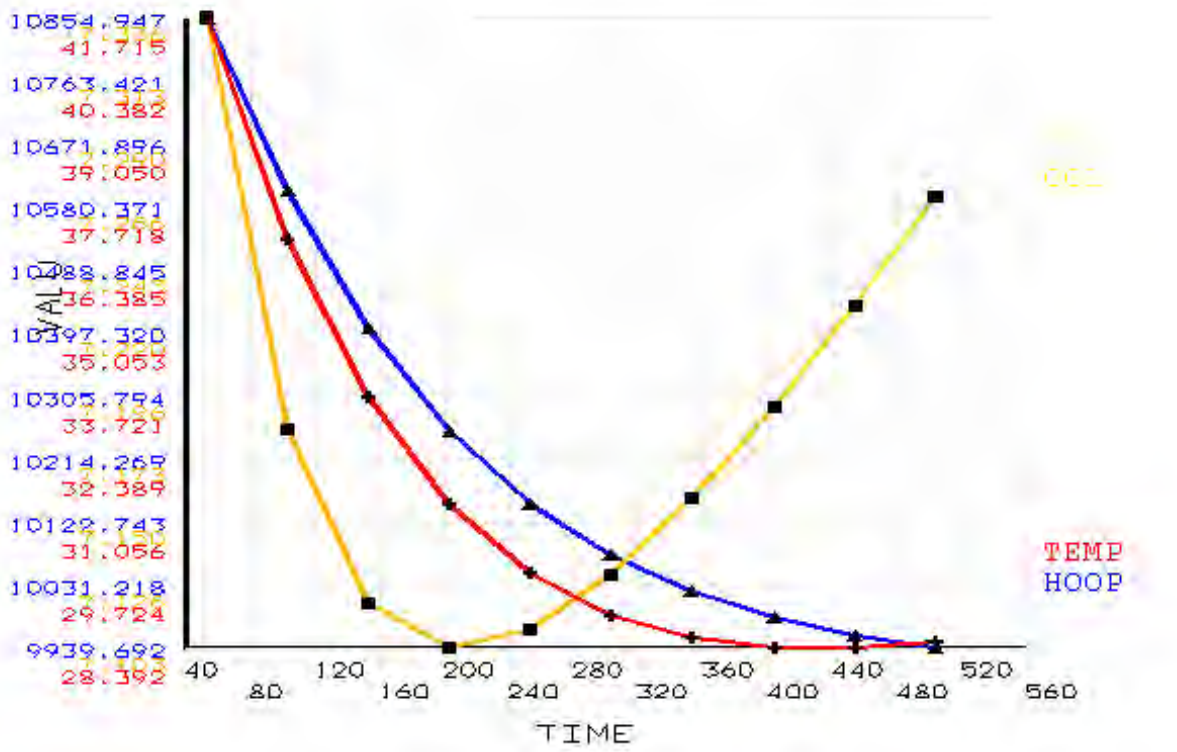

Figure 4.4 Critical parameters (CCL is critical crack length in inches, TEMP is temperature in ^{0}F, and HOOP is hoop stress in psi) plotted against time (sliding the trunnion into the hub during AP1 of the Christa McAuliffe Bridge).

Though this step is not important from the perspective of failure, as the critical crack lengths are high, an interesting interplay of temperatures, hoop stresses and critical crack length can be seen. As temperature and hoop stress fall, the critical crack length initially falls before rising. (see Equation (4.2b)).

4.7.1.4 Cooling down the trunnion-hub assembly

The hoop stress, temperature and the critical crack length during this step are plotted against time in Figure 4.5a. The results from the THGTM indicate that the lowest values of critical crack length during AP1 are observed during this step. This result is supported by experimental observation of crack formation during this step (see Chapter 1). This assumes special significance as Christa McAuliffe is one of the bridges that formed cracks during this step. Furthermore, the critical crack length remains low for a considerable period of time in contrast to what is observed in AP2 during its counterpart critical step: cooling of the hub (see Appendix B.7.2.2). This behavior assumes importance in our discussion of crack arrest (see Section 4.11). Initially, thermal and interference stresses reinforce each other and high hoop stresses occur as a result. As the trunnion-hub assembly nears steady state, the stresses due to interference dominate.

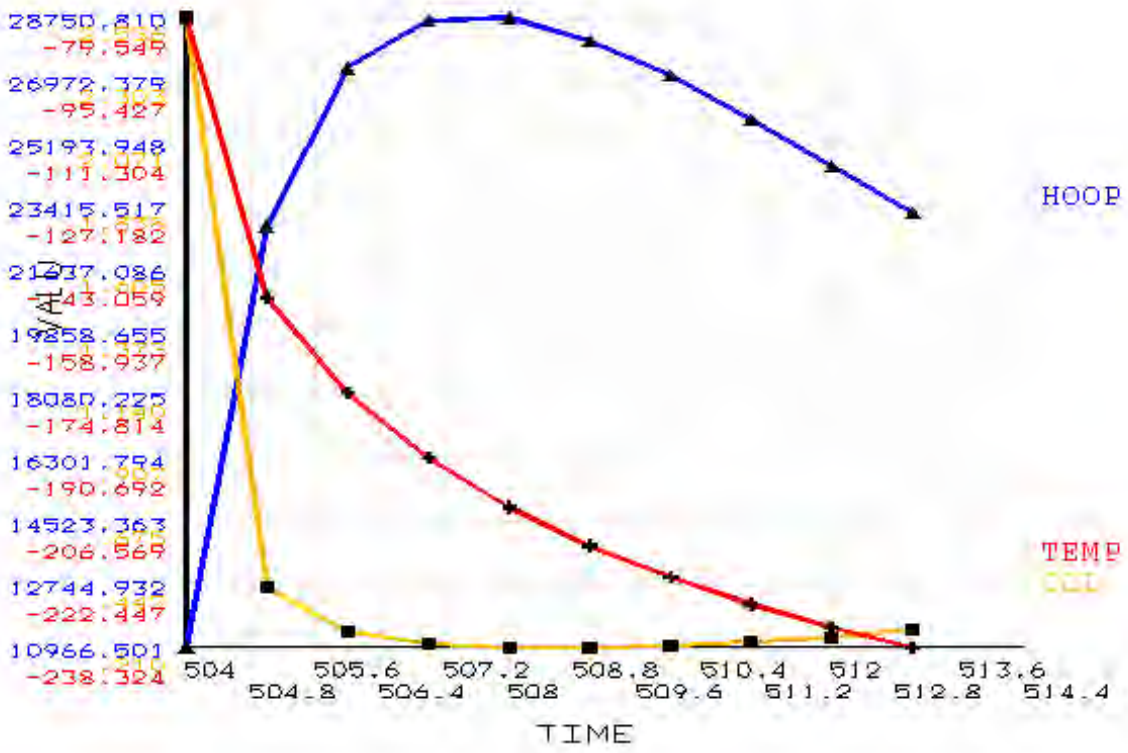

Figure 4.5a Critical parameters (CCL is critical crack length in inches, TEMP is temperature in ^{0}F, and HOOP is hoop stress in psi) plotted against time (cooling down of the trunnion-hub assembly during AP1 of the Christa McAuliffe Bridge).

Contour plots of the hoop stress and the temperature in the hub when the highest hoop stress is noticed are plotted in Figures 4.5b and 4.5c, respectively. Hoop stress and temperature plots when the lowest critical crack is observed are plotted in Figures 4.5d and 4.5e, respectively.

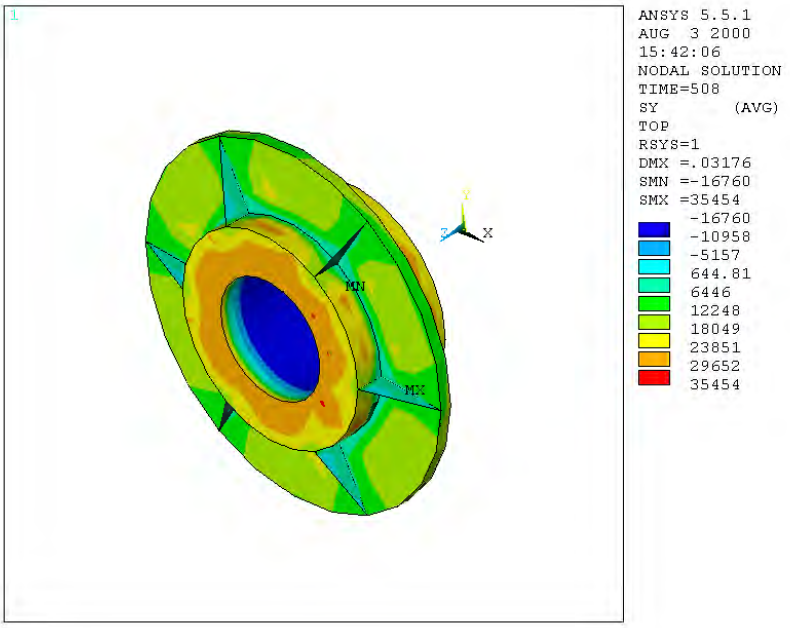

Figure 4.5b Hoop stress (psi) plot when the highest hoop stress during AP1 is observed.

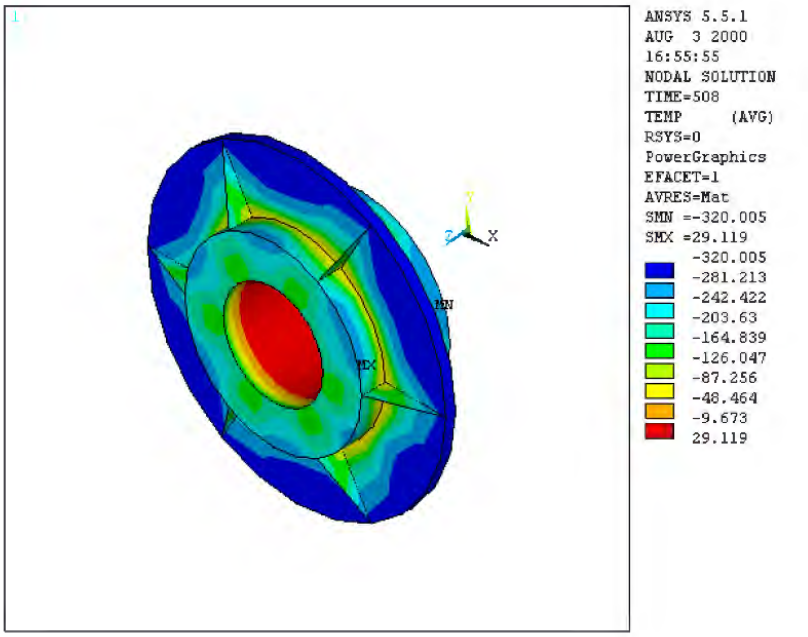

Figure 4.5c Temperature (^{0}F) plot when the highest hoop stress during AP1 is observed.

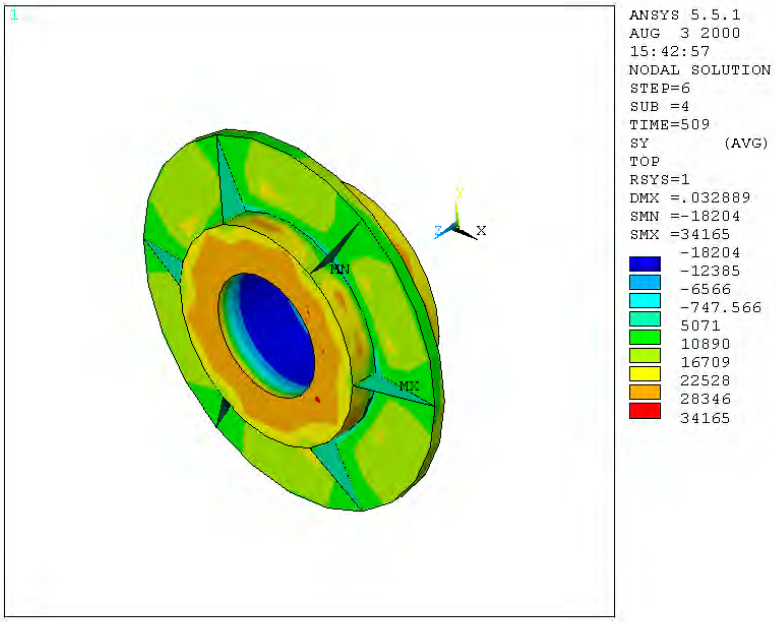

Figure 4.5d Hoop stress (psi) plot when the lowest critical crack length during AP1 is observed.

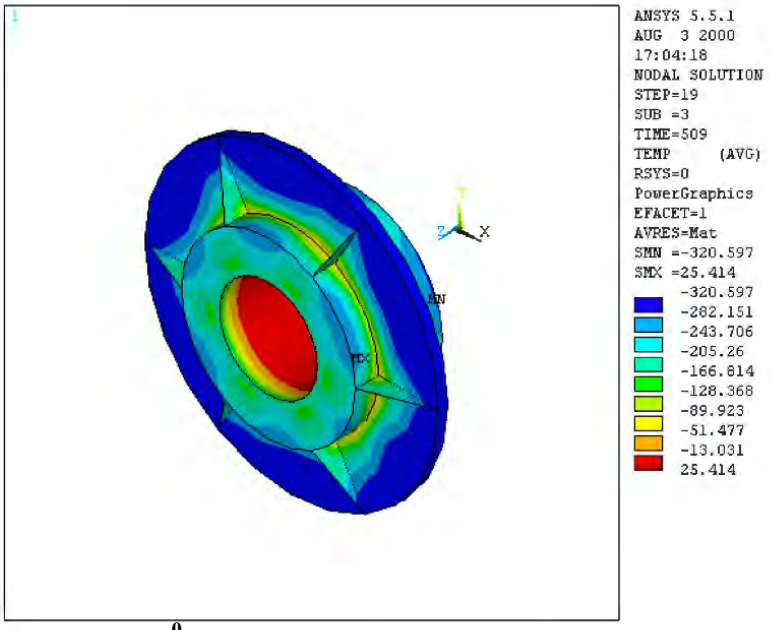

Figure 4.5e Temperature (^{0}F) plot when the lowest critical crack length during AP1 is observed.

4.7.1.5 Sliding the trunnion-hub assembly into the girder

The hoop stress, temperature and the critical crack length during this step are plotted against time in Figure 4.6 for this step. During this step, hoop stresses remain fairly stable primarily due to the remoteness of the inner radius of the hub from the hub girder interface. A rise in the temperature due to conduction and convection is accompanied initially with a rise, and later a fall in the hoop stress, confirming the somewhat non-intuitive behavior of thermal stresses. High values of the critical crack length indicate the low probability of crack propagation during this step.

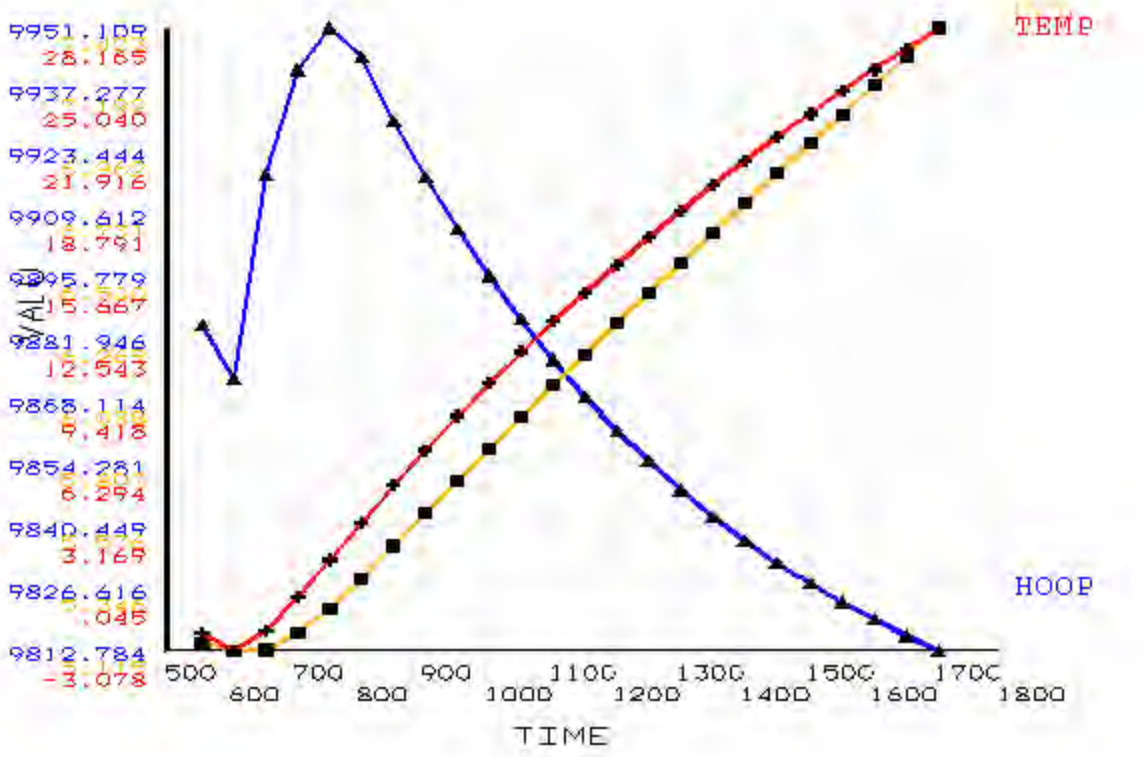

Figure 4.6 Critical parameters (CCL is critical crack length in inches, TEMP is temperature in ^{0}F, and HOOP is hoop stress in psi) plotted against time (sliding the trunnion–hub assembly into the girder during AP1 of Christa McAuliffe Bridge).

4.7.2 Assembly Procedure 2 (AP2)

4.7.2.1 Full assembly process

The stresses, temperatures and critical crack lengths at the chosen element are plotted against time in Figure 4.7. The time period for which each step of the assembly process is performed is given in Table 4.5.

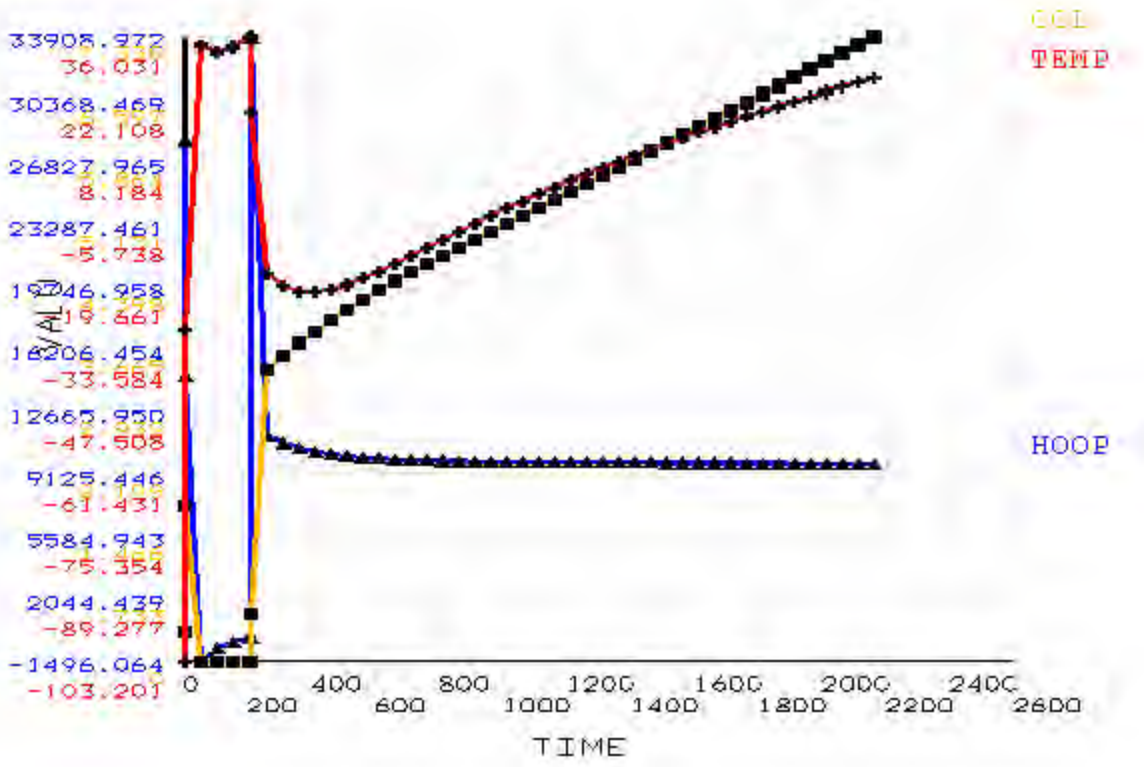

Figure 4.7 Critical parameters (CCL is critical crack length in inches, TEMP is temperature in ^{0}F, and HOOP is hoop stress in psi) plotted against time (full assembly process during AP2 of Christa McAuliffe Bridge).

Table 4.5 Time for each step of AP2 for the Christa McAuliffe Bridge.

STEP	STARTING TIME (min)	ENDING TIME (min)
Cooling down of the hub	0	2
Sliding the hub into the girder	3	202
Cooling down the trunnion	203	208
Sliding the trunnion into the hub-girder assembly	209	2158

4.7.2.2 Cooling down of the hub

The stresses, temperatures and critical crack lengths during this step are plotted against time in Figure 4.8a. A sharp thermal gradient across the radius at the inner radius of the hub initially results in high values of hoop stress. Over time, as the temperature gradient becomes less steep, the hoop stresses fall. The lowest value of critical crack length in AP2 is observed during this step. Note that the critical crack length rises almost instantaneously after reaching its lowest point indicating a possibility of crack arrest (see Section 4.11)

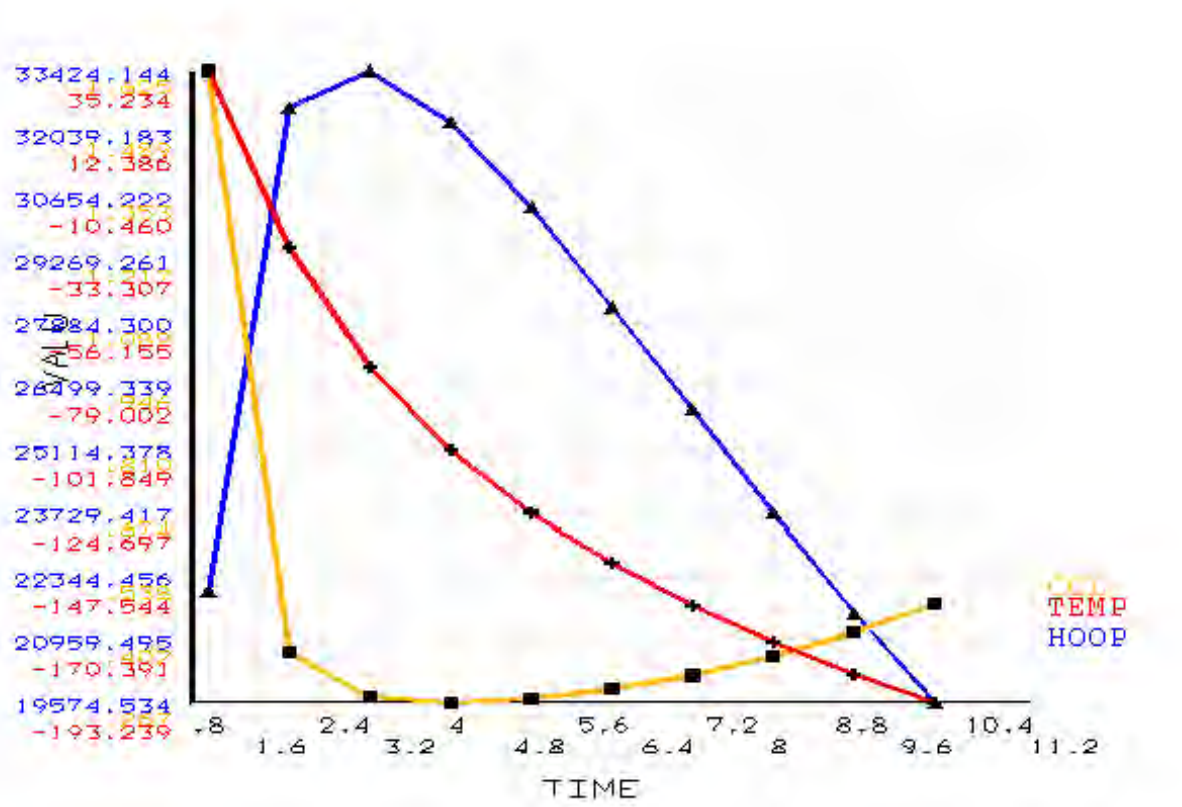

Figure 4.8a Critical parameters (CCL is critical crack length in inches, TEMP is temperature in ^{0}F, and HOOP is hoop stress in psi) plotted against time (cooling down of the hub during AP2 of the Christa McAuliffe Bridge).

Contour plots of the hoop stress and the temperature in the hub when the highest hoop stress is noticed are plotted in Figures 4.8b and 4.8c, respectively. Hoop stress and temperature plots when the lowest critical crack is observed are plotted in Figures 4.8d and 4.8e, respectively.

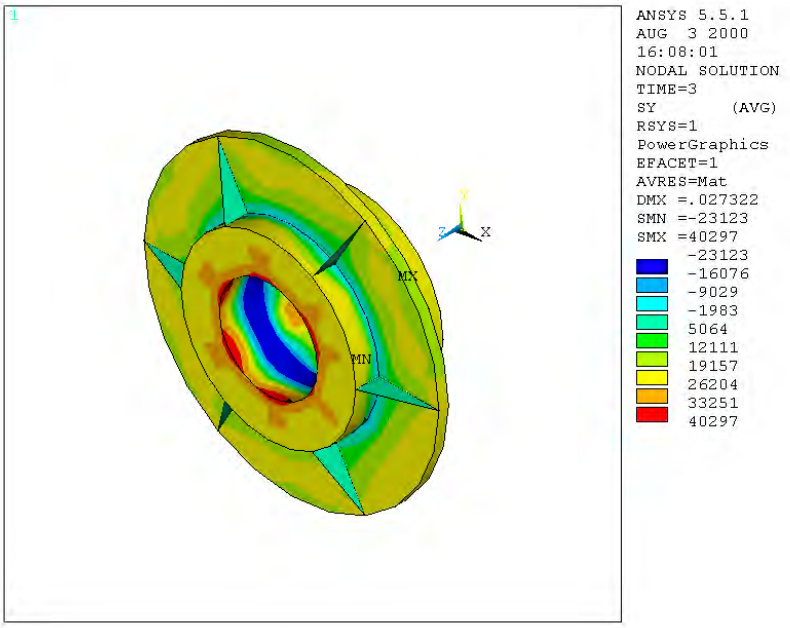

Figure 4.8b Hoop stress (psi) plot when the highest hoop stress during AP2 is observed.

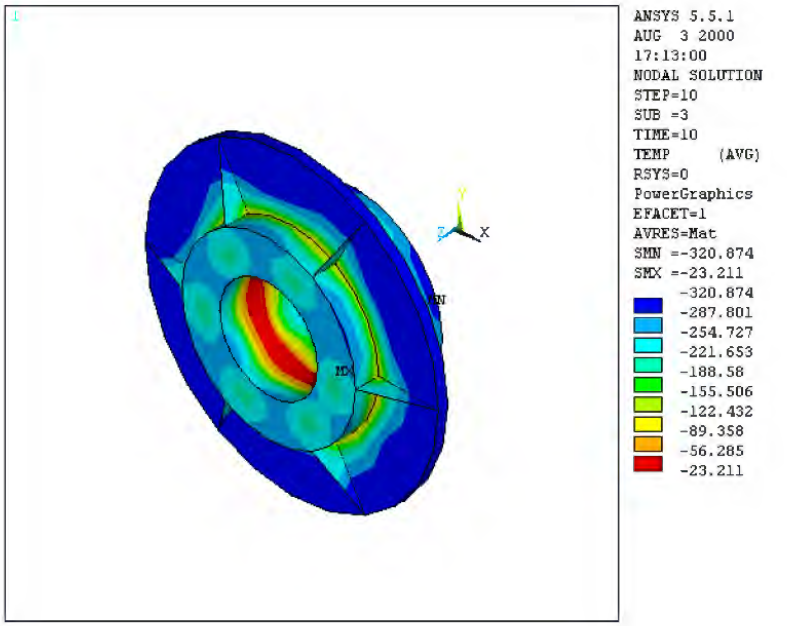

Figure 4.8c Temperature (^{0}F) plot when the highest hoop stress during AP2 is observed.

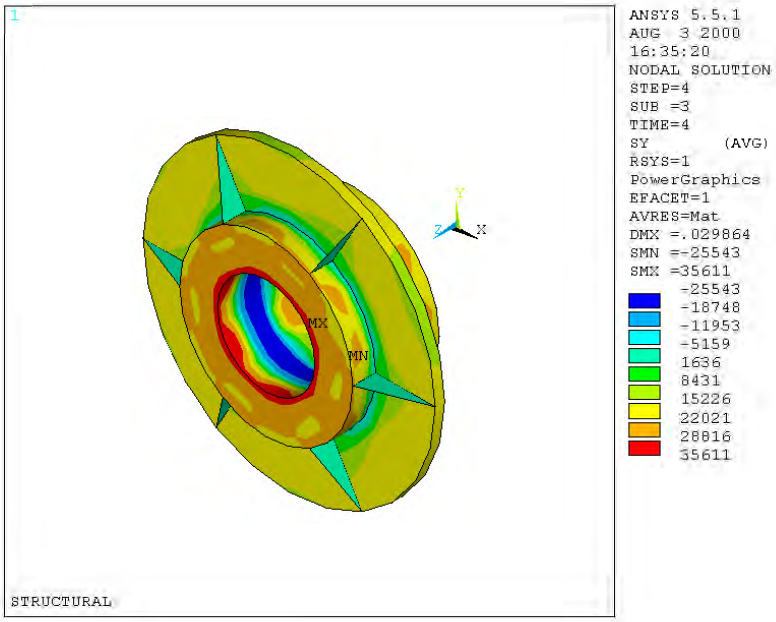

Figure 4.8d Hoop stress (psi) plot when the lowest critical crack length during AP2 is observed.

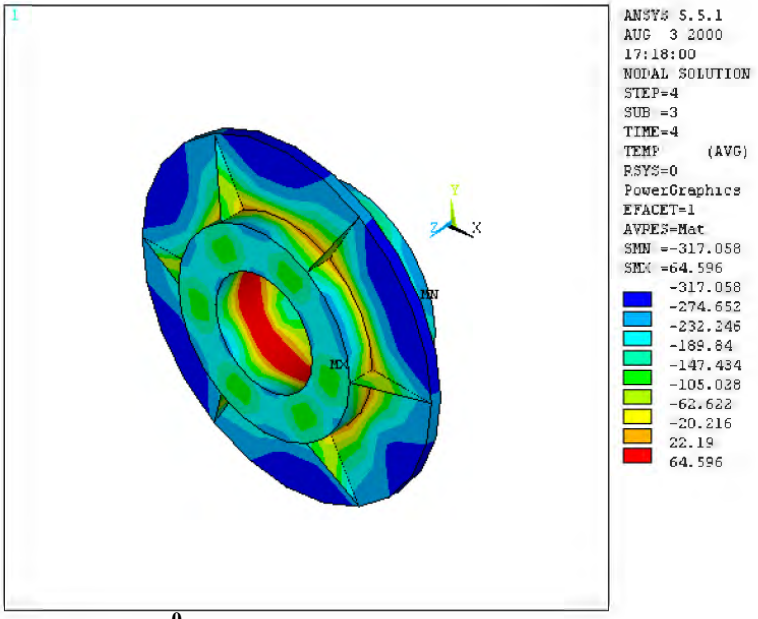

Figure 4.8e Temperature (^{0}F) plot when the lowest critical crack length during AP2 is observed.

4.7.2.3 Sliding the hub into the girder

The stresses, temperatures and critical crack lengths during this step are plotted against time in Figure 4.9. The hoop stresses during this step are compressive. The critical crack length is not defined for compressive hoop stresses, and hence, is shown as zero. The relatively low values of compressive hoop stress are explained by the remoteness of the inner radius of the hub from the hub-girder interface.

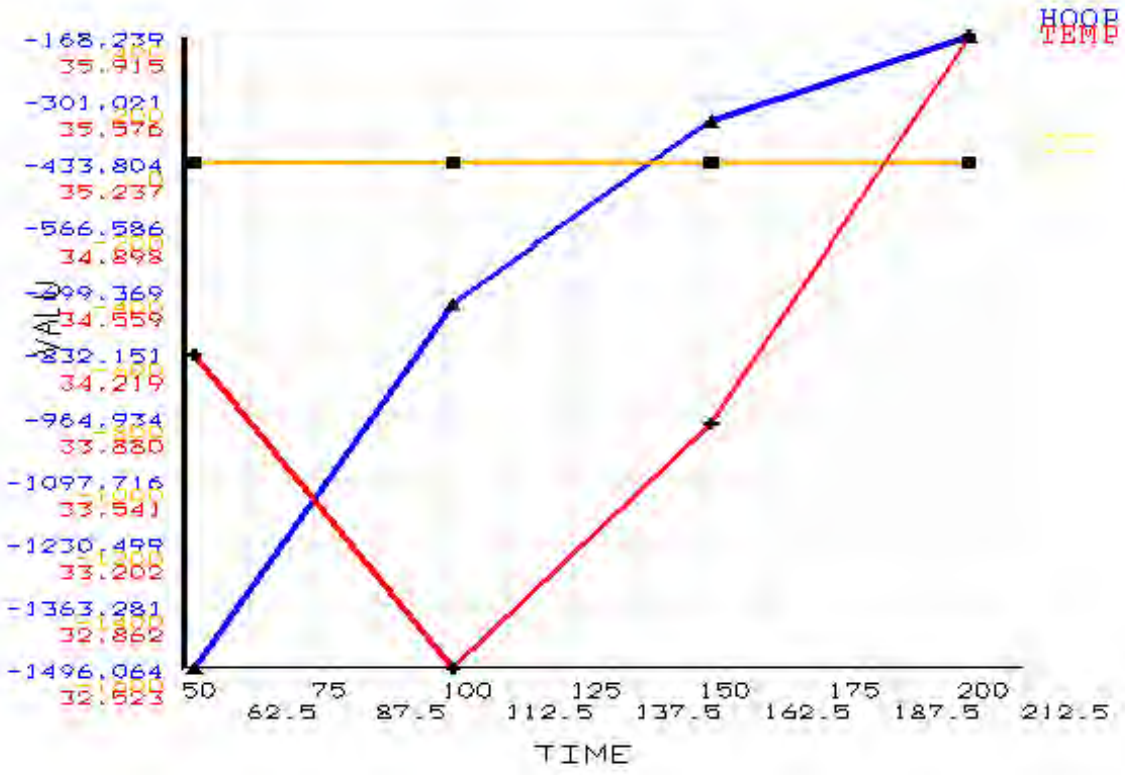

Figure 4.9 Critical parameters (CCL is critical crack length in inches, TEMP is temperature in ^{0}F, and HOOP is hoop stress in psi) plotted against time (sliding the hub into the girder during AP2 of the Christa McAuliffe Bridge).

4.7.2.4 Cooling down of the trunnion

The stresses in the hub are not affected during the cooling of the trunnion.

4.7.2.5 Sliding the trunnion into the hub-girder assembly

The stresses, temperatures and critical crack lengths during this step are plotted against time in Figure 4.10.

Almost immediately after contact, a combination of thermal stresses due to the sharp thermal gradient and interference stresses result in high hoop stresses. Over time, due to the effects of conduction and convection, the temperatures in the assembly begin to converge and interference stresses become dominant. High values of critical crack length indicate low probability of failure.

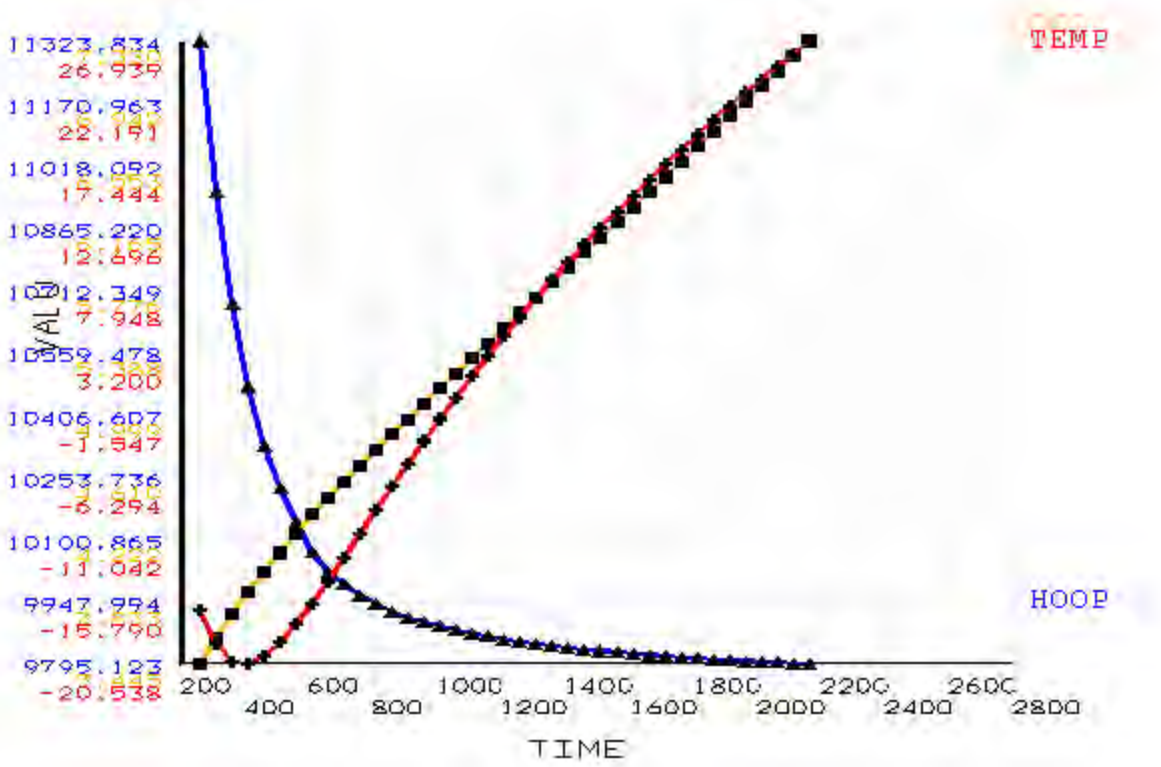

Figure 4.10 Critical parameters (CCL is critical crack length in inches, TEMP is temperature in ^{0}F, and HOOP is hoop stress in psi) plotted against time (sliding the trunnion into the hub-girder assembly during AP2 of the Christa McAuliffe Bridge).

4.8 Hillsborough Avenue Bridge

Possible critical points are studied in the hub using the THGTM. The element at the inner radius of the hub on the backing ring side is found to be the most critical. Figure 4.11 shows the chosen element in the hub.

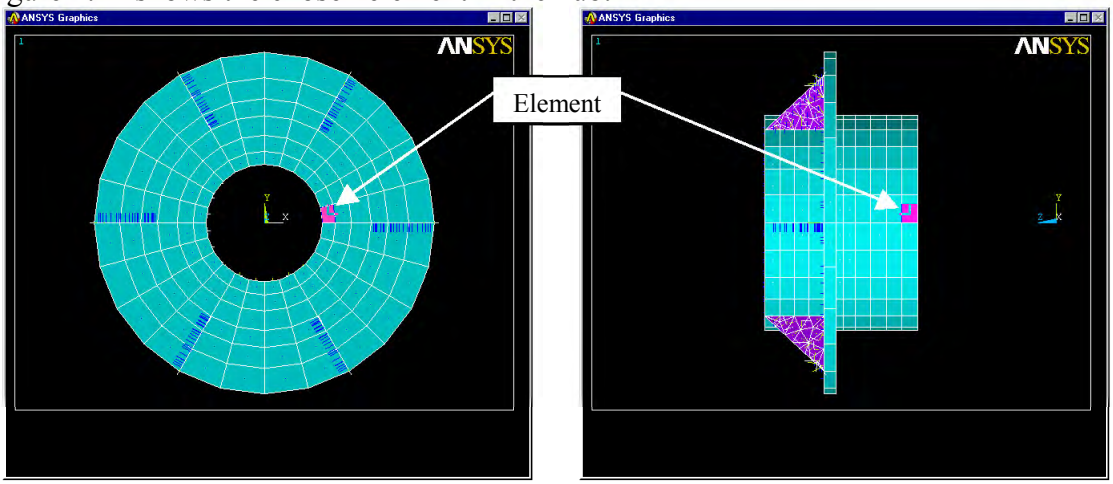

Figure 4.11 Front and side view of the chosen element in the Hillsborough Avenue hub

4.8.1 Assembly procedure 1 (AP1)

4.8.1.1 Full assembly process

The hoop stresses, temperatures and critical crack lengths at the chosen element are plotted against time in Figure 4.12. Time period for each step of the assembly process is performed is listed in Table 4.6.

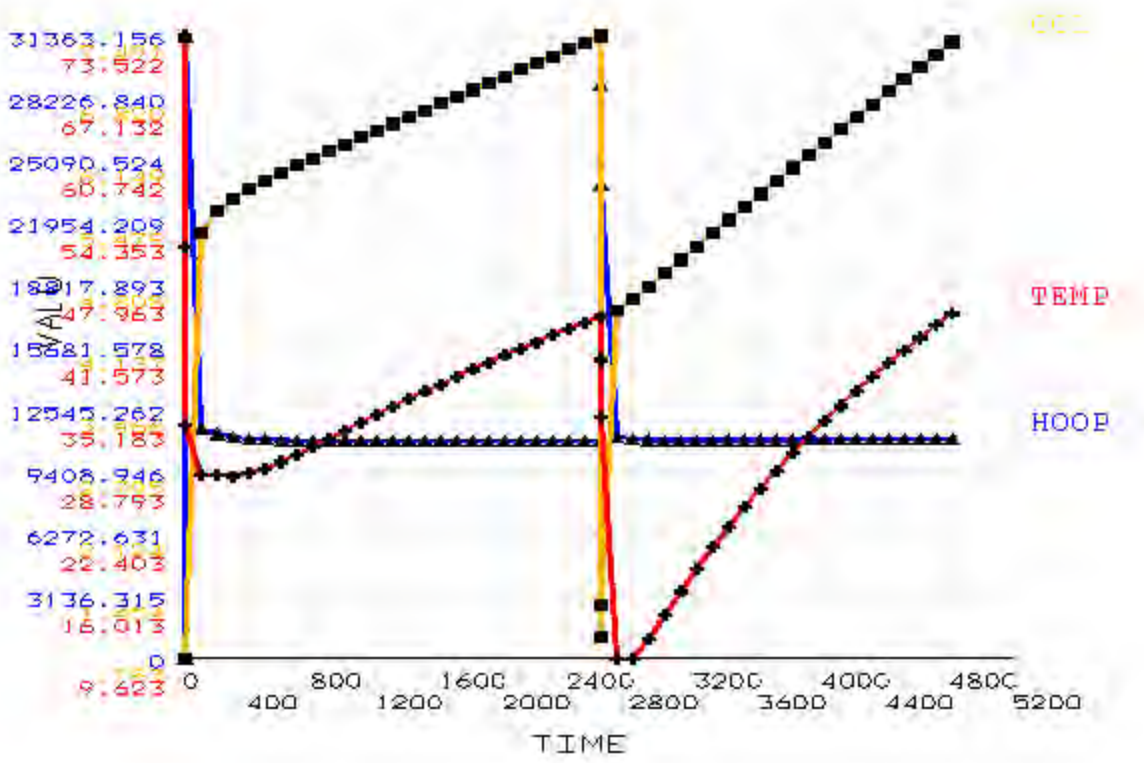

Figure 4.12 Critical parameters (CCL is critical crack length in inches, TEMP is temperature in ^{0}F, and HOOP is hoop stress in psi) plotted against time (full assembly process during AP1 of the Hillsborough Avenue Bridge).

Table 4.6 Time for each step of AP1 for the Hillsborough Avenue Bridge.

STEP	STARTING TIME (min)	ENDING TIME (min)
Cooling down of the trunnion	0	3
Sliding the trunnion into the hub	4	2603
Cooling down the trunnion-hub assembly	2604	2605
Sliding the trunnion-hub assembly into the girder	2606	4805

4.8.1.2 Cooling down of the trunnion

The stresses in the hub are not affected during the cooling down of trunnion.

4.8.1.3 Sliding the trunnion into the hub

The hoop stresses, temperatures and the critical crack lengths during this step are plotted against time in Figure 4.13.

A combination of stresses due to a sharp thermal gradient and interference stresses result in high hoop stresses after contact. As the temperature in the assembly becomes constant due to the effects of conduction and convection, stresses due to interference dominate. High values of critical crack length indicate low probability of failure.

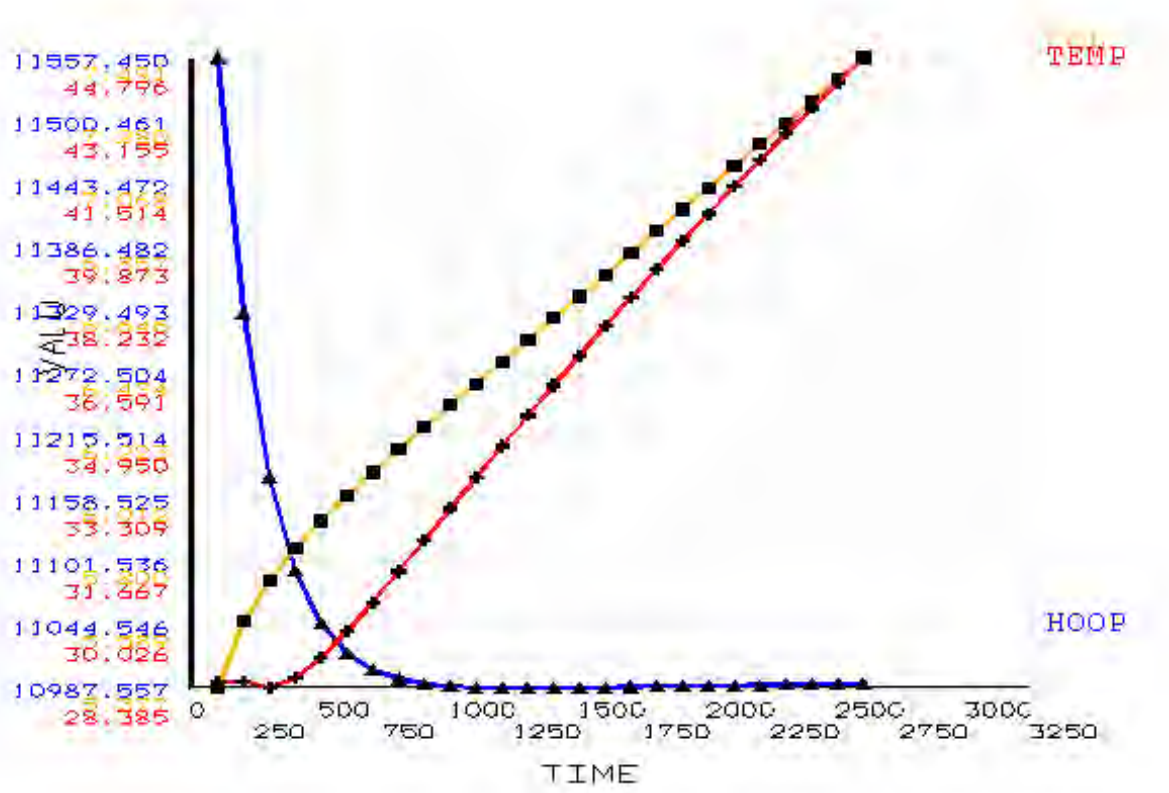

Figure 4.13 Critical parameters (CCL is critical crack length in inches, TEMP is temperature in ^{0}F, and HOOP is hoop stress in psi) plotted against time (sliding the trunnion into the hub during AP1 of the Hillsborough Avenue Bridge).

4.8.1.4 Cooling down the trunnion-hub assembly

The hoop stress, temperature and the critical crack length during this step are plotted against time in Figure 4.14. The results from the THGTM indicate that the lowest values of critical crack length during AP1 are observed during this step. Initially, thermal and structural stresses reinforce each other and high hoop stresses occur as a result. As the trunnion-hub assembly nears steady state, the stresses due to interference dominate. The trends of stresses and critical crack length are similar to what is observed in the Christa McAuliffe Bridge. The critical crack length remains low after its initial decline and shows no distinct upward trend noticed during the cooling of the hub in AP2 (see Appendix B.8.2.2). The highest value of hoop stress and lowest value of critical crack length occur almost together (though not precisely so, indicating a strong relationship between the two quantities).

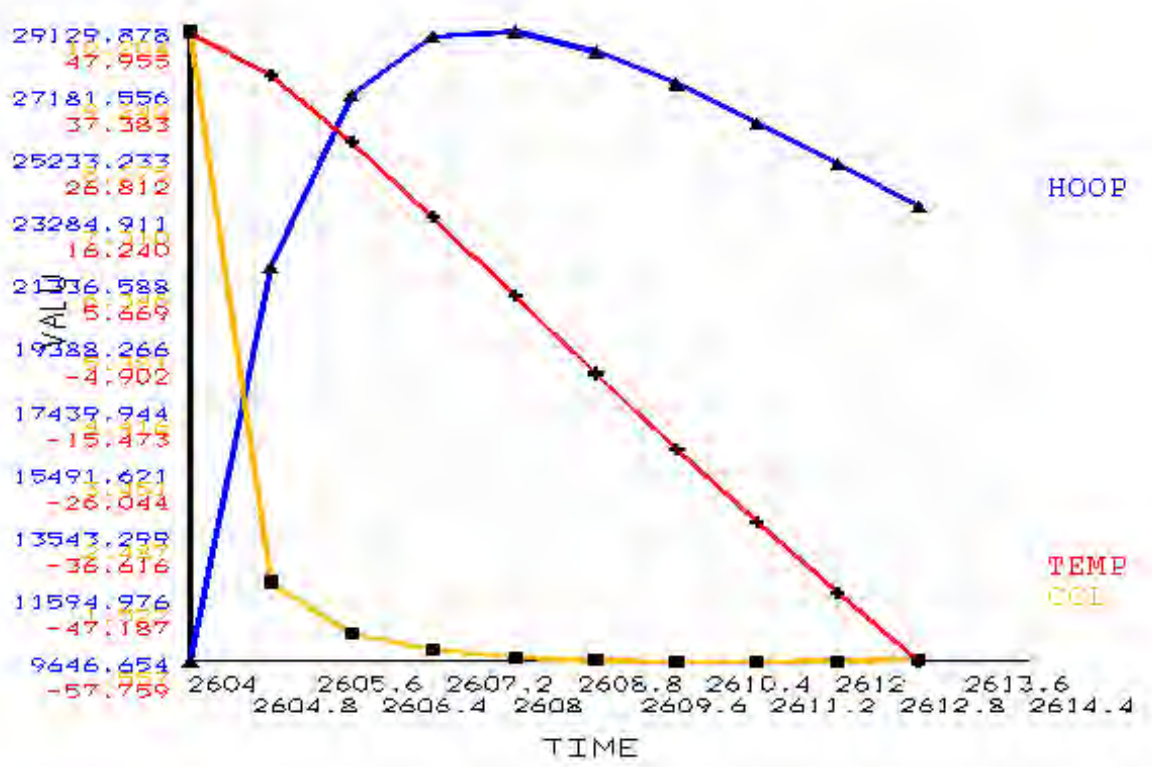

Figure 4.14 Critical parameters (CCL is critical crack length in inches, TEMP is temperature in ^{0}F, and HOOP is hoop stress in psi) plotted against time (cooling down of the trunnion-hub during AP1 of the Hillsborough Avenue Bridge).

4.8.1.5 Sliding the trunnion-hub assembly into the girder

The hoop stress, temperature and the critical crack length during this step are plotted against time in Figure 4.15. During this step, hoop stresses remain fairly stable primarily due to the remoteness of the inner radius of the hub from the hub girder interface. A rise in temperature is accompanied by initially a fall and then a rise in the hoop stress. An interesting point to note is that in the Christa McAuliffe, the trend is the opposite, that is, first rising and then falling, once again reinforcing the difference between different bridge assemblies. High values of critical crack length indicate a low possibility of crack formation during this step.

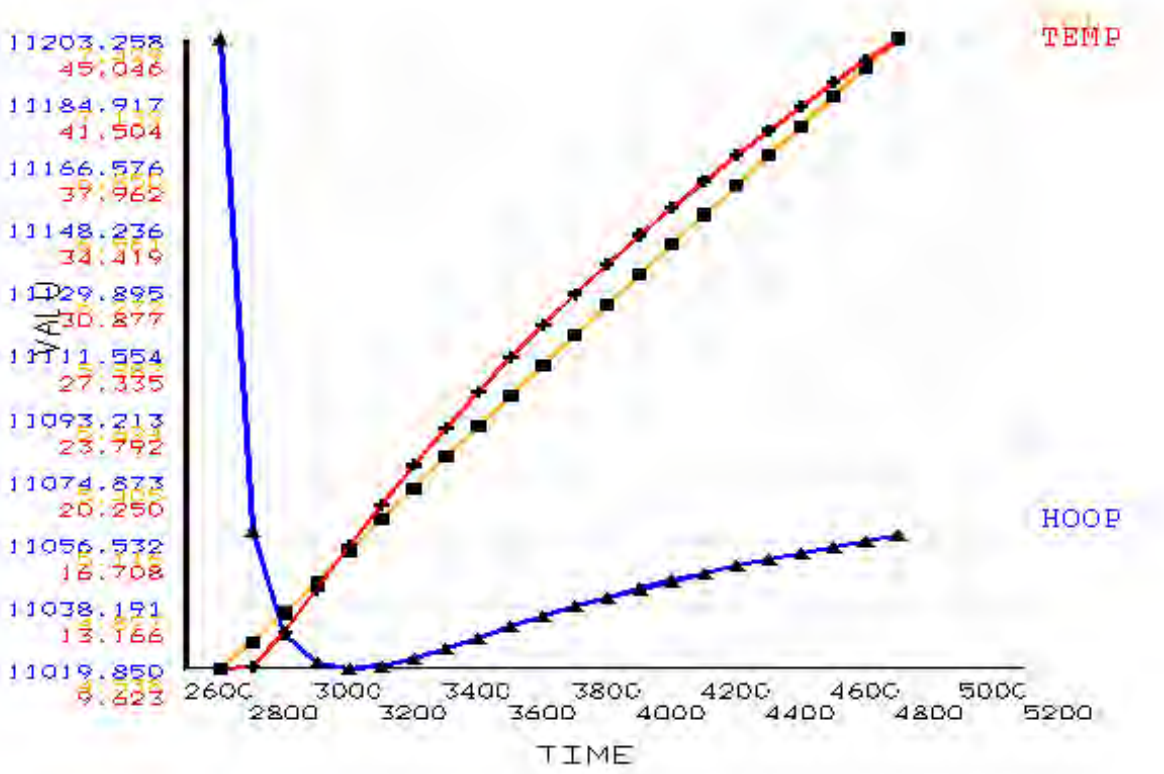

Figure 4.15 Critical parameters (CCL is critical crack length in inches, TEMP is temperature in ^{0}F, and HOOP is hoop stress in psi) plotted against time (sliding the trunnion-hub assembly into the girder during AP1 of the Hillsborough Avenue Bridge).

4.8.2 Assembly procedure 2 (AP2)

4.8.2.1 Full assembly process

The stresses, temperatures and critical crack lengths at the chosen element are plotted against time in Figure 4.16. Time period for each step of the assembly process is performed is listed in Table 4.7.

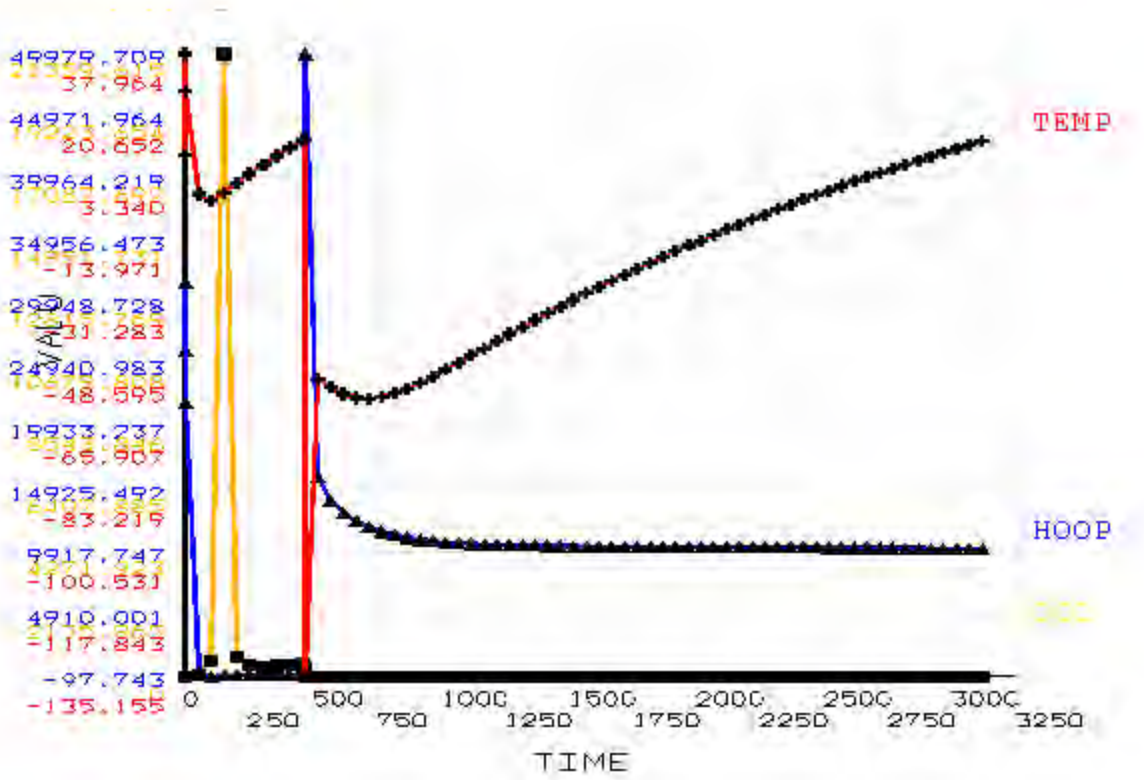

Figure 4.16 Critical parameters (CCL is critical crack length in inches, TEMP is temperature in ^{0}F, and HOOP is hoop stress in psi) plotted against time (full assembly process during AP2 of the Hillsborough Avenue Bridge).

Table 4.7 Time for each step of AP2 for the Hillsborough Avenue Bridge.

STEP	STARTING TIME (min)	ENDING TIME (min)
Cooling down of the hub	0	3
Sliding the hub into the girder	4	753
Cooling down the trunnion	754	760
Sliding the trunnion into the hub-girder assembly	761	3510

4.8.2.2 Cooling down the hub

The stresses, temperatures and critical crack lengths during this step are plotted against time in Figure 4.17. A sharp thermal gradient at inner radius of the hub initially results in high values of hoop stress at the inner radius of the hub. Over time, as the temperature gradient becomes less steep the hoop stresses decrease. The lowest value of critical crack length during AP2 is observed this step. The critical crack length (during the cooling down of the hub) in AP1 remains low after reaching its lowest point. Here, the critical crack length rises after reaching its lowest point. This may explain why though AP2 may produce lower values of critical crack length in the assembly, the probability of crack formation during AP1 maybe greater (see crack arrest in Section 4.11)

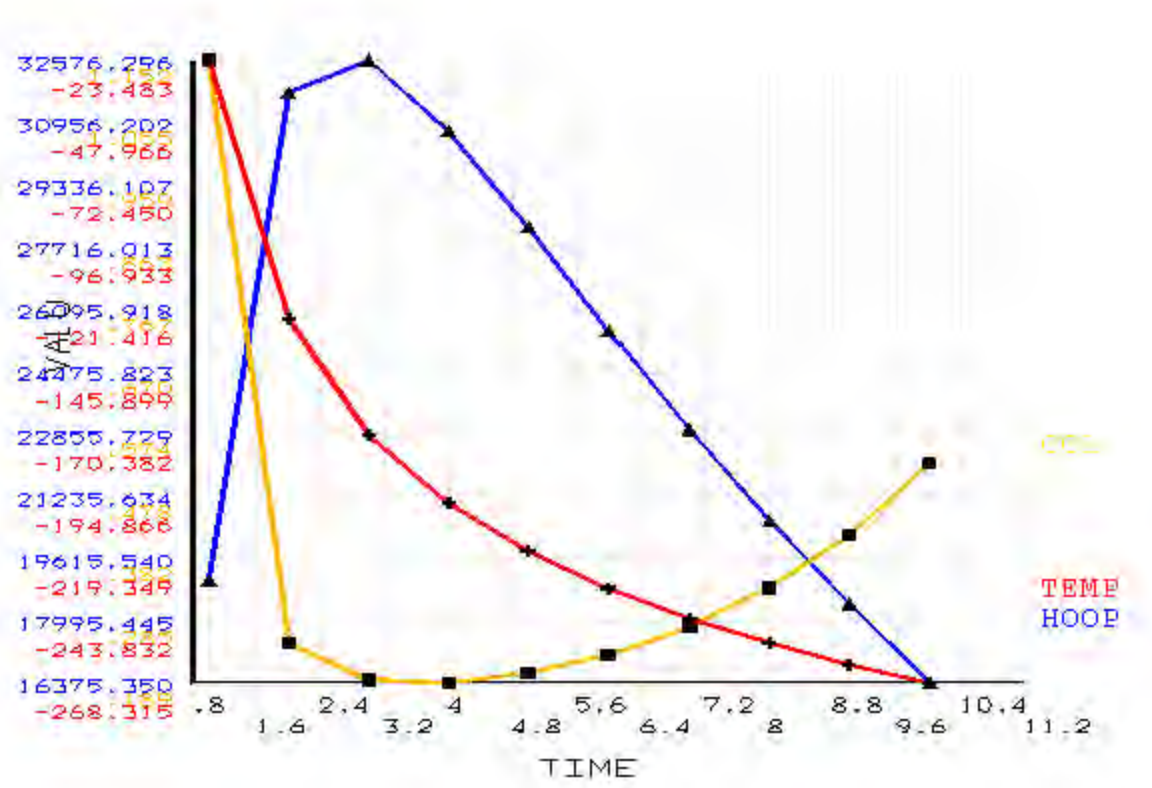

Figure 4.17 Critical parameters (CCL is critical crack length in inches, TEMP is temperature in ^{0}F, and HOOP is hoop stress in psi) plotted against time (cooling down of the hub during AP2 of the Hillsborough Avenue Bridge).

4.8.2.3 Sliding the hub into the girder

The stresses, temperatures and critical crack lengths during this step are plotted against time in Figure 4.18. The sharp 'blip' in the trend of critical crack length is explained by the extremely low value of tensile hoop stress at that point. The remoteness of the inner radius of the hub from the hub-girder interface results in low values of hoop stress. Points where the critical crack length is zero actually indicate compressive hoop stress for which the critical crack length is not defined.

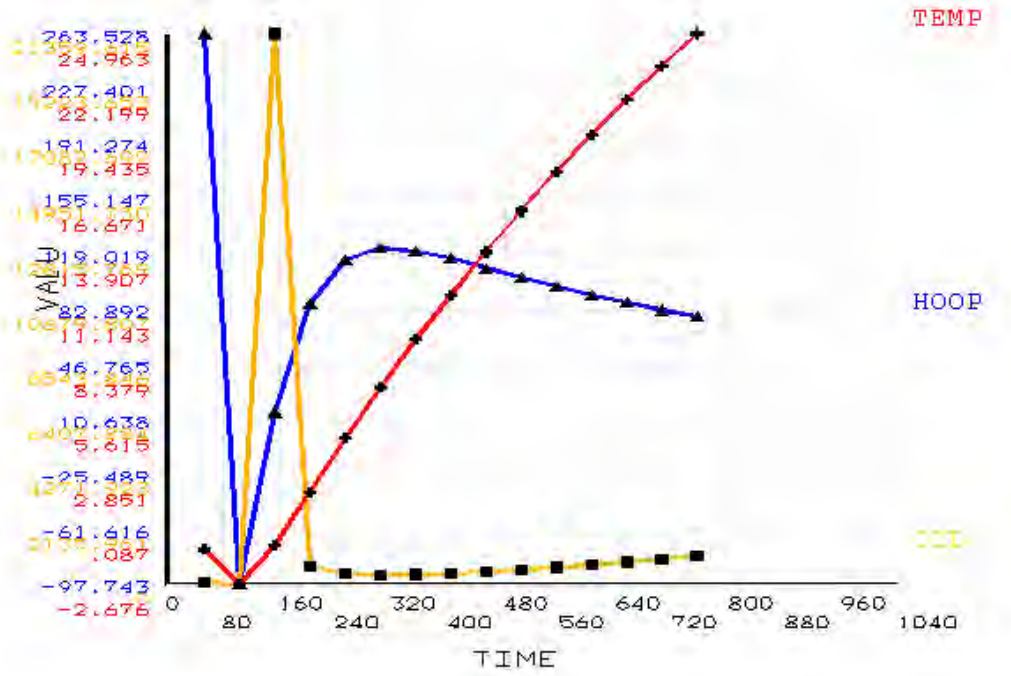

Figure 4.18 Critical parameters (CCL is critical crack length in inches, TEMP is temperature in ^{0}F, and HOOP is hoop stress in psi) plotted against time (sliding the hub into the girder during AP2 of the Hillsborough Avenue Bridge).

4.8.2.4 Cooling down of the trunnion

The stresses in the hub are not affected during the cooling down of the trunnion.

4.8.2.5 Sliding the trunnion into the hub-girder

The stresses, temperatures and critical crack lengths during this step are plotted against time in Figure 4.19. Almost immediately after contact a combination of thermal stresses due to the sharp thermal gradient and structural stresses due to interference result in high hoop stresses. Over time, due to the effects of conduction and convection the temperatures in the assembly converge to about the same temperature. High values of critical crack length indicate low probability of crack formation during this step.

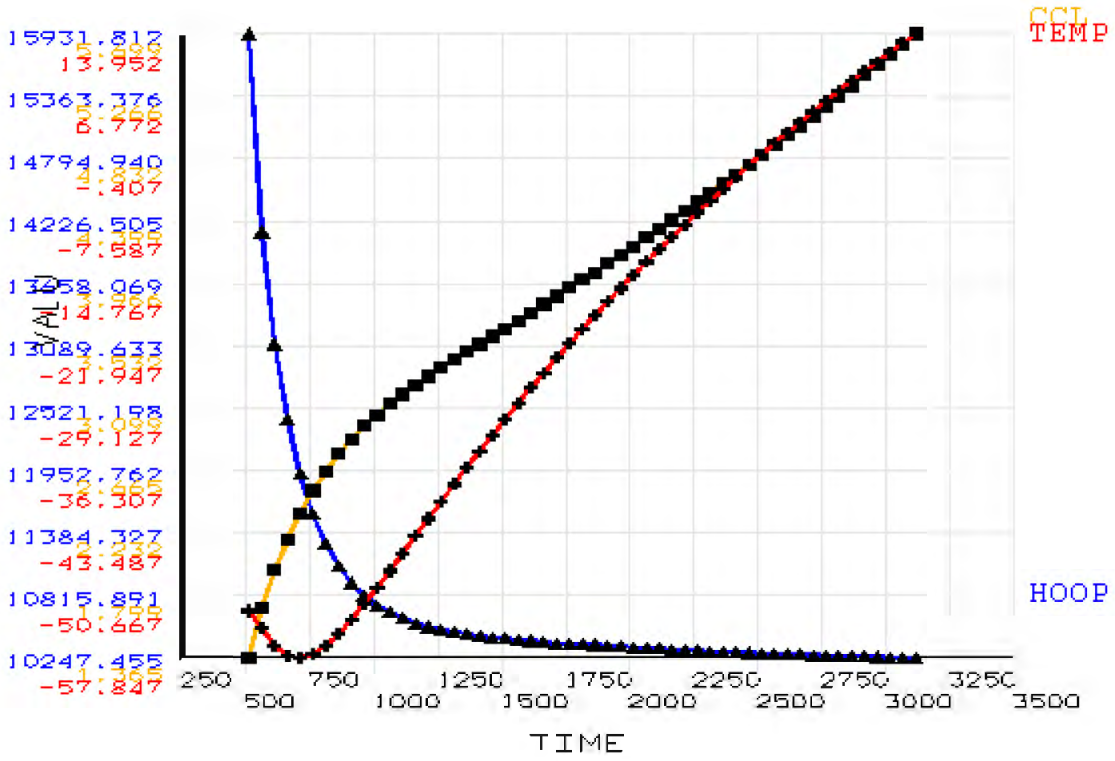

Figure 4.19 Critical parameters (CCL is critical crack length in inches, TEMP is temperature in ^{0}F, and HOOP is hoop stress in psi) plotted against time (sliding the trunnion into the hub-girder during AP2 of the Hillsborough Avenue Bridge).

4.9 17th Street Causeway

Possible critical points in the assembly are studied using the THGTM. The point on the inner radius of the hub on the gusset side is found to be the most critical (see Figure 4.20).

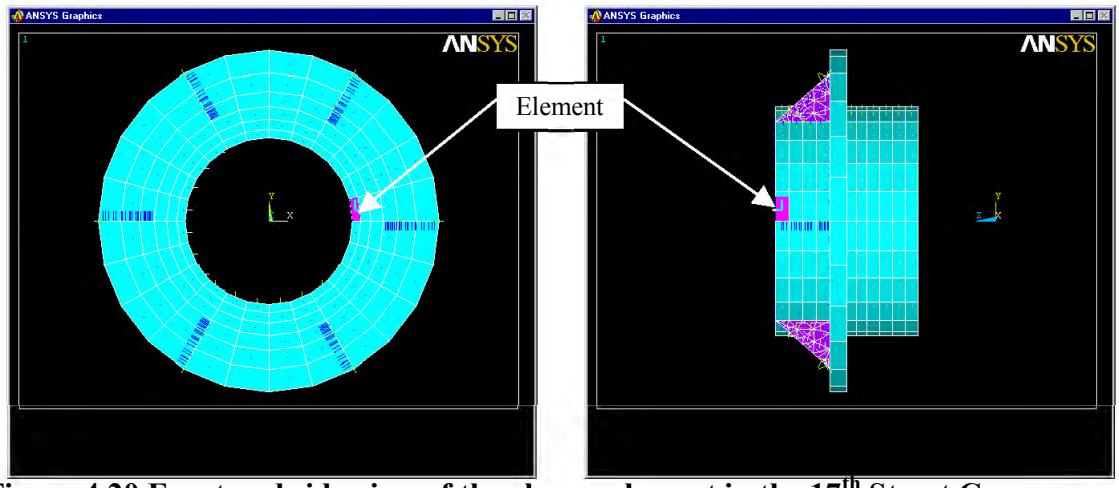

Figure 4.20 Front and side view of the chosen element in the 17th Street Causeway hub.

4.9.1 Assembly procedure 1 (AP1)

4.9.1.1 Full assembly process

The stresses, temperatures and critical crack lengths of the inner radius of the hub on the gusset side are plotted against time in Figure 4.21. Time periods for each step of the assembly process are listed in Table 4.8.

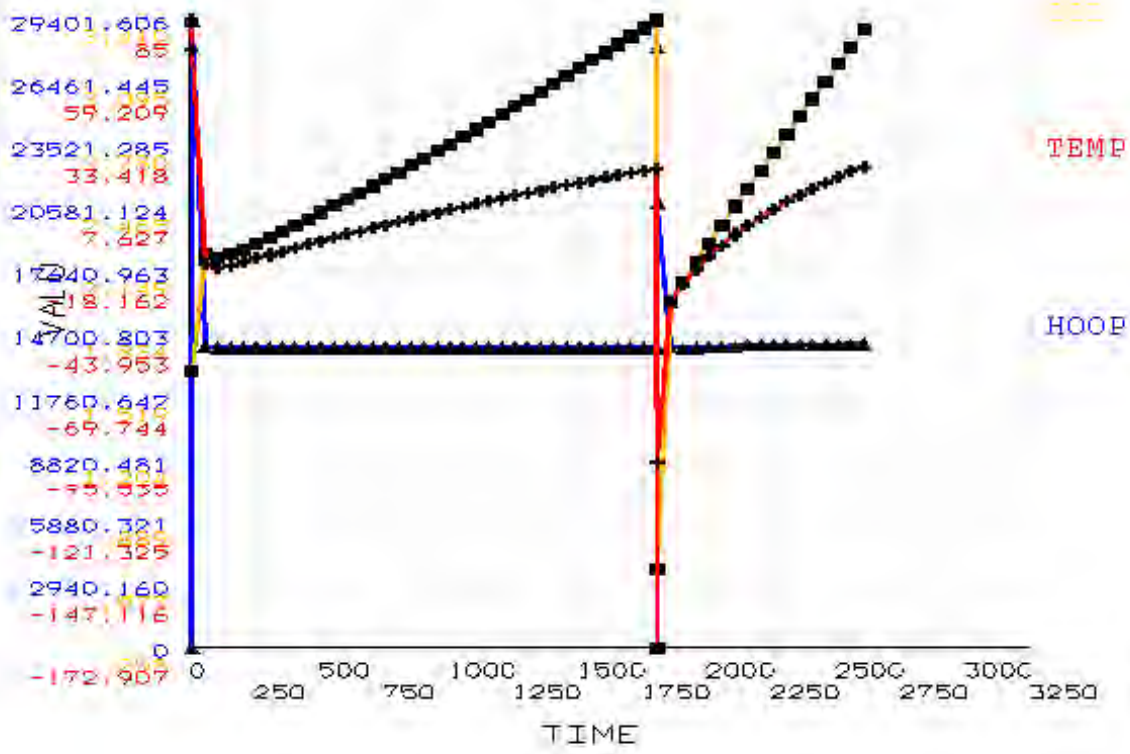

Figure 4.21 Critical parameters (CCL is critical crack length in inches, TEMP is temperature in ^{0}F, and HOOP is hoop stress in psi) plotted against time (full assembly process during AP1 of 17th Street Causeway Bridge).

Table 4.8 Time for each step of AP1 for the 17th Street Causeway Bridge.

Step	Starting time (min)	Ending time (min)
Cooling down of the trunnion	0	3
Sliding the trunnion into the hub	4	1803
Cooling down the trunnion-hub assembly	1803	1805
Sliding the trunnion-hub assembly into the girder	1806	2605

4.9.1.2 Cooling down of the trunnion

The stresses in the hub are not affected during the cooling down of the trunnion.

4.9.1.3 Sliding the trunnion into the hub

The hoop stress, the critical crack length and temperature during this step are plotted against time in Figure 4.22. Thermal and structural stresses due to interference

result in high hoop stresses after contact. As the temperature in the assembly converges due to the effects of conduction and convection, stresses due to interference become predominant. High values of critical crack length indicate a low possibility of failure.

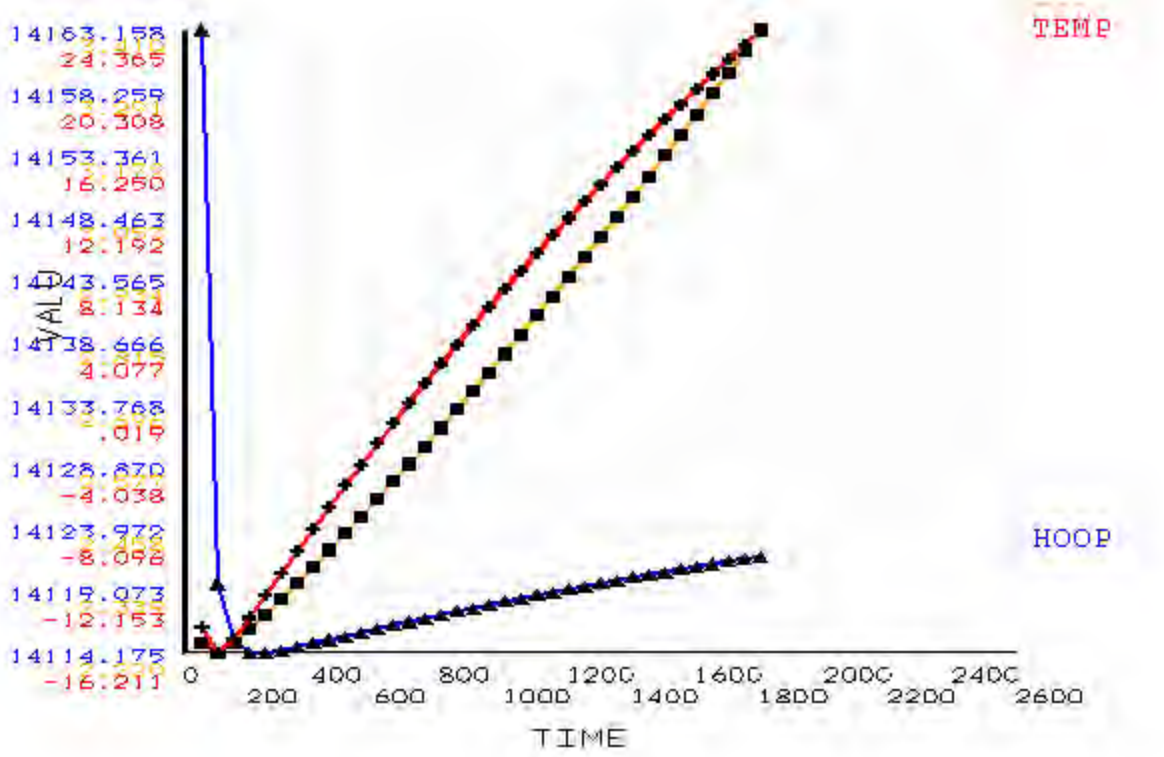

Figure 4.22 Critical parameters (CCL is critical crack length in inches, TEMP is temperature in ^{0}F, and HOOP is hoop stress in psi) plotted against time (sliding the trunnion into the hub during AP1 of 17th Street Causeway Bridge).

4.9.1.4 Cooling down the trunnion-hub assembly

The hoop stress, temperature and the critical crack length for this step are plotted against time in Figure 4.23. The results from the THGTM indicate that the lowest values of critical crack length during AP1 are observed during this step. Initially thermal and structural stresses reinforce each other and high hoop stresses occur as a result. As the trunnion-hub assembly nears steady state, the stresses due to interference dominate. An interesting point to note is that while the critical crack length in the Christa McAuliffe and Hillsborough assemblies stays low after its lowest point, here it rises steeply after its lowest point.

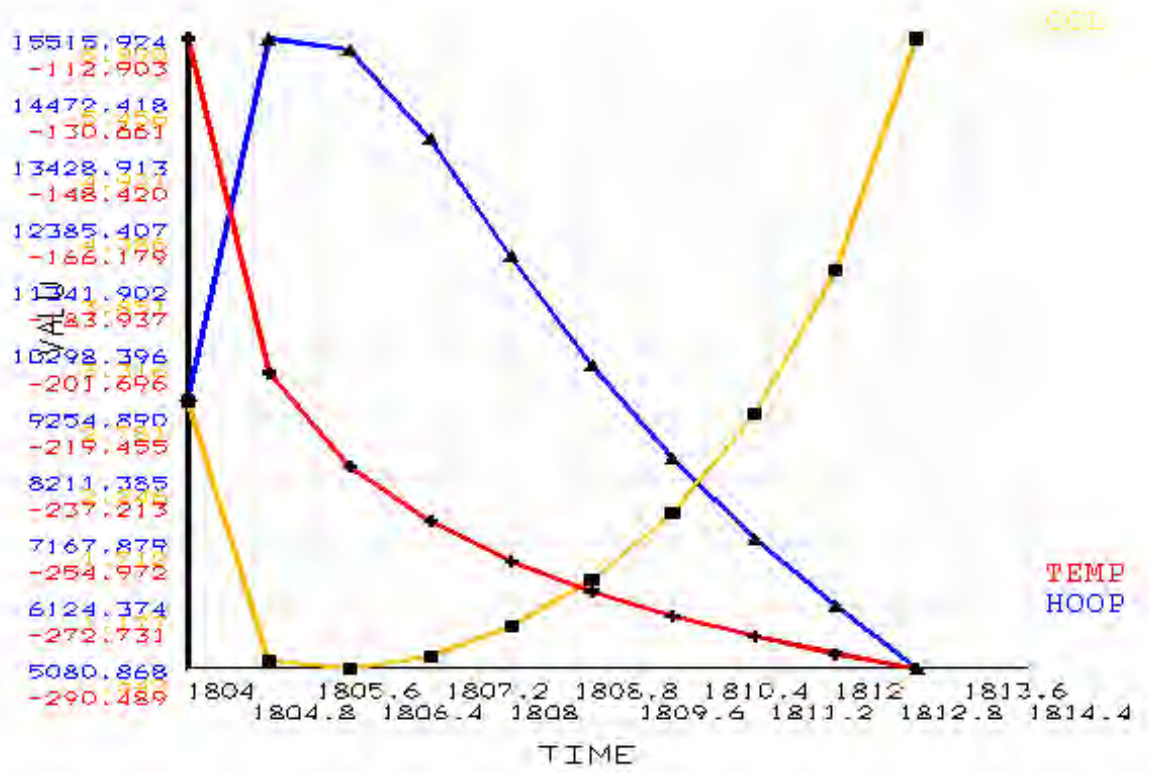

Figure 4.23 Critical parameters (CCL is critical crack length in inches, TEMP is temperature in ^{0}F, and HOOP is hoop stress in psi) plotted against time (cooling down of the trunnion-hub assembly during AP1 of the 17th Street Causeway Bridge).

4.9.1.5 Sliding the trunnion-hub assembly into the girder

The hoop stress, temperature and the critical crack length during this step are plotted against time in Figure 4.24. During this step, hoop stresses remain fairly stable primarily due to the remoteness of the inner radius of the hub from the hub girder interface. A rise in the temperature due to conduction and convection is accompanied with a rise in hoop stress. High values of critical crack length indicate a low probability of crack formation during this step.

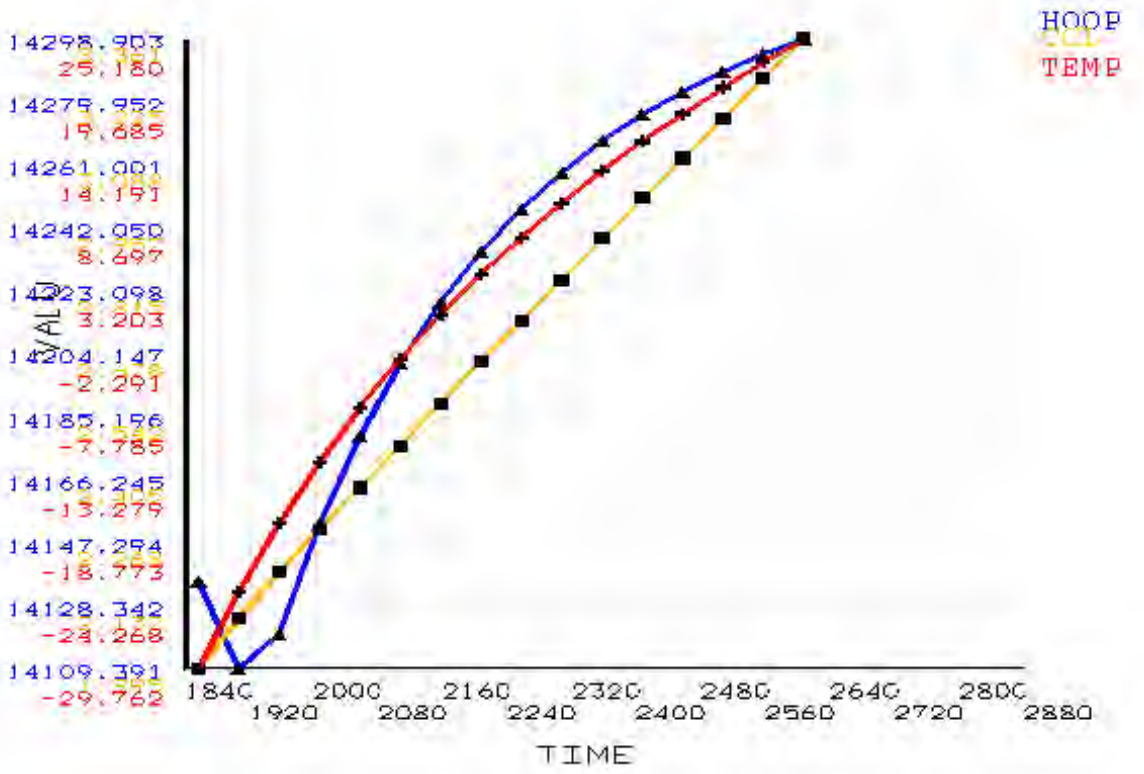

Figure 4.24 Critical parameters (CCL is critical crack length in inches, TEMP is temperature in ^{0}F, and HOOP is hoop stress in psi) plotted against time (sliding the trunnion-hub assembly into the girder during AP1 of the 17th Street Causeway Bridge).

4.9.2 Assembly Procedure 2 (AP2)

4.9.2.1 Full assembly process

The stresses, temperatures and critical crack lengths at the inner radius of the hub on the gusset side are plotted against time in Figure 4.25.

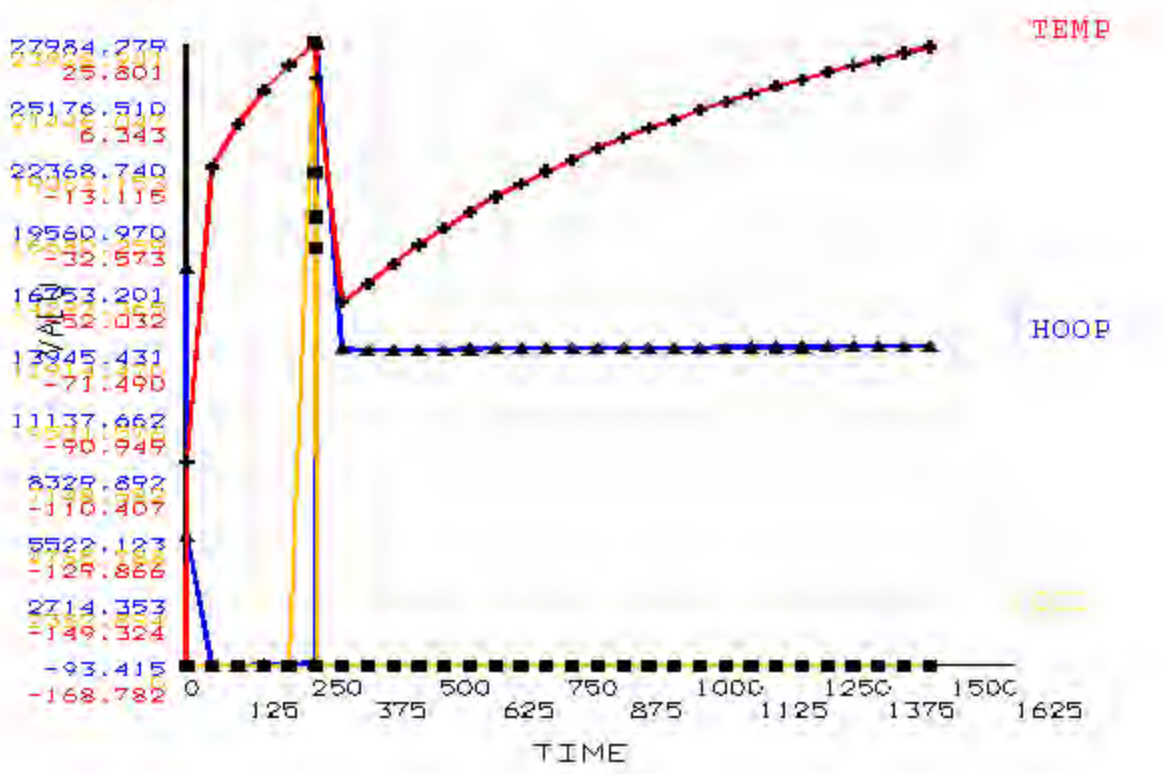

Figure 4.25 Critical parameters (CCL is critical crack length in inches, TEMP is temperature in ^{0}F, and HOOP is hoop stress in psi) plotted against time (full assembly process during AP2 of the 17th Street Causeway Bridge).

Table 4.9 Time for each step of AP2 for the 17th Street Causeway Bridge.

STEP	STARTING TIME (min)	ENDING TIME (min)
Cooling down of the hub	0	52
Sliding the hub into the girder	53	252
Cooling down the trunnion	252	256
Sliding the trunnion into the hub-girder assembly	257	1456

4.9.2.2 Cooling down of the hub

The stresses, temperatures and critical crack lengths during this step are plotted against time in Figure 4.26. A sharp thermal gradient at the inner radius of the hub initially results in high values of hoop stress at the inner radius interface. Over time, as the temperature gradient becomes less steep, the hoop stresses fall. The lowest value of critical crack length during AP2 is observed in this step. The critical crack length shows a distinctly different trend from that the trends observed in other bridges. Here, the critical crack length starts from a low value and climbs steeply as the temperature in the assembly falls, once again highlighting the differences between different bridges

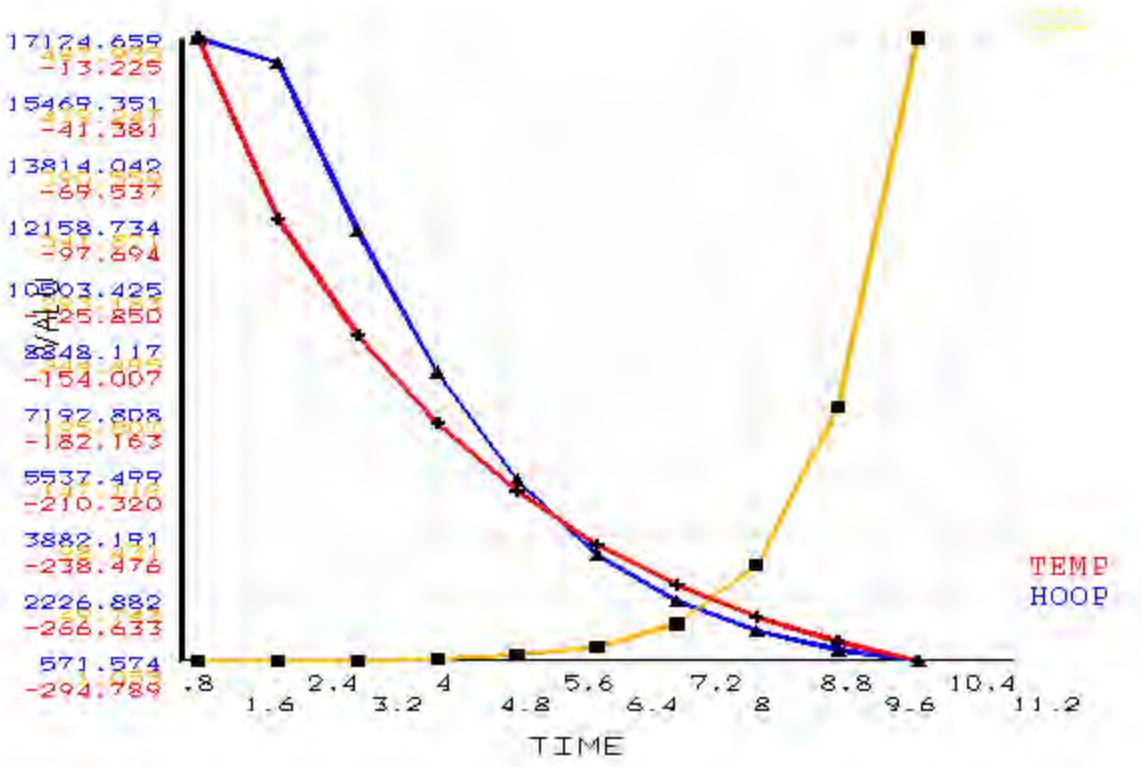

Figure 4.26 Critical parameters (CCL is critical crack length in inches, TEMP is temperature in ^{0}F, and HOOP is hoop stress in psi) plotted against time (cooling down of the hub during AP2 of 17th Street Causeway Bridge).

4.9.2.3 Sliding the hub into the girder

The stresses, temperatures and critical crack lengths during this step are plotted against time in Figure 4.27. The relatively low values of compressive hoop stress are explained by the remoteness of the inner radius of the hub from the hub-girder interface. The critical crack length is not defined for compressive hoop stress and hence is plotted as zero at these points.

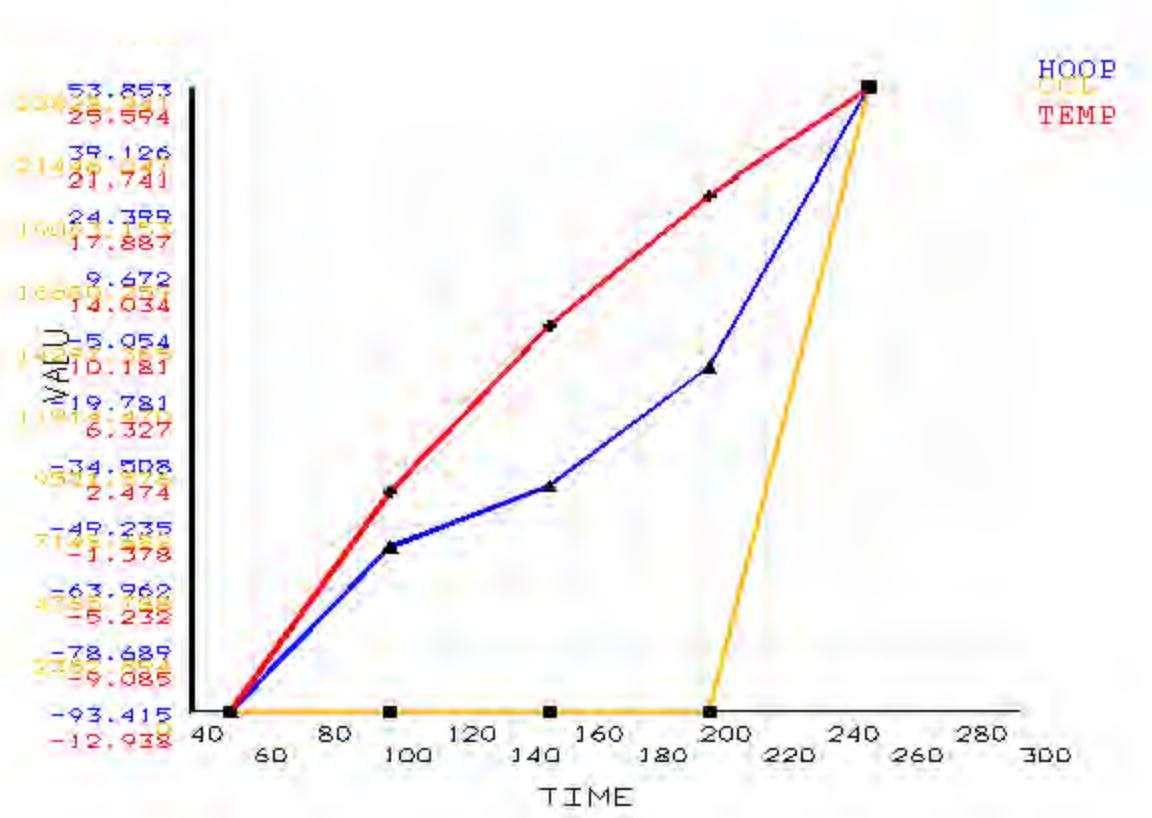

Figure 4.27 Critical parameters (CCL is critical crack length in inches, TEMP is temperature in ^{0}F, and HOOP is hoop stress in psi) plotted against time (sliding the hub into the girder during AP2 of the 17th Street Causeway Bridge).

4.9.2.4 Cooling down of the trunnion

The stresses in the hub are not affected during the cooling down of the trunnion.

4.9.2.5 Sliding the trunnion into the hub-girder assembly

The stresses, temperatures and critical crack lengths during this step are plotted against time in Figure 4.28. The behavior of hoop stress is somewhat different from that of other bridges. In the other two bridge assemblies, high initial hoop stress caused due to a thermal gradient is followed by a decrease in hoop stress as the assembly approaches steady state. Here the hoop stress increases and then decreases before increasing again. However the magnitude of this variation is is small. High values of critical crack length discount the probability of crack formation during this step.

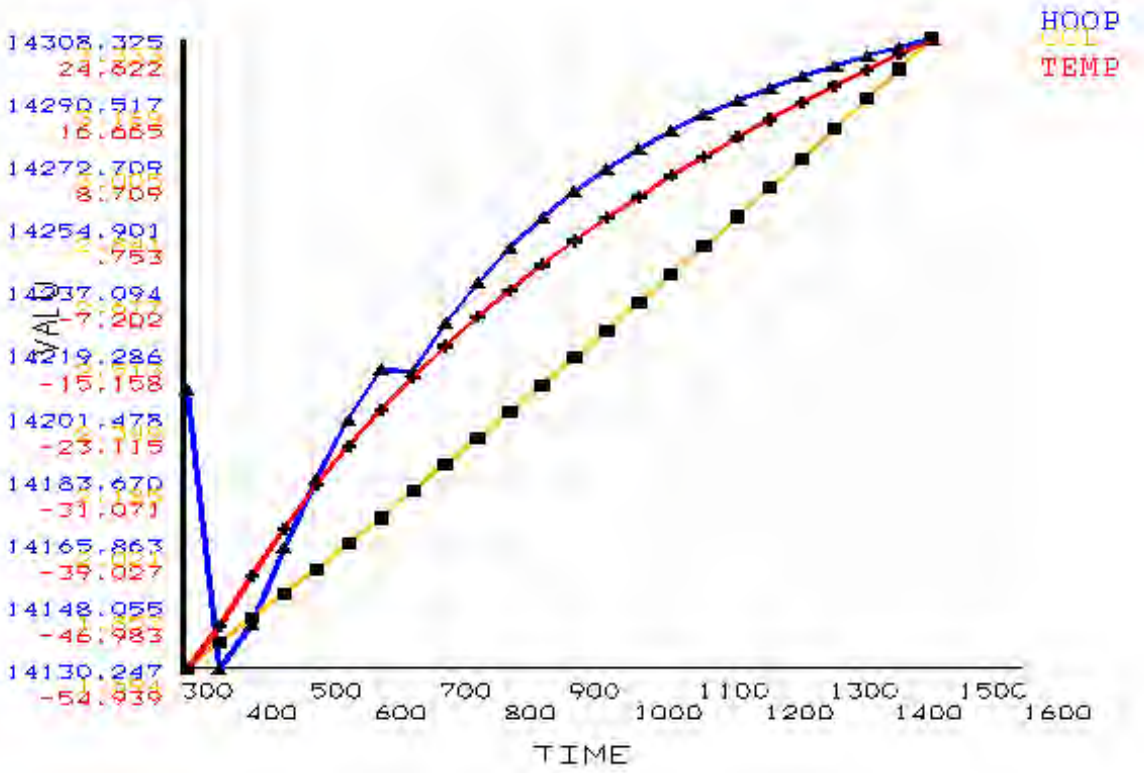

Figure 4.28 Critical parameters (CCL is critical crack length in inches, TEMP is temperature in ^{0}F, and HOOP is hoop stress in psi) plotted against time (sliding the trunnion into the hub-girder assembly during AP2 of the 17th Street Causeway Bridge).

4.10 Comparison

A comparison, for all of the bridges presented in the beginning of this chapter, of the highest hoop stress and critical crack length is presented in Table 4.10.

Table 4.10 Critical crack length and maximum hoop stress for different assembly procedures and different bridges.

BRIDGE	PARAMETER	AP1	AP2
Christa McAuliffe	Critical crack length (in)	0.2101	0.2672
	Maximum Hoop Stress (ksi)	28.750	33.424
Hillsborough Avenue	Critical crack length (in)	0.2651	0.2528
	Maximum Hoop Stress (ksi)	29.129	32.576
17th Street Causeway	Critical crack length (in)	0.6420	1.0550
	Maximum Hoop stress (ksi)	15.515	17.124

An examination of the results reveal significant differences in the behavior of each bridge. In some bridges, a lower critical crack length is found to occur during AP1 (that is, Christa McAuliffe and 17th Street Causeway) while in others (that is, Hillsborough Avenue) the opposite is true, however, only slightly. In addition, a slightly lower value of critical crack length during AP1 versus AP2 of Christa McAuliffe Bridge is observed. A simple comparison of critical crack lengths, however is not sufficient to

conclude the superiority of one assembly procedure over another for each bridge. A phenomenon called crack arrest described in the next section can explain how in some cases crack formation can be arrested in spite of low values of critical crack length during the assembly process.

The maximum hoop stress is less than the yield strength in all the bridge assemblies indicating that they will not fail.

4.11 Crack arrest

Crack arrest is the reverse of crack initiation. Small cracks present in the assembly grow fast after exceeding the fracture toughness of the material. Crack arrest may prevent these cracks from growing catastrophically. The condition required for this phenomenon to occur is evaluated by the parameter K_{Ia}, which is the critical crack arrest factor. Crack growth is arrested once

$$K \le K_{Ia} \tag{4.3a}$$

In Equation (4.3a), K is determined by the equation (Kanninen and Popelar, 1985)

$$K = f_e \sigma_\theta \sqrt{\pi a} \tag{4.3b}$$

where

K = calculated parameter based on the hoop stress, σ_θ, and the crack length, a,

σ_θ = tensile hoop stress, and

a = crack length.

The variation of K_{Ia} with temperature is shown in Figure 4.29a for A508 steel. It follows a trend similar to that of K_{Ic}.

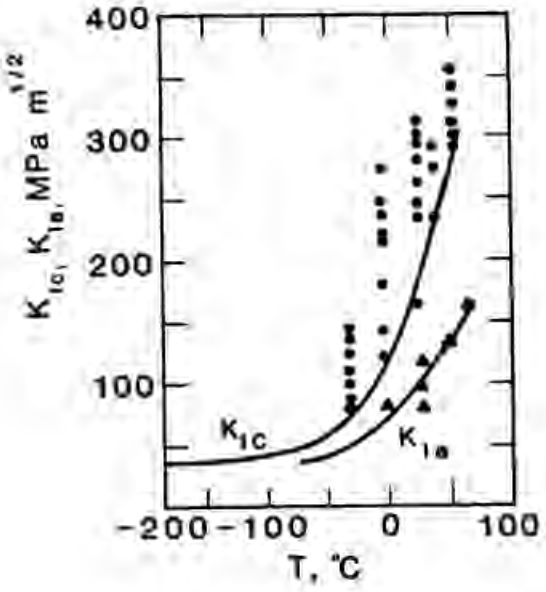

Figure 4.29a K_{Ia} and K_{Ic} against temperature for A508 steel (Kanninen and Popelar, 1985).

The crack length, a_a, at which crack arrest will occur is given by the Equation (4.3c).

$$a_a = \frac{K_{1a}^2(T)}{f_e^2 \pi \sigma_\theta^2} \tag{4.3c}$$

This phenomenon is of relevance to this study as sharp thermal gradients may result in low values of the fracture toughness, which may not necessarily lead to catastrophic crack growth. To illustrate this phenomenon, let us take the case of the Hillsborough Avenue Bridge. Figures 4.29b and 4.29c show the critical parameters during the cooling down of the trunnion-hub (AP1) and cooling down of the hub (AP2), respectively. The lowest value of critical crack length is lower during AP2 (0.1898 in) than during AP1 (0.5577 in). However, the critical crack length during AP1 remains low for a considerable period of time, whereas in AP2 it shows a sharp upward trend after its lowest point. From Figure 4.11a it is clear that the K_{Ia} and K_{Ic} follow similar trends. In AP2 crack growth initiated by $K > K_{Ic}$ may be arrested as $K \leq K_{Ia}$ with decrease in hoop stress. In AP1, the persistent low values of critical crack length indicate that the values a_a will also be low, thereby preventing crack arrest.

The possibility of crack arrest is greater when thermal stresses alone are present as they are transient and change rapidly. However, when a combination of both thermal and interference stresses are present, the possibility of crack arrest occurring is greatly reduced. Hence, crack arrest is more likely to occur during AP2 than during AP1.

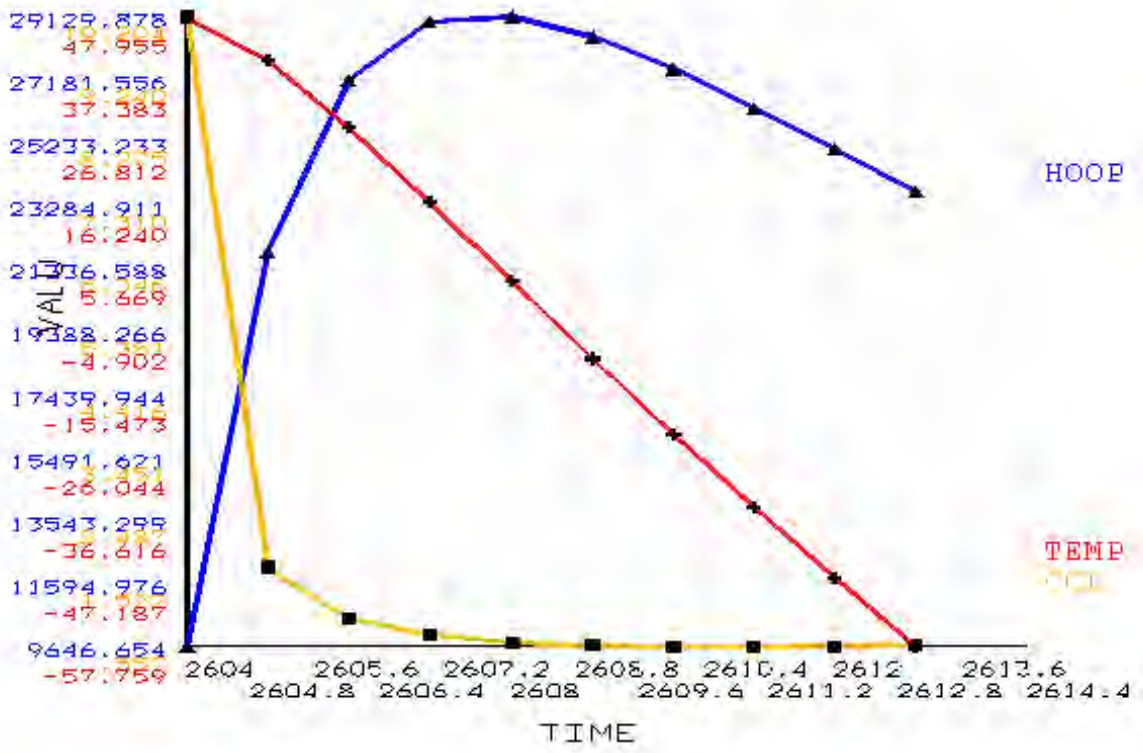

Figure 4.29b Critical parameters (CCL is critical crack length in inches, TEMP is temperature in ^{0}F, and HOOP is hoop stress in psi) plotted against time (cooling down of the trunnion-hub assembly during AP1 of the Hillsborough Avenue Bridge).

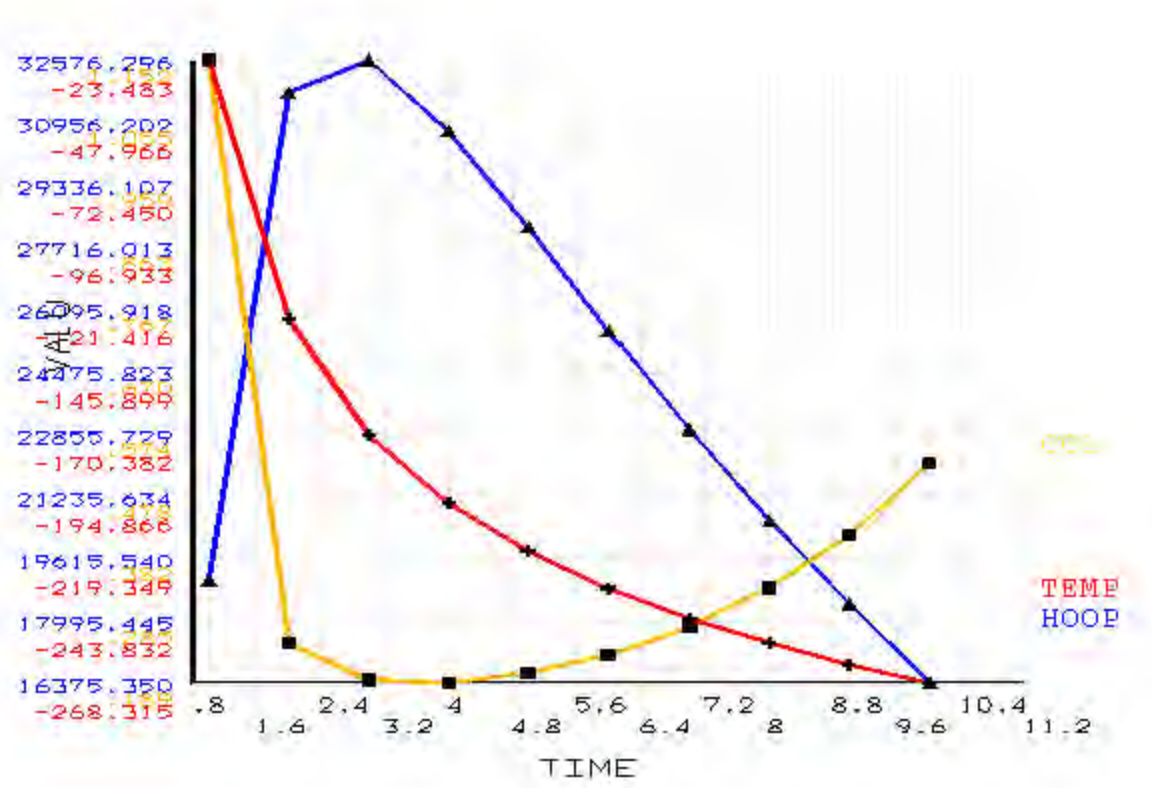

Figure 4.29c Critical parameters (CCL is critical crack length in inches, TEMP is temperature in ^{0}F, and HOOP is hoop stress in psi) plotted against time (cooling down of the hub during AP2 of the Hillsborough Avenue Bridge).

4.12 Possibility of failure during the insertion process and gap conduction

The most critical steps during the assembly process are determined to be the cooling processes. However, the possibility of failure during the warming up process also needs to be explored.

In this study male parts of the assembly are inserted into female parts as soon as the interference between them is breached. Hence, there is no gap conduction between the two parts. This is done principally because this models the worst case from the perspective of failure during the insertion of one part of the assembly into another. The reason for this explained next.

Thermal stresses are caused due to thermal gradients. Hence, the sharper thermal gradient (between the outer radius of the male part and inner radius of the female part) during the insertion of one part the assembly into another the greater are the thermal stresses. Cooling down a part of the assembly till the interference is breached results in a sharp thermal gradient between parts of the assembly. Whereas the male part down until there is gap between the two parts, and then subsequently warming parts of the assembly by a combination of convection and gap conduction up to the point of contact produces a less pronounced thermal gradient. This is so primarily because gap conduction results in faster heat flux and lowers the temperature difference between the outer radius of the male part and inner radius of the female part. Hence, the insertion of the male part into

the female part as soon as interference is breached is the worst case from the perspective of failure.

By modeling the worst case, we know which assemblies have a greater proneness to failure during the insertion process. For example, during AP1 of the Hillsborough Avenue Bridge, low values of critical crack length are noticed during AP1. Hence, it is advisable that during assembly we cool down parts of the assembly until there is a large gap between them during the assembly.

CHAPTER 5

EXPERIMENTAL SET-UP

5.1 Introduction

The objective of the experimental setup was to measure stresses and temperatures during the two different assembly procedures. This study utilized strain gages and thermocouples mounted on the trunnion, hub and girder. These sensors monitor strains and temperatures during all steps (cool down in liquid nitrogen and warm up in ambient air) as explained in Chapter 1.

Hence, the basic components of the setup were:

- A data acquisition system (to acquire data),
- A lap top computer (to initiate and control the data acquisition),
- Cryogenic strain gages (to measure strain),
- Thermocouples (to measure temperature), and
- Liquid nitrogen (cooling medium).

The details of some of these components are discussed in the following sections.

5.2 Data Acquisition System

The data acquisition system consisted of a chassis (see Figure 5.1) that carried signal-conditioning modules and was connected to a lap top computer by a PCMCIA card. The chassis employed was SCXI-1000 (National Instruments). This chassis can hold up to four SCXI modules. It powers SCXI modules as well as handles all timing, trigger, and signal routing between the SCXI modules.

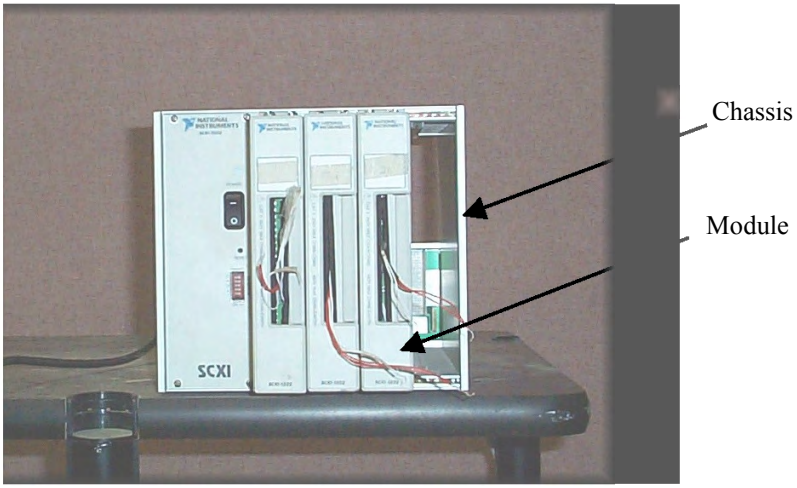

Figure 5.1 SCXI–1000 chassis with three SCXI-1122 modules.

The current study utilized three slots on the chassis. Each slot was occupied by a SCXI-1122 module. These modules monitor 48 channels of data, that is, 12 thermocouples and 36 strain gages (3 strain gages on each rosette).

The SCXI-1122 is a sixteen-channel isolated signal-conditioning module. It multiplexes sixteen inputs into a single isolation amplifier with gains ranging from 0.01 to 2,000. It also has one current and one voltage source for transducer excitation. It is

ideal for amplification and isolation of millivolt and volt inputs, thermocouples, and strain gages where scanning speeds are low. The low pass filter on the SCXI-1122 can be set to filter out noise at either 4Hz or 4000Hz. The "settling time" with a filter setting of 4 Hz is one second. This means that the fastest rate of data acquisition is one channel per second. This was adequate for the rate at which strains or temperatures were varying in the experiments carried out in this study. The filter was set to 4 Hz to filter out the 60 Hz noise from power lines.

The chassis was connected to the lap top computer via a PCMCIA card. The software used for acquiring the data was National Instruments LabVIEW (see Section 5.5 for details).

5.3 Strain Gages

The strain gages used were Measurements Group's, 'WK-06-125RA-350'. Here,

- The 'W' refers to the epoxy-phenolic resin encapsulation of the gage. 'K' refers to the strain-sensitive 'K-alloy' used in the foil grid. It is a modified Nickel-Chromium alloy in self-temperature compensated form, which can withstand -321^0F.
- '06' is the 'self-temperature compensation', the approximate thermal expansion coefficient of the structural material on which the gage is to be used (steel).
- '125' is the active gage length in mils (10^{-3} inch). 'RA' refers to the rectangular rosette grid and tab geometry.
- '350' is resistance of the gage in ohms.

A strain gage utilizes a Wheatstone bridge circuit to monitor change in resistance of the strain gage. The resistance changes when the strain gage gets deformed due to mechanical load. For a detailed explanation of the working of strain gage, refer to Dally and Riley (1993). All strain gages were coated with N-1 (chloroprene rubber) moisture proof coating.

5.4 Thermocouples

Thermocouples were chosen to measure the temperature because they are inexpensive, rugged, and can operate over a very wide range of temperatures Type-E thermocouples were chosen since this type gives the highest millivolt output per degree change in temperature in the cryogenic temperature range

The thermocouples used were Omega's '5TC-TT-E-20-120'. Here,

- '5TC' means ready made insulated thermocouples.
- 'TT' refers to the PFA teflon insulation.
- 'E' is the type of thermocouple (thermoelectric pair is chromel-constantan).
- The '20' and the'120' are the AWG and length of the wire, respectively.

A thermocouple operates on the principle that the junction of two dissimilar metals generates a voltage that varies with temperature. However, measuring this voltage is difficult because connecting the thermocouple to the data acquisition board measurement wires creates what are called the reference junctions or cold junctions. These additional junctions act as thermocouples themselves and produce their own voltages. Thus, the final measured voltage includes both the thermocouple and reference-junction voltages. The method of compensating for these unwanted reference-junction

voltages is called cold-junction compensation. This consists of an additional sensor (thermistor) mounted on the data acquisition module that measures the ambient temperature at the cold junction. The software can then compute the appropriate compensation for the unwanted thermoelectric voltages. For a detailed explanation of the working of a thermocouple, refer to Dally and Riley (1993).

5.5 LabVIEW Program

LabVIEW is a graphical programming development environment based on the G programming language for data acquisition and control, data analysis, and data presentation. Each LabVIEW program is called a "Virtual Instrument"(VI). Developing any VI involves setting up various sub-VIs (sub-routines), each for doing one particular task. Each VI has two windows, the "front panel" window that serves as the user interface and the "diagram" window where the actual code is written. The VI written for this study is called, "Strain-Temperature.vi". The front panel window and graphical code in the diagram window of this virtual instrument are shown in Figures 5.2 and 5.3.

The two graphs on the front panel display temperatures in Fahrenheit, and strain in microstrains (10^{-6}), respectively. The blocks on the right side of each graph are the "digital displays" for displaying the current value of each channel corresponding to the legend. "File header text" refers to any header or note that the user wants to save into the text file along with the data. Typical examples could include the details of the test being done or the positioning of the strain gages on the cylinder.

A delay period knob on the front panel gives the user the flexibility of changing the time interval between successive scans during the execution of the program. This delay refers to the delay period between consecutive scans not between successive channels (delay period between two successive channels is already fixed to one second as explained in Section 5.2). Typical cooling periods range from five to thirty minutes, while warm up typically takes four to eleven hours. A high rate of change of stress during cool down necessitates the maximum scan rate (one channel per second). The slow rate of change of stress in warm up means that a much lower scan rate can be used without losing any useful information. A slower scan rate reduces wear of the mechanical relays on the data acquisition module.

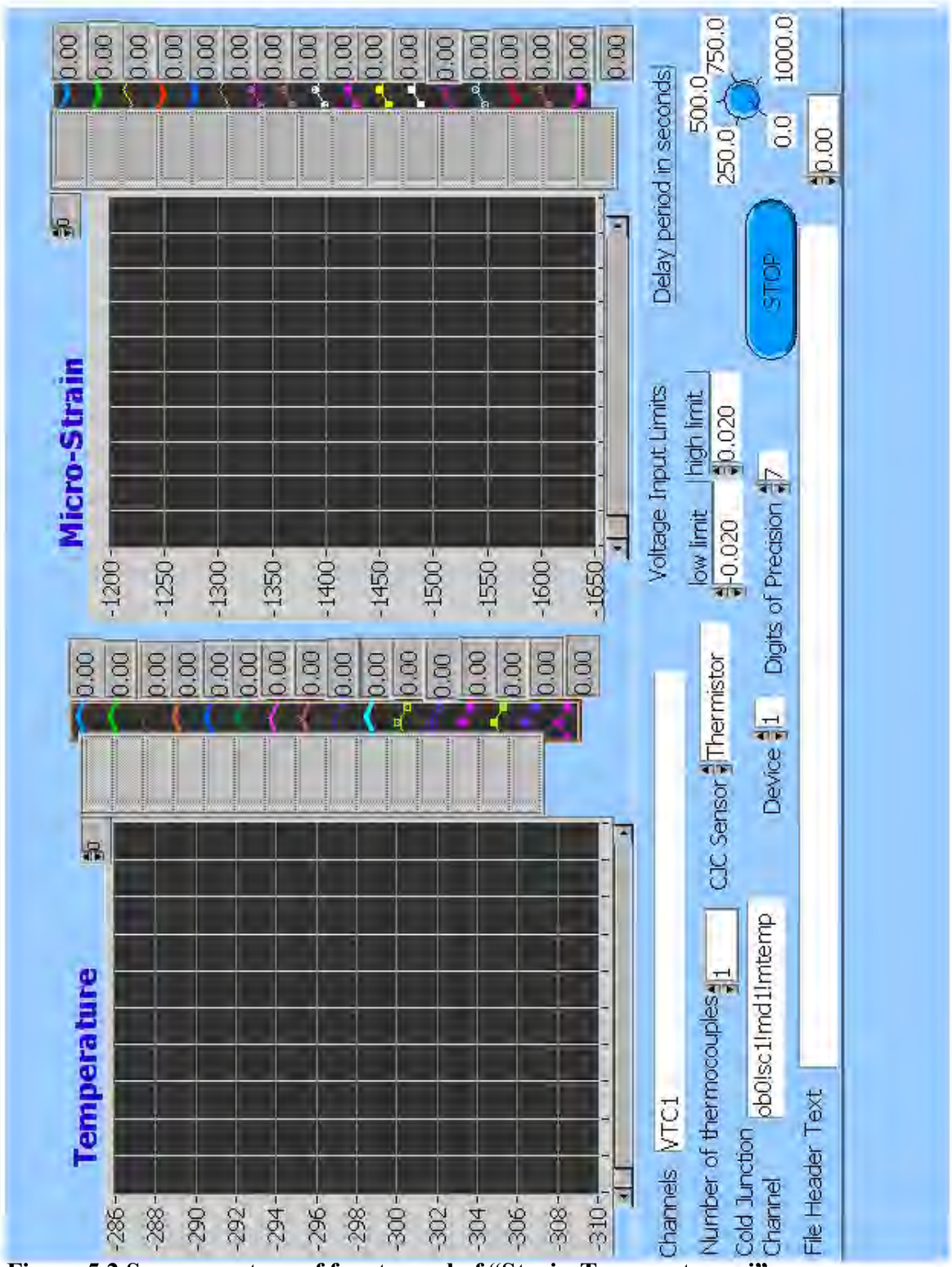

Figure 5.2 Screen capture of front panel of "Strain-Temperature.vi".

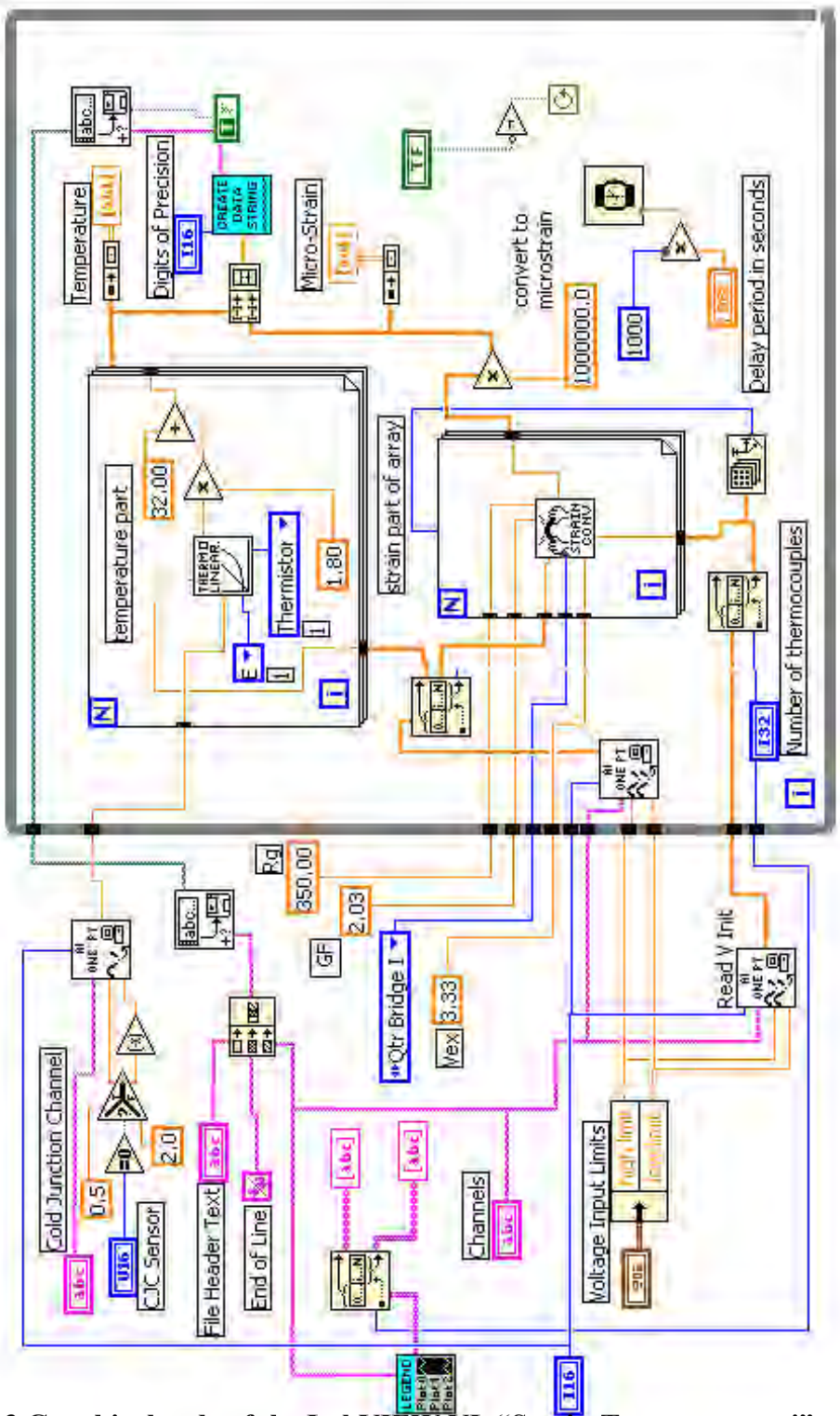

Figure 5.3 Graphical code of the LabVIEW VI, "Strain-Temperature.vi".

The 'Strain-Temperature' virtual instrument essentially does the following things:

- Reads the voltage output of each sensor into an array using "AI Sample Channels.vi"
- Splits this array into two sub-arrays, temperature and strain
- Converts voltages to temperatures using "Convert Thermocouple Reading.vi"
- Converts voltages to strains using "Convert Strain Gauge Reading.vi"
- Writes the data to a text file using "Write Characters to File.vi"

After the experiment is completed, the data in the text file is post-processed using Excel.

5.6 Post-Processing of Data

The post processing of the data mainly involves converting the strains recorded on each of the three channels of a rosette into hoop stress. To do this, first the 'recorded' strain has to be corrected to the 'true' strain by subtracting the 'apparent' strain from it.

Apparent strain is the strain induced in a strain gage purely due to a temperature change. In all experiments in the current study, a strain gage is mounted on the trunnion (or hub) room temperature, and then it is cooled in liquid nitrogen (-321^0F). This large change in temperature, alone produces a strain reading of approximately –1250 microstrains in the strain gage. This curve needs to be subtracted from the curve of recorded strain.

A typical apparent strain curve is shown in Figure 5.4. To obtain the apparent-strain curve, a thin specimen ($1" \times 0.5" \times 0.25"$) of the same grade of steel with the same type of strain gage mounted on it is subjected to a temperature excursion wherein there is no thermal stress produced in the specimen. This ensures that the strain being recorded is purely apparent strain.

For a detailed explanation of apparent strain, refer to Measurements Group Technical Note-504, 'Strain Gage Thermal Output and Gage Factor Variation with Temperature' (Measurement Group Technical Notes).

It is to be noted that this apparent strain, if uncorrected, can be a very significant source of error. For example, at the temperature of -321^0 F, the apparent strain value of a WK gage mounted on a steel substrate is close to –1250 microstrains, which translates approximately to an error of –37.5 ksi of stress (assuming an uni-axial stress state). After correcting for apparent strain, the true strains were converted to stresses using Hooke's Law, with a value of 30 Msi for Young's modulus of elasticity and a value of 0.3 for the Poisson's ratio.

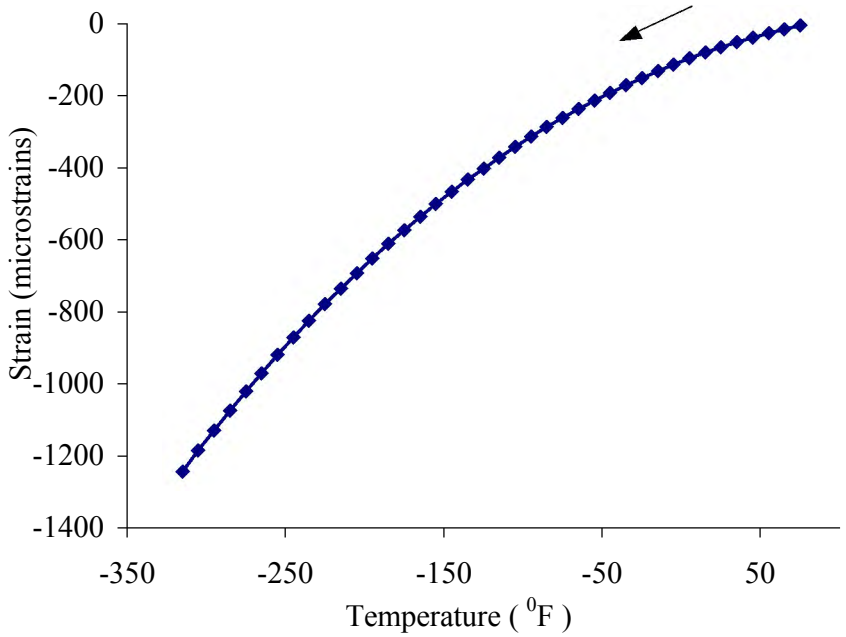

Figure 5.4 Typical apparent strain curve for WK strain gage on mild steel.

The experimental set-up described in this chapter was utilized to conduct a few verification experiments in the beginning of the study (see Appendix A).

These experiments were :

- Verification of thermocouples and their epoxy,
- Cantilever beam experiment, and
- Differential expansion between a steel sleeve and a brass bolt.

These simple experiments were designed to verify the working of the entire experimental set-up including all of its components (gages, thermocouples, bonding agents, moisture proofing agents and connecting wires). These experiments played a vital role in understanding the response of thermocouples and strain gages to the temperatures of liquid nitrogen. They served as preliminaries to the full-scale tests (see Chapter 7) done later. In addition to these preliminary experiments, a THG Assembly Procedure 1 was performed on a quarter-scale model, which is discussed in the next chapter.

CHAPTER 6

EXPERIMENTAL QUARTER-SCALE MODEL

6.1 Introduction

A preliminary THG assembly using AP1 was carried out on a trunnion and hub that were approximately one-fourth the dimensions of the full-scale components. The dimensions of the trunnion and hub are given in Table 6.1.

Table 6.1 Geometry of quarter-scale model.

Component	Internal Diameter (inches)	Outer Diameter (inches)	Height/ Length (inches)	Trunnion-Hub Interference (inches)
Trunnion	1.5	3.92	9.0	0.004
Hub	3.92	8.0	5.0	

6.2 Assembly of Quarter-scale Model using AP1

6.2.1 Steps in Assembly of Quarter-scale Model

The Quarter-scale Model was assembled using AP1, with a modification of the girder being excluded. So, the following steps were performed on the trunnion and the hub:

Step 1 Trunnion cool down
Step 2 Trunnion fitted into hub (see Figure 6.1)
Step 3 Cool down of the trunnion-hub

Figure 6.1 Cooled trunnion being inserted into the hub.

6.2.2 Positions of Gages (Quarter-scale Model)

Figures 6.2 and 6.3 show details of the positions of the gages on the trunnion and the hub, respectively. The thermocouples were mounted approximately half inch from

each strain gage. So, each mark in Figures 6.2 and 6.3 represents a set of one strain gage and one thermocouple. The positions of these gages on the trunnion were chosen with an objective of monitoring stresses at the trunnion inner diameter (Gage-A), outer diameter (Gage-B), near the trunnion-hub interface (Gages-D and DM) and one inch away from it (Gage-C). The notation 'DM' means mirror for Gage-D, since this Gage-DM was identical to Gage-D. The gages on the hub were placed on the hub inner diameter (Gages-E and F), mid-diameter (Gage-G), outer diameter (Gages-H and I) and on the curved surface below the top face (Gages-J and K).

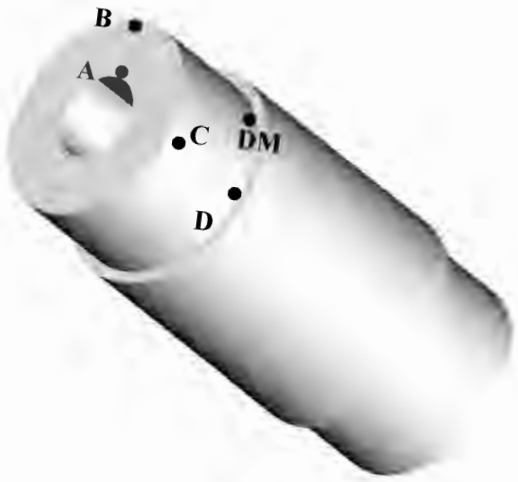

Figure 6.2 Positions of gages on quarter-scale trunnion.

Figure 6.3 Positions of gages on quarter-scale hub.

6.2.3 Results of Trunnion Cool down (Step 1)

As the first step of AP1, the trunnion was cooled down by immersion in liquid nitrogen. Figure 6.4 shows the surface temperature of the trunnion as recorded by the thermocouple, C-T. This cooling curve has three distinct zones, with different slopes (cooling rates). This is a result of "Pool-Boiling" heat transfer (Barron 1999), which takes place when the trunnion at room temperature is immersed in liquid nitrogen.

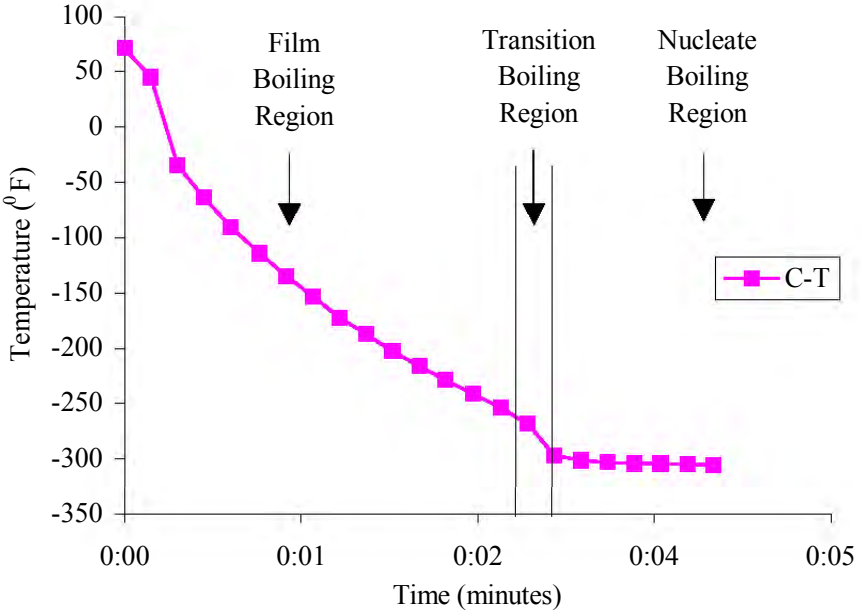

Figure 6.4 Temperature of the quarter-scale during cool down.

A typical Pool-Boiling curve for liquid nitrogen (Barron 1999) is shown in Figure 6.5. It has three regions; namely film boiling, transition boiling and nucleate boiling. Assuming that the saturation temperature is 70^0F, these three regions are defined by: film boiling from -260^0F to 70^0F, transition boiling from -290^0F to -260^0F and nucleate boiling from -320^0F to -290^0F. Figure 6.6 plots variation of the convection heat transfer coefficient with temperature. These values were derived from the heat flux plot versus ΔT, $(t_w - t_{sat})$ in Figure 6.5 (heat flux divided by ΔT gives h).

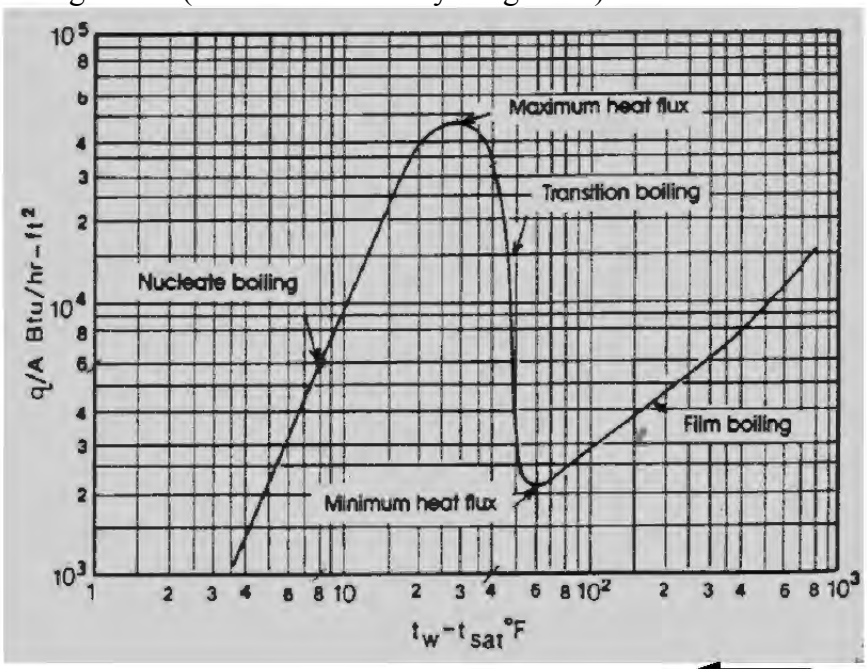

Figure 6.5 Boiling curve for pool boiling of liquid nitrogen.

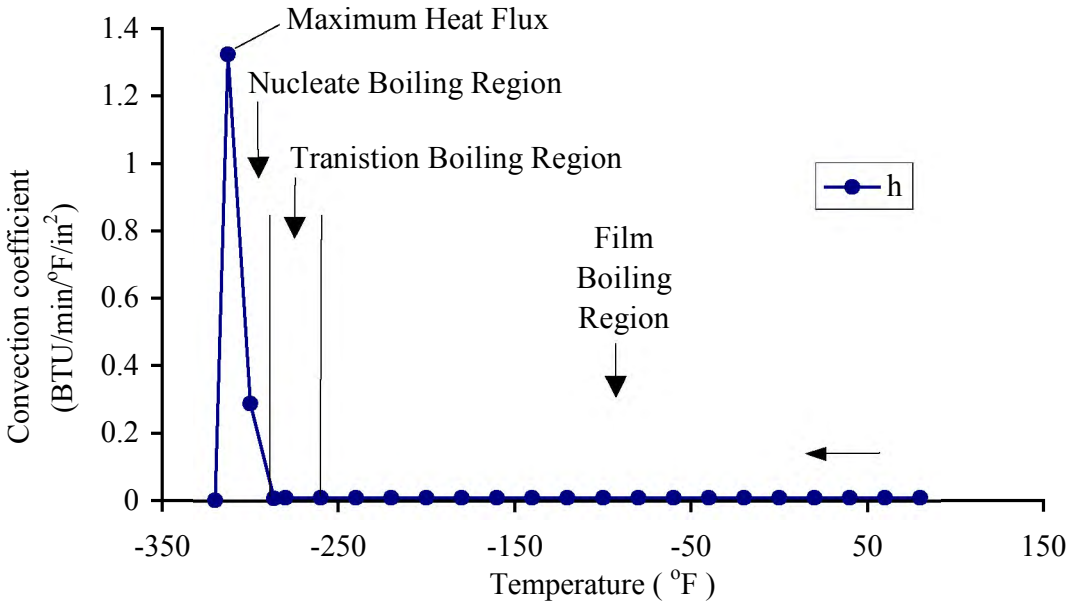

Figure 6.6 Variation of heat transfer coefficient with temperature.

Convective heat transfer is the product of the convection heat transfer coefficient (h), surface area (A) and the temperature difference (ΔT). When the trunnion is immersed into liquid nitrogen, there is a large temperature differential of approximately 400^0F between the trunnion and liquid nitrogen. This brings film boiling into play (far right of curve in Figure 6.5). The initial temperature differential results in a very high cooling rate, which can be noticed in the first thirty seconds of the cooling curve in Figure 6.4 (It is to be noted from Figure 6.6 that the value of *h* remains fairly constant (0.095 BTU/min/^{0}F/in^2) during film boiling).

As the trunnion begins to cool, the temperature difference keeps dropping, and the heat transfer follows the curve in Figure 6.5 from right to left. After film boiling, the heat transfer enters the transition boiling region. At the end of this transition region, the heat flux plot goes through a peak called "Peak Nucleate Boiling Point (PNBP)". This can also be seen in Figure 6.6, wherein the value of *h* rises approximately by a factor of 100. This phenomenon results in an increase in cooling rate, thereby making the cooling curve steeper at approximately the third minute in Figure 6.4.

Finally, when the temperature difference left between the trunnion and the liquid nitrogen drops to a small difference, the heat transfer enters the nucleate boiling region. During this cool down, the outer and inner diameter surfaces of the trunnion cool faster than the core, thereby resulting in a thermal gradient within the trunnion. The outer and inner surfaces tend to shrink faster than the core. This results in development of tensile hoop stresses on the outer surfaces of the trunnion. So, the hoop stress profiles shown in Figure 6.7 can be explained directly in relation to the above discussion of pool boiling heat transfer. Figure 6.8 shows the hoop stress as a function of time instead of temperature (Figure 6.7).

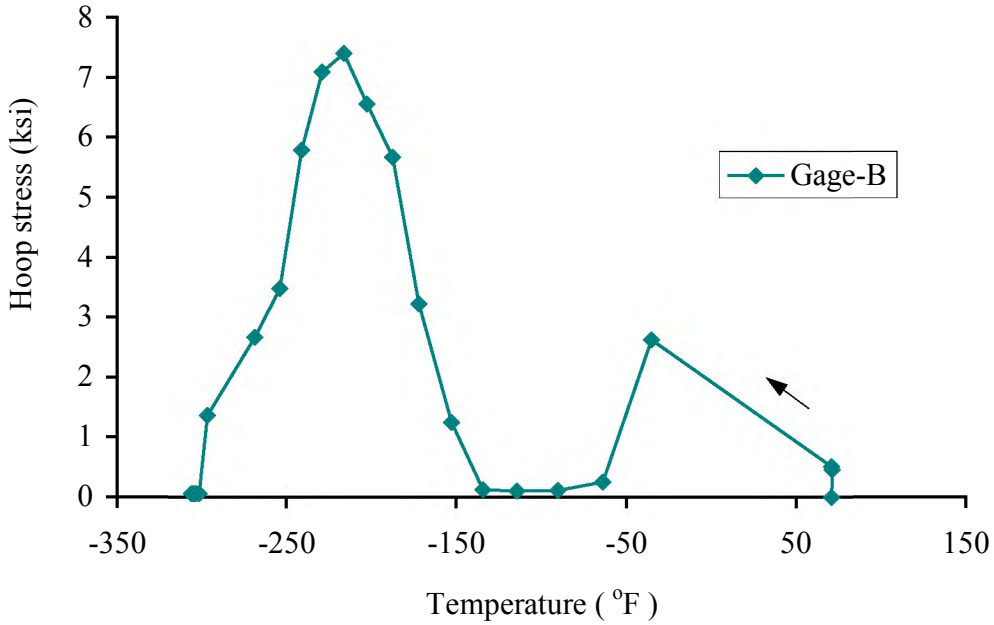

Figure 6.7 Hoop stress during trunnion cool down.

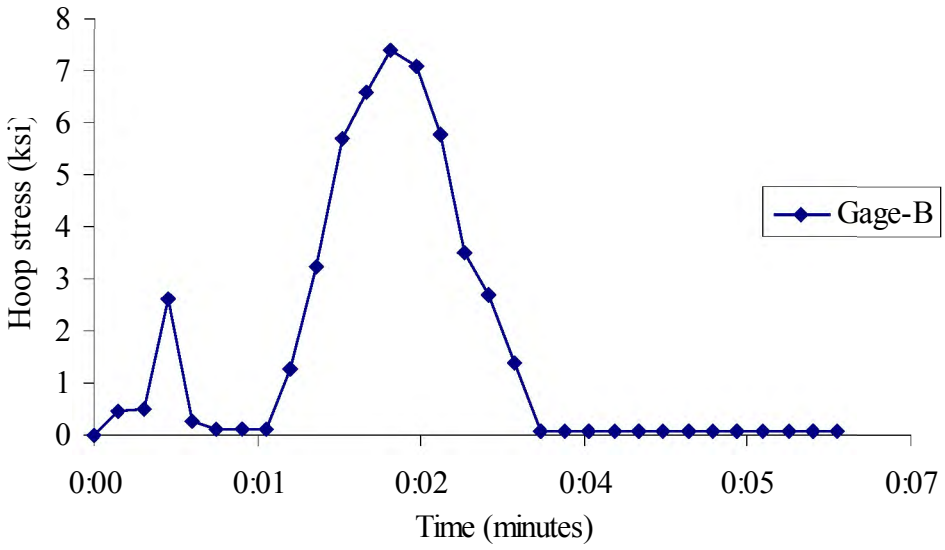

Figure 6.8 Hoop stress as a function of time.

This plot indicates that hoop stress peaks up at two points during the cooling curve. The first peak is a direct result of the high rate of heat transfer due to a large temperature difference at the start of the cooling curve. The second peak is a result of the PNBP. This phenomenon is repeated in the cool down of the trunnion and the hub of the full-scale models (Chapter 7).

Figure 6.9 illustrates the comparison of the hoop stresses as determined by the experiment against the stresses predicted by the finite element analysis model developed by Ratnam (2000). The comparison between the experimental and the FEA stresses is

not exact. One reason for this being that the value of *h* used in the FEA program was derived from a typical Pool-Boiling curve. This data is a function of several parameters such as surface roughness, geometry, orientation of the surface. Another reason that contributes to the difference between FEA and experimental stresses is that FEA applies the convection load as a 'step load'. If the load is applied as 'ramped', the results change significantly (15%) moving closer to experimental results. Simulating the actual loading as either a step or a ramp is a matter of choice, as neither case totally captures the actual physical conditions of the problem.

Also, the FEA model could not be programmed to incorporate the PNBP. Convergence problems were encountered in the solution for the FEA model in which the value of the convection heat transfer coefficient increased by a factor of 100 at PNBP. Since, the PNBP could not be incorporated into the FEA model, the stresses predicted by the FEA would be meaningful only for the region of film boiling. That is the reason why the FEA stresses in Figure 6.9 are shown only for the temperature range of -150^0F to 70^0F. The above-mentioned reasons hold true for Figure 6.10 as well.

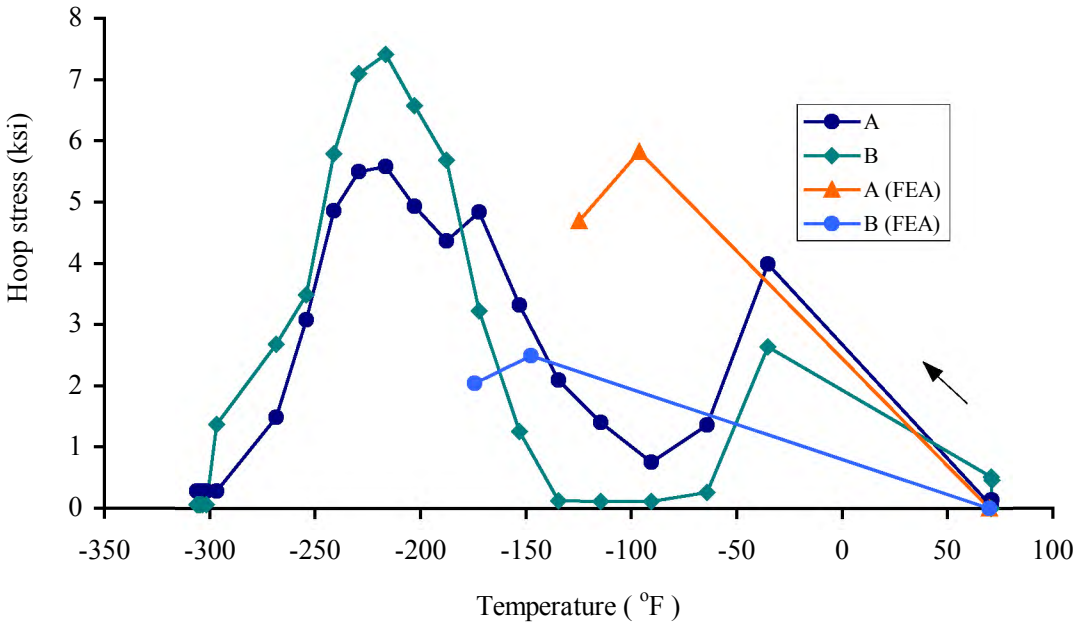

Figure 6.9 Experimental and FEA hoop stresses for gages A and B.

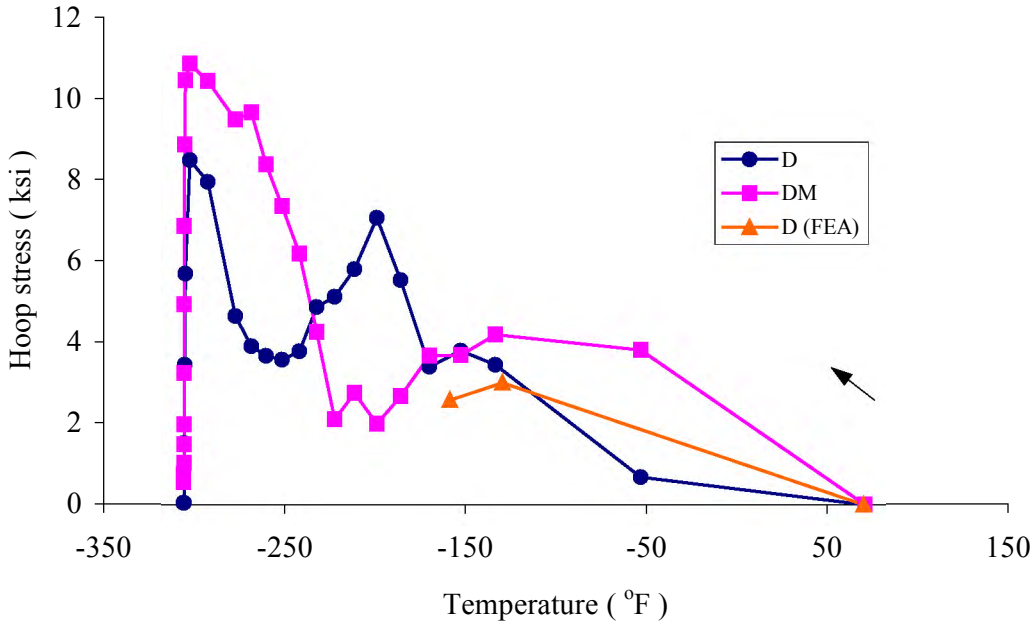

Figure 6.10 Experimental and FEA hoop stresses for gages D and DM.

It is evident from Figure 6.9 that the inner diameter cools differently from the outer diameter and therefore develops different stress. Although, it would be expected that gages D and DM (see Figure 6.10) would read the same stresses since they are at identical locations. The reason that these two gages read different stresses is the nature of the boiling process. Boiling of liquid nitrogen over a steel body (which was initially at room temperature), is a very turbulent process, therefore is not uniform from one point on the surface to the other. The values of the stresses differ due to this non-uniformity of the boiling phenomenon.

6.2.4 Results of Trunnion Warm up into the Hub (Step 2)

When the cold trunnion was inserted into the hub that was at room temperature, the heat transfer between them resulted in warm up of the cold trunnion and cool down of the hub for an initial period. After approximately seven minutes in this case of the quarter-scale model (see Figure 6.11), both the trunnion and the hub had achieved the same temperature (approximately -10^0F). From this point onwards, both of them warmed up together to room temperature.

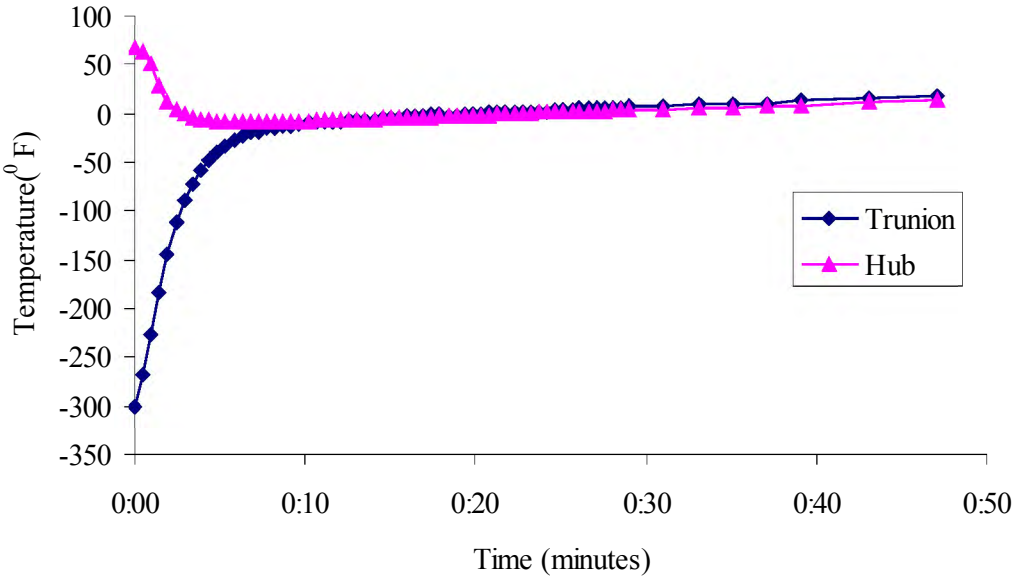

Figure 6.11 Trunnion and hub temperatures during trunnion warm up into the hub.

The hoop stresses developed in the hub during Step 2 of AP1 are shown in Figure 6.12. It illustrates stresses recorded by gages, E (representative of the hub inner diameter) and H, I, J, and K (representatives of the hub outer diameter).

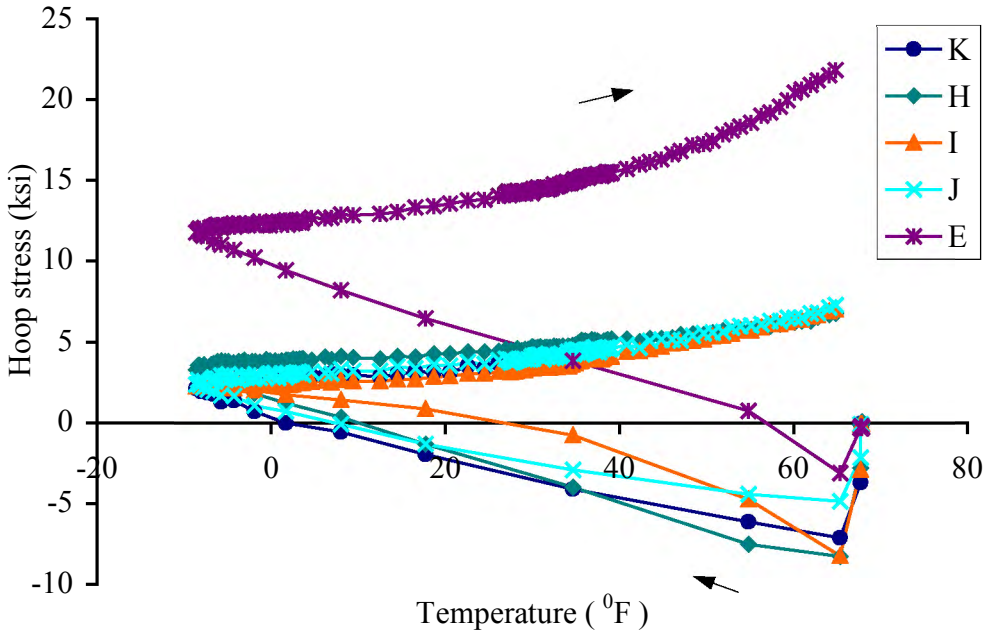

Figure 6.12 Transient stresses in hub.

The plots in Figure 6.12 start on the extreme right at the temperature co-ordinate of 70^0F. The hub was at this temperature before the cold trunnion was inserted into it. At this point, the inside of the hub is being cooled by the trunnion and the outside of the hub

is still in contact with ambient air. This thermal gradient generates thermal stresses in the hub, which are developed in the hub right at the outset (rightmost portion of the curve). As the hub cools further (curves moving from right to left), the temperature distribution within the hub becomes more uniform as a result of conduction heat transfer within the hub itself. So, the thermal stresses begin to decrease too.

As the trunnion warms up, it begins expanding within the hub. The interference fit between the trunnion and the hub starts to set in. This generates tensile stresses on the hub. With progress in the warm up, the interference increases since the trunnion diameter tries to achieve its original value, which is 0.004" bigger than the internal diameter of the hub. This increasing interference results in increase in the structural stress on the hub as temperature increases from -10^0F to 70^0F.

Gage-E picks up the highest stress since it is on the inner diameter of the hub. The remaining four gages (H, I, J and K) read close to each other (within 7%) since they are in geometrically identical positions. This warm up process (unlike the cool down process) is a slow process, and the change in structural stress as well as thermal stress occurs gradually and hence gives a more uniform stress field with respect to geometry.

During the warm up of the trunnion into the hub, the trunnion itself developed some stresses, but these were found to be in the range of –1 ksi to +4 ksi. These numbers are significantly lower than those in the hub. These stresses would not cause any damage or failure. Hence, their plots against time/temperature have been excluded. A comparison of the steady state stresses from experiment and from the finite element program is summarized in Table 6.2.

Table 6.2 Steady state hoop stresses at the end of trunnion warm up into the hub.

COMPONENT	GAGE LOCATION	GAGE	EXPERIMENTAL VALUES (ksi)	FEA VALUES (ksi)	PERCENTAGE DIFFERENCE (%)
Hub	Hub-inner diameter	E	21.774	19.614	10.43
	Hub-outer diameter	H	6.771	6.313	7.00
	Hub-outer diameter	I	6.988	6.313	10.14
Trunnion	Trunnion-inner diameter	A	5.368	4.237	23.55
	Trunnion-curved side	C	0.174	0.705	-120.81[4]
	Trunnion-curved side	DM	-2.912	-1.344	73.68

6.2.5. Results of Cool down of Trunnion-Hub (Step 3)

After the trunnion has completed warm up into the hub to room temperature, this trunnion-hub (TH) assembly is said to have achieved equilibrium, in that the temperatures and stresses would remain steady with time. This TH assembly is then immersed in liquid nitrogen. It is to be noted that the hub already had significant tensile stresses (approximately 21 ksi) on its inner diameter. The cool down induces further tensile thermal stresses on the hub, thereby aggravating the stress state. The total stress on the hub inner diameter rises to about 45 ksi. The temperature at which this peak stress occurs is approximately-200^0F. Figure 6.13 shows the hoop stresses in the hub during

[4] The percentage error is high since the values of stresses themselves are very low.

Step 3 of AP1. It illustrates stresses recorded by gages, E (representative of the hub inner diameter), and I and J (representatives of the hub outer diameter).

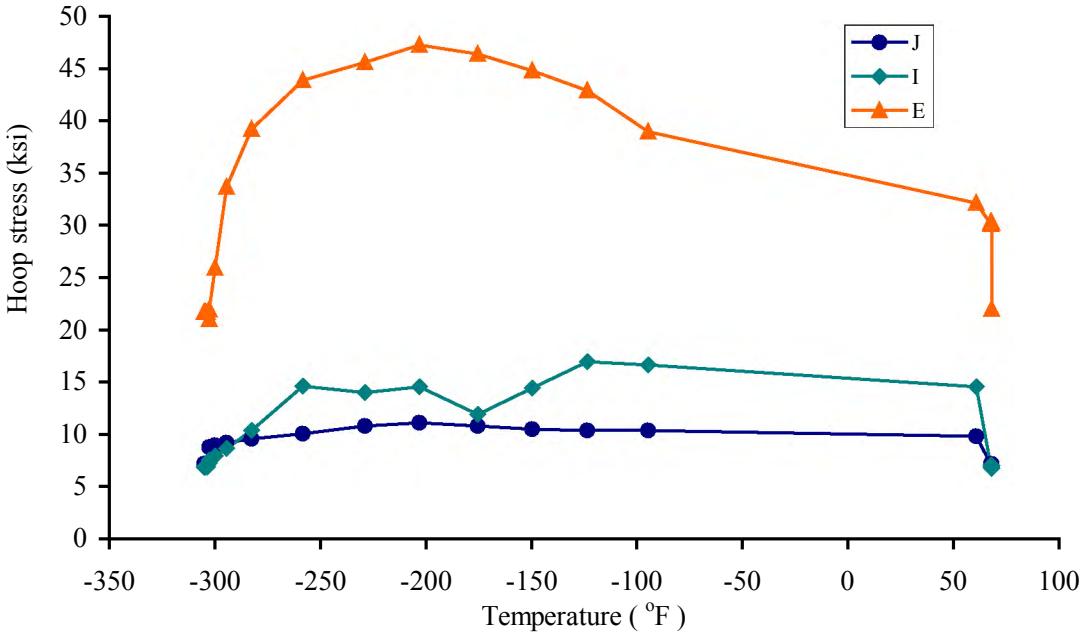

Figure 6.13 Hoop stresses induced in the hub during TH cool down.

The drawback of a high stress at a low temperature in this steel hub is that the steel is brittle at such low temperatures. The fracture toughness of steel decreases with a decrease in temperature (see Figure 6.14).

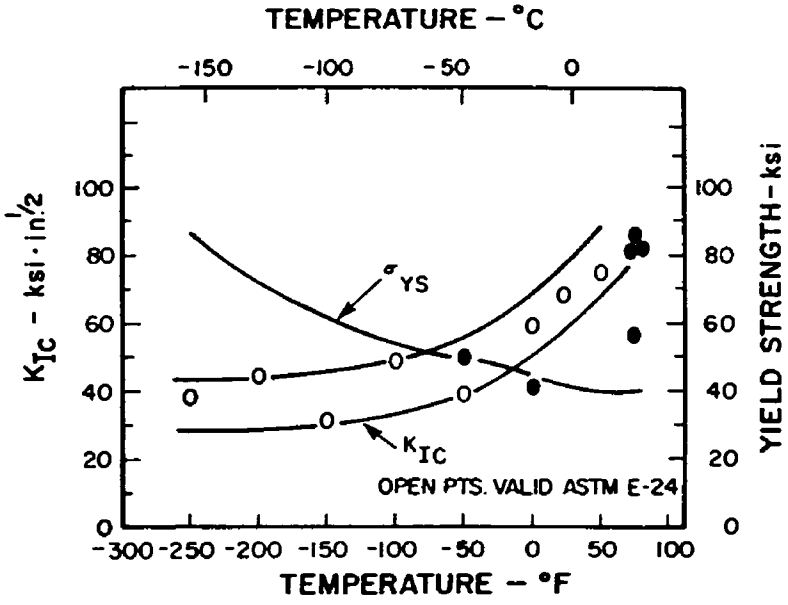

Figure 6.14 Fracture toughness and temperature (Blair et al., 1995).

Ratnam (2000) hypothesized that small cracks present in the assembly propagate catastrophically once they attain a critical crack length, a_c. The critical crack length[5] (Kanninen and Popelar, 1985) is given by:

$$a_c = \frac{K_{Ic}^2(T)}{f_e^2 \pi \sigma_\theta^2}) \tag{6.1}$$

where

a_c = critical crack length,

$K_{Ic}(T)$ = temperature dependent critical stress intensity factor,

f_e = edge effects, and

σ_θ = tensile hoop stress.

The critical crack length is dependent upon the fracture toughness, $K_{Ic}(T)$, and the hoop stress, σ_θ. The critical stress intensity factor, K_{Ic}, in turn is a function of temperature. K_{Ic} decreases with a decrease in temperature (see Figure 6.14). Therefore, when high stress occurs at a low temperature, the critical crack length falls to a very small value, thereby increasing the chances of crack propagation and consequent failure of the hub. For this particular hub with a 45 ksi stress at a temperature of -200^0F, the CCL is approximately 0.14 inch. It is to be noted that the values of the critical stress intensity factor were not available for the exact grade of steel used in this experiment. Hence, these CCL values provide only a reasonable estimate.

[5] See section 4.5 for a more detailed explanation of critical crack length.

CHAPTER 7

EXPERIMENTAL FULL-SCALE MODELS

7.1 Introduction

The quarter-scale model discussed in the previous chapter provided an understanding of the stress and temperature profiles developed during assembly procedure#1 (AP1). To compare the two assembly procedures, two exactly identical sets of trunnion, hub and girder were assembled, one using assembly procedure 1 (AP1) and the other using assembly procedure 2 (AP2). The stresses developed during these two procedures were compared against each other. The aim of these full-scale studies was to determine which of the assembly procedures was safer in terms of lower stresses and/or larger critical crack lengths. Nominal dimensions of the trunnion, hub and girder are shown in Table 7.1.

Table7.1 Nominal dimensions of full-scale trunnion and hub.

COMPONENT	INNER DIAMETER (inches)	OUTER DIAMETER (inches)	LENGTH OR THICKNESS[6] (inches)	INTERFERENCE (inches)
Trunnion	2.375	12.944	23	0.0077
Hub	12.944	17.760	11	0.0047
Girder	17.760	60.00[7]	0.75	

7.2 Assembly Procedure 1

7.2.1 Steps in the Assembly Procedure 1

Assembly procedure 1 was carried out on the full-scale model in four steps:

Step 1. The trunnion is shrunk by cooling in liquid nitrogen.

Step 2. This shrunk trunnion is then inserted into the hub and allowed to warm up to ambient temperature to develop an interference fit on the trunnion-hub interface.

Step 3. The resulting trunnion-hub assembly is shrunk by cooling in liquid nitrogen.

Step 4. This shrunk trunnion-hub assembly is then inserted into the girder and allowed to warm up to ambient temperature to develop an interference fit on the hub-girder interface.

7.2.2 Positions of Gages (AP1)

Figures 7.1 and 7.2 show details of the positions of the gages on the trunnion and the hub, respectively. The thermocouples were mounted about half an inch from each strain gage. So, each mark in Figures 7.1 and 7.2 represents a set of one strain gage and one thermocouple. The positions of these gages on the trunnion were chosen with an

[6] The tunnion and hub are expressed in terms of length and the girder is expressed in terms of thickness.

[7] The girder was approximated by a flat plate (60” ×60” × 0.75”) with a hole of diameter 17.76”.

objective of monitoring stresses at trunnion inner diameter (Gage-1), mid-diameter (Gage-2), outer diameter (Gage-3), near the trunnion-hub interface (Gages-6 and 7) and 2" away from it (Gages-4 and 5). The gages on the hub were primarily focused on the hub inner diameter (Gages-10, 11, 13 and 15).

The other gages were on the hub mid-diameter (Gages-9 and 12), outer diameter (Gages-8 and 14), and on the cylindrical surface at the hub outer radius (Gages-16, 17 and 18).

Figure 7.1 Gages on trunnion of AP1.

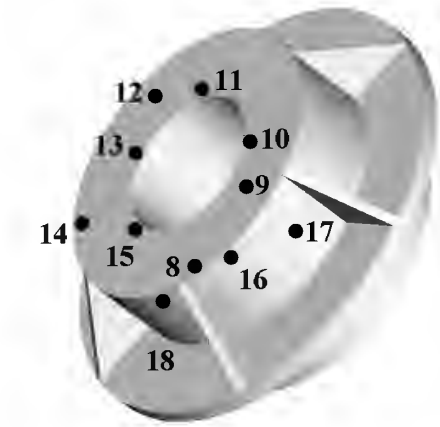

Figure 7.2 Gages on hub of AP1.

One strain gage and one thermocouple were placed on the diameter of the hole in the girder. This gage would find the stress in the girder at the hub-girder interface.

7.2.3 Results of Trunnion Cool down (Step 1)

Figures 7.3 and 7.4 show trunnion being cooled and the hoop stresses developed in this step.

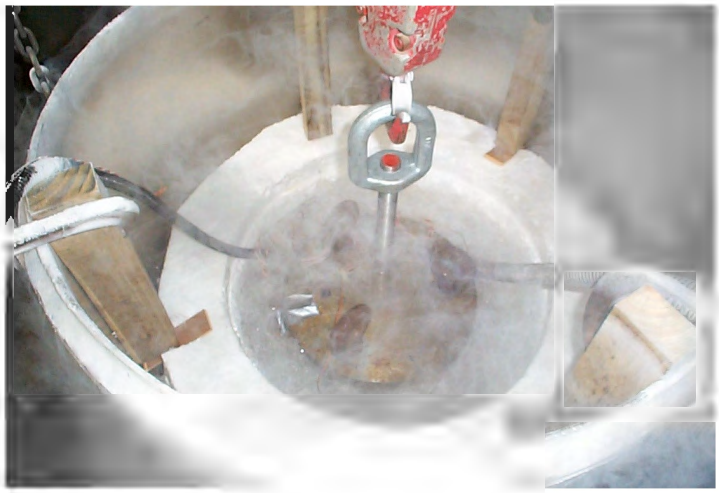

Figure 7.3 Trunnion immersed in liquid nitrogen (Step 1 of AP1).

It is to be noted that these stresses are qualitatively similar to those obtained during the cool down of the quarter-scale trunnion (see Section 6.2.3). All gages of the trunnion were included in this plot.

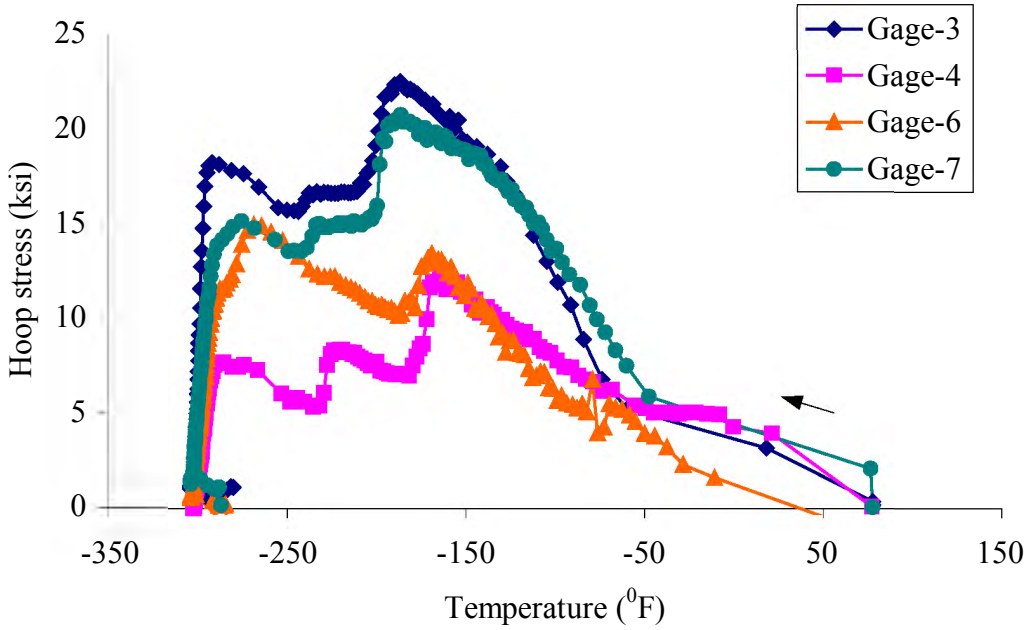

Figure 7.4 Hoop stresses during cool down of trunnion (Step 1 of AP1).

7.2.4 Results of Trunnion Warm up into Hub (Step 2)

At the end of Step 1, the trunnion had shrunk due to cooling in liquid nitrogen. However, it was found that the inner diameter of the hub had a taper on it. The nominal inner diameter of the hub should have been 12.944". The diameters measured along the depth and in two perpendicular directions (0^0 and 90^0) are shown in Table 7.2.

Table 7.2 Taper on the inner diameter of the full-scale hub.

POSITION	DIRECTION 0^0	DIRECTION 90^0
1" from the top	12.943"	12.942"
Middle	12.938"	12.939"
1" from bottom	12.938"	12.939"

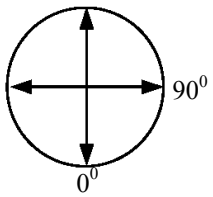

As a result of this taper (accurate to ±0.0005), two aspects of the current study had to be altered.

- This taper caused the clearance (achieved by the cooling of the trunnion) to be insufficient for a successful assembly. Hence, the hub had to be heated (see Figure 7.5) to 200^0F to get an extra 0.01" of clearance.
- This taper was of the same order of magnitude as the interference itself. In addition, the hub had to be heated to perform the assembly. These two factors would affect the results of the experiment significantly in comparison to the manner in which the FEA had modeled the assembly procedure. So, a comparison of the transient stresses from the experiment against those predicted by the FEA was ruled out. However, the steady state stresses could still be compared (see Section 7.3.6)

Figure 7.5 shows the hub being heated by induction coils wrapped around it. Heat dissipation was prevented by enclosing the hub within heat blankets

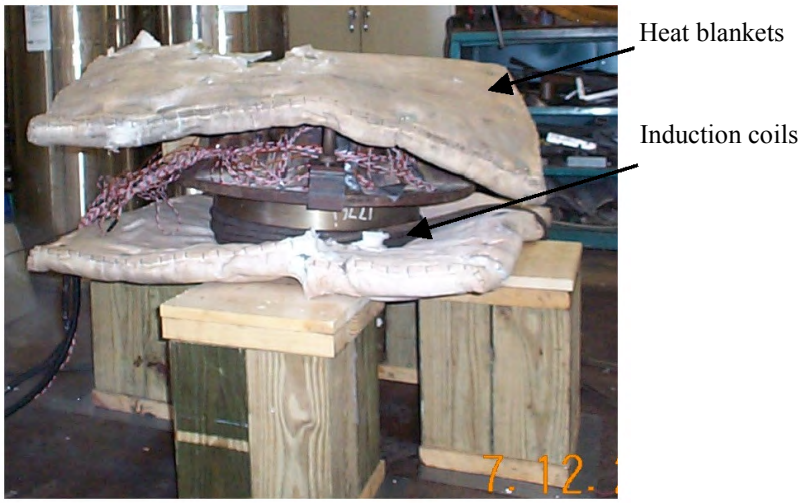

Figure 7.5 Hub heated with induction coils.

The hub was heated overnight using this arrangement to ensure that the entire hub would be at a steady state uniform temperature of 200^0F, when the trunnion would be inserted into it. Right before the cold trunnion was taken out of the dewar, the heating coils and blankets were taken off the hub and it was centered onto the wooden blocks. Figure 7.6 shows the hub being supported on wood blocks. These wood blocks had been aligned with marks on the ground, so that they would be centered with respect to the overhead crane, which would lower the cold trunnion into the hub. Also, the hub was aligned into a pre-marked circle on these wooden blocks. Both these marking schemes ensured that the trunnion would be concentric with the hub during the process of the assembly. Also, the "stopper blocks" were cut to a specific height so that the trunnion

would ‘stop’ at the right point when it was lowered into the hub, with the shoulder on the trunnion coming flush with the top face of the hub.

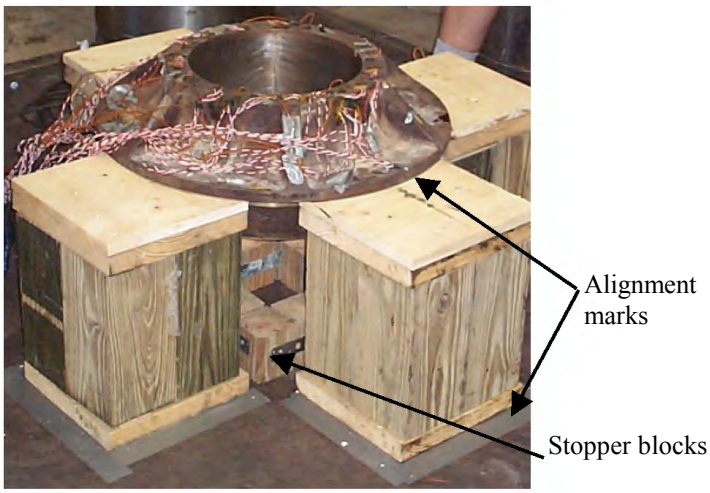

Figure 7.6 Hub supported on wood blocks.

With the hub centered correctly, the cold trunnion was removed from the dewar and its diameter was measured with a micrometer (see Figure 7.7). This diameter was checked against the inner diameter of the hub to ensure that there was enough clearance for the assembly to be performed successfully. The trunnion was 0.015” bigger than the hub inner diameter at room temperature. Cooling the trunnion gave a shrinkage of 0.025” and an additional 0.01” was obtained by heating the hub. So, the net clearance for the assembly was approximately 0.02”.

Figure 7.7 Measurement of shrunk diameter of cold trunnion with a micrometer.

Figure 7.8 illustrates Step 2 of AP1, the cold trunnion being inserted into the hub. Figure 7.9 shows the cold trunnion fitted inside the hub. The trunnion has condensed moisture from the ambient air to form a thin layer of ice on itself.

Figure 7.8 Insertion of cold trunnion into the hub (Step 2 of AP1).

Figure 7.9 Completed Step 2 of AP1 with the cold trunnion inserted into the hub.

When the trunnion warms up into the hub, the hub develops structural tensile stresses due to the interference between the trunnion and the hub. The hoop stresses developed in the hub during the process of the trunnion warming up inside it are shown in Figure 7.10. Gages 10 and 15 are plotted as representative of the hub inner diameter.

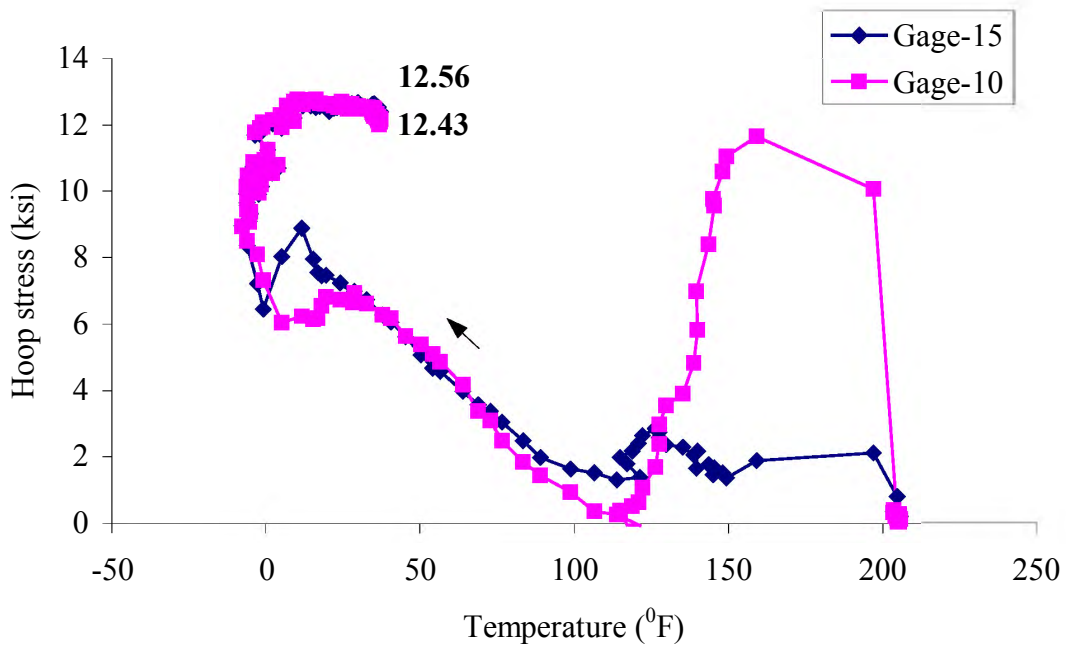

Figure 7.10 Hoop stress at hub inner diameter during trunnion-hub warm up (Step 2 of AP1).

It is to be noted that at the inner diameter of the hub, there is a steady state stress of approximately 12.5 ksi at the end of Step 2.

7.2.5 Results of Trunnion-Hub Cool down (Step 3)

After the trunnion-hub warm up to room temperature, this sub-assembly is cooled in liquid nitrogen (Step 3) so that it can be fitted into the girder (Step 4). Figure 7.11 shows the cooled trunnion-hub being taken out of the liquid nitrogen dewar. As discussed in Section 6.2.5, this process of the combined cool down of the trunnion-hub is the most critical part of AP1. The hub already has significant tensile stress (12.5 ksi) at its inner diameter as shown in Figure 7.10.

Figure 7.11 Cooled trunnion-hub taken out of the liquid nitrogen dewar.

The cool down subjects the hub to a thermal shock thereby generating thermal stresses over and above the existing structural steady state stresses (see Figure 7.12). All gages on the hub were included in this plot.

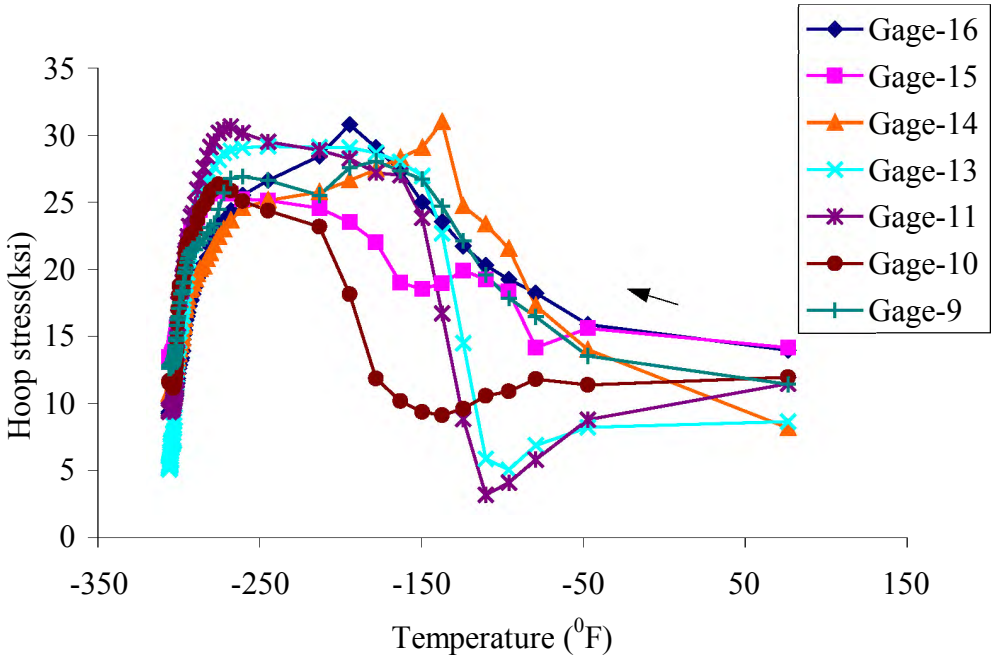

Figure 7.12 Hoop stress in hub during combined trunnion-hub cool down.

7.2.6 Results of Trunnion-Hub Fitted into the Girder (Step 4)

After Step 3, the trunnion-hub had shrunk and was inserted into the girder hole, to complete the THG assembly (see Figures 7.13 and 7.14).

Figure 7.13 Insertion of cooled trunnion-hub into the girder.

Figure 7.14 Completed THG assembly using AP1.

During this step, both the trunnion and the hub experience compression due to the interference fit at the hub-girder interface. Hence, both the trunnion and the hub develop compressive stresses (in the range of –1 ksi to –2.5 ksi). Again, these stresses are not plotted since they do not make any significant changes to the existing stresses in the components. The girder experiences tension due to the trunnion-hub warming up into it (steady state stress approximately 4.5 ksi).

7.3 Assembly Procedure 2

7.3.1 Steps in the Assembly Procedure 2

Assembly procedure 2 was carried out on the full-scale model in four steps:

Step 1. The hub is shrunk by cooling in liquid nitrogen.

Step 2. This shrunk hub is then inserted into the girder and allowed to warm up to ambient temperature to develop an interference fit on the hub-girder interface.

Step 3. The trunnion is shrunk by cooling in liquid nitrogen.

Step 4. This shrunk trunnion is then inserted into the hub-girder assembly and allowed to warm up to ambient temperature to develop an interference fit on the trunnion-hub interface.

7.3.2 Positions of Gages (AP2)

Figures 7.15 and 7.16 show details of the positions of the gages on the trunnion and the hub, respectively. The thermocouples were mounted about half inch from each strain gage. So, each mark in Figures 7.15 and 7.16 represents a set of one strain gage and one thermocouple. The positions of the gages on the trunnion were chosen with an objective of monitoring stresses at trunnion inner diameter (Gage-1), outer diameter (Gage-2), near the trunnion-hub interface (Gage-7) and 2” away from it (Gage-5). The gages on the hub were placed on the hub inner diameter (Gages-10, 11, 12, 13 and 16), mid-diameter (Gages-9 and 15), outer diameter (Gage-14) and on the cylindrical surface at the hub outer radius (Gages-18, 19 and 20).

Figure 7.15 Positions of the gages on the trunnion.

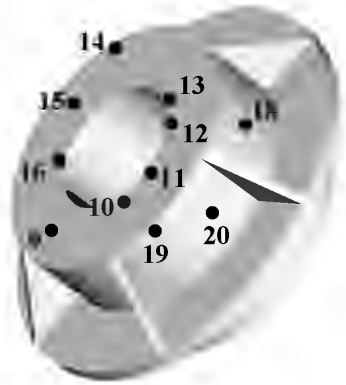

Figure 7.16 Positions of the gages on the hub.

7.3.3 Results of Hub Cool down (Step 1)

Step 1 of AP2 is the cool down of the hub in liquid nitrogen (see Figures 7.17 and 7.18).

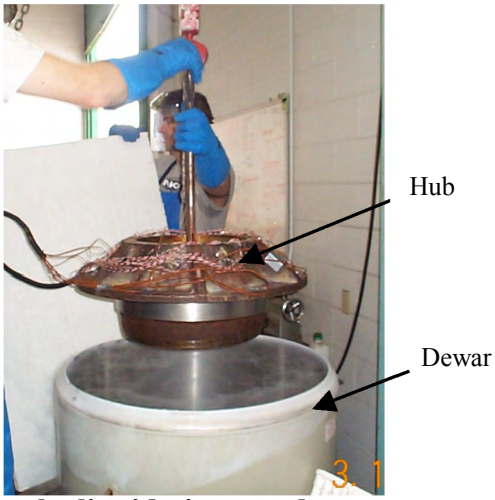

Figure 7.17 Hub lowered into the liquid nitrogen dewar.

Figure 7.18 Cooled hub pulled out of the dewar.

As explained earlier, the hub is subjected to a thermal shock when it is immersed in liquid nitrogen. The hoop stresses developed on the hub inner diameter during this time are shown in Figure 7.19. All four gages on the hub inner diameter have been included in this plot.

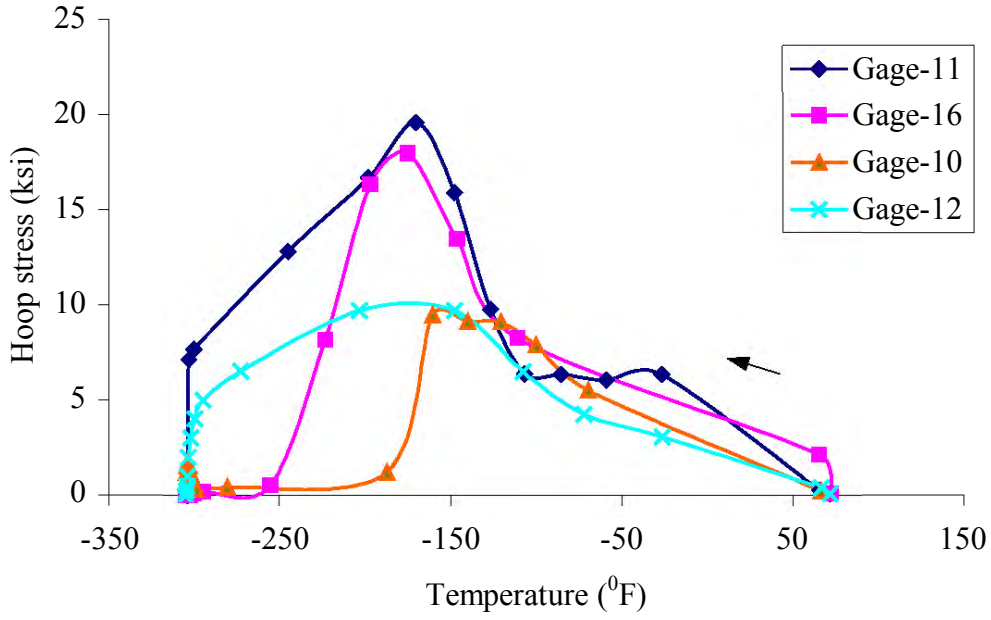

Figure 7.19 Hoop stresses on inner diameter of hub during cool down.

7.3.4 Results of Hub Warm up into the Girder (Step 2)

After the hub shrinks by cooling in liquid nitrogen, it is then inserted into the girder (see Figure 7.20) to create the hub-girder sub-assembly.

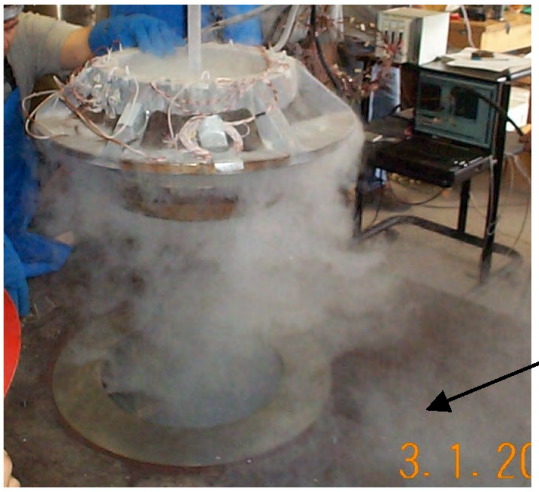

Figure 7.20 Cold hub lowered into the girder (Step 2 of AP2).

Figure 7.21 shows the completed hub-girder sub-assembly. Note the thin layer of ice formed by condensing the moisture from the ambient air.

Figure 7.21 Hub-girder sub-assembly (Step 2 completed).

At the end of hub warm up into the girder, the hub gages read steady state stresses in the range of –1 ksi to –2 ksi, and the gage on the girder read 5.5 ksi of hoop stress (FEA predicted value was 5.9 ksi).

As explained in Section 7.2.4, the hub had to be heated to 200^0F for getting extra clearance for the trunnion to be inserted into it (see Figure 7.22).

Figure 7.22 Induction heating coils for heating the hub-girder.

7.3.5 Results of Trunnion Cool down (Step 3)

In accordance with Step 3 of AP2, the trunnion is cooled by lowering it into the liquid nitrogen dewar (see Figure 7.23).

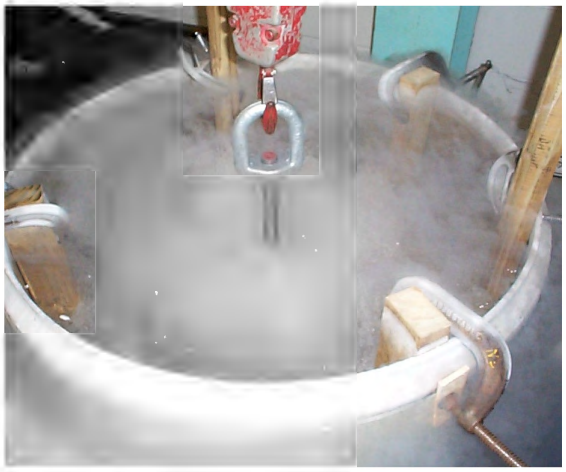

Figure 7.23 Trunnion cooled in the liquid nitrogen dewar.

Filling the liquid nitrogen dewar up to the top, would need close to ten tanks of liquid nitrogen. Since the full-scale trunnion was only 13 inches in diameter, donuts were made out of Styrofoam and piled onto each other to occupy the volume between the trunnion and the dewar (see Figure 7.24). This saved close to four tanks of liquid nitrogen.

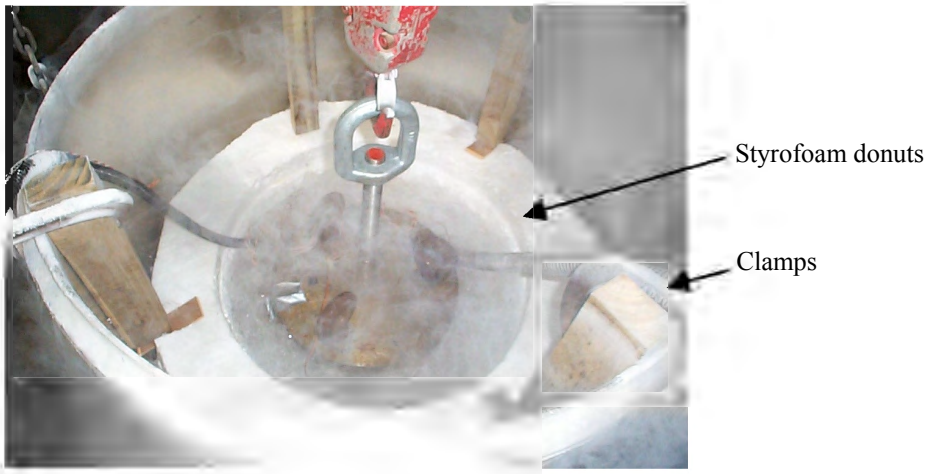

Figure 7.24 Styrofoam donuts in liquid nitrogen dewar.

The cooled trunnion was taken out of the dewar (see Figure 7.25) and shrink-fitted into the heated hub-girder assembly.

Figure 7.25 Cold trunnion taken out of the dewar.

The plot of hoop stresses during cool down of the trunnion (see Figure 7.26) is observed to be qualitatively similar to that of the quarter-scale trunnion in Section 6.2.3. All working gages on the trunnion have been included in this plot.

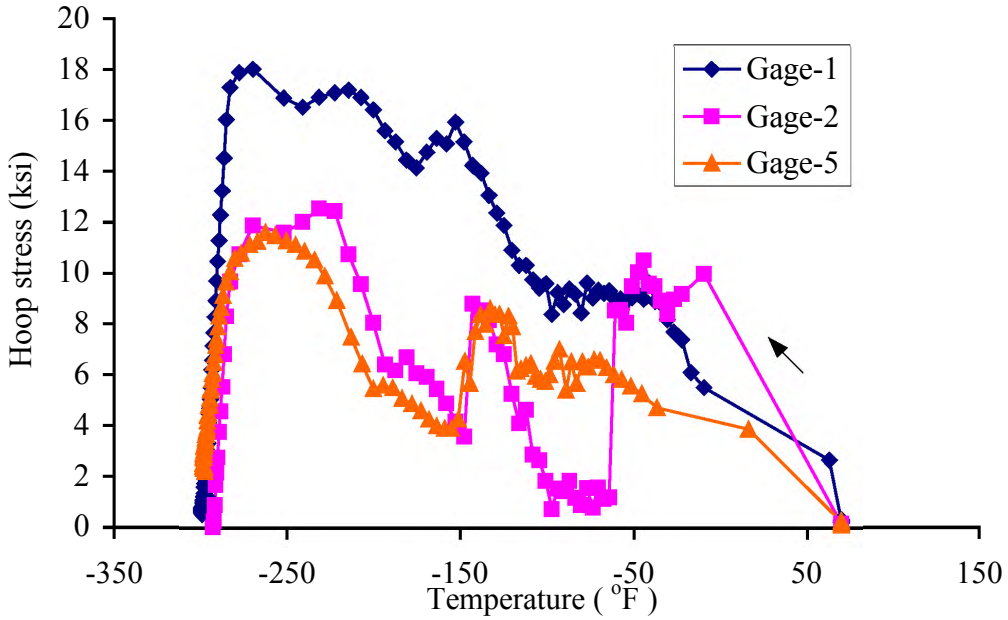

Figure 7.26 Hoop stresses during cool down of trunnion.

7.3.6 Results of Trunnion Warm up into the Hub-Girder (Step 4)

The cold trunnion that was inserted into the hub-girder in Step 3 is allowed to warm up to room temperature. Figures 7.27 and 7.28 show the completed THG assembly.

Figure 7.27 Assembled trunnion-hub-girder.

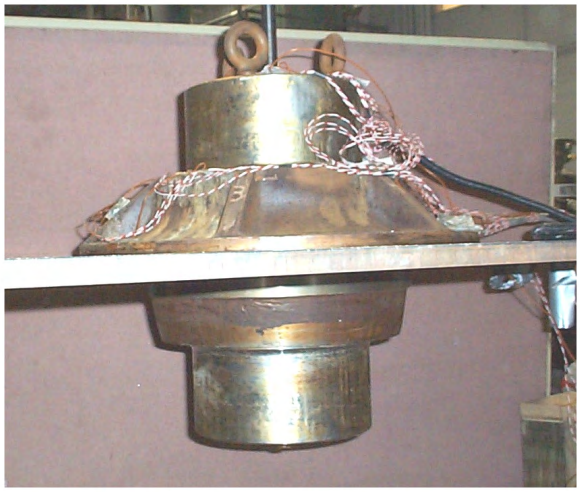

Figure 7.28 THG assembly lifted by the overhead crane.

The transient stresses developed in the hub during this Step 4 of AP2 are shown in Figures 7.29 and 7.30.

Figures 7.29 shows the hoop stresses on the inner diameter of the hub as a function of temperature. The stresses were recorded by gages 10, 12 and 16 during the process of the trunnion warming up into the hub-girder. The curve begins from the temperature-axis point of 200^0F and moves left as the hub first cools due to the cold trunnion. At about -37^0F, both the trunnion and the hub-girder have achieved close to the same temperature. After this, the hub starts to warm up which means the curves are now moving rightwards. During this warm up, the thermal stresses start to decrease and the net resultant stress at the end of the curve is mainly the steady state structural stress due to the interference between the trunnion and the hub. The small variation between the three 'identical' gages can be attributed to the minor differences in their radial and/or angular positions. Figures 7.30 shows a similar plot for gages 9 and 15, which were on the mid-diameter of the hub.

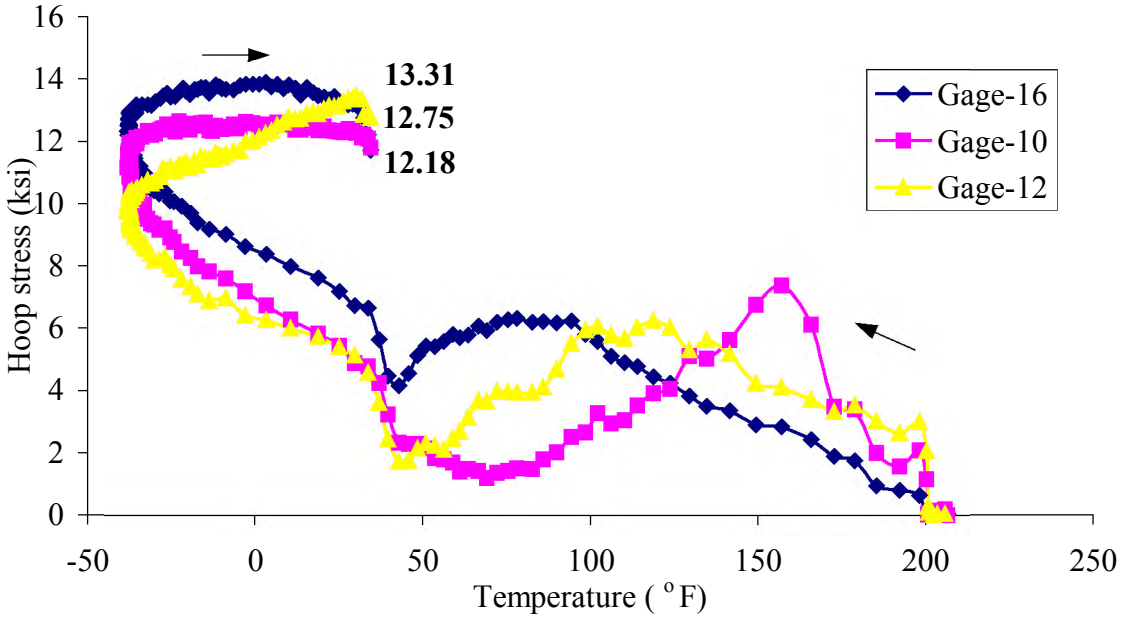

Figure 7.29 Transient stresses on hub inner diameter during Step 4 of AP2.

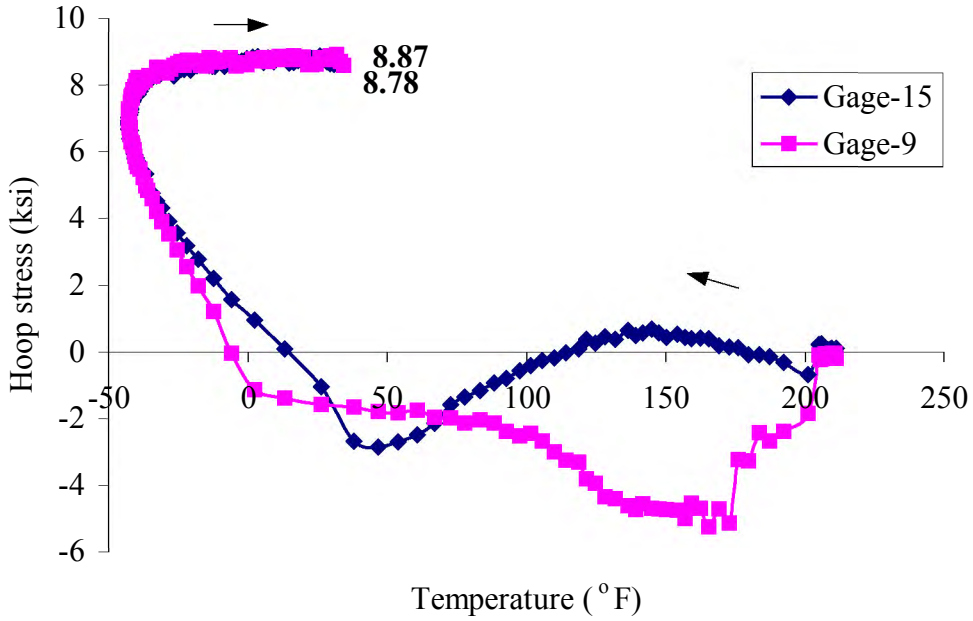

Figure 7.30 Transient stresses on hub mid-diameter during Step 4 of AP2.

The steady state hoop stresses (see Table 7.3), recorded from three gages (10, 12 and 16) on the inner diameter of the hub were found to be within 5 to 14 % of the FEA predicted stresses. And, those on the mid-diameter were within 26% of the FEA value.

Table 7.3 FEA and experimental steady state hoop stresses comparison for the hub.

Gage Position	Gage Number	Experimental Stress Value (ksi)	FEA Stress Value (ksi)	Percentage Difference (%)
Inner diameter	12	13.31	14.00	-5.02
	16	12.75	14.00	-9.33
	10	12.18	14.00	-13.89
Mid-diameter	15	8.72	11.25	-25.30
	9	8.90	11.25	-23.36

CHAPTER 8

SUMMARY OF RESULTS FOR FULL-SCALE TESTING (PHASE II)

The earlier chapter presented a detailed step-by-step description of all the steps involved in assembly procedure#1 (AP1) and assembly procedure#2 (AP2). Detailed results of each step were discussed along with the details of that particular step. These step-by-step results have been summarized into hoop stress plots for the assembly procedures. This chapter discusses the comparison of these "Time-History" plots for each assembly procedure.

8.1 Comparisons of AP1 and AP2 Based on Hoop Stress and CCL

The hoop stress on the inner diameter of the hub developed during both these assembly procedures are shown in Figures 8.1 and 8.2. Both plots have been marked into the four steps that constitute each procedure.

In Figure 8.1 for AP1, Step 1 is trunnion cool down. The hoop stress in the hub remains zero during this step. In Step 2, the cold trunnion is inserted into the hub. Consequently, the hoop stress rises to a steady state value of approximately 12.5 ksi. Step 3 is the most critical step in AP1, the trunnion-hub being cooled down results in the peak hoop stress of approximately 25.7 ksi. During Step 4, the trunnion-hub warm up into the girder, and the steady state stress on the hub inner diameter is approximately 12.8 ksi.

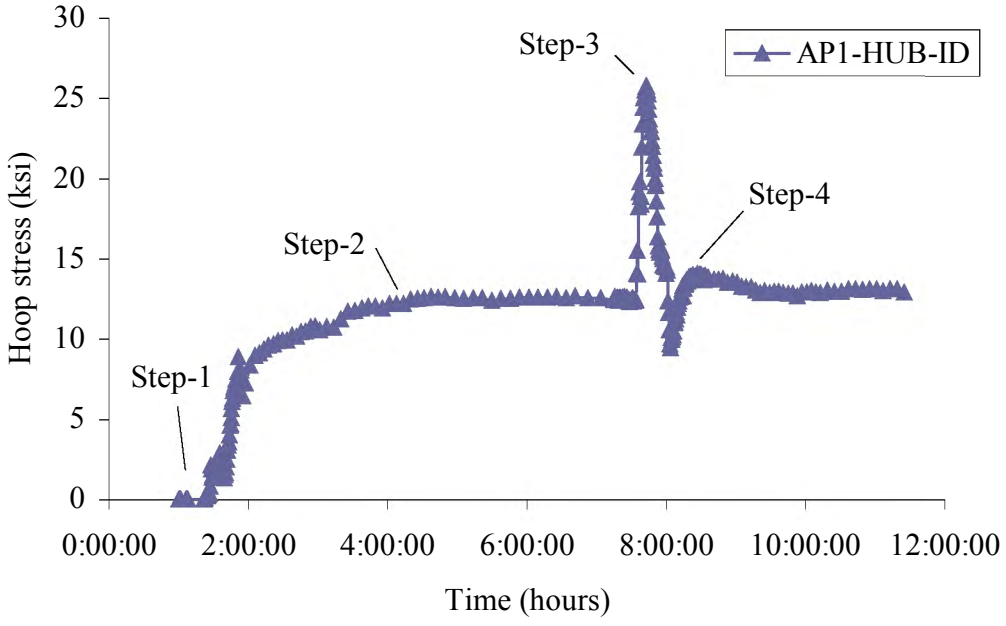

Figure 8.1 Hoop stress on hub inner diameter during all steps of AP1.

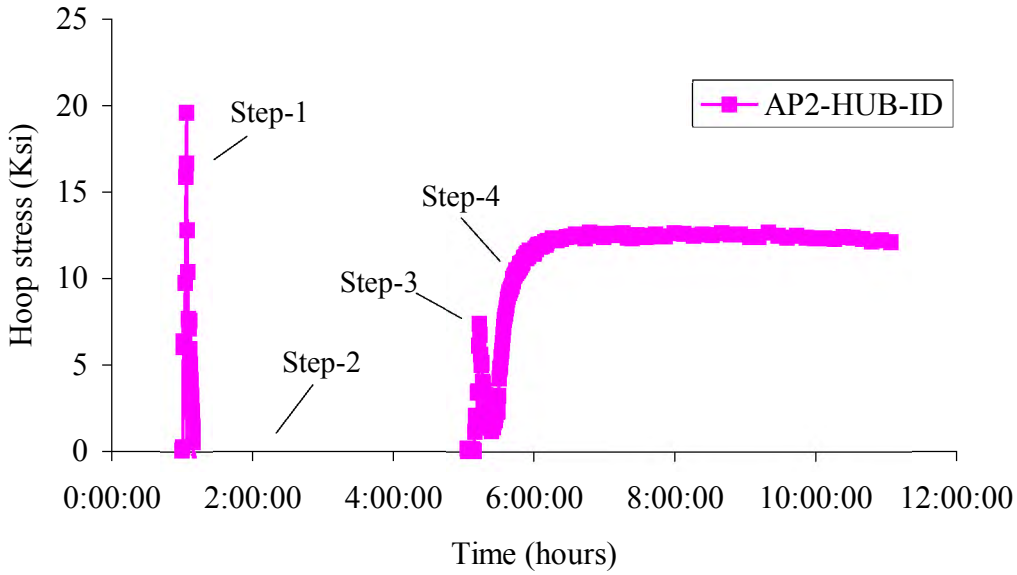

Figure 8.2 Hoop stress on hub inner diameter during all steps of AP2.

The plot for AP2 is also divided into the four assembly steps (see Figure 8.2). Step 1, being hub cool down, results in a peak stress of approximately 19.5 ksi on the hub inner diameter. In Step 2, the hub warms up into the girder, and the compressive stress on the hub inner diameter is less than 1 ksi. If shown on the plot, these stresses require the X-axis to start at a Y co-ordinate of –1 ksi. This affects the readability of the graph and also these low stresses can be neglected in comparison to peak stresses of 20 and 26 ksi. Hence, it has been omitted from the plot for the sake of clarity. In Step 3, the trunnion is inserted into the hub-girder. This trunnion expands within the hub, creating tensile stresses on the hub inner diameter. The steady state value of this stress is approximately 12.1 ksi.

After studying these plots in detail individually in Figures 8.1 and 8.2, they are combined on the same graph in Figure 8.3 for the purpose of comparison.

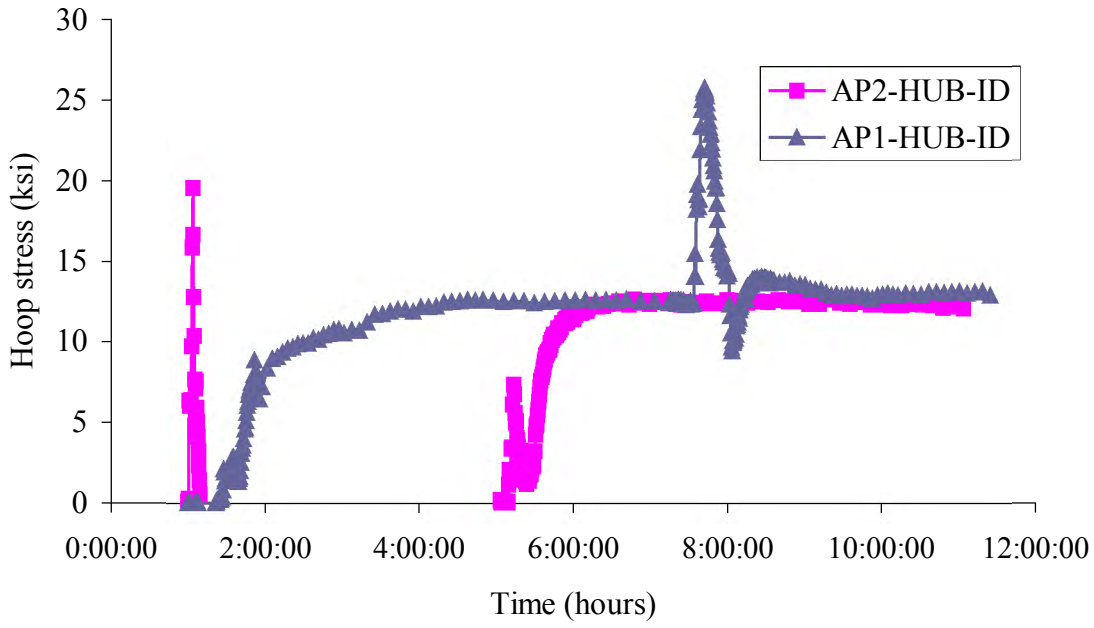

Figure 8.3 Comparison of the assembly procedures based on hoop stress.

Figure 8.3 presents a very clear and concise comparison of the hoop stress between AP1 and AP2. It illustrates the peak stress in Step 3 of AP1 to be higher than the peak stress in Step 1 of AP2.

Table 8.1 shows the values of the critical crack length[8] (determined from experimental data) during each of the two assembly procedures. Table 8.2 shows values of CCL as predicted by the FEA program. The difference between the experimental and the FEA values can be attributed to several reasons discussed in Section 7.2.4 such as taper on the hub, heating the hub, convection coefficient and ramped load.

Table 8.1 CCL comparisons of the two assembly procedures (experimental data).

ASSEMBLY PROCEDURE	CCL (inches)	YIELD STRENGTH (ksi)	HOOP STRESS (ksi)	TEMPERATURE (^{0}F)	TIME
AP1	0.3737	96	25.7	-278	8th minute into trunnion-hub cool down (Step 3 of AP1)
AP2	0.7610	65	19.5	-171	3rd minute into hub cool down (Step 1of AP2)

[8] Fracture toughness values were needed to calculate CCL from hoop stress. It is to be noted from Figure 6.14 (for ASTM E-24 steel) that the fracture toughness decreases with decreasing temperature. The. Hence, these CCL values are reasonable estimates.

Table 8.2 CCL comparisons of the two assembly procedures (FEA data).

ASSEMBLY PROCEDURE	CCL (inches)	YIELD STRENGTH (ksi)	HOOP STRESS (ksi)	TEMPERATURE (^{0}F)	TIME
AP1	0.2037	53	37.0	-92	3rd minute into trunnion-hub cool down (Step 3 of AP1)
AP2	0.6196	53	21.5	-92	1st minute of trunnion warm up into hub (Step 3 of AP2)

The comparison of AP1 and AP2 based on hoop stress can also be discussed on the basis of the factor of safety (see Table 8.3). This factor of safety (FOS) is the ratio of hoop stress in the hub to the yield strength[9] of steel.

Table 8.3 FOS comparisons of the two assembly procedures (experimental data).

ASSEMBLY PROCEDURE	FOS	YIELD STRENGTH (ksi)	HOOP STRESS (ksi)	TEMPERATURE (^{0}F)	TIME
AP1	2.95	56	19.0	-124	4th minute into trunnion-hub cool down (Step 3 of AP1)
AP2	3.29	64	19.5	-171	3rd minute into hub cool down (Step 1of AP2)

8.2 Comparisons of AP1 and AP2 Based on Von-Mises Stress

Figure 8.4 compares the Von-Mises stresses on the hub inner diameter during the two assembly procedures. The peak stress of 49 ksi in AP1 is observed in Step 3 (trunnion-hub cool down). At this time, the hub has both high radial and hoop stresses that add up to give very high values of Von-Mises stresses. The peak in AP2 is during the cool down of the hub. It is to be noted that this peak is significantly lower than that of AP1.

[9] It is to be noted from Figure 6.14 that the yield strength is a function of the temperature (that is, it is increasing with decreasing temperature). This makes FOS a significant parameter to be studied.

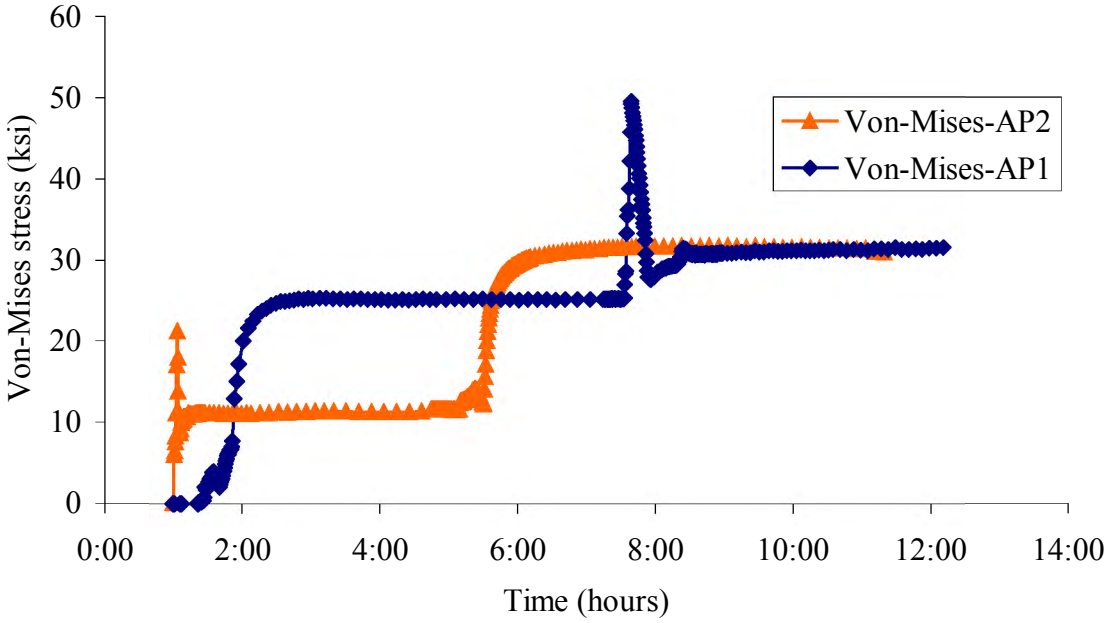

Figure 8.4 Comparison of the assembly procedures based on Von-Mises stress.

CHAPTER 9

CONCLUSIONS AND RECOMMENDATIONS

9.1 Conclusions

9.1.1 Conclusions for Parametric FEA (Phase I)

Our hypothesis at the beginning of this study was that AP2 resolves the problems associated with AP1. The results broadly agree with this hypothesis. However each bridge is different and needs to be analyzed separately. There can be possible situations where AP1 may turn out to be a better process. One common problem associated with both assembly processes studied is thermal shock. In AP2, the sharp thermal gradient sometimes leads to very low values of critical crack length (CCL). In AP1, a combination of high thermal and interference stresses results in possibility of crack formation. A lower thermal gradient can improve both the assembly processes.

Some recommendations during assembly are:

- Before choosing the assembly procedure for a bridge, the THGTM should be run and the following questions need to be answered:
  a. What are the values of the critical crack length during the critical steps in the assembly process? During which process does a lower value of critical crack length exist?
  b. How long do the values of critical crack length remain low? Are there indications of crack arrest?
  c. What are the highest values of hoop stress and when do they occur?
  d. What are values of critical crack length and hoop stress during the two warming up processes?
- Avoid sharp thermal gradients to result in lower thermal stresses. It is advisable to perform a part of the cooling process in a medium with a lower convective heat transfer coefficient and boiling point than liquid nitrogen before dipping it in liquid nitrogen. For example, immersion in liquid nitrogen could be preceded by immersion in a mixture of dry ice and alcohol.
- In general, it is better to cool parts of the assembly until there is a reasonable gap between the male and the female part before insertion. This is particularly true if the THGTM indicates low values of critical crack length during the process.

9.1.2 Conclusions for Full-Scale Testing (Phase II)

Table 9.1 summarizes the comparisons of assembly procedure 1 (AP1) and assembly procedure 2 (AP2) based on all three criterions, hoop stress, CCL (see section 4.5 for a detailed description of CCL) and Von-Mises stress. Table 9.1 clearly illustrates that AP2 is significantly better compared to AP1 in terms of all three criterions. Although, these results may or may not change by changing the geometry or interference values in the THG assembly. The FEA results (see Table 8.2**)** agree with this conclusion as well.

Table 9.1 Summary of comparisons of AP1 and AP2.

PROCEDURE	HOOP STRESS (ksi)	CRITICAL CRACK LENGTH (CCL) (inches)	VON-MISES STRESS (ksi)	FACTOR OF SAFETY (FOS)
AP1	25.7	0.3737	49.2	2.95
AP2	19.5	0.7610	30.9	3.29

The numbers for CCL in Table 9.1 were calculated at the locations of the strain gages at different times and the smallest numbers gives the critical crack length for the whole assembly. Note that as temperature decreases, the fracture toughness decreases (see Figure 6.14) and hence, the values of the critical crack length.

The maximum hoop and Von-Mises stresses in Table 9.1 are calculated by finding these stresses at the strain gage locations throughout the assembly procedure. The factor of safety is calculated from finding the minimum of the ratio between the yield strength and hoop stress at the strain gage locations. Since yield strength is a function of temperature, maximum hoop stresses do not necessarily result in lower factors of safety. Also note that the maximum Von-Mises stress does not coincide with the time when the maximum hoop stress occurs in AP2. The maximum Von-Mises stress occurs when the whole assembly reaches steady state, while the maximum hoop stress occurs when the trunnion is placed in the hub-girder.

The critical crack length (CCL) and factor of safety (FOS) in Table 9.1 is based upon the fracture toughness and yield strength in Tables 8.1 through 8.3. Note that these values for fracture toughness and yield strength are temperature dependent, thereby making the CCL and FOS temperature dependent also.

9.2 Recommendations

Based on the results of this experimental study, the following are some recommendations for FDOT:

- Lay down inspection specifications for determining if voids or cracks in the cast hub are bigger than 0.3 inch. (CCL for AP1 was found to be 0.3 inch).
- Specify tight machining tolerances for the inner diameter of the hub, indicating true position and perpendicularity tolerances. A taper along the depth could also contribute to chances of trunnion getting stuck in the hub during assembly procedure (for example, Venetian Causeway).
- Consider heating the outer component as an alternative to cooling the inner component. Heating has two distinct advantages over cooling in liquid nitrogen. First, it is a slow process as to not create large thermal stresses. Second, heating the steel does not make it brittle. Cooling the steel casting makes it more brittle and more susceptible to crack propagation.
- Consider gradual cooling, whenever the hub is being cooled by itself (AP2) or as a trunnion-hub assembly (AP1), in a convection-cooling chamber using liquid nitrogen as opposed to immersion in liquid nitrogen. The same shrinkage can still be obtained for carrying out a successful assembly. The advantage is that the trunnion or hub does not get a thermal shock associated with direct immersion. The disadvantage is that it would be slower to carry out.

- Consider staged cooling wherein the trunnion or hub is first cooled from room temperature to 0^0F, then dry-ice/alcohol is used to cool it down further to -109^0F, before being cooled to -321^0F (liquid nitrogen). This staged cooling is better than immersing the trunnion directly in liquid nitrogen since in any given stage the temperature change is smaller, resulting in significantly lower thermal stresses.

9.3 Future work

Some areas for future work could be:

- Study the effect of warming one component while cooling the other component in something other than liquid nitrogen, such as dry ice/alcohol.
- Studying the effect of thickness of hub on the hoop stress developed. Conduct design optimization of geometry of the bridge to understand their influence on stress distribution. Increasing the hub thickness would make it stronger but it could also increase the thermal gradient along the radial direction possibly resulting in higher thermal stress.
- The AASHTO LRFD Movable Bridge Specifications require that the trunnion hub be tightly fit into structural parts with an ANSI/ISO H7/s6 fit. The specifications further require that the hub flanges bolt to the girder webs to transfer torsional and axial loads. Mechanical assemblies similar to this do require an interference fit, and are not generally assembled with a clearance at the interface. Research work on eliminating the interference fit and providing a clearance at the hub-girder interface, must consider various aspects such as rigidity and permanence of the assembly, importance of accuracy of location, trunnion alignment through rotation of the leaf and bore pressure requirements.

9.4 Availability of resources

Numerous resources are available at the University of South Florida for analysis of trunnion-hub-girder assemblies for future designs. Some of these resources are:

- Downloadable bridge design tools (http://www.eng.usf.edu/~besterfi/bascule/bascule.zip). and files for ANSYS finite element analysis (http://www.eng.usf.edu/~besterfi/bascule/fem.zip).
- Faculty (e.g., Dr. Glen H Besterfield and Dr. Autar K. Kaw) to analyze new bridge designs on a contractual basis.
- Training opportunities on how to use the programs for trunnion-hub-girder assembly design.

The parametric finite element program, developed as part of this research, could be best utilized to predict the thermal/structural characteristics at assembly and possibly avoid construction delays. For instance, the model could be used to analyze low-level interference fits at the trunnion-hub interface.

Numerous other information pertaining to this research project is also available on the web at http://www.eng.usf.edu/~besterfi/bascule/ (see Appendix E).

REFERENCES

Barron, R. F., (1999), *Cryogenic Heat Transfer*, Taylor and Francis Company, PA, pp. 161-172.

Brentari E. G. and Smith R. V., (1964), "Nucleate and Film Pool Boiling Design Considerations for 0_2, N_2, H_2 and He," *International Advances in Cryogenic Engineering,* 10b, pp. 325-341.

Dally, J. W. and Riley, W.F., (1993), *Instrumentation for Engineering Measurements*, John Wiley and Sons, New York, pp. 129-134,153-155.

Denninger, M. T., (2000), "Design Tools for Trunnion-Hub Assemblies for Bascule Bridges," Masters Thesis, University of South Florida.

Hare, D. A. and Moore, Sr. T. C., (2000), Evaluation of GE-167 Silicone Rubber (RTV) For Possible Service As A Moisture-Barrier For Certain Strain Gage Applications, *NASA Technical Memorandum-210087*, pp. 2-4.

Kanninen, M. F. and Popelar, C. H., (1985), *Advanced Fracture Mechancis, Oxford Engineering Science Series*, Oxford University Press, New York.

Logan, D. L., (1992), *A First Course in Finite Element Method*. 2nd Ed, *PWS-Kent Series in Engineering*, PWS-Kent Publishing Co., Boston.

Measurements Group Technical Notes, Strain Gage Thermal Output and Gage Factor Variation with Temperature, see http://www.measurementsgroup.com/guide/tn/tn504/504index.htm

Moore, T. C., (1997), Recommended Strain Gage Application Procedures for Various Langley Research Center Balances and Test Articles, *NASA Technical Memorandum-110327*, pp. 20-25.

Noda, N., (1987), "Transient Thermoelastic Contact Problem in a Cylinder with a Position-Dependent Heat Transfer Coefficient," *Journal of Thermal Stresses,* 10, pp. 57-69.

Noda, N., (1985), "Transient Thermoelastic Contact Stresses in a Short-Length Circular Cylinder," *Journal of Thermal Stresses,* 8, pp. 413-424.

Noda, N., (1984), "Transient Theromelastic Contact Problem in a Long Circular Cylinder," *Journal of Thermal Stresses,* 7, pp. 135-147.

Oliviera, R. and Wu, X. R., (1987), "Stress Intensity Factors for Axial Cylinders Subjected to Thermal Shock," *Engineering Fracture Mechanics,* 27, pp. 185-197

Ootao, Y., Akai, T. and Tanikawa Y., (1995), "Three-Dimensional Transient Thermal Stress Analysis of a Non-Homogenous Hollow Circular Cylinder Due to a Moving Heat Source in the Axial Direction," *Journal of Thermal Stresses,* 18, pp. 497-512

Ozisik, M. N., (1977), *Basic Heat Transfer*, McGraw-Hill Book Company, New York.

Pourmohamadian, H. and Sabbaghian, M., (1987), "Transient and Residual Thermal Stresses in a Solid Cylinder with Temperature Dependent Material Properties," *ASME Pressure Vessel and Piping,* 98-8, pp. 33-41.

Radebaugh, R. and Marquardt, E., (1993), Cryogenic Instrumentation, Recent *Advances in Cryogenic Engineering,* ASME, 267, pp. 18-19.

Ratnam, B., (2000), *Parametric Finite Element Modeling of Trunnion Hub Girder Assemblies for Bascule Bridges*, Masters Thesis, University of South Florida,.

Reed, R. P., (1983), *Materials at Low Temperatures*. ASM International, Materials Park, Ohio.

Shigley, J. E. and Mischke, C.R., (1986), *Standard Handbook of Machine Design*, McGraw Hill Company, New York, pp. 19.9-19.11.

Blair, M., Stevens, T. L., and Linskey, B., (1995) Steel Castings Handbook, 6th Ed., ASM International, Materials Park, Ohio.

Thomas, J. R. Jr., Sing, J. P., Tawil, H., Powers, L., and Hasselman, D. H. P., (1985), "Thermal Stresses in a Long Circular Cylinder Subjected to Sudden Cooling During Transient Convection Heating" *Journal of Thermal Stresses,* 8, pp. 249-260.

Urgural, A. C. and Fenster, S. K., (1995), Advanced Strength and Applied Elasticity, 3rd Ed., Prentice-Hall, New Jersey.

Kowalkowski, M. K., Rivers, H. K. and Smith, R. W., (1998), Thermal Output of WK-Type Strain Gauges on Various Materials at Cryogenic and Elevated Temperatures, *NASA Technical Memorandum-208739*, pp.8-16.

APPENDIX A

TRUNNION-HUB-GIRDER DESIGN TOOLS

A.1 Introduction

Shrink fitting is a technique used to create an interference fit between the inner and outer members of a system, for example the trunnion and hub, respectively. The inner member is cooled down to a temperature that will allow sufficient change in its outer diameter (if circular in shape), until it can slide into the outer member. The change in size can be calculated using the coefficient of thermal expansion of the material and the temperature change. Once the inner member has been cooled and inserted into the outer member, the system is allowed to reach steady state. As the system reaches steady state temperature, the inner member expands back to its original shape, and an interference fit is formed. This fit allows for a bond, in a friction joint, between the two members. However, in high-load situations, this fit is usually supplemented with another joint, for example, bolts. A bolted joint is slip-critical.

As a step to work towards the solution of this problem, the bascule bridge design, fabrication, and operation must be analyzed and understood. To aid in this process several design tools have been developed. These design tools provide a general understanding of the physical (THG) system, and demonstrate how it reacts to various loading situations.

The first design tool simulates an actual bridge layout, and finds the actual torque necessary to raise the bridge leaf, given various parameters (for example, material properties and wind loading).

Due to the shrink fitting done to the system, and based on the type of standard fits at the interfaces of the trunnion-hub and hub-girder, interferences are created at the two interfaces. These interferences cause pressures at the interfaces and, correspondingly, develop hoop (also called circumferential and tangential), radial, and Von-Mises stresses in the THG assembly. The second design tool finds all of these stresses, as well as the radial displacements in each member (trunnion, hub, and girder). The results provide the design engineer with an idea of how the given diametrical interferences (from shrink fitting) affect the stresses in the various members of the THG assembly.

A third tool is developed to find all of the critical stresses (radial, hoop, and Von-Mises) in the THG assembly at steady state. The results from this tool are tabulated to show these stresses for various combinations of the material properties and geometric dimensions of the trunnion, hub, and girder. The design engineer can then use these as design parameters.

The fourth design tool is for developing the bolt pattern used to supplement the hub-girder interference fit. The amount of torque resisted by the hub-girder comes from two sources – hub-girder interference and the bolts. The torque resisted by the bolts is based on the number of bolts, diameter of bolt circles, bolt material and size, material and geometric dimensions of the hub and girder, etc. This design tool allows the user to test various bolt patterns. The designer then tabulates results for direct use.

The first three design tools are briefly described in the remainder of this Appendix. The fourth design tool is not elaborated on further here because it is out of the scope of the initial research project.

A.2 Technical information

To understand the complexity of the design tools used to analyze the trunnion-hub-girder (THG) assembly, an overview of their technical aspects is needed. Remember, the first design tool is used to simulate actual bridge design. It provides the user with an understanding of how much actual torque is created during the opening/closing of a bascule bridge. The next design tool calculates the approximate steady state stresses and displacements in the THG assembly, given diametrical interferences, due to shrink fitting. This design tool also calculates and displays a stress profile along the radius of the entire THG assembly. The third design tool is used to find all of the critical stresses in the THG assembly. These stresses can vary with material properties, as well as with the dimensions of the trunnion, hub, and girder. This design tool allows the user to examine multiple design schemes involving the THG geometry and materials. In this technical analysis, approximate steady-state stress equations are developed for calculating the compressive radial stress at the trunnion-hub and hub-girder interfaces. These stresses determine the amount of torque the assembly can resist before slipping at the interfaces. Also calculated are the hoop and Von-Mises stresses, which determine the failure of the assembly.

All of the equations and technical information used to develop these design tools and user-friendly programs can be found in Denninger (2000). They have been left out of this final report for brevity.

A.3 Graphical user-interface model

A user-friendly PC based design package is developed for the THG assembly design (see Figure A.1). This program allows the user to simulate various designs of the THG assembly. The inputs to the program are explained step-by-step, and are related to the technical information given in Denninger (2000). Then the outputs of the program are explained.

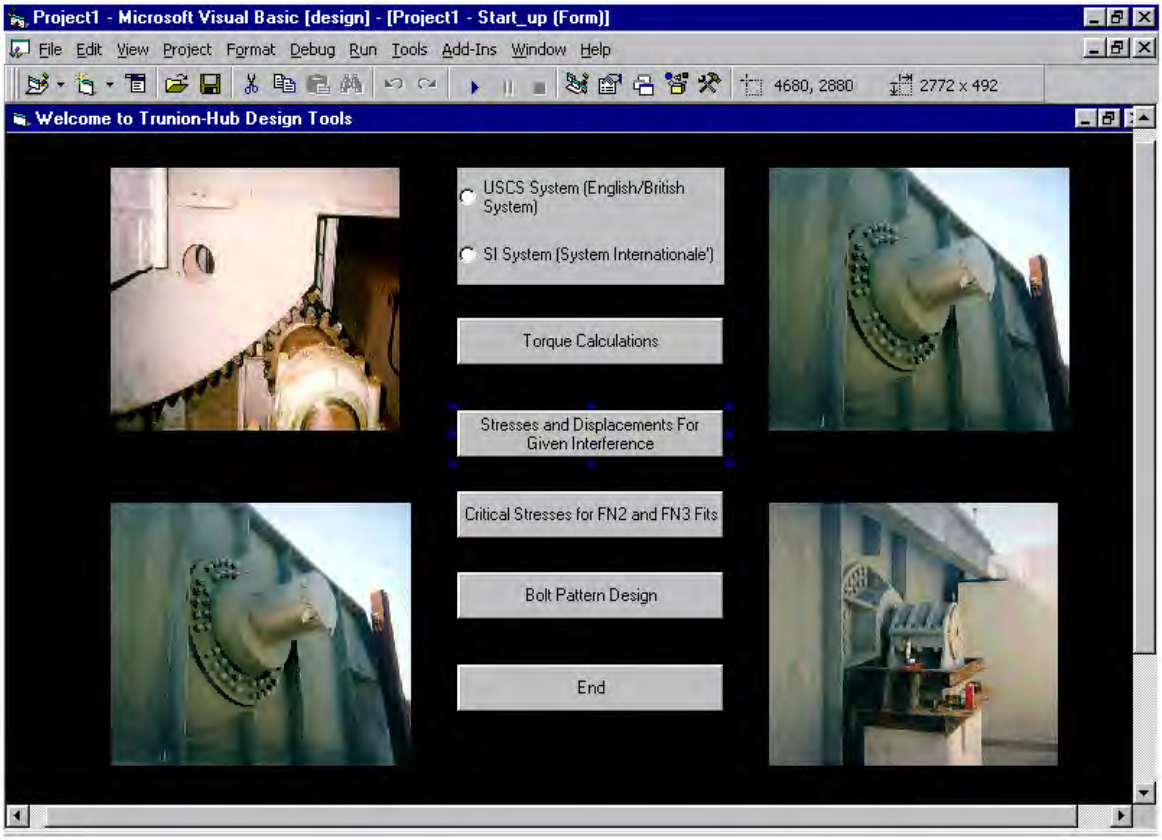

Figure A.1 Main menu of the trunnion-hub design tools program.

Trunnion-hub design Tools (see Figure A.1) is a Graphical User Interface (GUI) designed to run on personal computers and takes advantages of their extensive number of programming tools, graphics packages, portability, and low cost.

THG assembly is comprised of several design tools. These are "Design Tool 1 – Torque Calculations for THG assembly", "Design Tool 2– Stresses in the THG assembly with given interference", "Design Tool 3 – Stresses in the THG assembly with given standard interference fits" and "Design Tool 4 – Torque resisting capability of the THG assembly due to bolts and hub-girder FN2 fit."

A.4 Design tool 1 – Torque calculations.

The first design tool calculates the torque that the THG assembly is required to resist, given actual bascule bridge criteria entered by the user. The user is required to input the dimensions of a bascule leaf, as related to the diagram shown (Figure A.2). The user must also input values such as the unbalanced load at the tip of the span, the dead weight load of the leaf, the wind load, the diameter of the trunnion, the starting coefficient of friction of the roller bearing, and the angle of opening of the bascule leaf. As discussed in Denninger (2000), the design tool sums the three torques affecting the bearing (wind load, unbalanced load, and starting friction) to find the total torque that the assembly must resist. This design tool provides the user the torques that must be resisted by the bascule THG assembly.

A.4.1 Example problem

The following is an example problem using the first design tool, "Torque Calculations for THG Assembly".

Example: Given for a typical South Florida bridge are the following parameters: a = 48.75 ft, b = 31.5 ft, c = 18.75 ft, d = 120 ft, e = 66 ft, σ_w = 20 psf (AASHTO Condition C), μ_{start} = 0.004, w_l = 53.30 x 10^6 lbf, w_u = 2696 lbf, d_b = 3.281 ft, and θ_o = 57.5°. Find the distance to the centroid from the trunnion centerline, the wind load affecting the leaf and each girder, and the torque that is generated by wind load, friction load, and unbalanced load. Then determine the total torque that the roller bearing assembly must resist.

Solution: The above data is input to the Design Tool 1 interface, as shown in Figure A.2.

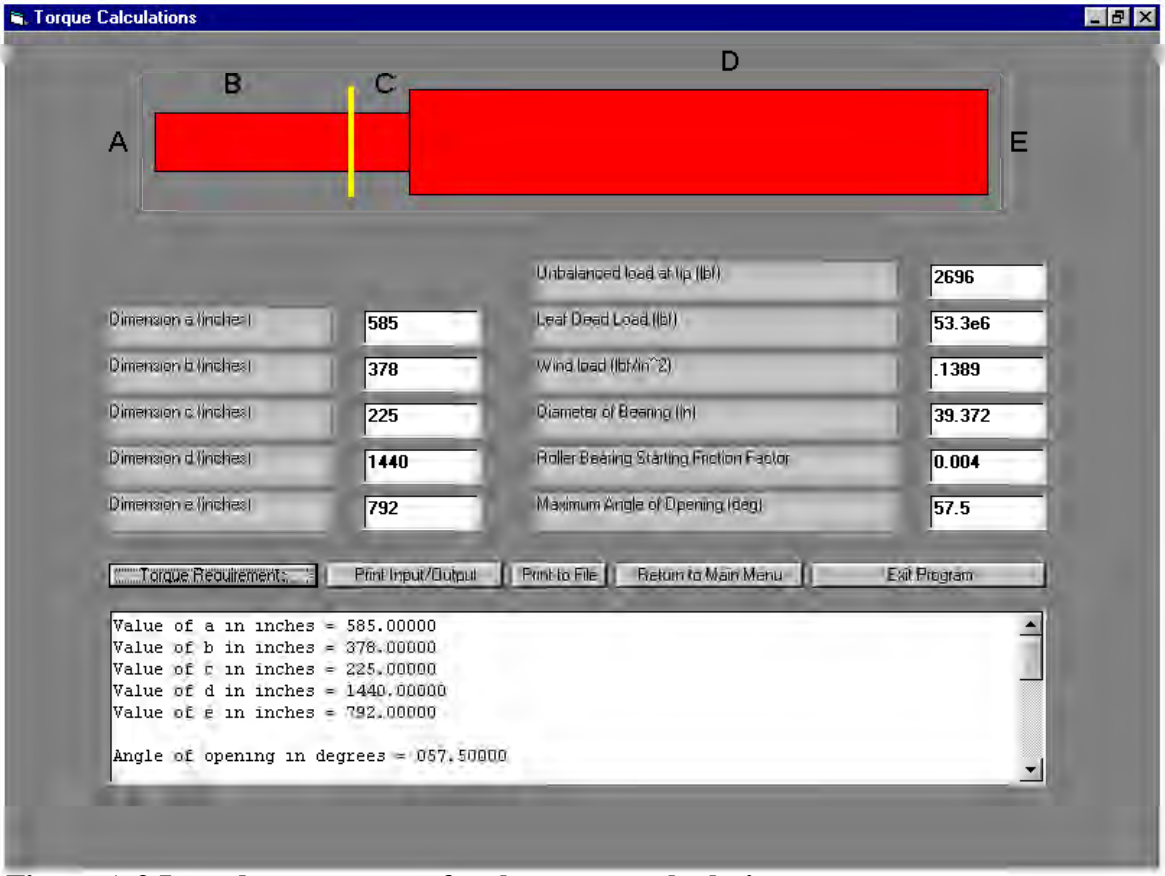

Figure A.2 Introductory screen for the torque calculation program.

From the results given by the program, the wind load is 0.139 lb/in^2, unbalanced weight on leaf tip is 2696 lbs, and leaf dead load is 53,300,000 lbs. The diameter of the trunnion is 39.37 inches, and centroid distance from trunnion is 859 inches. The Wind load on leaf is 149023 lbs, wind load on each girder is 74512 lbs, and wind moment on girder 53,973,000 in-lbs. The unbalanced moment is 2,411,900 in-lbs, friction moment is 4,197,100 in-lbs and total moment on TGH assembly is 60,582,000 in-lbs

A.5 Design tool 2 - Interference stresses due to shrink-fitting.

One of the design tools calculates the critical radial stresses at the trunnion-hub and hub-girder interfaces, and hoop and Von-Mises stress in the THG assembly for input diametrical interferences. This program gives the user a comprehension of how the stresses vary through the assembly radius, and is an academic tool for the designer to get a technical "feel" of the complexity of the problem due to the two interferences.

This program follows the equations given in Denninger (2000), for a composite cylinder made of three cylinders with a diametrical interference at each of the two interfaces. The three cylinders approximate the trunnion, hub and girder. The inputs to the program are the elastic modulus of each cylinder, Poisson's ratio for each cylinder, the inner and outer radii of each cylinder, and the specified interference at each of the two interfaces. The program then outputs a radial profile of the radial, hoop, and Von-Mises and radial displacement across the entire THG assembly.

A.5.1 Example problem

The following is an example problem for this design tool, "Interference Stresses Due to Shrink-Fitting".

Example: A compound cylinder is made of three cylinders (with a solid inner shaft) as shown in Figure A.3 with the radii given as $r_O^1 = 8.39$ in, $r_O^2 = 15.39$ in, and $r_O^3 = 36.5$ in. The Young's modulus and Poisson's ratio of all the cylinders is given as E = 30 Msi, ν=0.3, respectively. The diametrical interference at the interface of the Cylinder 1 and Cylinder 2 is given as δ_1=0.0080 in and δ_2=0.010 in, respectively. Find the pressure at the interfaces, and the maximum hoop and Von-Mises stresses in the compound cylinder.

Solution: The above data is input to the Design Tool 2 interface, as shown in Figure A.3.

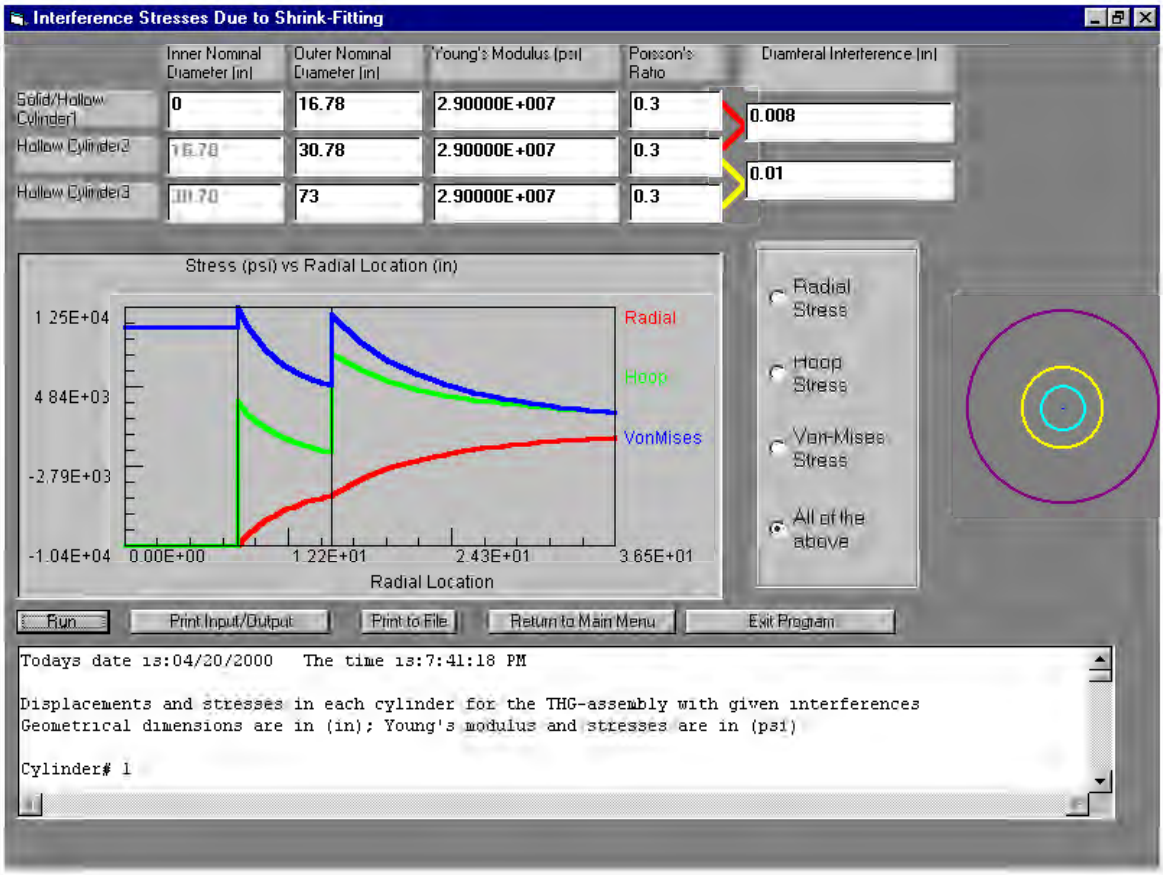

Figure A.3 Introductory screen for the interference stresses due to shrink-fitting program.

From the results given by the program, the interference pressures at the two interfaces are –10.42 ksi and –5.563 ksi. The maximum tensile hoop stress in the assembly of 7.968 ksi exists in Cylinder 3 at the inside radius. The maximum Von-Mises stress of 12.48 ksi exists in Cylinder 2 at the inside radius.

A.6 Design tool 3 - Interference stresses due to FN2 and FN3 fits.

Another design tool is very similar to the previous one, except now the user specifies the industry standard interference fit (FN2 or FN3) at each of the two interfaces. The critical stresses, as just discussed in the previous section, are then calculated. This program allows the designer to check what the approximate steady state stresses would be after assembly. In this program, the user can see if the hoop stresses (both compressive and tensile, if applicable) are more than the yield stresses, which may cause hoop cracks in that respective cylinder. The Von-Mises stress is also given to show how these stresses directly compare with the yield strength of the material.

A.6.1 Example problem

The following is an example problem using the third design tool, "Interference Stresses Due to FN2 and FN3 Fits".

Example: A compound cylinder is made of three cylinders (with a solid inner shaft) as shown in Figure A.4 with the radii given as $r_o^1 = 8.39$ in, $r_o^2 = 15.39$

in, and r_O^3 = 36.5 in. The Young's modulus and Poisson's ratio of all the cylinders is given as E = 29 Msi, ν=0.3, respectively. FN2 fits are assumed at each of the two interfaces. Find the critical stresses in the THG assembly.

Solution: The above data is input to the Design Tool 3 interface, as shown in Figure A.4.

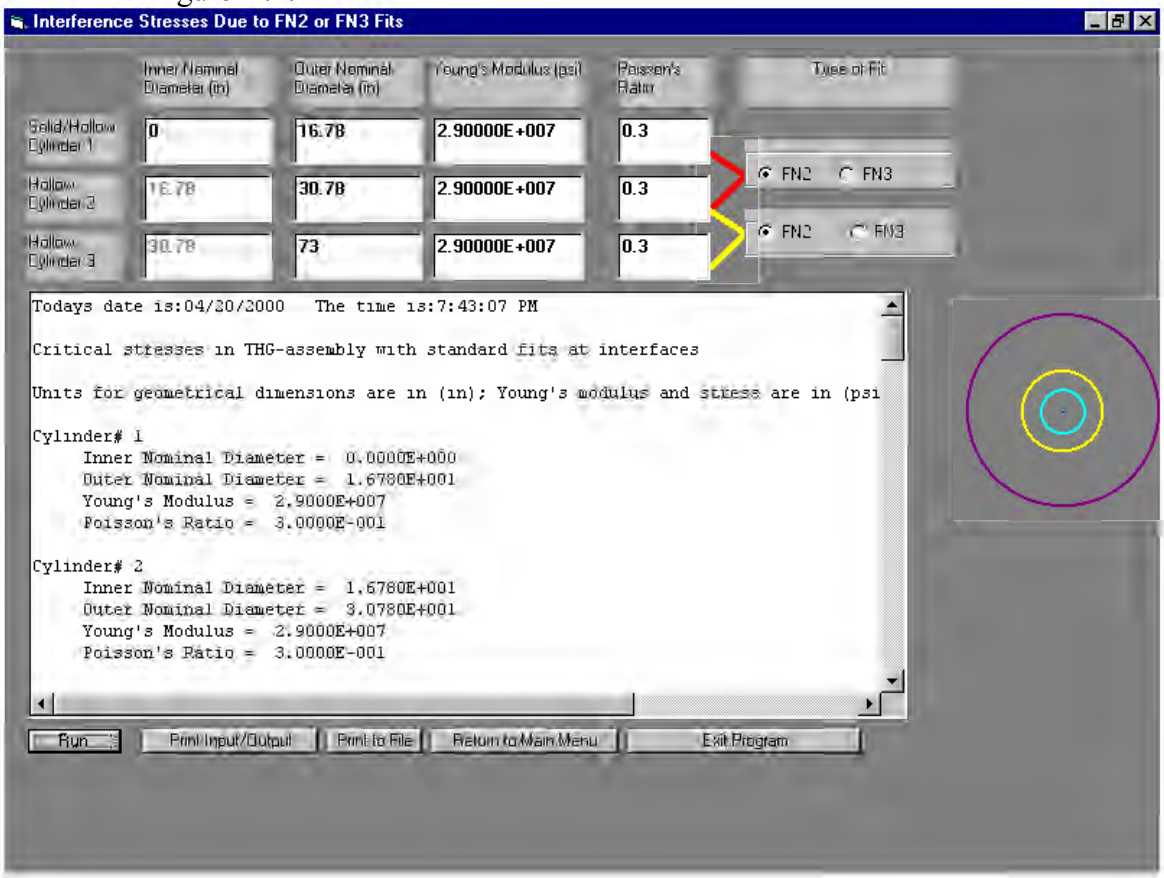

Figure A.4 Introductory screen for the interference stresses due to FN2 and FN3 fits program.

From the results given by the program, the interference pressures at the two interfaces are –5.99 ksi and –3.18 ksi. The maximum tensile hoop stress in the assembly of 8.263 ksi exists in Cylinder 3. The maximum Von-Mises stress of 13.11 ksi exists in Cylinder 2.

A.7 Conclusions

In summary, the first design tool simulates an actual bridge layout, and finds the actual torque necessary to raise the bridge leaf. The second design tool calculates radial, hoop, and Von-Mises stresses, as well as the radial displacements in each member (trunnion, hub, and girder). The third design tool, which is very similar to the second design tool, finds all of the critical stresses in the THG assembly at steady state as a function of the type of fit.

The primary benefit of these design tools is that they make the design and analysis of THG assemblies less tedious for the user. The programs allow the user to operate in a user-friendly, visual basic interface, and provide feedback on input data when it is

incomplete. The types of calculations that are done by the software are based on established methods of elasticity, bridge design, as well as the Allowable Stress Design and Load and Resistance Factor Design philosophies.

A.8 Software installation and system requirements

The following are the minimum computer system requirements for the installation of Bascule Bridge Design Tool:

1. Personal computer running Microsoft Windows 95/98 or Windows NT
2. 32 MB RAM
3. Internet connection for downloading program
4. WinZip software to unzip the zipped file of the installation program - WinZip can be downloaded free for 30 days from http://www.winzip.com
5. Microsoft Mouse
6. Printer recommended
7. SVGA or higher resolution video adapter

Bascule Bridge Design Tool can be installed in the following manner:

1. Go to the WWW address of http://www.eng.usf.edu/~besterfi/bascule/bascule.zip
2. Close all the applications except virus checkers.
3. Download the "bascule.zip" program to a temporary directory.
4. Unzip the program using a zip utility such as WinZip that can be downloaded free for 30 days from http://www.winzip.com.
5. Click on "setup.exe" file out of the unzipped files and follow the instructions.
6. Follow the instructions given on the screen. You can change the directory to anything you want.
7. Once the installation is complete, the program "THG-Assembly" will be part of the Program in the Start Menu.

APPENDIX B

USER MANUAL

B.1 Introduction

ANSYS was chosen as the parametric Finite Element Method (FEM) software of choice principally because of its strength in thermo-structural analysis. Also, the two ANSYS languages - ANSYS Parametric Design Language (APDL) and User Interface Design Language (UIDL) allow us to develop user friendly interfaces that can be used by a design engineer. Using a parametric model, transient stresses in the two alternative assembly procedures for different bridges are compared and our hypothesis is tested using time-history plots of temperature and stress.

The model, as the name suggests, is parametric, allowing the user to modify geometries, material and thermal properties of assembly materials and convective media, interference values, temperature of cooling and ambient convective media, and loading times. Also, depending on the required degree of accuracy, the user can also change mesh density and time steps. Options for different THG assemblies and different assembly procedures are included in the model. The results, such as, temperature and stress, are displayed both as a function of position (time fixed) in contour plots and as a function of time (position fixed).

One of the principal contributions of this work is creating a user friendly parametric model, which shall from now be called the Trunnion-Hub-Girder Testing Model (THGTM), to analyze existing Trunnion-Hub-Girder (THG) assemblies and design new assemblies. However, for brevity and simplicity, care was taken not to compromise the more important goals of accuracy and flexibility. Some intermediate knowledge of finite element modeling as regards to element shape testing, costs of mesh refinement, efficiency of computational time, accuracy trade-off, thermal-structural field interaction, limitations and assumptions of the model are expected of the user.

A step-by-step guide for using the THGTM is presented in this appendix. The program allows the user to analyze existing assemblies and design new assemblies. The two assembly procedures, assembly procedure 1 (AP1) and assembly procedure 2 (AP2), are modeled in the THGTM. This program allows the user to change materials, meshing parameters, loads and time increments. One useful feature of this program is that it allows the user to determine the exit points during the different steps in the analysis. Results are presented both in time history graphs (position fixed) and contour plots (time fixed).

The THGTM has a user-friendly interface in the form of dialog boxes, pick menus and toolbars. While every attempt has been made to make the program simple and user friendly, this has not been achieved at the cost of denying the user the flexibility over issues such as mesh density, computational time and accuracy. It is assumed that the user has some basic knowledge of finite elements with regards to element shape testing, thermo-structural field interaction, effects of mesh refinement on computational time, and computational time versus accuracy trade-off. The user should read Chapter 3 to understand and appreciate the modeling approach and assumptions used in the model. The program has been written principally in ANSYS Parametric Design Language (APDL) including a few commands from User Interface Design Language (UIDL).

B.2 Modeling of the assembly procedures

During the actual assembly of the trunnion-hub-girder (THG), the male part is cooled down till there is a clearance between the two parts of the assembly. Initially, convection with air and conduction in the gap between the two parts results in the parts coming into contact. After contact, conduction at the contact surfaces and convection with air at the free surfaces results in an interference fit between the two parts of the assembly. However, due to difficulties in modeling dynamic gap conduction using the sequential coupled field approach, a modified approach is used. In this model, the male part of the assembly is inserted in the female part as soon as the interference between the two parts is breached and hence no gap conduction is modeled.

The two cooling processes in each assembly procedure are analyzed separately and the results presented in ancillary files.

B.3 Running the trunnion-hub-girder testing model

A step-by-step guide to run the THGTM is presented next.

B.3.1 Starting the trunnion-hub-girder testing model

B.3.1.1 Step 1

On the desktop go the START menu and enter

START>Programs>ANSYS 5.5> Interactive

The interactive window in Figure B.1 is displayed.

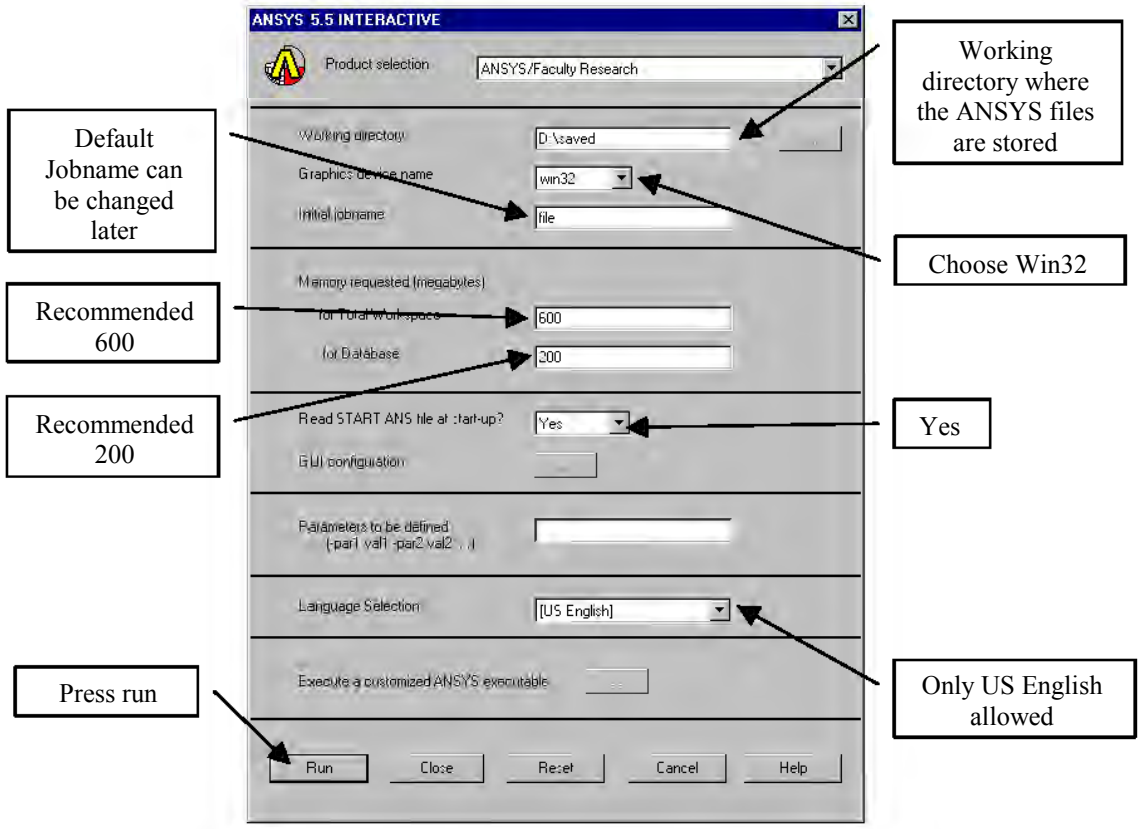

Figure B.1 Interactive.

Working directory: This directory contains all the ANSYS files. If one of the hard drives is getting full the working directory can be changed. The following files, available at www.eng.usf.edu/~besterfi/bascule/fem.zip must be copied to the new working directory.

thgtm1.mac: Input file for AP1
thgtm2.mac: Input file for AP2
hills: parameters for the Hillsborough Avenue Bridge
hallen1: parameters for the Hallendale Beach Boulevard Bridge
christa: parameters for the Christa McAuliffe Bridge
cause17: parameters for the 17th Street Causeway Bridge
thpost.mac: input file for the time-history postprocessor
myset.mac: input file for dimensioning the parameters

There is also a file ndraw.mac in the c:\tdraw directory. Do not delete any of these files. If you do delete them inadvertently then go to www.eng.usf.edu/~besterfi/bascule/fem.zip and download the files again. If you want to move this program to another computer, then do the following three steps.

1. Copy 'Start55.ans' from D:\ANSYS55\DOCU to the new \ANSYS55\DOCU directory of the drive where ANSYS is installed.
2. Copy all the required files to the new working directory.
3. Create a new directory c:\tdraw and copy ndraw.mac into it.

B.3.1.2 Step 2

On clicking on RUN in ANSYS 5.5 in the interactive menu shown in Figure B.3.1.1, the various ANSYS windows and input menus appear on the screen as shown in Fig B.3.1.2. A description of the menus and windows is as follows:

Main Menu: The main menu is the interactive interface for the ANSYS processors, operations and preferences.

Utility Menu: The utility menu is for performing the file operations and other non-processor dependent operations in ANSYS.

Output Window: The ANSYS output window displays the output of the ANSYS operations. In this model the output is not shown on the output window. Instead it is directed to an output file.

ANSYS Toolbar: The toolbar has many tools which will be used in the THGTM.

Graphics Window: The graphical output (solid model, meshing, results etc.) are displayed in the ANSYS graphics window.

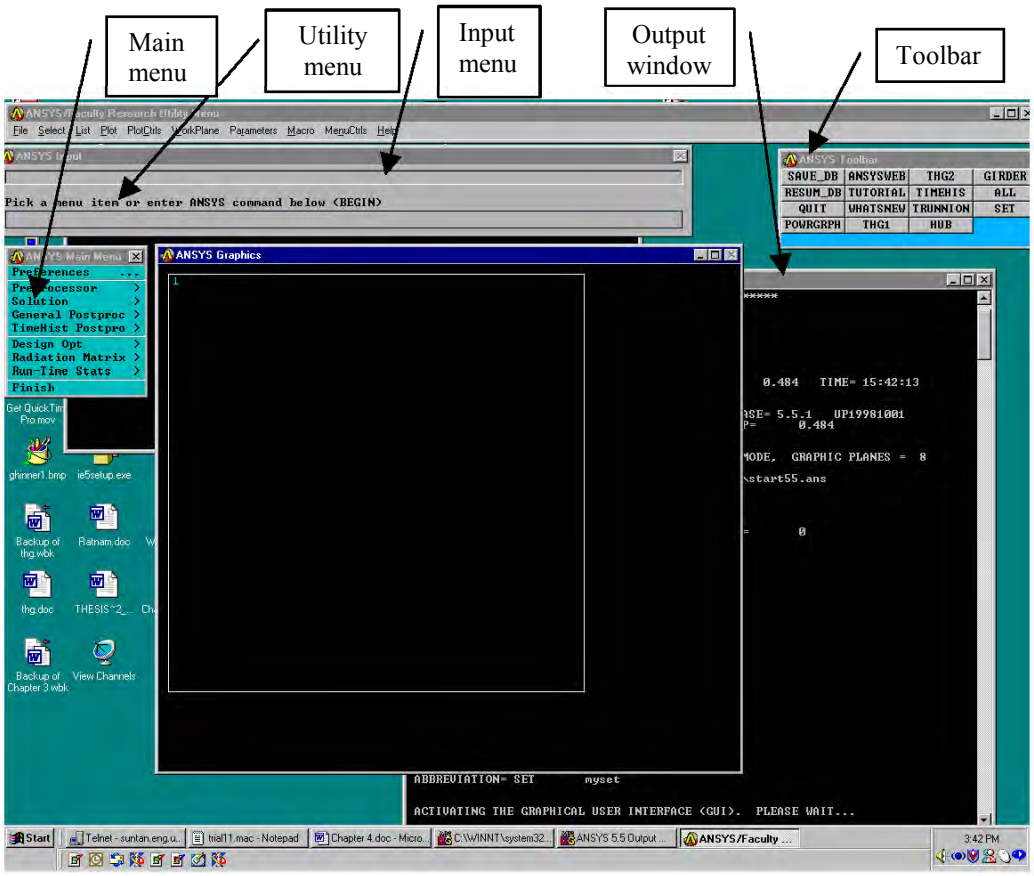

Figure B.2 ANSYS windows.

B.3.1.3 Step 3

Go to the ANSYS toolbar as shown in Figure B.3 and click on THG1 for AP1 and THG2 for AP2.

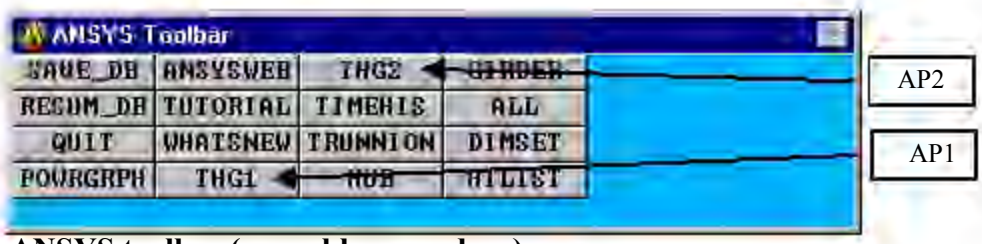

Figure B.3 ANSYS toolbar (assembly procedure).

B.3.2 Entering filenames

The filenames of the different parts of the analysis are entered in this section. As we are using a sequential coupled field process, both structural and thermal filenames are required for any run. Step 4 and Step 5 allow the user to enter the filenames for the complete thermal and structural analyses while Step 6, Step 7, Step 8, and Step 9 allow the user to enter filenames for the ancillary analyses. *Note that all filenames must be entered in single quotes*. For example for the Hillsborough Bridge using AP1 the thermal filename can be 'Thill1'.

B.3.2.1 Step 4

The thermal filename for the complete analysis is entered in the dialog box shown in Figure B.4.

Figure B.4 Thermal filename.

B.3.2.2 Step 5

The structural filename for the complete analysis is entered in the dialog box shown in Figure B.5

Figure B.5 Structural filename.

B.3.2.3 Step 6

For AP1, the thermal filename for the cooling down of the trunnion is entered in the dialog box shown in Figure B.6a

Figure B.6a Trunnion cooling thermal filename.

For AP2, the thermal filename for the cooling down of the hub is entered in the dialog box shown in Figure B.6b.

Figure B.6b Hub cooling thermal filename.

B.3.2.4 Step 7

For AP1, the structural filename for the cooling down of the trunnion is entered in the dialog box shown in Figure B.7a.

Figure B.7a Trunnion cooling structural filename.

For AP2, the structural filename for the cooling down of the hub is entered in the dialog box shown in Figure B.7b.

Figure B.7b Hub cooling structural filename.

B.3.2.5 Step 8

For AP1, the thermal filename for the cooling down of the trunnion-hub is entered in the dialog box in Figure B.8a.

Figure B.8a Trunnion-hub cooling thermal filename.

For AP2, the thermal filename for the cooling down of the trunnion is entered in the dialog box shown in Figure B.8b.

Figure B.8b Trunnion cooling thermal filename.

B.3.2.6 Step 9

For AP1, the structural filename for the cooling down of the trunnion-hub is entered in the dialog box shown in Figure B.9a.

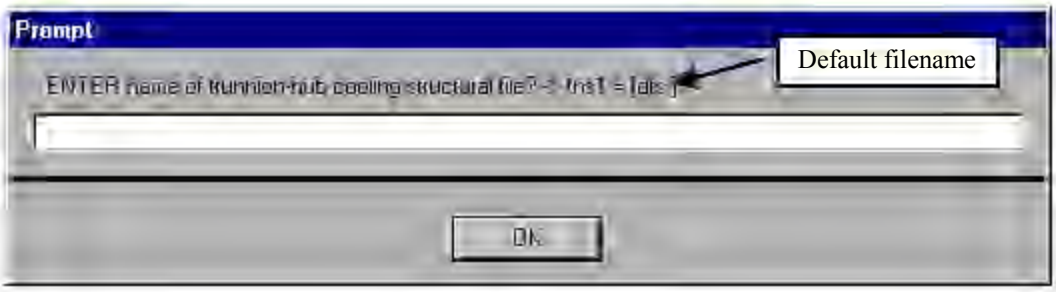

Figure B.9a Trunnion-hub cooling structural filename.

For AP2, the structural filename for the cooling down of the trunnion is entered in the dialog box shown in Figure B.9b.

Figure B.9b Trunnion cooling structural filename.

A series of error messages shown in Figure B.9c will appear.

Figure B.9c Error message.

These error messages are caused due to a bug in the ANSYS software and do not affect the program in any way. Keep on clicking OK to ignore the errors till the next multi-prompt dialog box appears.

B.3.3 Material and geometric parameters

The steps described in this section allow the user to enter material and geometric parameters. The user is given the choice of using one of the existing geometries of the THG assemblies or entering his/her own geometrical parameters.

B.3.3.1 Step 10

A multi-prompt dialog box similar to the one shown in Figure B.10 appears allowing the user to choose the material of the THG assembly.

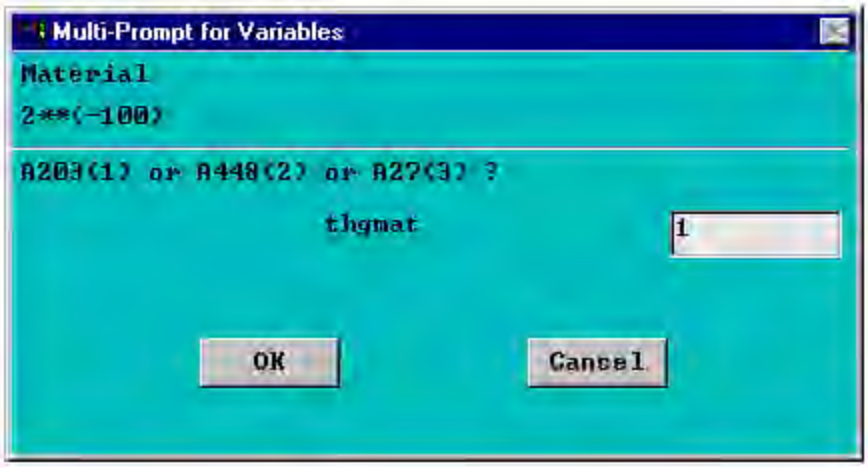

Figure B.10 Material choice menu.

B.3.3.1 Step 11

The user is given a choice between using the existing geometries for the bridges or entering his or her own geometric parameters. The multi-prompt dialog box shown in Figure B.11 allows the user to choose between the following: choice=1 is to use one of the saved bridges and choice=2 is to design a new bridge.

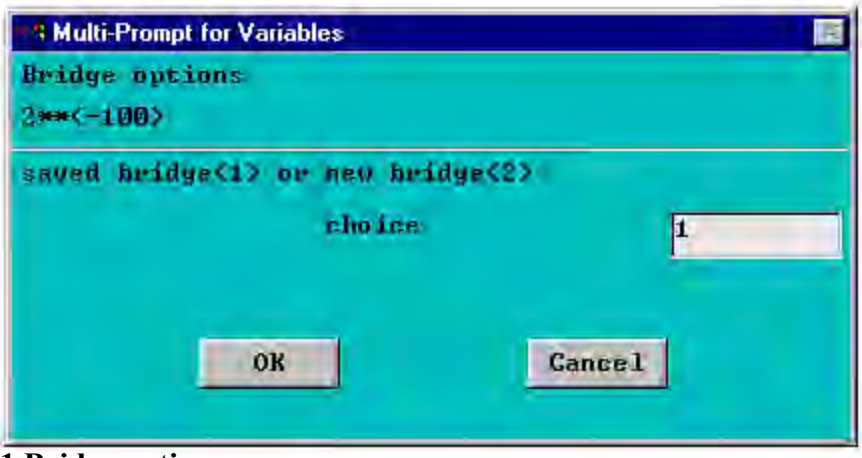

Figure B.11 Bridge options menu.

The next step depends upon the 'choice' parameter entered in Step 11. Ignore all the error messages till you get the next multi-prompt dialog box.

B.3.3.3 Step 12 (choice=1)

This option allows you to choose one of the existing THG assemblies. Ignore all the error messages till you get multi-prompt dialog box similar to the one shown in Figure B.12.

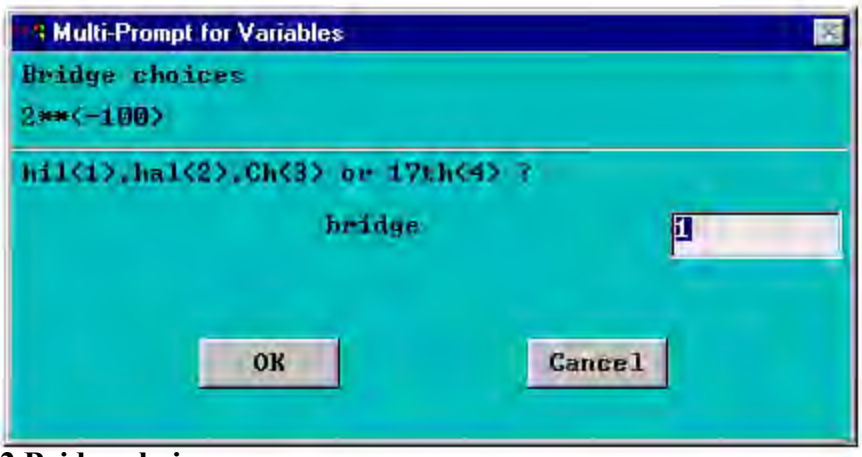

Figure B.12 Bridge choices menu.

The multi-prompt dialog box shown in Figure B.12 allows the user to choose between the following: bridge=1 is to use Hillsborough Avenue Bridge; bridge=2 is to use Hallendale Beach Boulevard Bridge; bridge=3 is to use Christa McAuliffe Bridge; and bridge=4 is to use 17th Street Causeway Bridge.

B.3.3.4 Step 12 (choice=2)

This option allows you to build a THG assembly with user defined geometric parameters. Ignore all the error messages till you get a multi-prompt dialog box. The default parameters are set for the Christa McAuliffe Bridge.

B.3.3.4.1 Step 12a (choice=2)

Figure B.13a shows the trunnion dimensions to be entered. All dimensions are in inches.

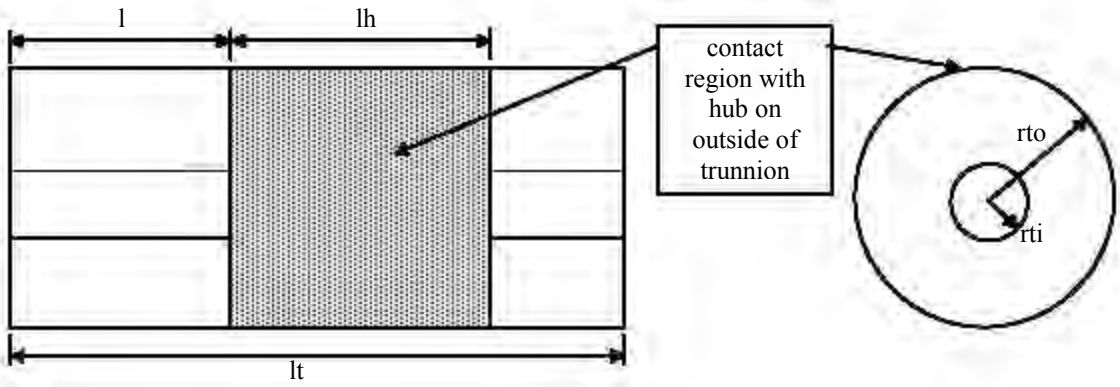

Figure B.13a Trunnion dimensions.

The dimensional parameters to be entered are

lt	=	total length of the trunnion,
l	=	Extension of the trunnion on the gusset side (length to hub on the trunnion on the gusset side),
lh	=	total length of the hub,
rti	=	inner radius of the trunnion, and
rto	=	outer radius of the trunnion (inner radius of the hub)

Figure B.13b shows the multi-prompt dialog box for entering the trunnion dimensions.

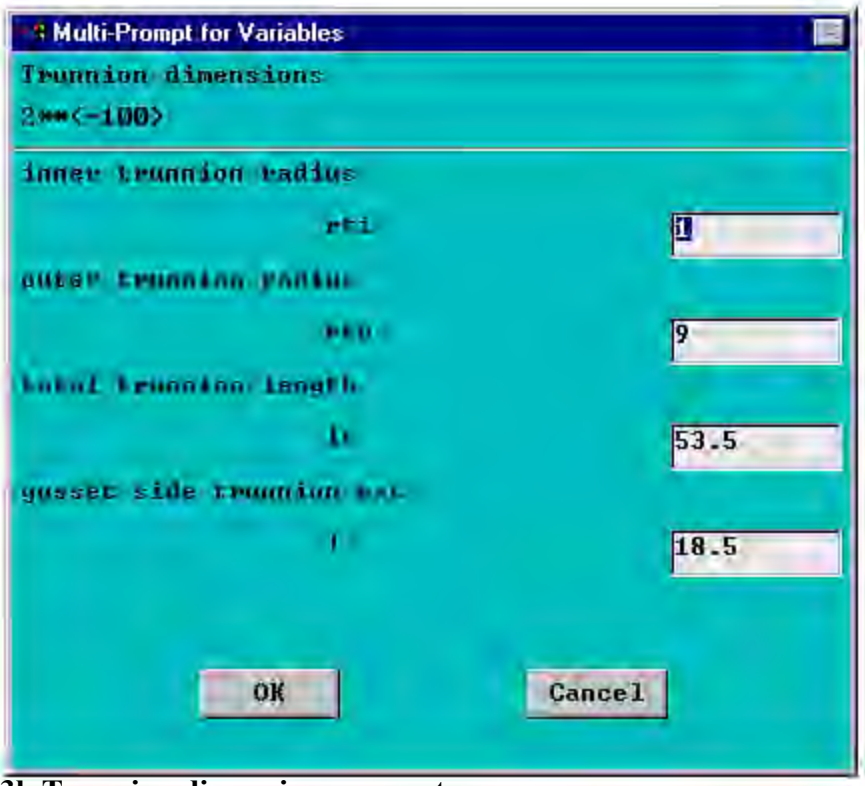

Figure B.13b Trunnion dimension parameters.

After entering the trunnion parameters click OK. Ignore the error messages by clicking OK to each of them till the next multi-prompt dialog box appears on the screen.

B.3.3.4.2 Step 12b (choice=2)

The hub dimensions to be entered are shown in Figure B.3.3.4.2a. All dimensions are in inches.

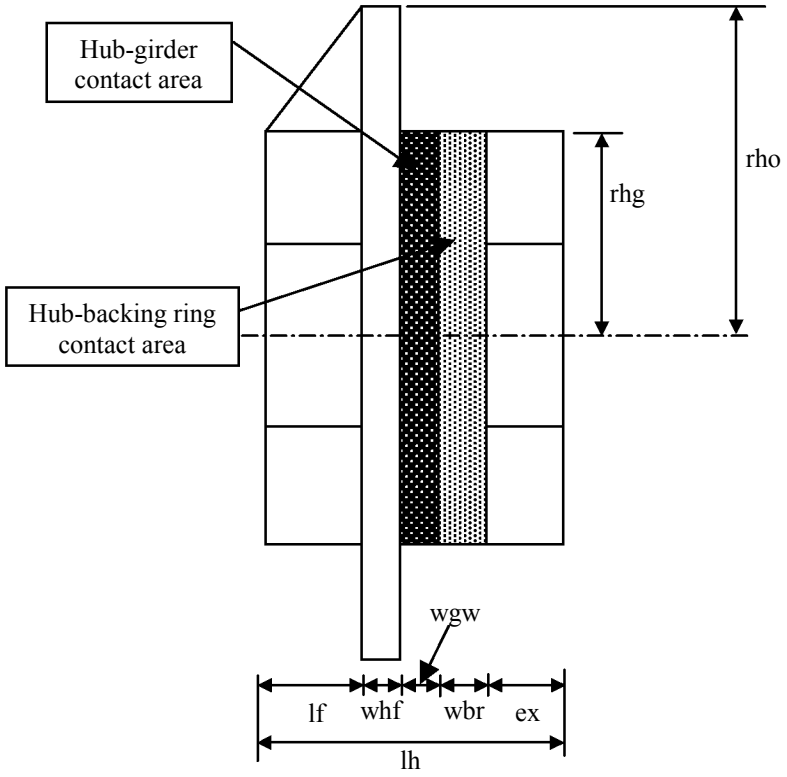

Figure B.14a Hub dimensions.

The dimensional parameters to be entered are

rhg	=	outer radius of the hub (minus flange),
rho	=	outer radius of the hub flange,
wbr	=	backing ring width,
wgw	=	width of the girder (web),
whf	=	width of hub flange,
lf	=	distance to hub flange,
lh	=	total length of the hub,
tg	=	gusset thickness, and
ex	=	distance from the end of the backing ring to the end of the hub.

The hub dimensions can be entered in the multi-prompt dialog box shown in Figure B.14b.

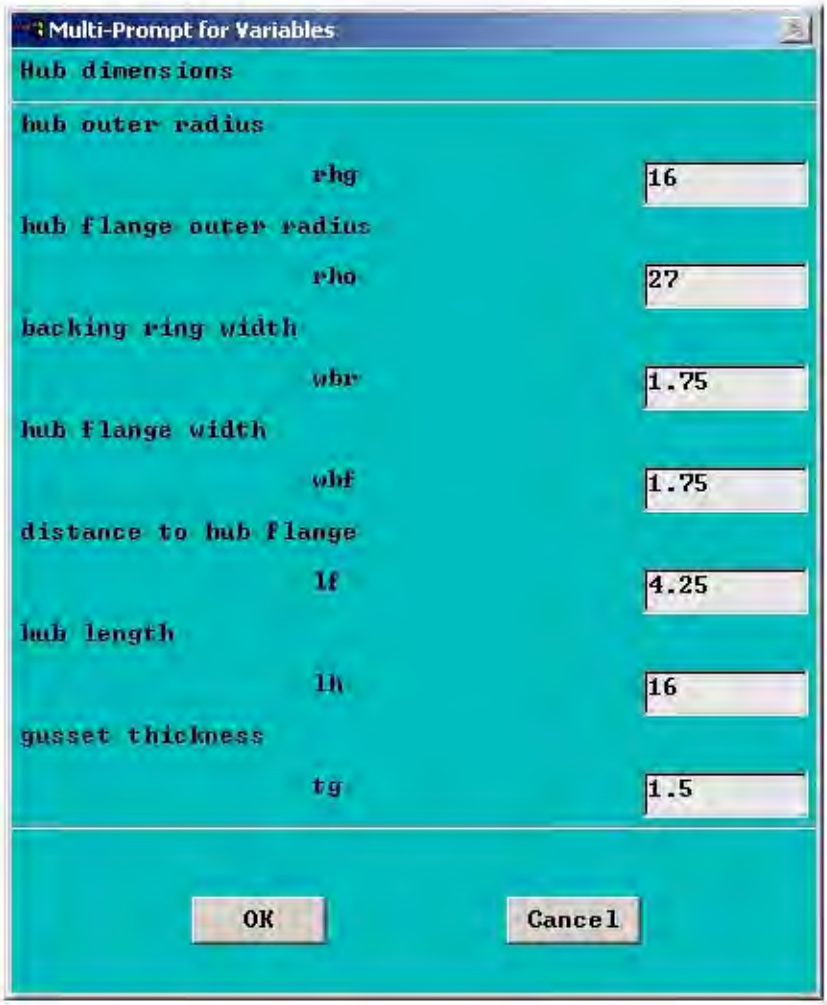

Figure B.14b Hub dimension parameters.

After entering the trunnion parameters click OK. Ignore the error messages by clicking OK to each of them till the next multi-prompt dialog box appears on the screen.

B.3.3.4.3 Step 12c (choice=2)

The dimensions to be entered for the girder are shown in Figure B.15a. All dimensions are in inches.

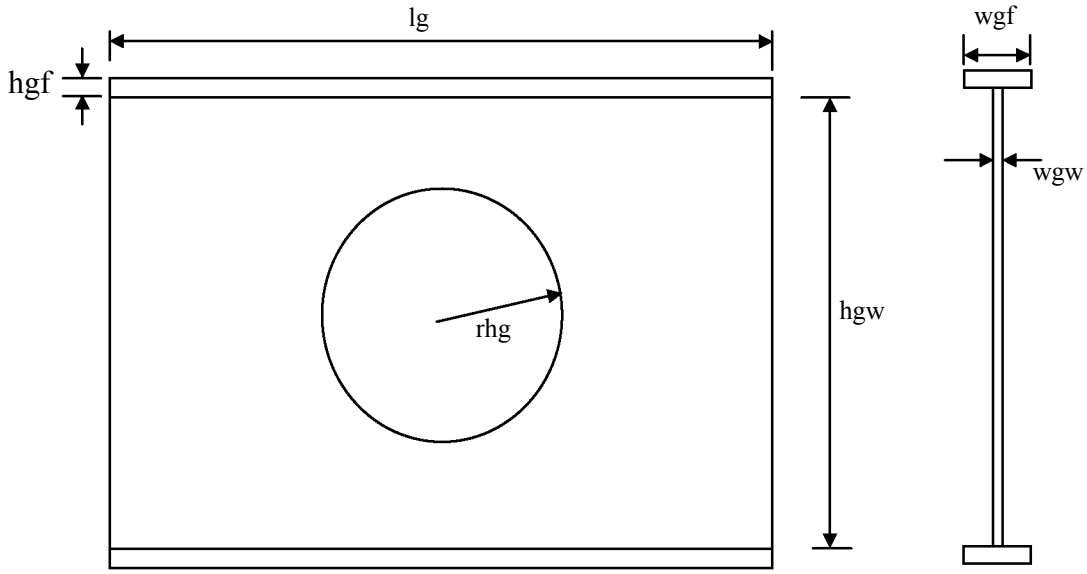

Figure B.15a Girder dimensions.

The dimensional parameters to be entered are

wgf = width of the girder flange,
hgw = height of the girder web,
lg = width of the girder,
hgf = height of the girder flange, and
wgw = width of the girder web.

The girder dimensions can be entered in the multi-prompt dialog box shown in Figure B.15b.

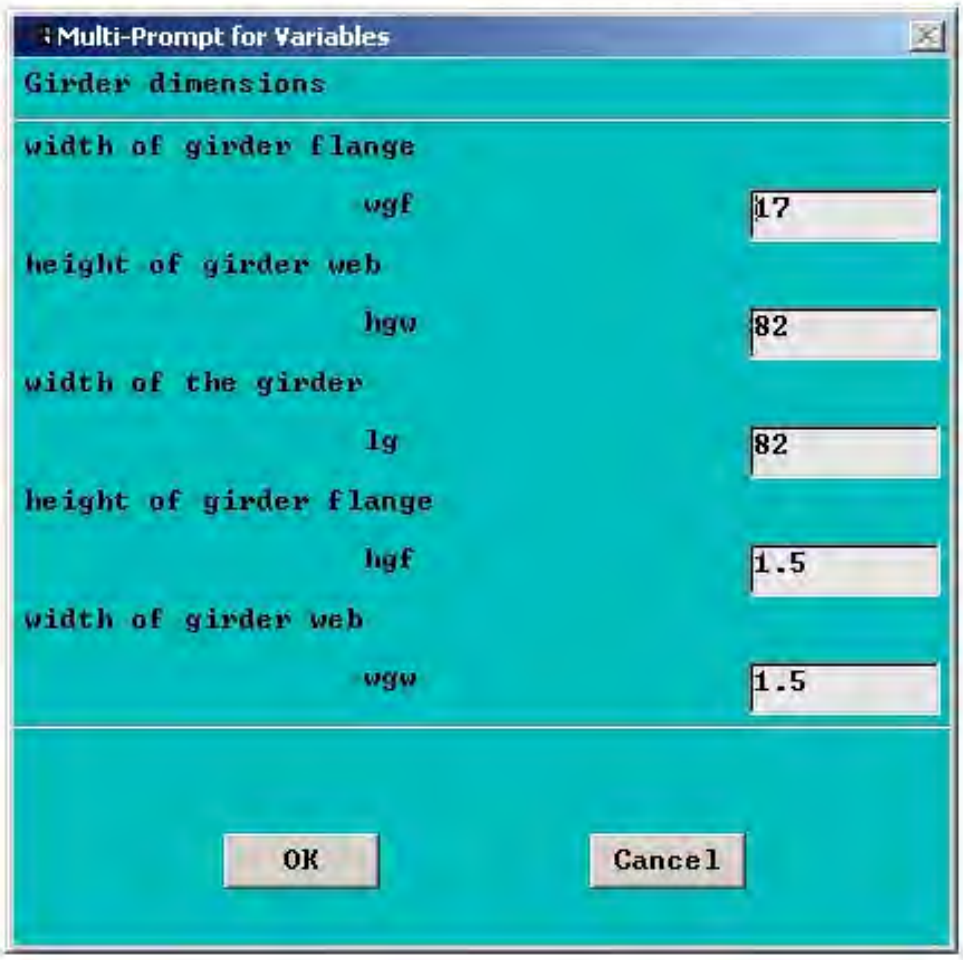

Figure B.15b Girder dimension parameters.

Click OK to ignore all the error messages till the next multi-prompt dialog box appears on the screen.

B.3.4 Meshing input

The meshing details of the THG assembly are entered here. Some meshing parameters have restrictions as regards to the range of values that can be used. The acceptable values are shown in the parentheses for these parameters.

B.3.4.1 Step 13

The divisions along the girder are entered here. Figure B.16a shows the girder division parameters to be entered.

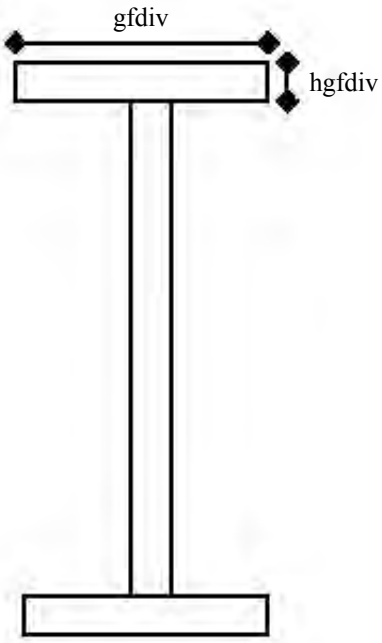

Figure B.16a Girder divisions.

The girder division parameters to be entered are

gfdiv = number of divisions along the girder flange width, and
hgfdiv = number of divisions along the girder flange height

Figure B.16b shows the multi-prompt dialog box where the girder dimension parameters to be entered.

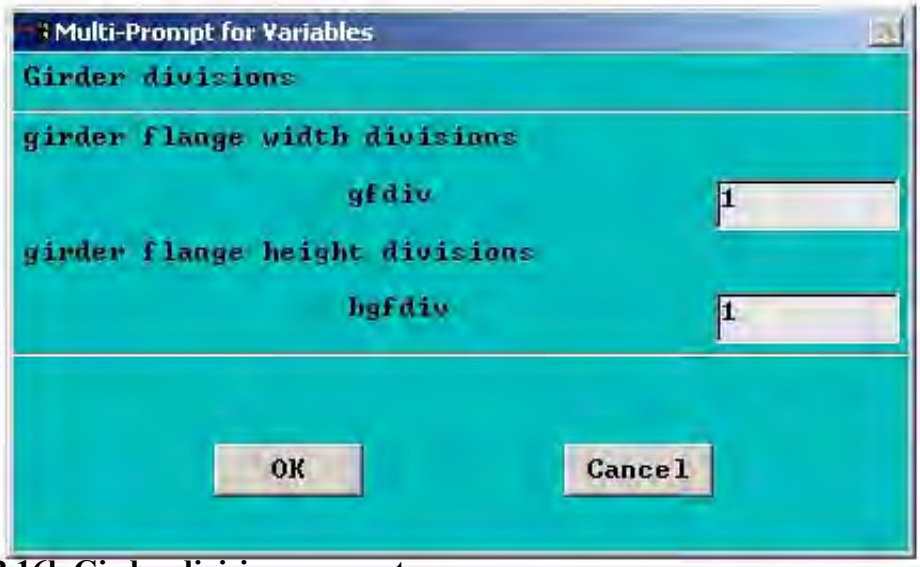

Figure B.16b Girder division parameters.

After entering the parameters click OK. Ignore all the error messages till the next multi-prompt dialog box appears on the screen.

B.3.4.2 Step 14

Meshing parameters along the length, that is, number of divisions along the length are during this step. Figures B.17a and B.17b show the meshing parameters to be entered.

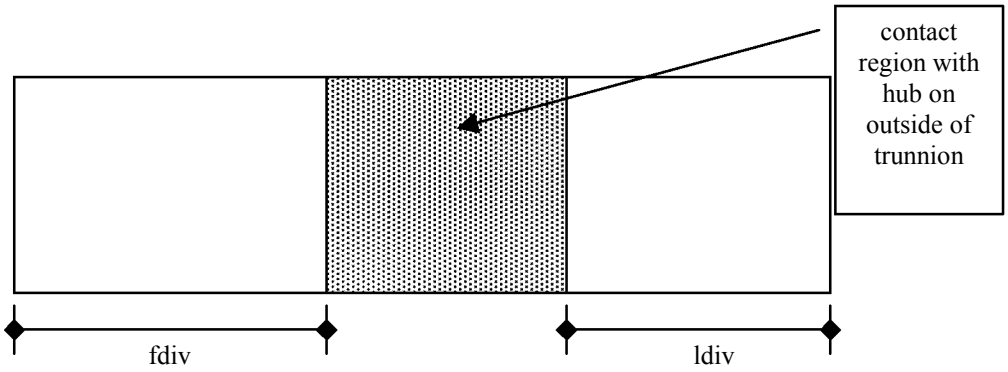

Figure B.17a Divisions along the length (trunnion).

The meshing parameters to be entered are

fdiv = number of divisions along the length to the hub on the gusset side, and
ldiv = number of divisions along the length to the hub on the backing ring side.

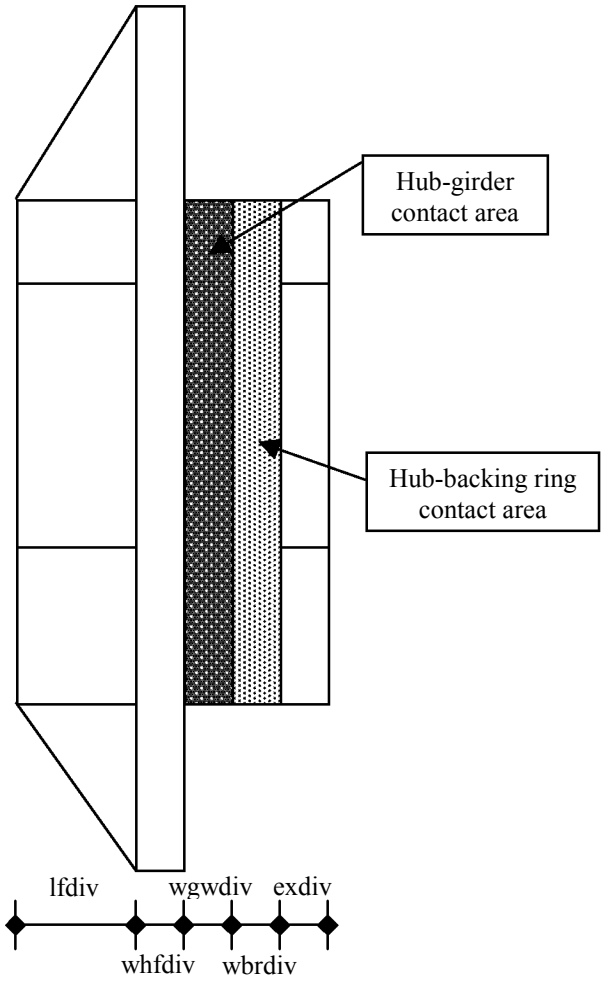

Figure B.17b Divisions along the length (hub).

The relevant dimensional parameters are explained in Appendices B.3.3.4.1, B.3.3.4.2 and B.3.3.4.3.

fdiv = number of divisions along f,
exdiv = number of divisions along ex,
whfdiv = number of divisions along whf,
wbrdiv = number of divisions along wbr,
wgwdiv = number of divisions along wgw,
whfdiv = number of divisions along whf,
lfdiv = number of divisions along lf, and
ldiv = number of divisions along l.

Figure B.17c shows the multi-prompt dialog box where the parameters are to entered.

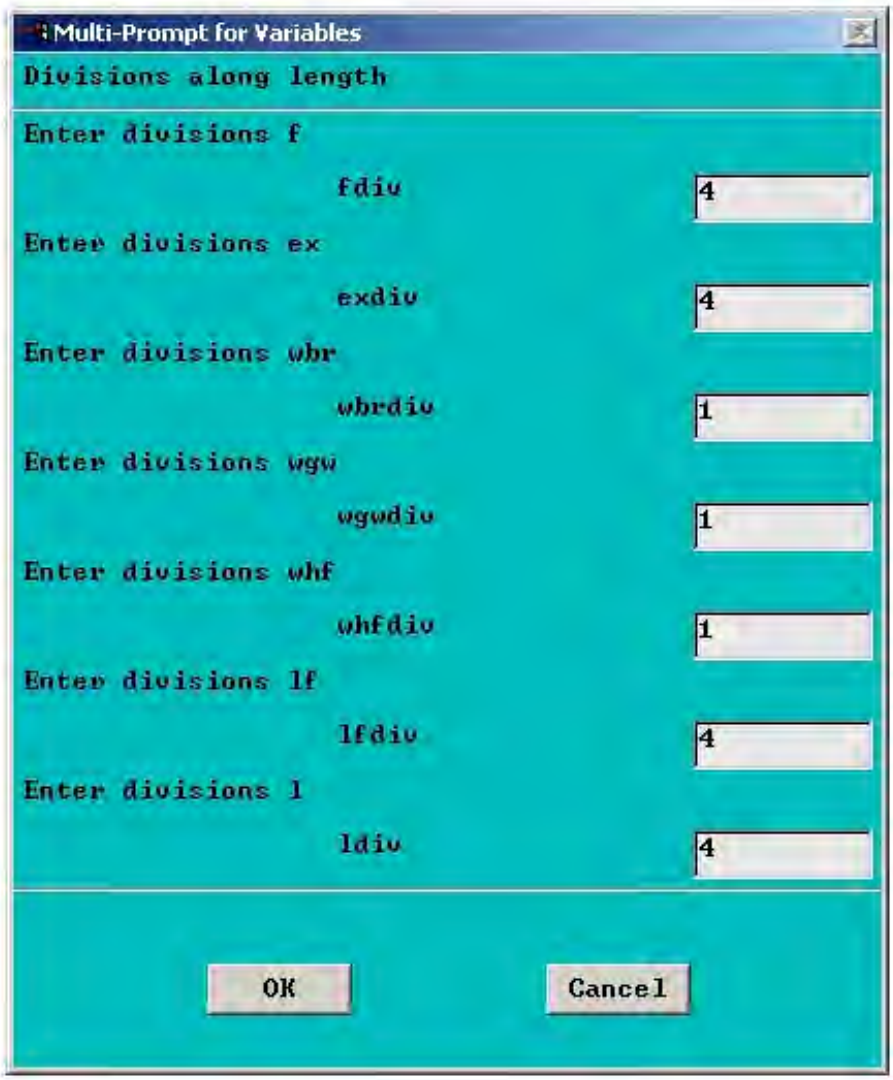

Figure B.17c Divisions along the length parameters.

After entering the parameters click OK. Ignore the error messages till the next multi-prompt dialog box appears on the screen.

B.3.4.3 Step 15

Some more meshing parameters, such as, number of radial and circumferential divisions, are entered here. The number of radial divisions is the same for the trunnion, hub and the girder. This is done so that the components contact each other smoothly. Figures B.18a, B.18b and B.18c show the radial and circumferential divisions to be entered for the trunnion, the hub and the girder

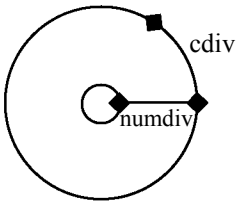

Figure B.18a Trunnion radial and circumferential divisions.

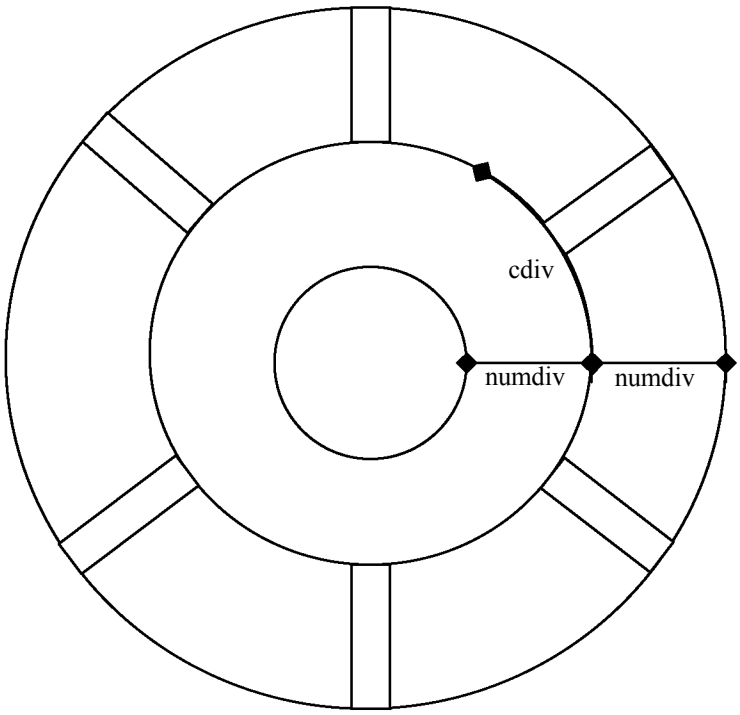

Figure B.18b Hub radial and circumferential divisions.

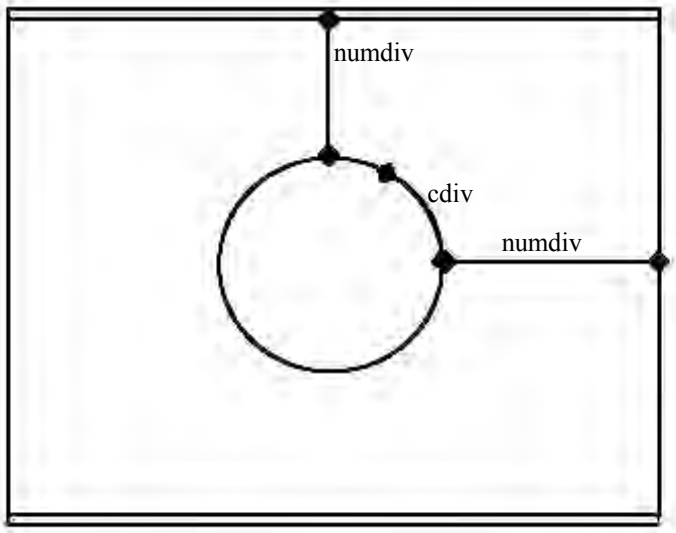

Figure B.18c Girder radial and circumferential divisions.

The radial and circumferential divisions to be entered are:

numdiv = number of divisions in the radial direction in each the trunnion, the hub and the girder, and

cdiv = number of divisions in the circumferential direction for every 60^0 (between a pair of gussets).

Note that restricted values for 'numdiv' are odd numbers greater or equal to three (that is, 3, 5, 7, 9, …), and restricted numbers for 'cdiv' are multiples of 4 (that is, 4, 8, 12, …). Figure B.3.4.3d shows the multi-prompt dialog where the radial and circumferential parameters are to be entered.

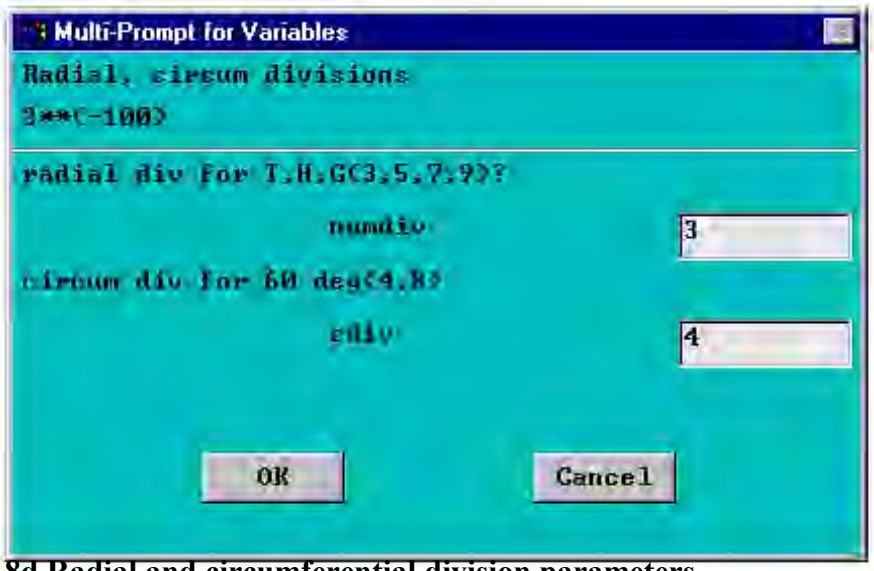

Figure B.18d Radial and circumferential division parameters.

Click OK. Ignore all the error messages which follow till the next multi-prompt dialog box appears on the screen.

B.3.4.4 Step 16

The radial interference between the trunnion and hub (thInt) and the hub and girder (hgInt) are entered at this step. The interference values for FN2 and FN3 fits can be obtained using the Bascule Bridge Design Tools (Denninger, 2000). Click OK after entering the values. All parameters to be entered are in inches. Ignore the error messages till you get the next multi-prompt dialog box (see Figure B.19) and the hourglass cursor changes back into the arrow.

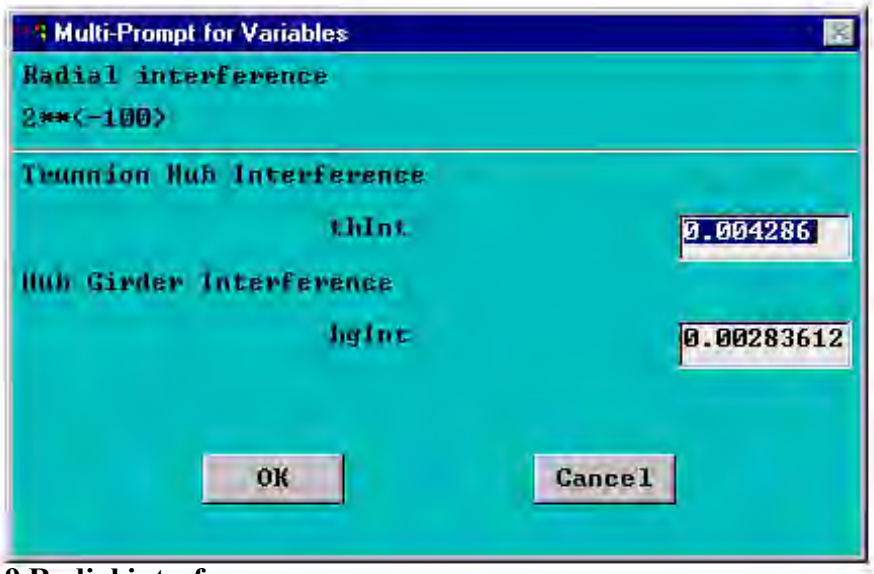

Figure B.19 Radial interference.

B.3.5 Loading input

B.3.5.1 Step 17

The cooling medium bulk temperature (Tcool) and the ambient air bulk temperature (Tbulk) are to be entered in the multi-prompt dialog box shown in Figure B.20. Note that all units are ^{0}F. After entering the values, click OK. Ignore the series of error messages by clicking OK till you get a multi-prompt dialog box.

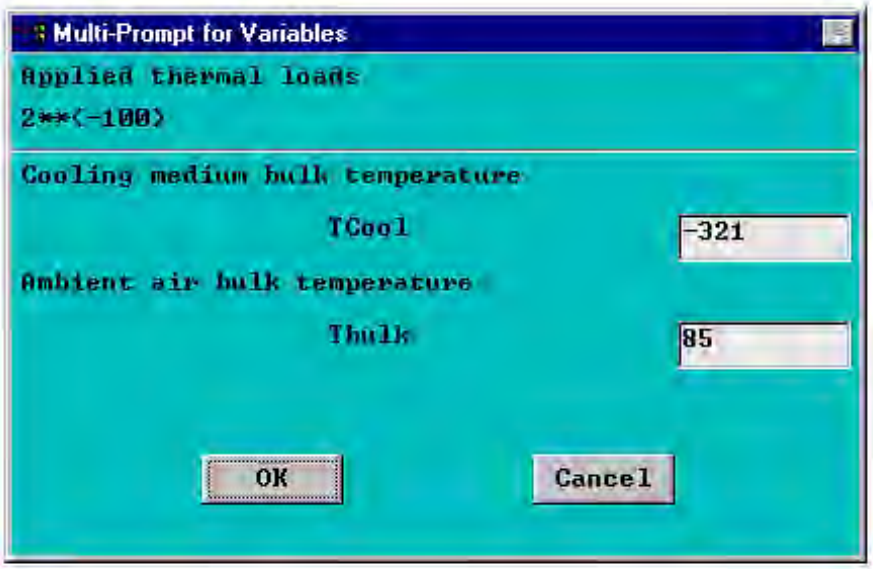

Figure B.20 Applied thermal loads.

B.3.5.2 Step 18

The time temperature and time increment options are entered in this step. AP1 and AP2 have different input files and hence have their own distinct set of input parameters.

For AP1, the time-temperature options are entered in the multi-prompt dialog box shown in Figure B.21a. An explanation of the parameters to be entered is also included in this section.

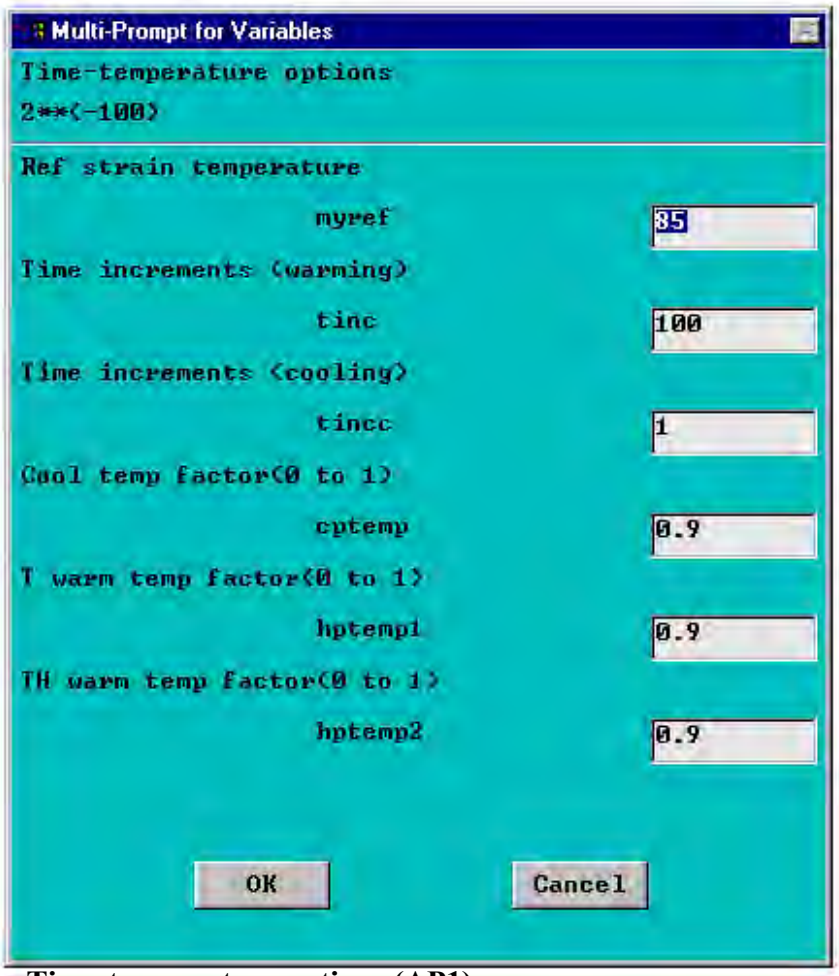

Figure B.21a Time-temperature options (AP1).

For AP2, the time-temperature options are entered in the multi-prompt dialog box shown in Figure B.21b.

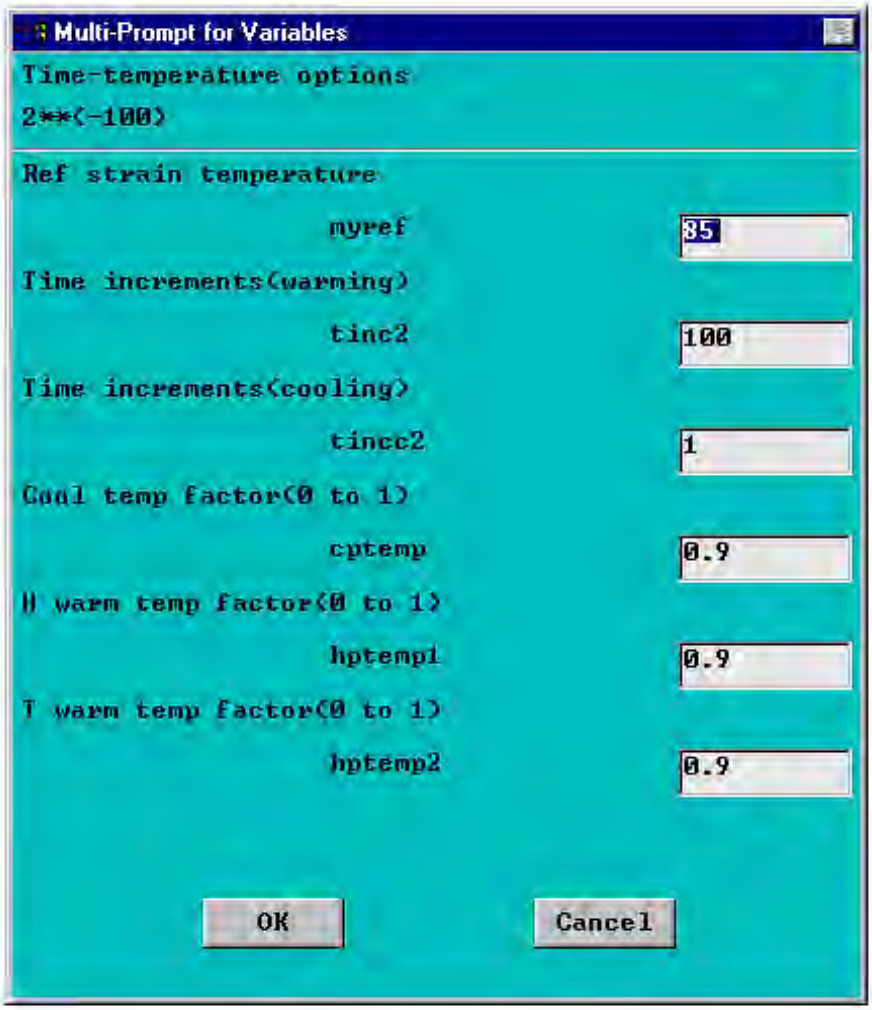

Figure B.21b Time –temperature options (AP2).

In Figure B.21b, the following input parameters are described:

Reference strain temperature (myref): The reference temperature is the temperature at which the strains are zero. Normally, the reference temperature should be the same as the ambient air temperature. The ambient air temperature should be entered unless the reference temperature is different from ambient air temperature.

Time increments for warming (tinc, tinc2) and time increments for cooling (tincc, tincc2): The time increments denote the time intervals at which the results are saved. The larger the time increment, the less accurate the result, the fewer the points on the load history and hence the less is the computational time. Time increments for the warming and cooling process should be chosen balancing the needs of accuracy, conserving computational time and required number of points in the loading history. Typically, the time increments during warming could be a larger (25-200 minutes) than the time increments during cooling (1-4 minutes), as warming is a slower process than cooling. The values in the brackets are only a suggested range of values. The user can choose any integer time increment he or she considers fit.

Cool temperature factor (cptemp): This parameter determines the point at which the cooling process is to be stopped. The cooling process stopped once the minimum temperature in the assembly falls below the stop temperature determined by Equation (B.1a)

$$T_s^c = TCool + (1 - cptemp) * (TBulk - TCool) \quad \text{(B.1a)}$$

where

T_s^c = warm temperature criterion,
TBulk = ambient air bulk temperature, and
TCool = cooling medium bulk temperature.

Note that, large values (0.95 to 0.9999) are recommended for the cool temperature factor. In this model we use the sequential coupled field approach and hence, the thermal analysis for the cooling process is performed before the structural analysis. 'cptemp' determines the parameter for exiting the thermal analysis during cooling. If a small value of cptemp is used then it can cause the thermal analysis to exit even before the time point at which the gap between the two bodies is breached in the structural analysis. However, the cptemp=1 should not be used as a body theoretically attains the bulk temperature of the surrounding medium only after infinite units of time.

Warm temperature factor (hptemp1 and hptemp2): The duration of the warming up process is determined by the warm temperature factor. The warming up process is stopped once the minimum temperature in the assembly exceeds the temperature determined by the stop temperature determined by Equation (B.1b).

$$T_s^w = TBulk - hptemp(i) * (TBulk - TCool), \quad i = 1, 2 \quad \text{(B.1b)}$$

where,

T_s^c = cool temperature criterion,
TBulk = ambient air bulk temperature,
TCool = cooling medium bulk temperature, and
hptemp(*i*) = warm temperature factor for each of the two warming up processes.

In Equation (B.1b), i=1, 2 denotes the first warming up process and the second warming up process, respectively.

B.3.5.3 Step 19

Additional parameters required for performing the stand alone runs of the cooling processes are entered in this step, that is, the time for which each cooling process is to be analyzed. For AP1 the ancillary cooling parameters are entered in Figure B.22a. where coolt1 is the trunnion cooling time and coolt2 is the trunnion-hub cooling time.

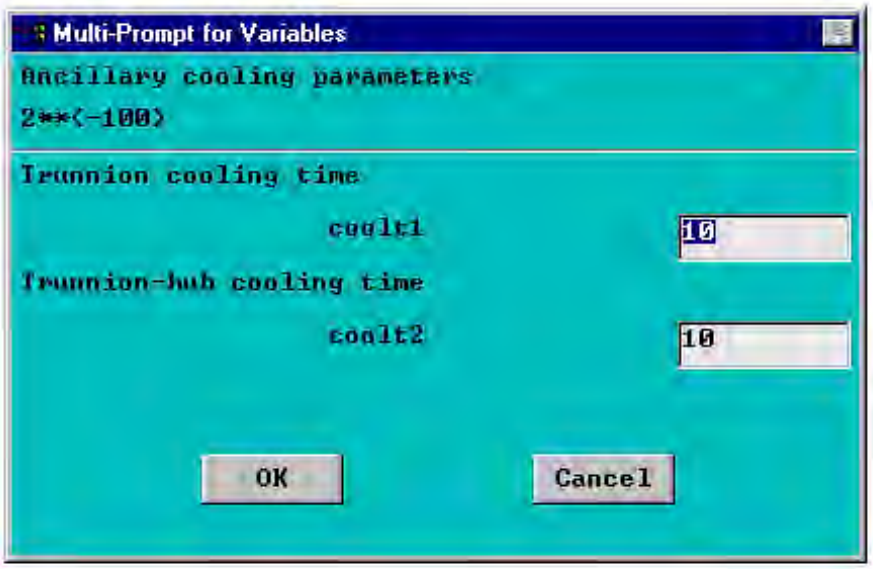

Figure B.22a Ancillary cooling parameters (AP1).

For AP2, the ancillary cooling parameters are given in Figure B.22b where coolt1 is the hub cooling time and coolt2 is the trunnion cooling time.

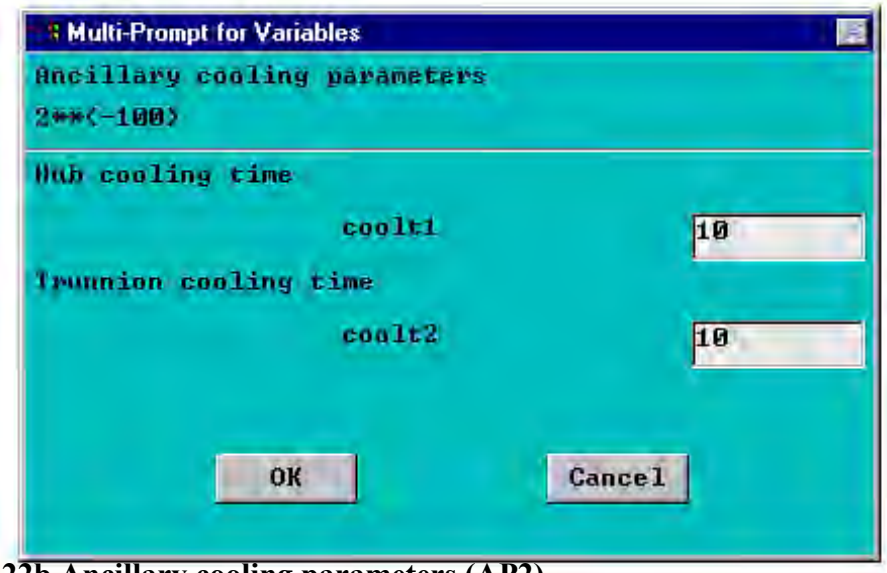

Figure B.22b Ancillary cooling parameters (AP2).

B.3.5.4 Step 20

In this step we define the equation of fracture toughness as a function of temperature. Figure B.23a shows the multi-prompt dialog box where the coefficients and the constants are entered. The factor for the edge effects is also input in this step. The equation of fracture toughness is assumed to be a fourth degree equation of temperature

$$K_{Ic} = (\text{fourth}) * T^4 + (\text{third}) * T^3 + (\text{second}) * T^2 + (\text{first}) * T + cterm, \qquad \text{(B.2a)}$$

where fourth, third, second, first, T and *cterm* are coefficient coefficients of the equation. The critical crack length (CCL), a_c, is given by

$$a_c = \frac{K_{Ic}^2(T)}{fedge^2 \pi \sigma_\theta^2} \qquad \text{(B.2b)}$$

where

$K_{Ic}(T)$ = temperature dependent critical stress intensity factor,
$fedge$ = edge effects factor, and
σ_θ = hoop stress.

Figure B.23a Fracture coefficients and constants.

After entering all of the parameters required for the run in Figured B.23a, click OK. The time required for the solution to run depends upon mesh density, time increments, temperature factors, time parameters, meshing prameters, temperature factors and ancillary parameters. While the solution is running, Figure B.23b appears on the screen.

Figure B.23b ANSYS process status bar.

The time required to complete a run depends on the bridge, meshing parameters, time increments, temperature factors and ancillary parameters. A run takes a minimum of 5 hrs. Once the ANSYS process status bar shown in Figure B.23b disappears from the screen, the solution is complete and ready for further post-processing. The required ANSYS files have been saved in the working directory. Go to Appendices B.5 and B.6 to do the post-processing. Note that, the program does not have exit options or warnings if wrong values are entered. Hence, if any wrong values are input, exit ANSYS by pressing Ctrl+Alt+Del.

Once the solution is complete, pick all the ANSYS processes shown in Figure B.23c and end them by clicking on END TASK.

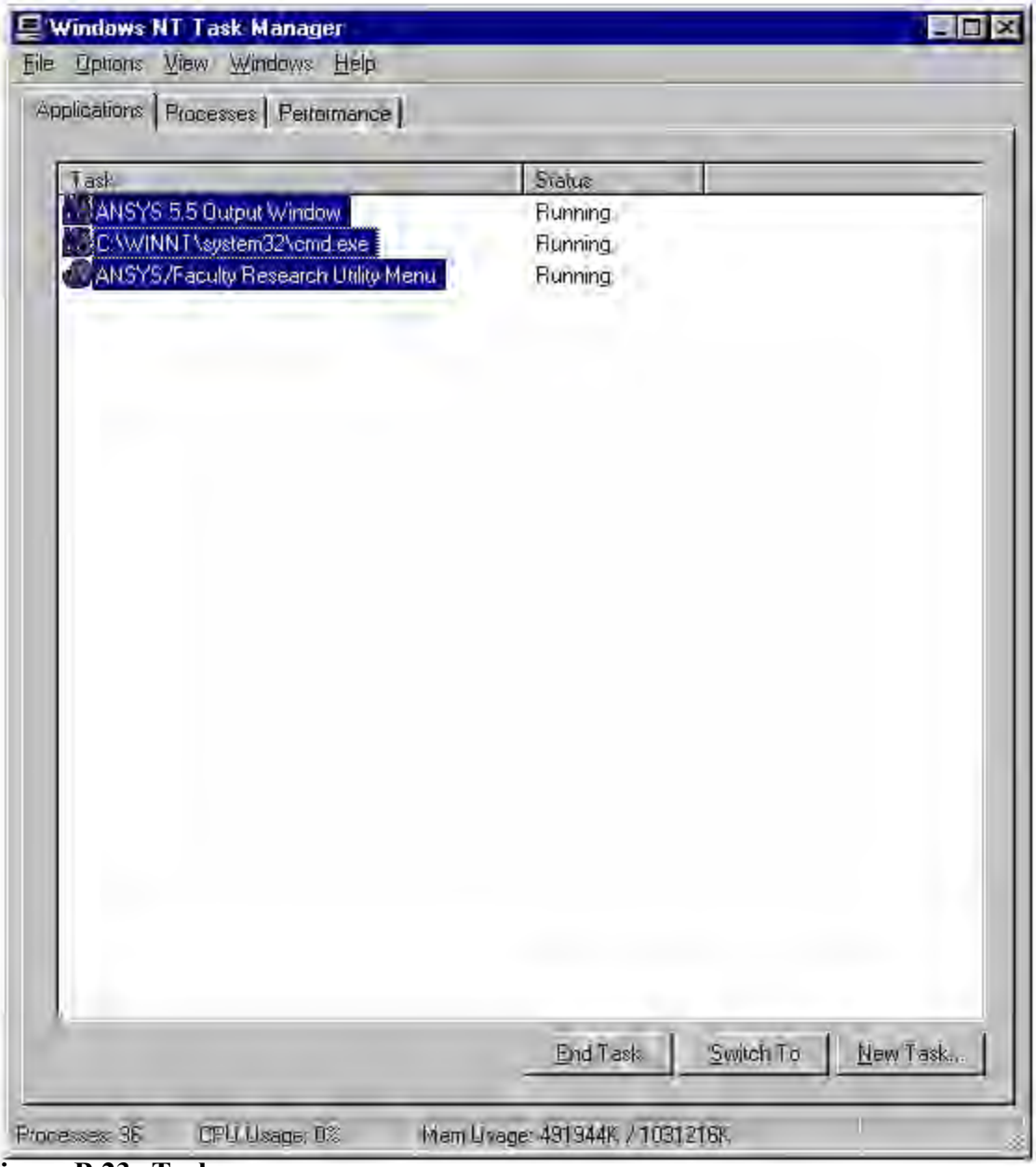

Figure B.23c Task manager.

B.3.6 Trunnion-hub-girder testing model crash

The THGTM can crash due to two possible situations. In Situation 1 the disk drive is full and there is no space to store the ANSYS files. The remedy for this situation is to free up some disk space and run the program again. In Situation 2 ANSYS is out of memory. This situation is unlikely as the recommended values should normally be sufficient. The remedy for this situation is to increase the database space and workspace memory in interactive menu in Step 1 (refer to Figure B.1) of Appendix B.3

B.4 Resuming an already saved job

This section describes how the results of previous runs can be reviewed.

B.4.1 Step 1

Follow Step 1 and Step 2 of Appendix B.3, that is, enter

File>Utlilty menu>Change jobname

The textbox in the Figure B.24 asks the user to 'enter a new jobname'. The user should enter the jobname of the previously saved runs. Note that, filenames in the THGTM are case sensitive.

Figure B.24 Enter filename.

The filename must correspond to one of the previously saved runs. The filename to be entered will depend upon the type of post-processing to be performed subsequently. To enter one of the two post-processors, follow the guidelines presented next.

General Postprocessor:

Stresses: Enter the name of the structural file in Figure B.24.

Temperatures: Enter the name of the thermal file in Figure B.24.

Time history postprocessor:

Stresses and temperatures: Enter the name of structural file in Figure B.24.

Once the filename is entered, click OK.

B.4.2 Step 2

Go to the Utility menu and enter the following.

File>Utility Menu>Resume Jobname.db

B.4.3 Step 3

On the ANSYS toolbar (see Figure B.25a) click on DIMSET

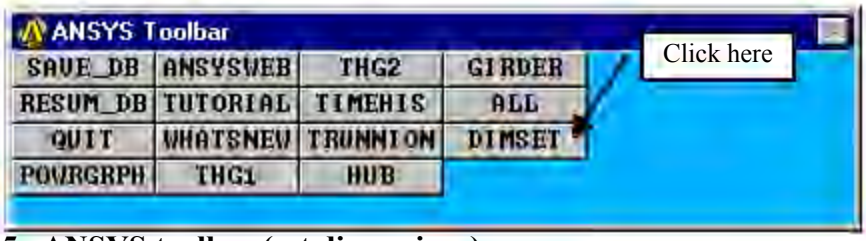

Figure B.25a ANSYS toolbar (set dimensions).

This step is required to dimension some arrays and set the results to the last set. The results can now be seen in the general postprocessor (described in Appendix B.5) or in the time history postprocessor (described in Appendix B.6). Sometimes on clicking DIMSET you will get a series of messages similar to the one shown in Figure B.25b.

Figure B.25b Re-dimensioning verification box.

Keep clicking 'yes' till such messages do not appear anymore. Note that if you fail to click the DIMSET button on the ANSYS toolbar, the general postprocessor and the time history postprocessor may not work as desired.

B.5 General postprocessor

The General postprocessor allows us view the results in the form of contour plots (time fixed). Prior to performing the steps described next the user should have either:

1. Performed a run of the program (Step 1 to Step 20) in Appendix B.3, or
2. Resumed a previous run (Step 1 to Step 3) of Appendix B.4.

B.5.1 Step 1

Choose the time point of interest by entering the following.

ANSYS Main Menu>General Postproc>Results Summary

Figure B.26 shows a summary of the results. The first column 'SET' denotes the set number of the results, 'TIME/FREQ' denotes the time for which the results have been saved, 'LOAD STEP' denotes the load step number of the results, and 'SUBSTEP' denotes the number of substeps in a loadstep. In the results summary make a note of the point of interest.

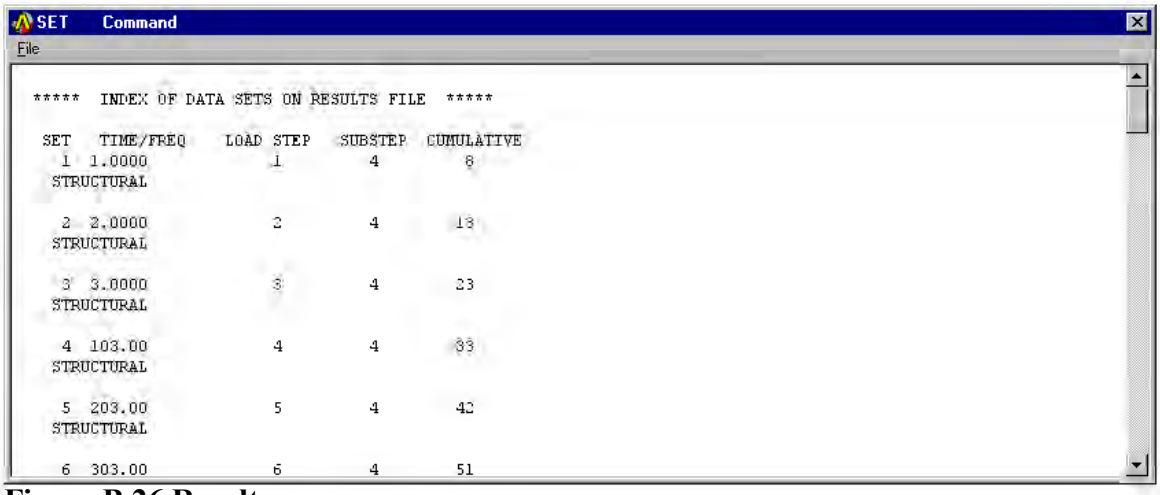

Figure B.26 Results summary.

B.5.2 Step 2

Go to the ANSYS Main Menu and enter the following.

ANSYS Main Menu> General Postproc>-Read Results-By Time-Frequency

Enter the time of interest chosen from the results summary described in Appendix B.5.2 in the dialog box shown in Figure B.27.

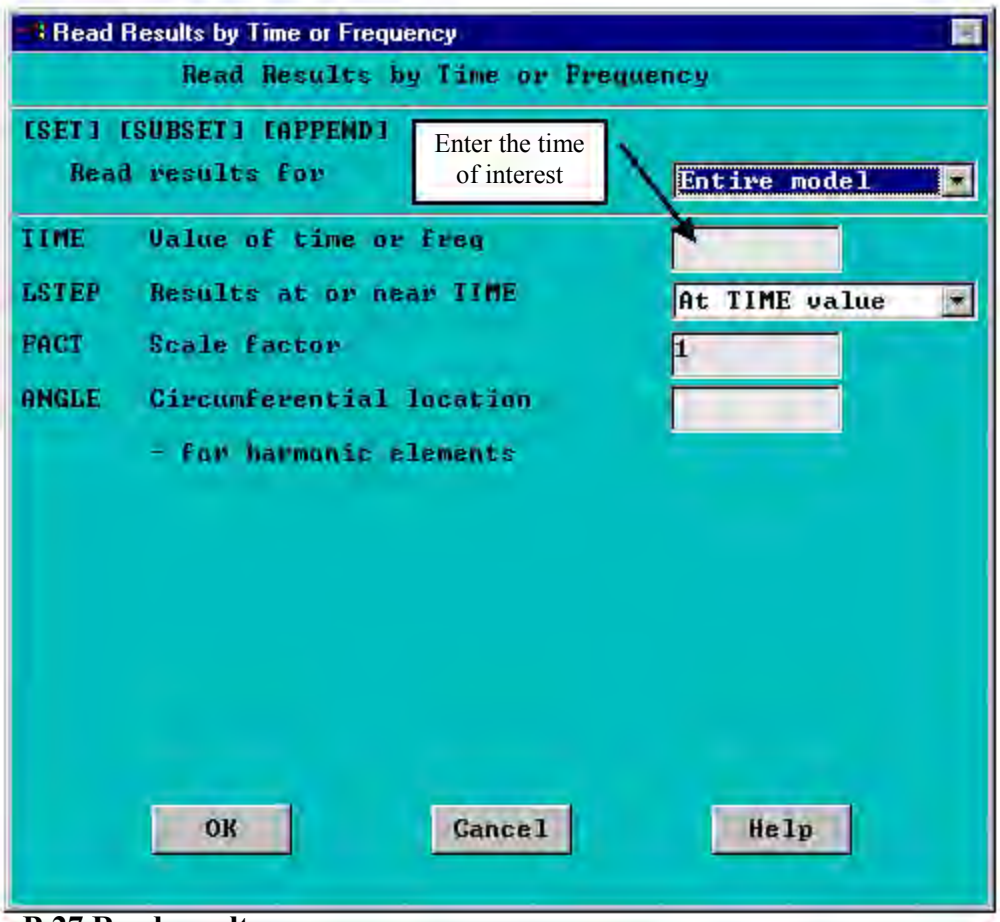

Figure B.27 Read results.

B.5.3 Step 3

Go to the ANSYS Main Menu and enter the following.

ANSYS Main Menu> General Postproc>Plot Results> Nodal Solu

The dialog box shown in Figure B.28a appears. Pick the quantity that needs to be plotted and click OK. Note that, the results are displayed in the cylindrical co-ordinate system as shown in Figure B.28b. Hence stresses in the x and y direction denote the radial stress and the hoop stress, respectively.

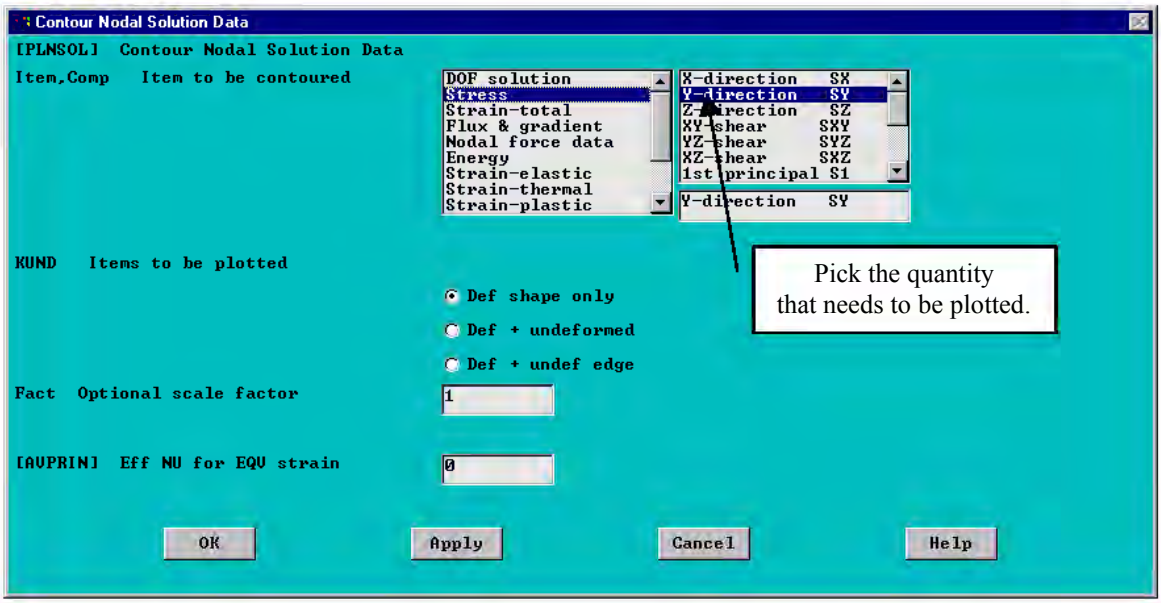

Figure B.28a Plot results.

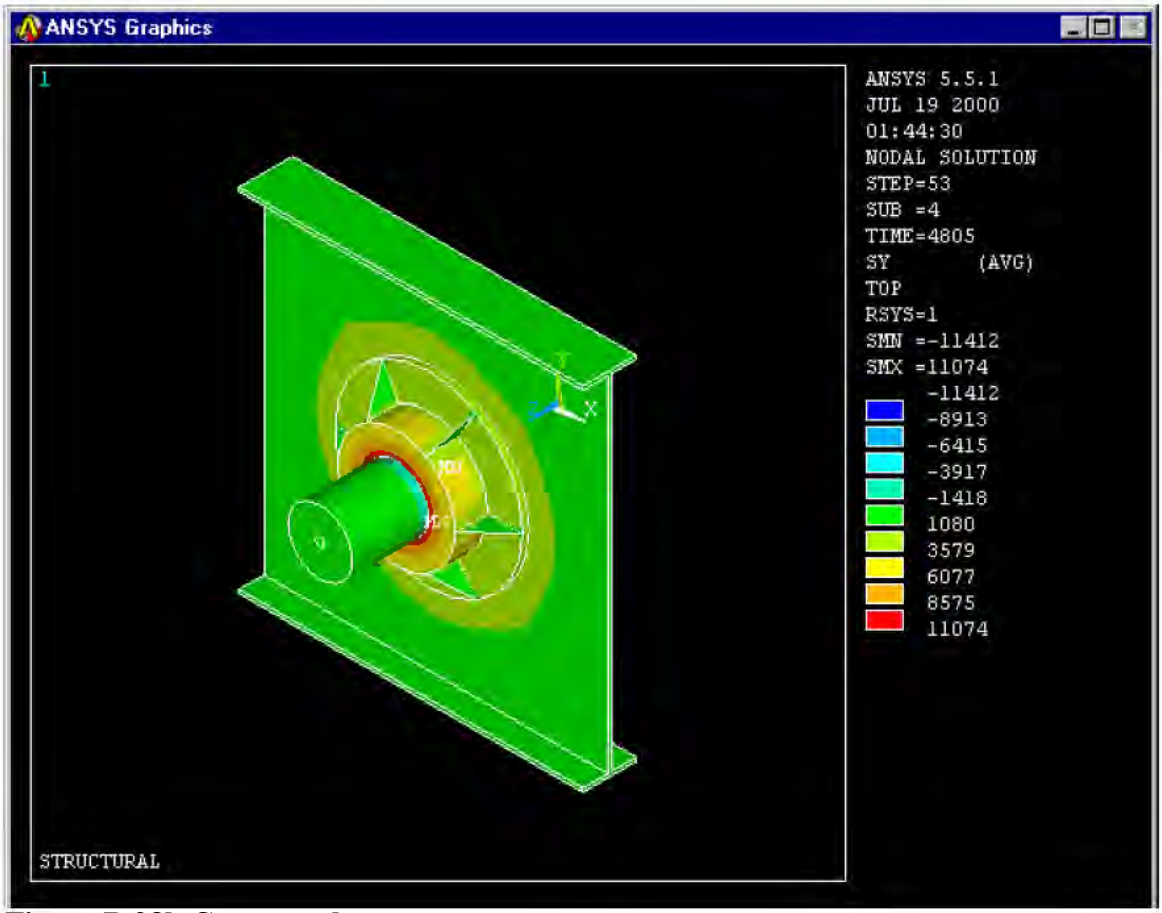

Figure B.28b Contour plot.

Repeat Step 1 to Step 3 to view different quantities at different or the same times.

B.5.4 Plotting parts of the assembly

Contour plots of individual parts of the assembly can be plotted by choosing them on the ANSYS toolbar as shown in Figure B.29.

Figure B.29 ANSYS toolbar (choose part of interest).

Follow steps 1-3 of the general postprocessor described in Appendix B.5. Once you are finished with the General Postprocessor click ALL on the ANSYS toolbar to select all entities

B.6 Time history postprocessor

The time history postprocessor plots variables against time. The THGTM has been programmed to plot hoop stress, temperature and critical crack length versus time. Prior to performing the steps described next the user should have either:

1. Performed a run of the program (Step 1 to Step 20) in Appendix B.3, and click on DIMSET on the ANSYS toolbar, or
2. Resumed a previous run (Step 1 to Step 3) of Appendix B.4.

B.6.1 Step 1

On the ANSYS toolbar shown in Figure B.30 click on TIMEHIS.

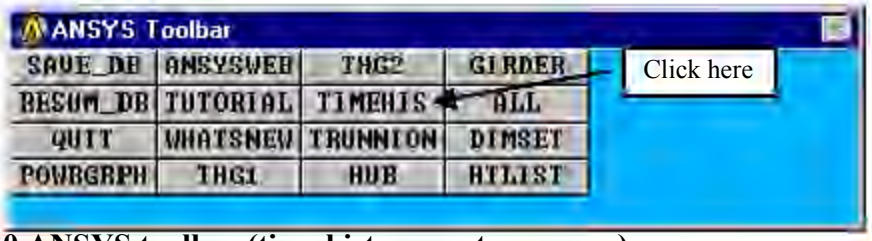

Figure B.30 ANSYS toolbar (time history postprocessor).

B.6.2 Step 2

You will get a dialog box like the one shown in Figure B.31a.

Figure B.31a Enter part of interest.

Enter ‘t’ for trunnion, ‘h’ for hub and ‘g’ for girder. The requested part of the assembly with the elements attached to it is plotted. The working of the time history postprocessor is explained with the help of an example. For example, if ‘h’ is entered, the elements attached to the hub are plotted as shown in Figure B.31b.

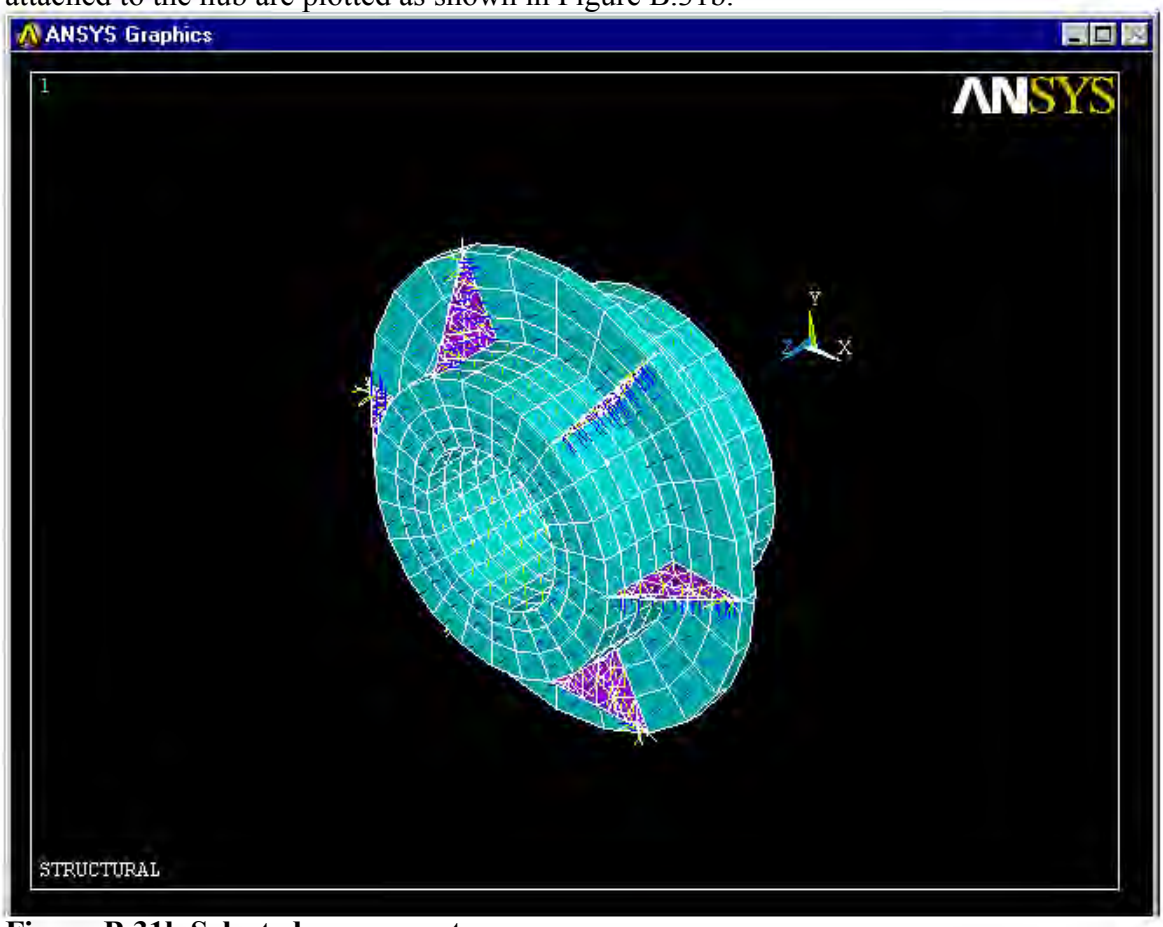

Figure B.31b Selected component.

A pick menu shown in Figure B.31c also appears.

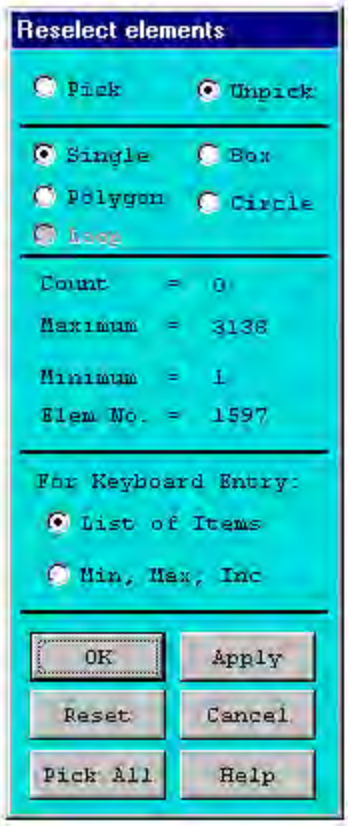

Figure B.31c Pick elements.

If we move the cursor over the ANSYS Graphics window the pick arrow points upwards indicating that we are in a pick mode. The desired element can be 'picked' by left clicking the mouse over it and Clicking OK. However, in practice it is often difficult to click at the right location and often misplaced clicks result in the wrong element being selected. A technique described next will help the user pick the correct element. The previous example is continued here.

B.6.3 Step 3a

Go to the Utility Menu and enter the following.

Utility Menu>PlotCtrls>Pan, Zoom, Rotate

The Pan-zoom-rotate menu shown in Figure B.32 appears on the screen.

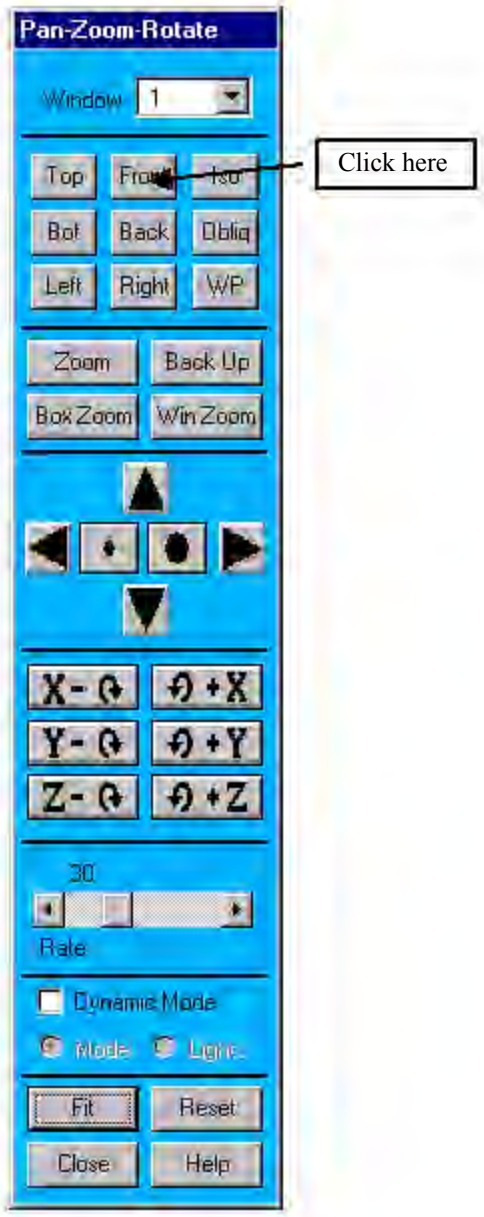

Figure B.32 Pan-zoom-rotate.

B.6.4 Step 3b

Click 'Front' in Figure B.32 and choose the element which has the same radial and hoop co-ordinates of our point of interest as shown in the Figure B.33

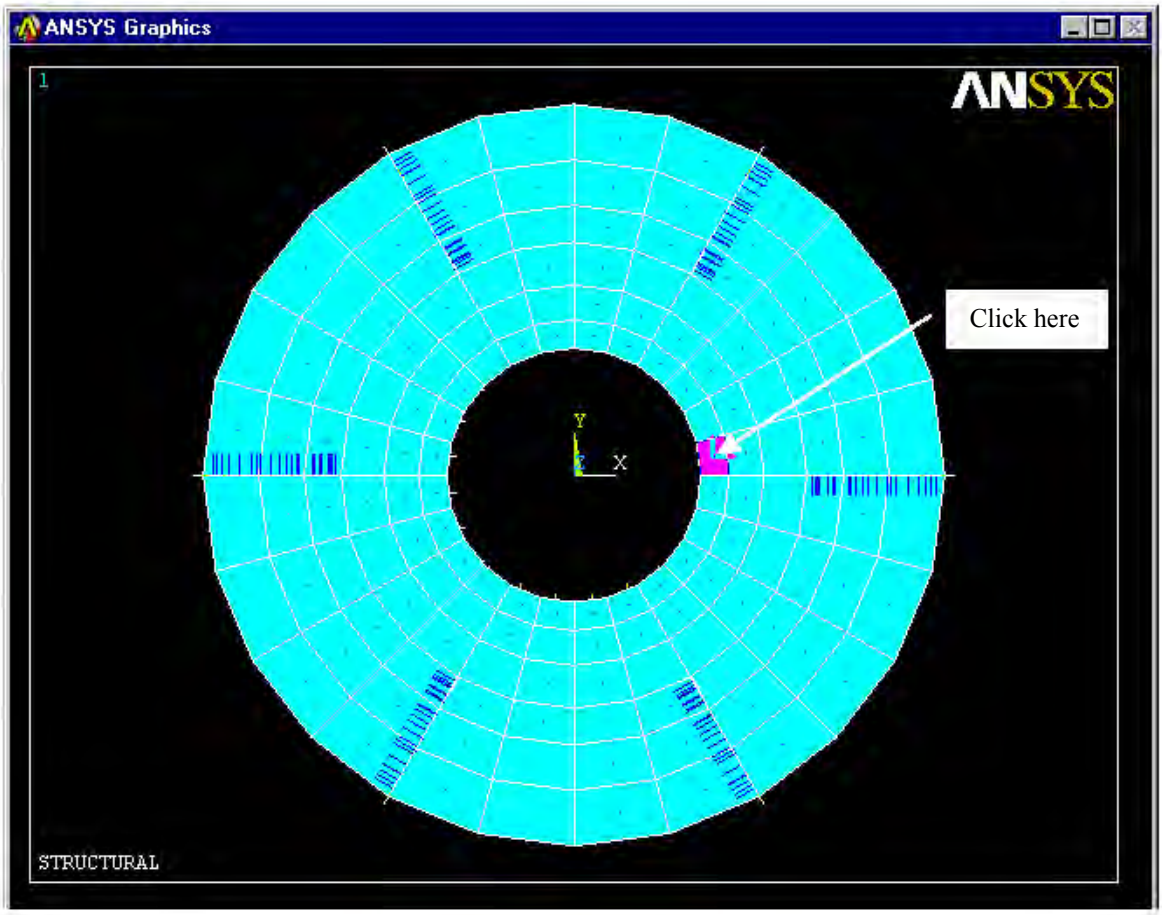

Figure B.33 Front view.

B.6.5 Step 3c

Click 'Right' on the pan, zoom and rotate dialog box in Figure B.32 and the right view of the part in question appears as shown in Figure B.34.

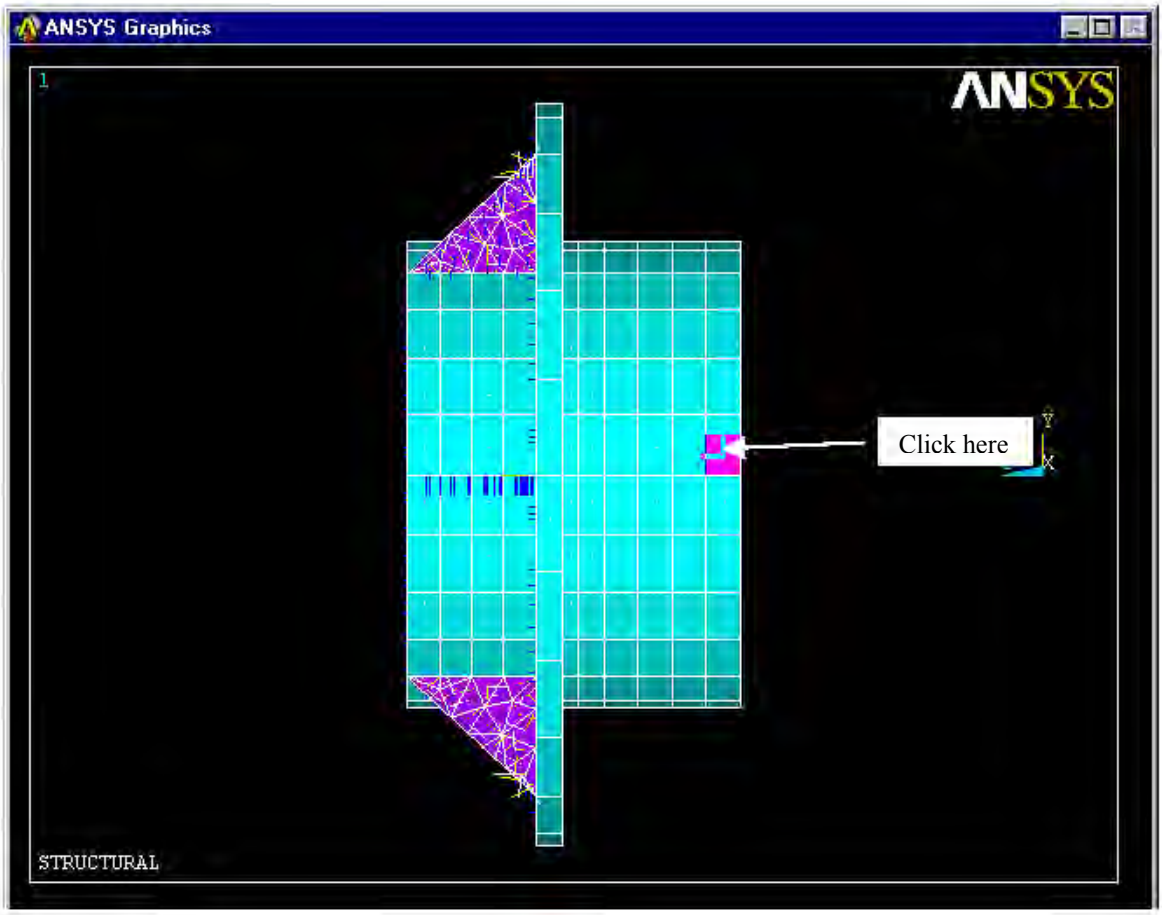

Figure B.34 Right view.

B.6.6 Step 3d

If there is more than one element with the same r and θ co-ordinate then the dialog box similar to the one shown in Figure B.35 will appear on the screen.

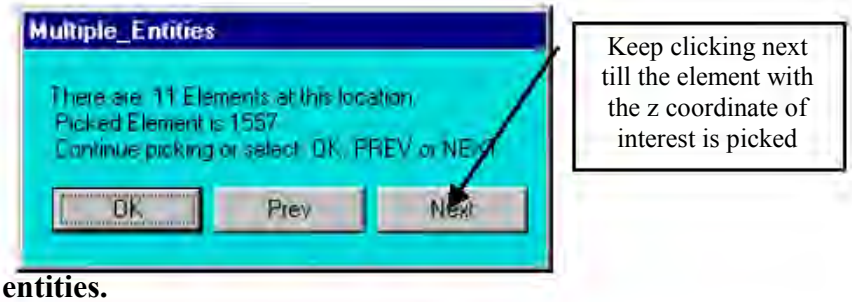

Figure B.35 Multiple entities.

Each time you click the next element with same z co-ordinate is chosen. Continue clicking till the element of interest is chosen. Then click OK on the 'reselect elements' menu.

In case you select the wrong element, you can enter the unselect mode by a right mouse click. After unselecting the unwanted element, you can enter the select mode again by right clicking again.

B.6.7 Step 3e

On clicking OK the element chosen is plotted. The view of the element can be changed using the Pan Zoom and Rotate. A dialog box similar to the one shown in Figure B.36a appears.

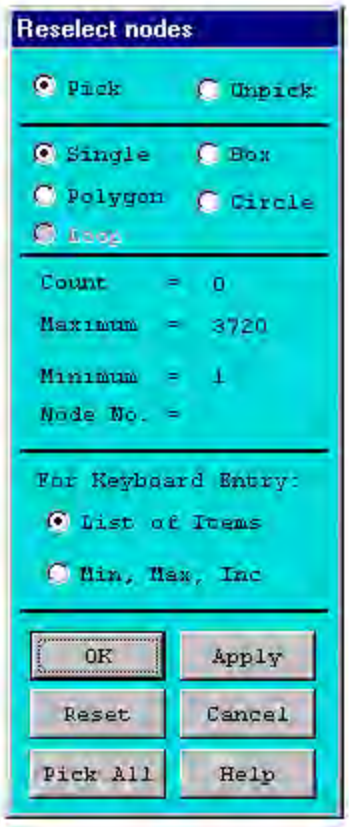

Figure B.36a Pick nodes.

Select the node of choice by clicking near it on the ANSYS Graphics window and clicking OK. In case you select the wrong node you can enter the unselect mode by a right mouse click. After unselecting the unwanted node you can enter the select mode again by right clicking again.

It will take some time for the results to appear on the screen. Wait for the hourglass on the screen to disappear. A graph similar to the one shown in Figure B.36b appears on the screen.

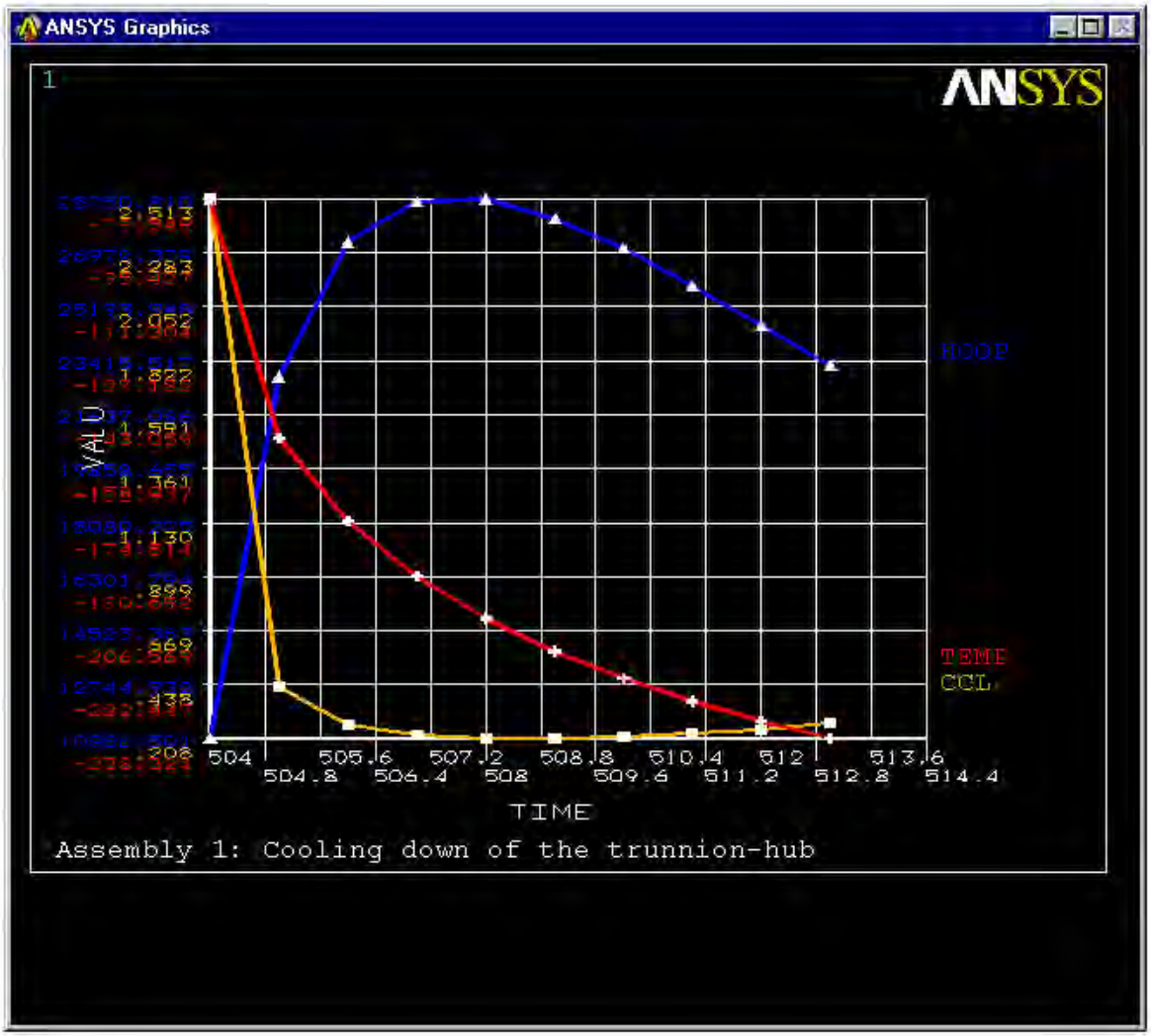

Figure B.36b Time history plot.

To print the graph, enter the following.

Utility Menu>Plot Ctrls>Hard Copy> to printer

To save the graph, enter the following.

Utility Menu>Plot Ctrls>Hard Copy>to file

The graph is saved as a bitmap file (*.bmp) in the working directory.

B.6.8 Options

To list the results, on the ANSYS toolbar shown in Figure B.37a, click on HTLIST.

Figure B.37a ANSYS toolbar (list results).

The results are listed in the format shown in Figure B.37b.

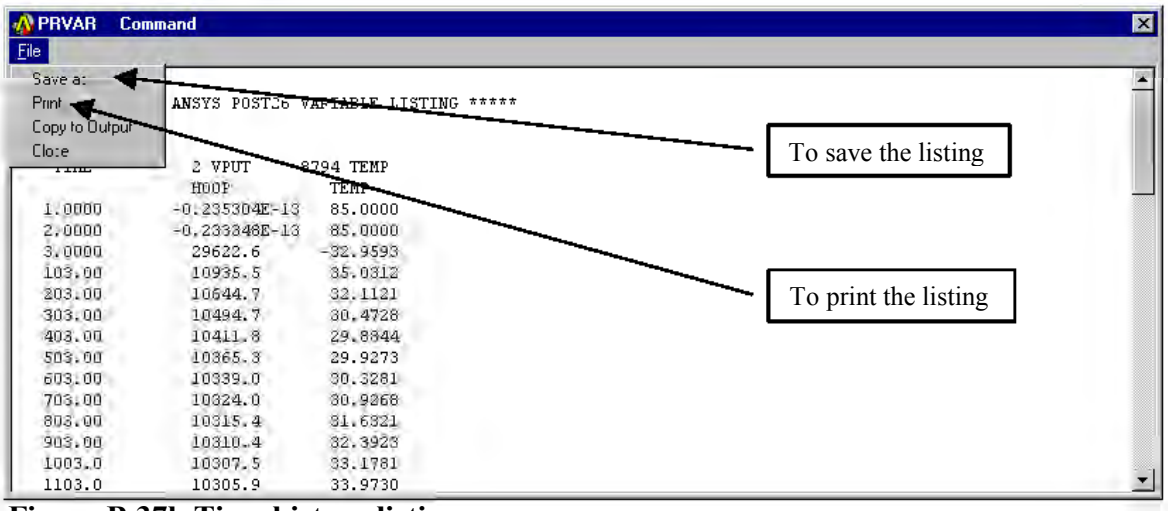

Figure B.37b Time history listing.

The pull down menus allow you to save and print the listing.

APPENDIX C

VERIFICATION EXPERIMENTS

C.1 Introduction

Owing to the high costs involved in the machining of the trunnion, hub and girder, the full-scale testing is a non-repeatable experiment. Hence, it is important to verify that all components of the experimental set-up work perfectly through the range from ambient temperature (80^0F) to the boiling temperature of liquid nitrogen (-321^0F). Also, the results produced by the data acquisition system need to be validated. Hence, a few verification experiments were carried out.

C.2 Verification of Thermocouples and Their Epoxy

Six type E thermocouples were inserted into a steel cylinder (shown in Figure C.1). Radial-1, Radial-2 and Radial-3 were probe-type thermocouples that had been inserted radially and were cemented into 17/64" holes with a 120^0 spacing, at depths of ½", 1", and 1 ¼" respectively. Axial-1, Axial-2, and Axial-3 were bare-end thermocouples cemented into 1/8" diameter holes with a spacing of 120 degrees, drilled on a 1 1/8" diameter circle located axially on the test sample. These thermocouples reached depths of ½", 1", and 1 ½", respectively. This cylinder was dropped into liquid nitrogen and then allowed to warm up to about 55^0F.

The results of this experiment are shown in Figure C.2. It was observed that the cool down was a rapid process (six minutes) while the warm up was relatively very slow (three hours). It was also observed that both the bare-end and the probe-type thermocouples performed perfectly in the experiment. Hence, it was concluded that the bare-end type of thermocouple would be used in this research project since they required less physical alteration to test samples thereby reducing possible stress related effects.

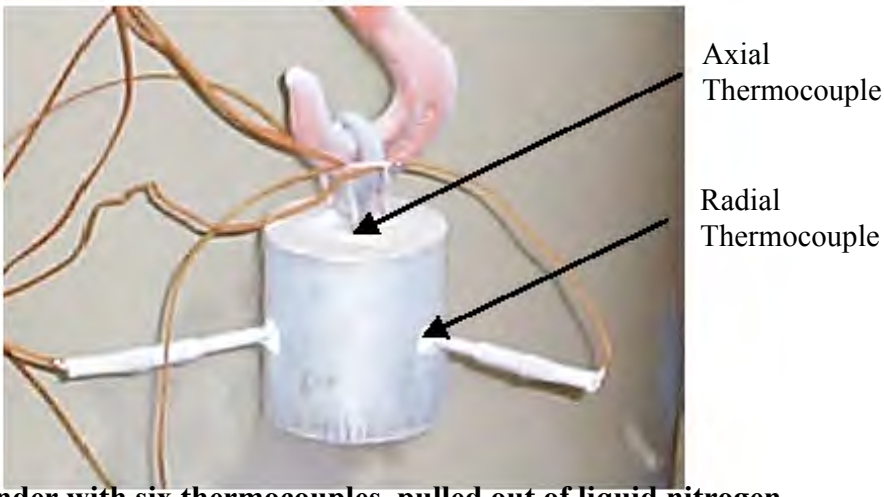

Figure C.1 Steel cylinder with six thermocouples, pulled out of liquid nitrogen.

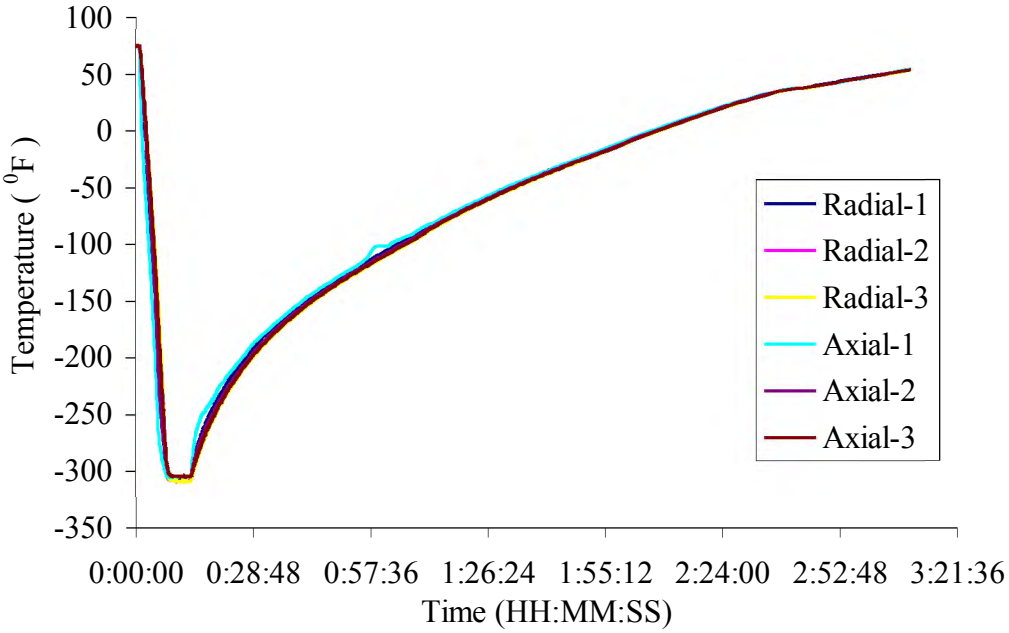

Figure C.2 Cool down in liquid nitrogen and warm up in ambient air.

C.3 Cantilever Beam Experiment

In this experiment two strain gages were mounted on a steel cantilever beam (shown in Figures C.3 and C.4). This beam was then loaded with known weights at its free end. The strains recorded by DAQ system were used to calculate bending stresses in the beam. These results were compared with theory and they are summarized in Table C.1.

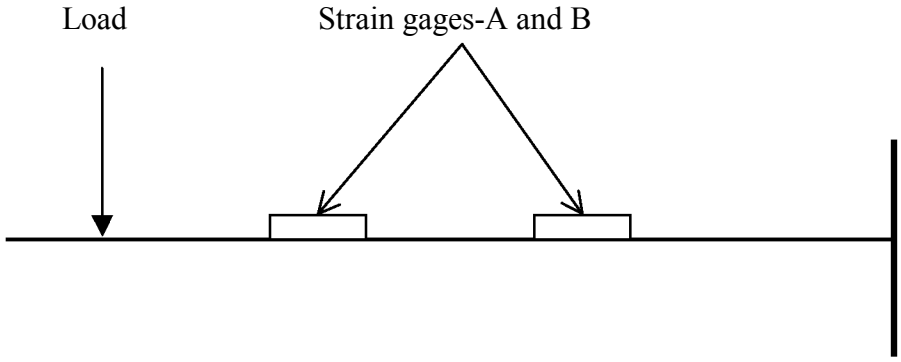

Figure C.3 Schematic diagram of cantilever beam.

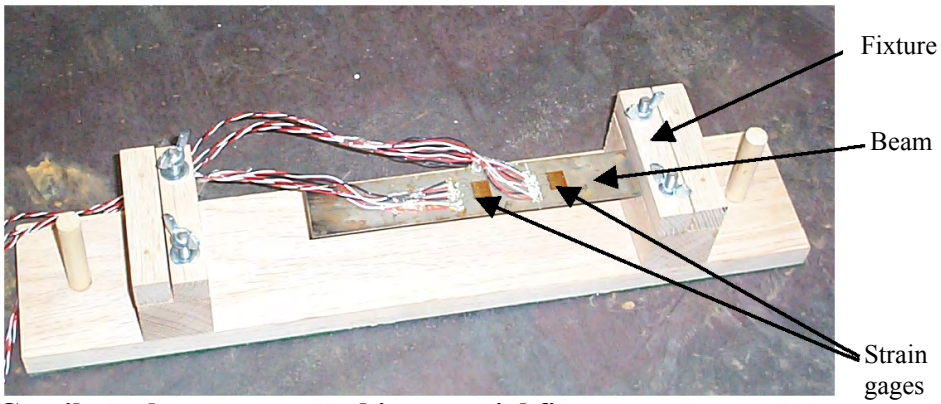

Figure C.4 Cantilever beam supported in a special fixture.

Table C.1 Comparison of theory and experimental strains for both strain gages.

Strain Gage A			Strain Gage B		
Theoretical Strain (με)	Experimental Strain (με)	Percentage Difference (%)	Theoretical Strain (με)	Experimental Strain (με)	Percentage Difference (%)
7.55279	8.99744	17.45778	5.17506	5.94593	13.86333
16.33094	17.10076	4.60529	10.90856	11.37992	4.22959
16.41534	17.76512	7.89795	10.93496	12.26548	11.46971
25.01385	27.00618	7.65986	16.66280	18.32154	9.48273
29.35967	31.35308	6.56667	19.90675	21.85052	9.30986
32.70040	34.13041	4.27950	21.78314	23.18094	6.21738
40.43038	42.17485	4.22363	26.93241	26.44175	-1.83859

To summarize the results presented in Table C.1, theoretical and DAQ stresses were averaged over the seven loads and the percentage errors based on these averaged values were evaluated to be 6.19 % for strain gage-A and 6.11% for strain gage-C.

The difference between the theory and DAQ results can be attributed to the adhesive, which is used to bond the strain gage to the beam. The thickness and stiffness of this glue line have a significant effect on the results because the steel beam itself is just 0.029" thick.

The data from this experiment was also used to plot "Load vs. Strain" for the two strain gages. As expected from theory of elasticity, these graphs were nearly linear. The graphs are shown in Figure C.5. Note that in Figure C.5, R^2 is the coefficient of determination.

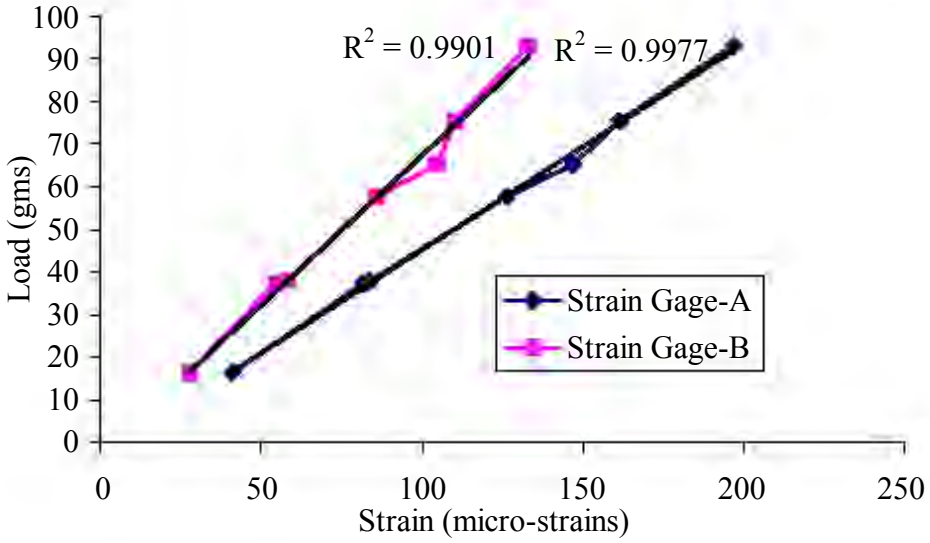

Figure C.5 Plot of applied load versus strain in Gage-A and Gage-B.

C.4 Differential Expansion Between a Steel Sleeve and a Brass Bolt

This experiment was done to verify whether the strain gages performed well when immersed in liquid nitrogen and to measure "thermal output" which is essentially the strain produced in a strain gage purely due to temperature change. This is then deducted from the "recorded" strain to get "mechanical" strain.

As shown in Figures C.6 and C.7, the steel sleeve was constrained at its two ends by brass nuts (mounted on the brass bolt). This sleeve-bolt assembly was immersed in liquid nitrogen. The coefficient of thermal expansion of the bolt is greater than that of the sleeve. Therefore, the bolt would contract more than the sleeve thus providing a net compressive force on the sleeve. This stress was measured by a strain gage mounted on the sleeve and then compared to a theoretical value.

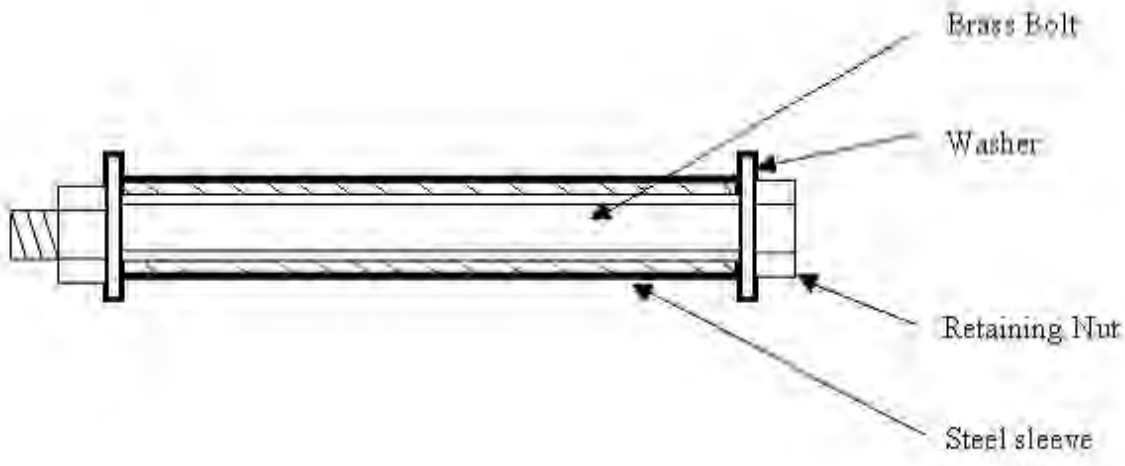

Figure C.6 Sectional view of sleeve-bolt assembly.

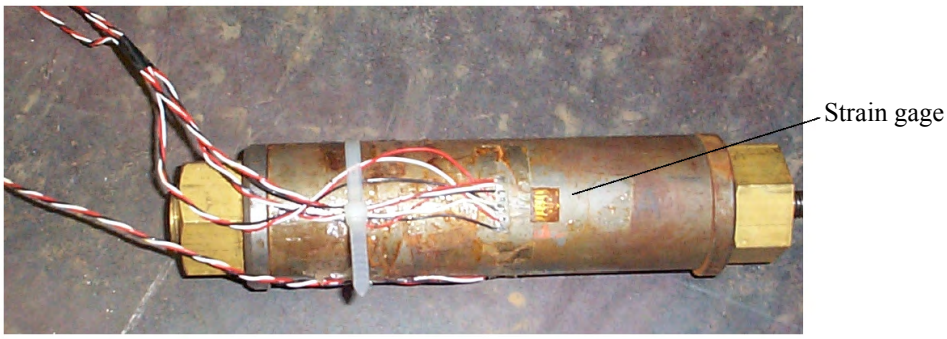

Figure C.7 Actual sleeve-bolt assembly.

The equations for unrestrained contraction are:

$$\delta_{steel} = \alpha_{steel} \cdot \Delta T \cdot L \tag{C.1a}$$

$$\delta_{brass} = \alpha_{brass} \cdot \Delta T \cdot L \tag{C.1b}$$

The load-displacement equations are:

$$\delta_{steel} = \frac{P.L}{(A.E)_{steel}} \tag{C.2a}$$

$$\delta_{brass} = \frac{P.L}{(A.E)_{brass}} \tag{C.2b}$$

For equilibrium:

$$P_{steel} = P_{brass} = \frac{(\Delta T.(\alpha_{steel} - \alpha_{brass})).((A.E)_{steel} \times (A.E)_{brass})}{(A.E)_{steel} + (A.E)_{brass}} \tag{C.3}$$

The theory predicted the compressive stress in the sleeve to be –15.5 ksi, while the experimental result is –7.3 ksi. However, the theory did not account for the variation of the coefficient of thermal expansion of both metals with temperature. This variation is quite considerable; the value of the coefficient of thermal expansion decreases by almost a factor of three over the range from room temperature to that of liquid nitrogen. Hence, an "equivalent" value of the coefficient of thermal expansion was used to compute the "theoretical " stress. This modified value of theoretical stress was –8.0 ksi. This was in good conformance with the experimental value. (Absolute percentage difference of 9.25 %)

APPENDIX D

X-RAY REPORT

Curtis F. McKnight Testing Laboratories Inc. (Tampa, FL) was asked to x-ray the hub before doing the full-scale tests. The inspection report by the laboratory (given in the next 5 pages) states, " Upon review of the radiographs, it is to noted that 4 gross indications of shrinking/gas are present in the major cylinders section above the flange (non-gusseted end). These are the size and nature that is far in excess of level 5 of the ASTM E186 or E446 reference radiographs, while no acceptance standards have been imposed in the case of this trunnion, it is to note that the severity of the indications on this specimen would likely not be acceptable to any industry standards, military or civilian. It is not known as to whether any particular contract and or design specifications have been imposed and subsequently no acceptance or rejection of this specimen is made."

CURTIS F. McKNIGHT
TESTING LABORATORIES, INC.
7708 E. BROADWAY
TAMPA, FLORIDA 33619
Ph: (813) 626-0287

Page 1 of 1 Pages

RADIOGRAPHIC REPORT

CUSTOMER PG+H
ADDRESS 1512 4th Ave Tampa Fl
PURCHASE ORDER NO.
DATE 8-17-00
CUSTOMER JOB NO.
WORK ORDER NO. 00-0669
REPORT NO.
SYSTEM Bridge Trunion

WELD NO.	VIEWS	DIA.	THICKNESS	ACCT.	REJ.	REMARKS / CODE
WEB	0-1	3/4	[redacted]			
	1-2	3/4	[redacted]			
	2-3		3/4			
	3-4		3/4			
	4-5		3/4			
	5-0		3/4			
BOTTOM D7	0-1		1 5/8			
	1-2		1			
	2-3		0 1/2			
	3-4		|			
	4-5		|			
	5-0		|		
BOTTOM D8	0-1		|		
	1-2		|		Shrinkage Level 5
	2-3		|		
	3-4		|		
	4-5		|		
	5-0		|		
TOP	0-1		1 5/8			Shrinkage Level 5
	1-2		2 1/2			Shrinkage Level 5
	2-3		|		Shrinkage Level 5
	3-0		|		Shrinkage Level 5

MATERIAL TYPE CS | WELDING PROCESS

WELD JOINT: OPEN ROOT ☐ INSERT ☐ BACKING ☐

MFG. STAGE: PARTIAL ☐ FINAL ☐ BEFORE PWHT ☐ AFTER PWHT ☐ EXCAVATED AREA ☐ OTHER

DEVELOPED: FOR 8 min Time AT 68 °

SOURCE: IR 192 ☑ CO 60 ☐ S/N B333
X-RAY ☐ KV.
SOURCE/SPOT SIZE .1 X .1 SFD 15/22/18
CI/MA. 95 MA/MIN. 35-18

PENETRAMETER: TYPE ASTM PENE. MATERIAL CS
PENE. SIZE 20/40/25 N/A INFO ONLY ☐

PENE. PLACEMENT: SOURCE SIDE ☑ FILM SIDE ☐
SEPARATE BLOCK ☐ LIKE PART ☐

SHIM: MATERIAL n/a THICKNESS

FILM: MFG./TYPE AGFA SPEED D7-D8
LOAD Double SIZE 7 x 17

SCREENS: Pb ☑ OTHER ☐
THICKNESS: FRONT .010 BACK .010

LOCATION MARKER: SOURCE SIDE ☑ FILM SIDE ☐
AT ____ SPACING & NO. AT ____ INCH/DEGREES INTERVALS

REQUIRED SENSITIVITY: 2T ☐ 4T ☐ OTHER INFO

VIEWING TECHNIQUE:
SINGLE FILM ☐
COMPOSITE FILM ☑

EXAMINATION:
SINGLE WALL ☑
DOUBLE WALL ☐

RADIOGRAPHER S Comeaux CERT. LEVEL II

PROCEDURE CFM 10.3 TECH. NO.

EVALUATION BY:
NAME [signature] CERT. LEVEL II DATE 8-17-00
TO ACCEPTANCE STD. INFO ONLY

NOTES:

SKETCH:

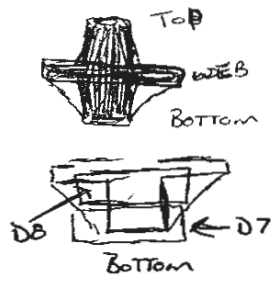

CODE
1. Crack
2. Lack of Fusion
3. Incomplete Penetration
4. Slag
5. Porosity
6. Undercut
7. Burn Thru
8. Unfused Insert
9. Crater Crack
10. Crater Pit
11. Excessive Melt Thru
12. Tungsten
13. Surface Ind.
14. Film Artifact

Form RT002 9/91

CURTIS F. McKNIGHT
TESTING LABORATORIES, INC.

TESTING and INSPECTION

7708 E. BROADWAY
TAMPA, FL 33619
(813) 626-0287

INSPECTION REPORT

Date August 23, 2000

Customer P G & H Engineering — WO# 00-0619

Address 1512 4th Ave. — Type of Inspection Visual

Tampa, Fl. 33605 — Applicable Specifications

Customer Purchase Order No. B18929

Description and/or Serial No. Bridge Trunions

RESULTS OF INSPECTION

Upon review of the radiographs, it is noted that 4 gross indications of shrinking / gas are present in the major cylinders section above the flange (non-gusseted end). These are the size and nature that is far in excess of level 5 of the ASTM E186 or E446 reference radiographs, while no acceptance standards have been imposed in the case of this trunion, it is of note that the severity of the indications on this specimen would likely not be acceptable to any industry standards, military or civilian. It is not known as to whether any particular contract and or design specifications have been imposed and subsequently no acceptance or rejection of this specimen is made. See attached shooting sketches for locations of indications and radiographic geometry.

AWS QC 1 KEN C. McKNIGHT 92040381 CWI

Prepared by Ken C McKnight — Approved by

Ken C. McKnight, CWI

WEB View
Bottom
Bottom
3/4"
Film
D7 Film 93cu 37sec
Placement

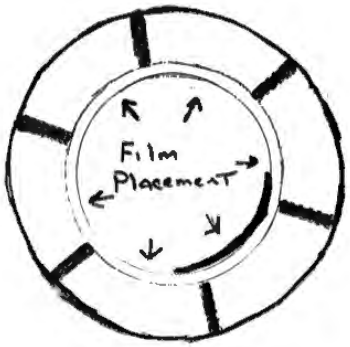

Bottom H
View

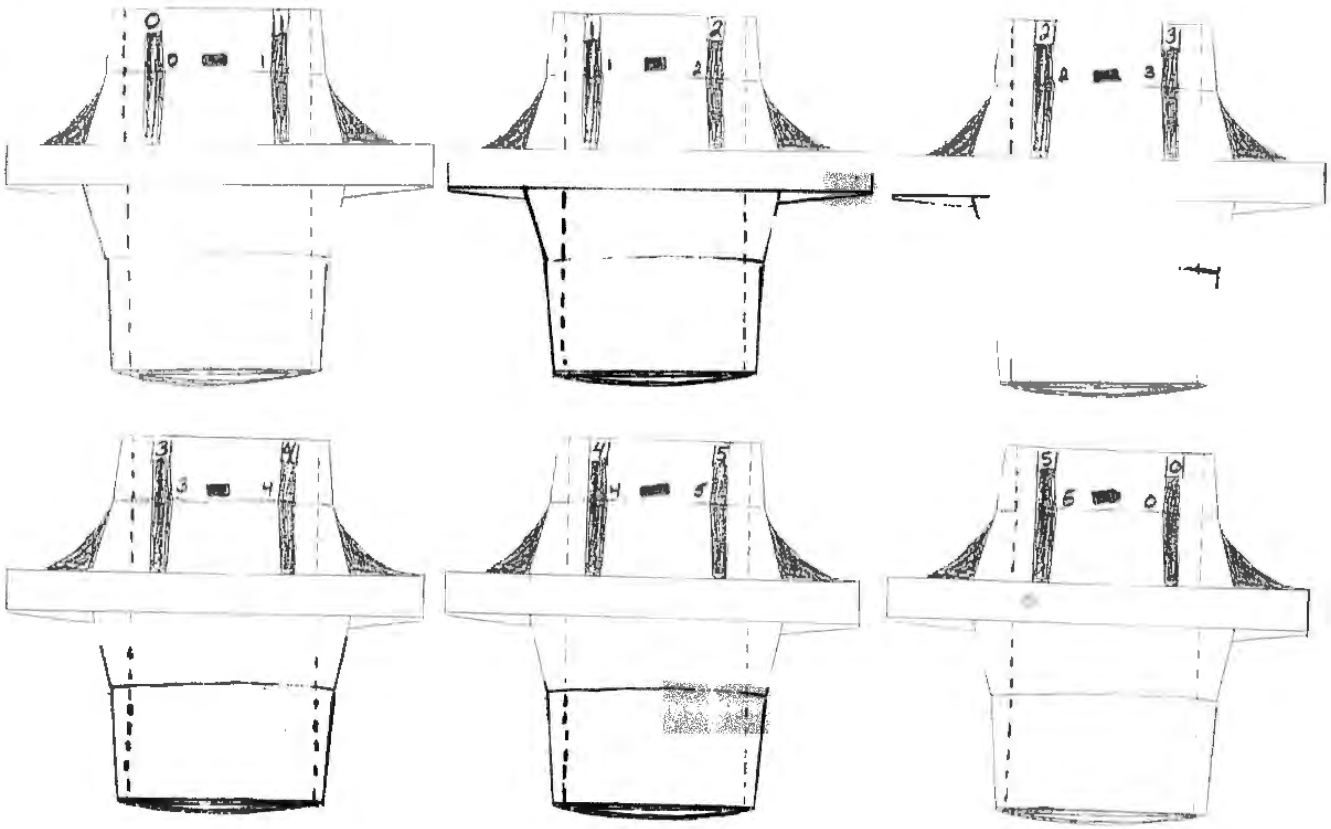

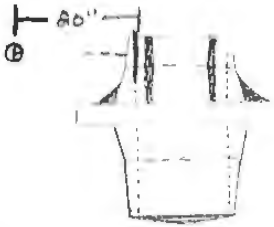

D7 Co 4
6 expos

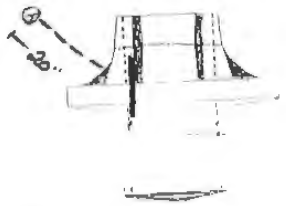

D8 C
6 pos

Top Half
Views
17"
14 1/8"
14 1/8"
14 1/2"
Film
Film
Film
Film
6 1/2"
D7 93C 70SEL
1 expos
Panoramic

The x-rays of the hub from the top view are given in Figures D.1a through D.1d. See the x-ray report presented previously in this appendix for a description of these views. Note the presence of void in the casting in Figures D.1a through D.1d

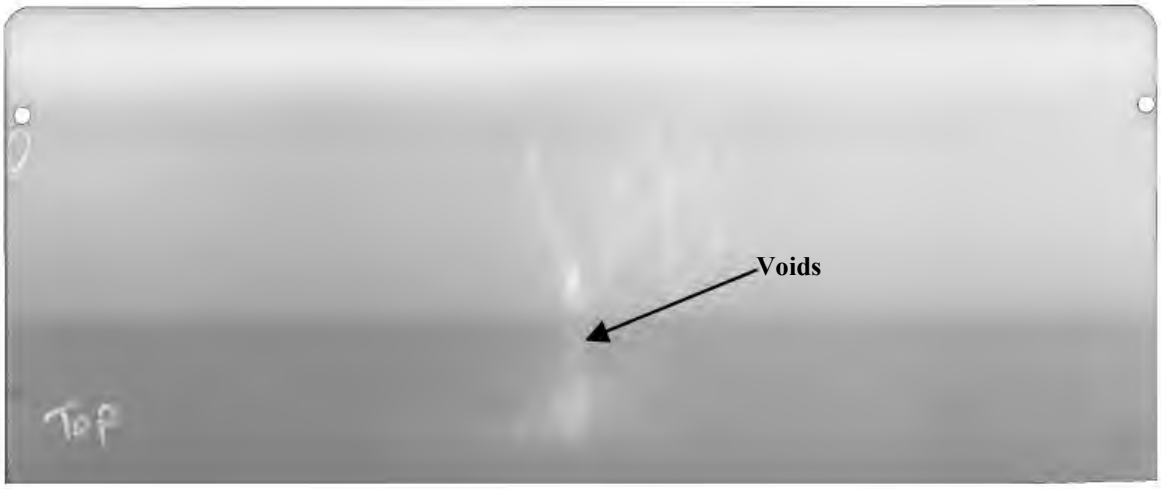

Figure D.1a X-ray of the hub from the top view (0-1).

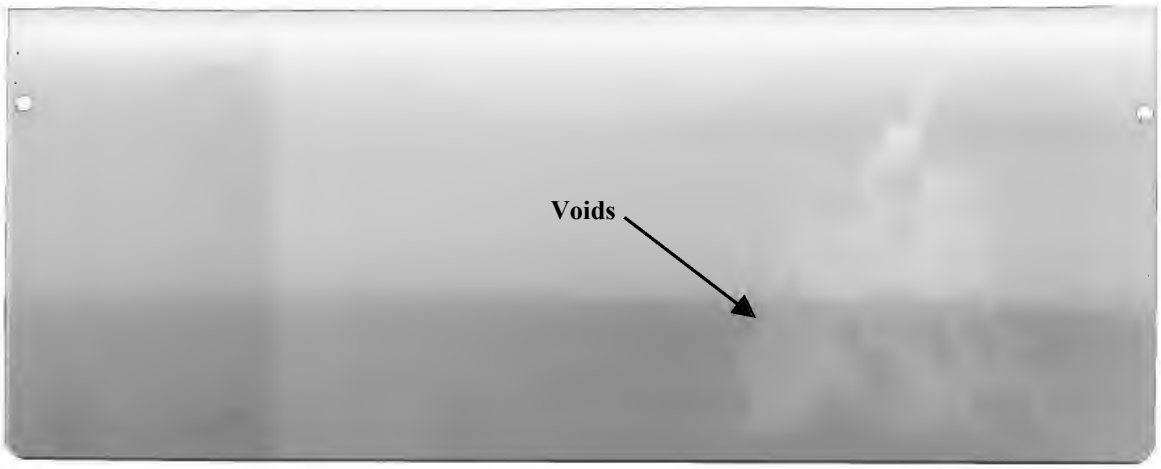

Figure D.1b X-ray of the hub from the top view (1-2).

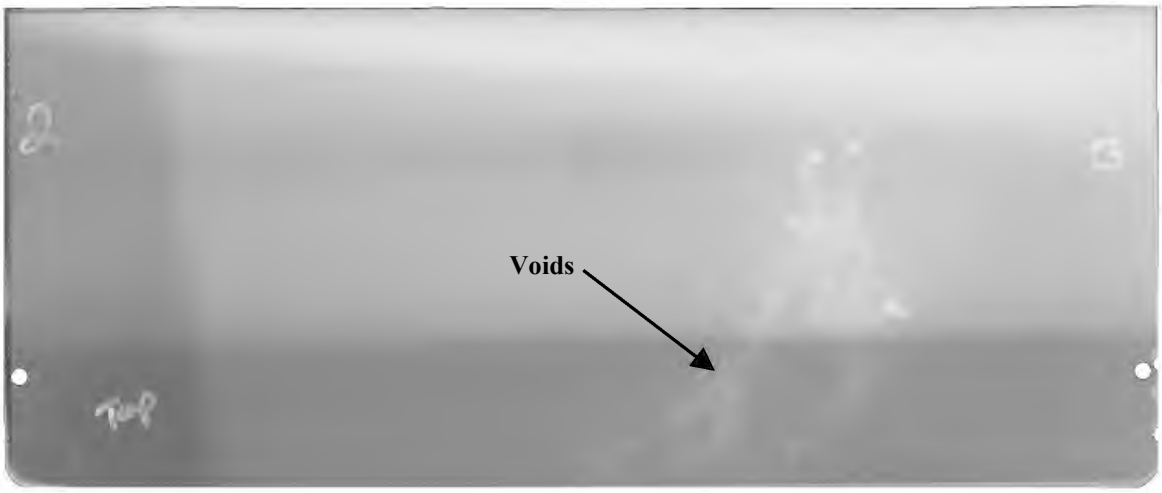

Figure D.1c X-ray of the hub from the top view (2-3).

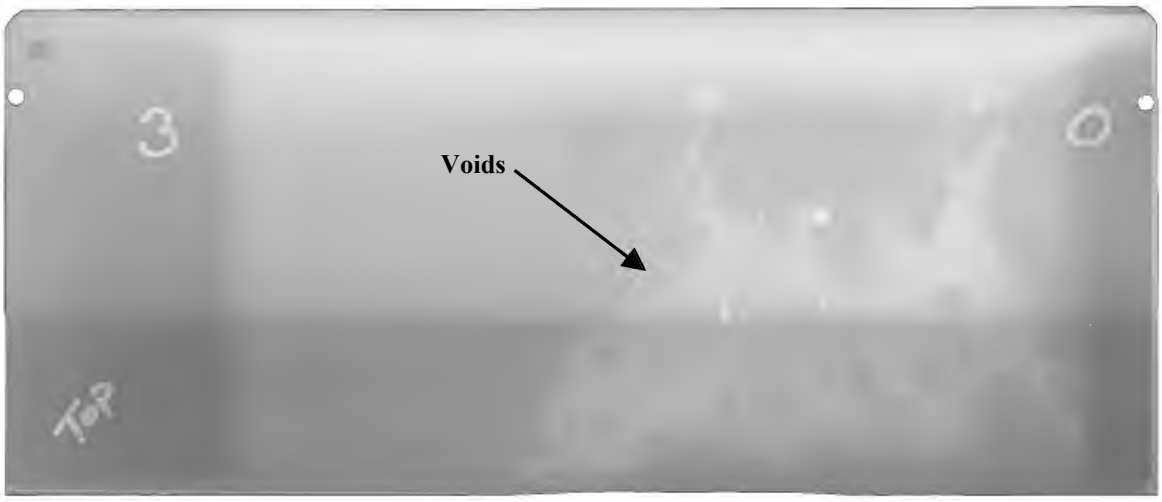

Figure D.1d X-ray of the hub from the top view (3-0).

The x-rays of the hub from the web view are given in Figures D.2a through D.2f. See the x-ray report presented previously in this appendix for a description of these views.

Figure D.2a X-ray of the hub from the web view (0-1).

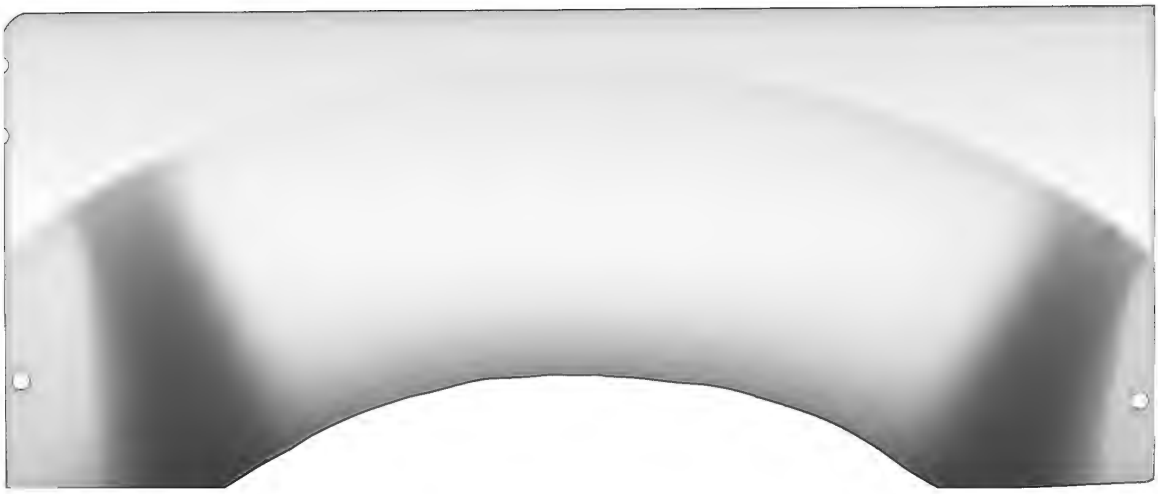

Figure D.2b X-ray of the hub from the web view (1-2).

Figure D.2c X-ray of the hub from the web view (2-3).

Figure D.2d X-ray of the hub from the web view (3-4).

Figure D.2e X-ray of the hub from the web view (4-5).

Figure D.2f X-ray of the hub from the web view (5-0).

APPENDIX E

WEB SITE

The web site (see Figure E.1) titled "bascule bridge trunnion-hub-girder design" for this research project is located at http://www.eng.usf.edu/~besterfi/bascule/.

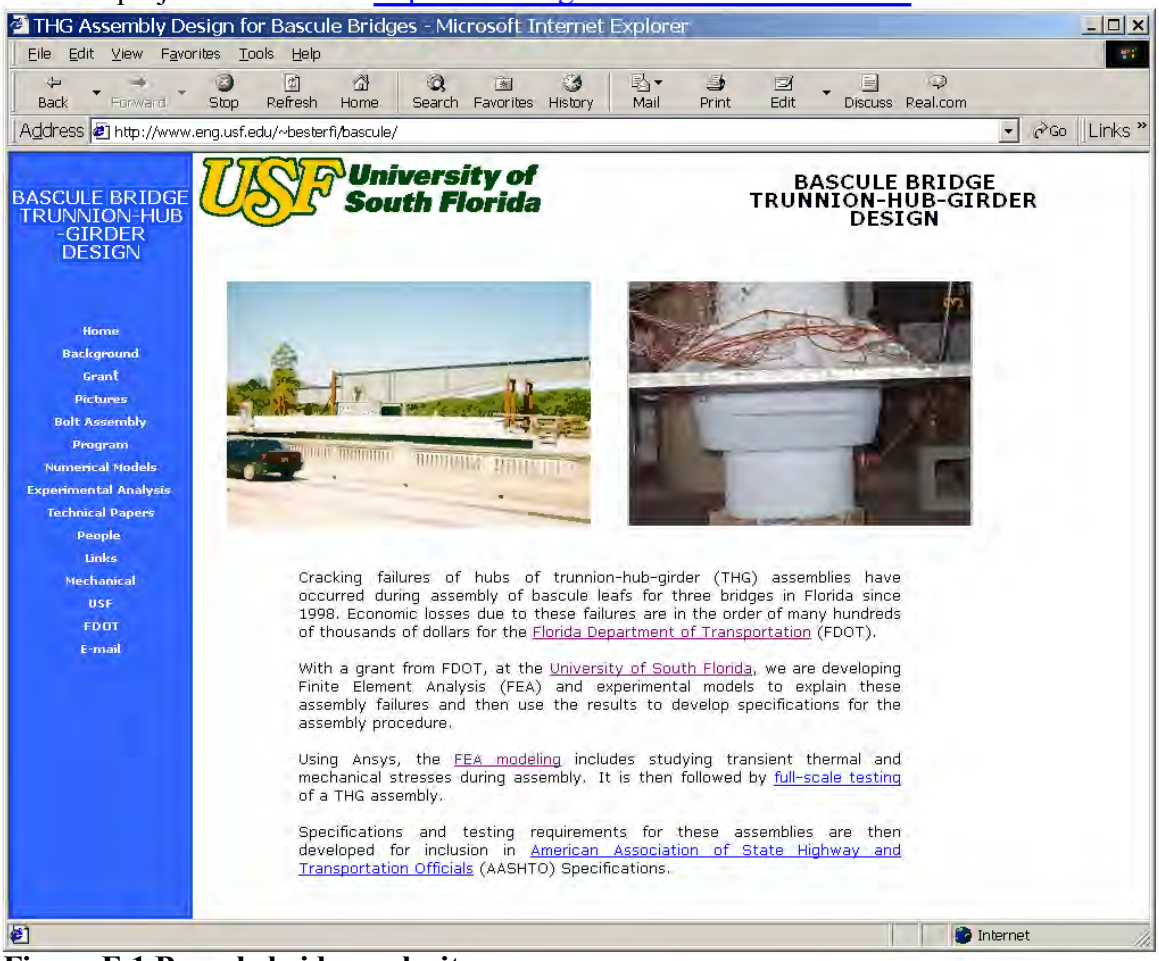

Figure E.1 Bascule bridge web site.

The following information is accessible from the web site:

- Description of the grant,
- People involved with the research project,
- Pictures of various component of a THG assembly for several bridges,
- Downloadable programs,
- Published papers,
- Numerical (FEA) results,
- Experimental results,
- Three Master's degree thesis,
- Final report submitted to FDOT,
- Video clips of experimental testing, and
- Links to various related sites.